# Final Report

## Design of a Cutting Edge Low-Emission Low-Noise Aircraft

Group 1


Delft University of Technology

TU Delft

This page is left empty intentionally.

# Final Report

## Design of a Cutting Edge Low-Emission Low-Noise Aircraft

by

## Group 1


| Student Name | Student Number |
|---|---|
| M.J. van Laar | 4282817 |
| V.P. Petrov | 4554418 |
| S.C.P. Wijnands | 4668561 |
| D.S. Taraczky | 4823141 |
| J. Smeets | 4862163 |
| S. Rooze | 4992644 |
| T.S. Vermeulen | 4995309 |
| R. Vaznelyte | 5019214 |
| D.S. Ruijs | 5025028 |
| J. Chen | 5076412 |


| | |
|---|---|
| Tutor: | Francesco Avallone |
| Coaches: | Fabio Beltrame & Nan Yue |
| Teaching Assistant: | Lars Dijkstra |
| Project Duration: | April 19, 2022 - June 21, 2022 |
| Faculty: | Faculty of Aerospace Engineering, Delft |

Cover: Artistic impression of the Lightning2 aircraft in flight.
Background image taken from `https://wallpapersmug.com/w/wallpaper/clouds-and-sunset-sea-of-clouds-2e0a0c15760/download` - Accessed: 16-06-2022

TU Delft

LH2

# Executive Overview

This executive overview provides the reader with a content-based summary of the Lightning2 DSE project. First, the project timeline and planning is outlined, after which each chronological step and deliverable in this project are briefly presented and summarised.

**Project Timeline & Planning**: The overview of the project is maintained using a dedicated Gantt chart, where the project is divided into five phases, being Phase 1: Project Planning, Phase 2: Literature Study and Requirements Analysis, Phase 3: Conceptual Design, Phase 4: Initial Sizing, and Phase 5: Detailed Sizing. The final report will be finished on June 17, 2022 with a symposium presentation on June 23, 2022.

**Mission Need Statement & Project Objective Statement**

Mission Need Statement

Design a new cutting-edge aircraft concept similar in size to the Airbus A320, which emits at least 50% less $NO_x$, 45% less $CO_2$, and 65% less perceived noise.

Project Objective Statement

Design a low-emission and low-noise aircraft with a unit price of $100 million with 10 students in 10 weeks.

**Key Client Requirements**: From the client, a set of requirements for the aircraft were derived. The key requirements here are a design time of five years, a reduction of 90% in $NO_x$, 45% in $CO_2$, and 65% in perceived noise emissions, relative to aircraft that entered service in the year 2000. This all should not be at the expense of safety, reliability, or cost compared to the A320. Furthermore, all parts should be recyclable and on-ground operations should be gas emission free. To remain competitive in the market, the design should be adaptable when technology advances.

**Key Project Risks**: Before continuing with the design, project and technical risks were identified. The key resulting risks are summarised in Table 1, including their mitigation strategies.

**Table 1:** *High project and technical risks.*

| Risk ID | Risk | Mitigation |
|---|---|---|
| **R.O.6** | Unrealistic project schedule. | Schedule with multiple levels and low task dependency. |
| **R.O.10** | Exceeding page limit. | Allocate approximate page limits to each chapter. |
| **R.O.8** | Unrealistic objectives. | Perform research into requirement feasibility. |
| **R.T.C.6** | Costly design changes. | Perform a extensive research into requirement feasibility. Set up contract with definite requirements. |
| **R.T.C.7** | Inaccurate cost estimate. | Implement financial buffer. |
| **R.T.S.1** | Scarce materials & resources | Create back-up structures with different materials. |
| **R.T.S.6** | Third party delivery delays. | This risk has to be accepted. |

**Market Analysis**: The key characteristics of the commercial aviation market have been analysed and the intersection of sustainability and low-cost carriers has been identified as a potential gap in the market. The growth in this sector, combined with the resilience of short-haul flights to the Covid-19 shock, provide confidence to the team that the final product will fit this market gap.

The current and expected competition with short/medium-haul flights is analysed, by considering the high-speed rail network (assuming further unification amongst countries) and futuristic options such as Hyperloop.

To immediately compete with current A320-type aircraft, operational distribution of flight ranges are analysed combined with geographical mapping. Figure 1 depicts the main operational areas of the intended aircraft.

**Figure 1:** *Range of the Lightning2 aircraft. Each circle shown has a radius of 3 700 km.*

Key market dynamics and trends are identified that pertain to the commercial aviation sector in broader terms (low-cost carriers, sustainability, and recyclability). Additionally, market factors pertaining specifically to airport hydrogen infrastructure and fuel cell integration in aircraft are discussed. Under the assumption of a 30 year active selling period of the aircraft, a first estimation of aircraft orders amounts to 1 800 units.

**Financial Analysis:** A financial analysis of the Lightning2 aircraft was conducted to estimate the unit cost, the operational costs and the return of investment. The program requires an initial investment of 19.7 billion USD, which will be doubled after 30 years of manufacturing, as indicated by the return of investment of 230 %. The unit cost is estimated to be 57 million USD.

**Table 2:** *The summary of the financial analysis. All cost estimations are expressed in FY2022.*

| **Parameter]** | **Value** |
|---|---|
| Initial investment [USDmil.] | 19 700 |
| Unit manufacturing cost [USDmil.] | 49.29 |
| Unit cost [USDmil.] | 57.71 |
| Market price (exc. VAT) [USDmil.] | 90.00 |
| Operational costs [USD/nm] | 62.29 |
| Return on investment [%] | 232.6 |
| Break-even point [Units] | 554 |

**Preliminary Design Options**: Before a design concept can be chosen, different concepts need to be outlined first. Below, a concise description of each of the three final concepts is given. These concepts are a conventional aircraft, box wing, and blended wing body.

**Design concept 1**: The first design uses a conventional wing configuration and a partial turboelectric propulsion system. In partial turboelectric propulsion, the wing-mounted turbofan engines produce thrust, but also generate electricity with the use of generators to drive (multiple) electric fans. An electric fan is placed at the back of the fuselage and uses Boundary Layer Ingestion (BLI) to increase fuel efficiency. The concept will have a low wing configuration with a backward sweep. Finally, a T-tail empennage is chosen because of the placement limitation as result of the electric fan at the back of the fuselage. This concept is shown in Figure 4.

**Design concept 2**: The second concept is the box wing, which has many similarities with the conventional concept. The box wing has two wings: the front wing is a low wing with backward sweep, and the aft wing is a high wing with forward sweep to limit the connecting distance between the wings. The box concept has the same propulsion system as the conventional concept with the turbofans placed under the front wing, while also using a T-tail as empennage. This concept is shown in Figure 2.

**Design concept 3**: The third option is a blended wing body, which will have a hydrogen propulsion system using fuel cells to generate power for the distributed propulsion. With distributed propulsion, the small engines are placed along the span of the aircraft to reduce the overall fuel consumption and noise. The distributed propulsion is placed at the upper side of the wing at the trailing edge to make optimal use of BLI. Because of the aerodynamic properties of the blended wing body, no empennage is needed to ensure stability. This concept is shown in Figure 3.

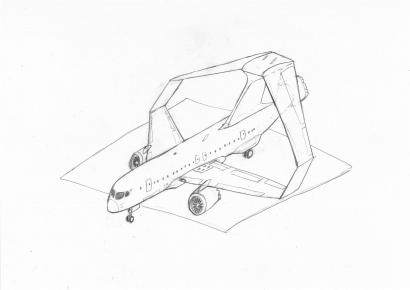

**Figure 2:** *Drawing of the box wing concept.*

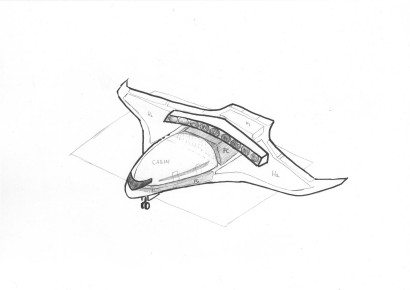

**Figure 3:** *Drawing of the blended wing body wing concept.*

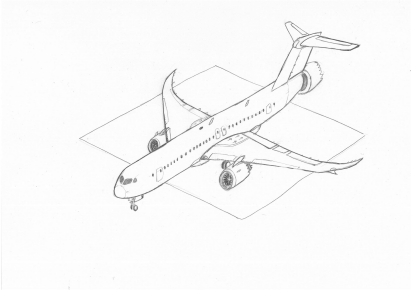

**Figure 4:** *Drawing of the conventional wing concept.*

**Design Trade-Off**: For the final design trade-off, five criteria are selected on the basis of which the three concepts can be scored. Each criteria is comprised of multiple metrics that encompass the most important points. The criteria weights and scores are summarised in Table 3. The criteria weights are established based on the AHP method and consultation with an external expert, Raymond van der Meer (NLR). Based on this trade-off, the Blended Wing Body is deemed the best design option.

**Table 3:** *The final trade-off summary table.*

| | **Emissions** | **Noise** | **Adj.** | **DTR & F.** | **Weight** | **Total** |
|---|---|---|---|---|---|---|
| **W.F.** | 22.3% | 9.9% | 5.5% | 29.7% | 32.6% | 100% |
| **CON** | $CO_2$ & $NO_x$. [0.68] - *red* | Loud turbofans. [0.30] - *yellow* | Small expected efficiency increase. [0.29] - *red* | Abundance of literature. [2.75] - *green* | MTOW = 77.940 kg. [1.08] - *red* | **5.17** *yellow* |
| **BOX** | Less $CO_2$ & $NO_x$ than CON. [1.15] - *yellow* | Loud turbofans + more leading edge noise. [0.27] - *red* | Additional wing area. [0.35] - *yellow* | More literature than BWB, less manufacturable than CON. [0.97] - *yellow* | MTOW = 72.648 kg. [1.63] - *yellow* | **4.69** *red* |
| **BWB** | Water vapour. [1.83] - *green* | Noise shielding and distributed propulsion. [0.77] - *green* | Available space in wing. [0.44] - *green* | Lack of literature & airport infrastructure. [0.89] - *red* | MTOW = 62.457 kg. [2.68] - *green* | **5.61** *green* |

**Sensitivity Analysis**: To test the robustness of the final design choice against variations in criteria weights, a sensitivity analysis is performed. Based on this, additional confidence was gained in the decision, as only one out of eleven test altered the outcome of the design concept. The first test consists of equalling all criteria weights, effectively deeming each criteria equally important for the aircraft design, as shown in Table 4. Subsequently, the weight factor of each criteria is increased and decreased by 50% one by one, tabulated in Table 5. In both tables, the right-most column highlights the highest scoring design option. Green signals the same outcome as the final trade-off summary table, red signals a different design option outcome.

**Table 4:** *Design criteria weights - equal.*

| Criteria | Emissions | Noise | Adjustability | D.T.R. & F. | Weight | Concept |
|---|---|---|---|---|---|---|
| **Weight Factor** | 20% | 20% | 20% | 20% | 20% | BWB |

**Table 5:** *Design criteria weights - Shift & Re-Distribution.*

| | Criteria | Emissions | Noise | Adj. | D.T.R. & F. | Weight | Concept |
|---|---|---|---|---|---|---|---|
| **Weight Factor** | **Emissions (+50%)** | 33.4% | 7.1% | 2.7% | 26.9% | 29.9% | BWB |
| | **Emissions (-50%)** | 11.1% | 12.7% | 8.2% | 32.5% | 35.4% | BWB |
| | **Noise (+50%)** | 21.0% | 14.9% | 4.2% | 28.5% | 31.4% | BWB |
| | **Noise (-50%)** | 23.5% | 5.0% | 6.7% | 30.9% | 33.9% | BWB |
| | **Adjustability (+50%)** | 21.6% | 9.2% | 8.2% | 29.0% | 32.0% | BWB |
| | **Adjustability (-50%)** | 23.0% | 10.6% | 2.7% | 30.4% | 33.3% | BWB |
| | **D.T.R. & F. (+50%)** | 18.6% | 6.2% | 1.7% | 44.6% | 28.9% | CON |
| | **D.T.R. & F. (-50%)** | 26.0% | 13.6% | 9.2% | 14.9% | 36.4% | BWB |
| | **Weight (+50%)** | 18.2% | 5.8% | 1.4% | 25.6% | 49.0% | BWB |
| | **Weight (-50%)** | 26.4% | 14.0% | 9.5% | 33.8% | 16.3% | BWB |

**Detailed Design Phase:** After the blended wing body design concept was chosen, the detailed designing of the (sub-)systems was performed in the final phase of the project, falling within the Design Synthesis Exercise scope. Focus was placed on the propulsion system, the aerodynamic design, structural analysis of the liquid hydrogen tank, the wingbox and the fuselage, the stability & control, and performance characteristics of the aircraft.

**Propulsion System Design:** the Lightning2 makes use of distributed propulsion due to its many benefits in fuel consumption and noise. The distributed propulsion consists of 10 4 MW electric ducted fans which produce a total thrust of 228 kN at sea level. The electricity is produced by Proton Exchange Membrane Fuel cells from PowerCellution, which can deliver up to 37.4 MW of power during take-off. The parameters of the propulsion system are given in Table 6.

**Table 6:** *Propulsion system summary.*

| Parameter | Value | Parameter | Value |
|---|---|---|---|
| Number of engines [-] | 10 | Length nacelle [m] | 2.73 |
| Total sea level thrust [kN] | 228 | Total DP width [m] | 18.1 |
| Fan diameter [m] | 1.65 | Number of fuel cell stacks [-] | 299 |
| Maximum nacelle width [m] | 1.76 | Fuel cell volume [$m^3$] | 11.4 |
| Number of blades [-] | 8 | Total propulsion system weight [tons] | 23.0 |

**Aerodynamic Analysis** The aerodynamic analysis primarily focused on creating the wing planform and selecting an airfoil for both the wing and the fuselage. This was done using XFLR5 as well as the DATCOM methods to analyse the airfoils and the total aircraft. In Table 7, the summary of the most important values of the wing planform are shown. In Figure 5, the planform is shown from a top-view. Furthermore, Figure 6 and 7 shown the airfoils used for the wing and the fuselage, respectively.

**Table 7:** *Aerodynamic analysis summary.*

| Parameter | Value |
|---|---|
| $S_{fuselage}$ [m$^2$] | 211.30 |
| $S_{wing}$ [m$^2$] | 162.28 |
| $\Lambda_{LE,wing}$ [deg] | 52.12 |
| $\Gamma$ [deg] | 3 |
| $\alpha_{cruise}$ [deg] | 3.1 |
| $c_{r_{wing}}$ [m] | 11.86 |
| $c_{t_{wing}}$ [m] | 3.45 |
| $b$ [m] | 36 |
| Wing airfoil [-] | Eppler 325 |
| Wing incidence angle [deg] | 0.21 |

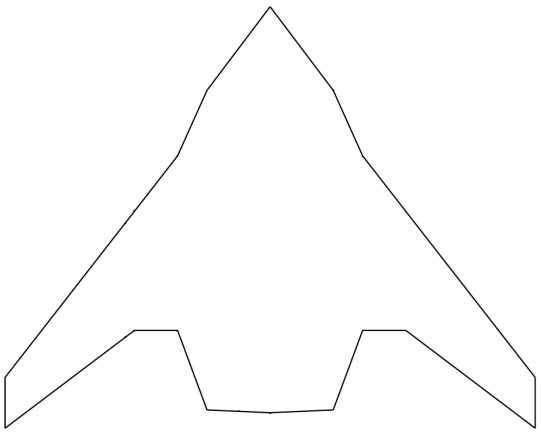

**Figure 5:** *Top-view of the final wing planform*

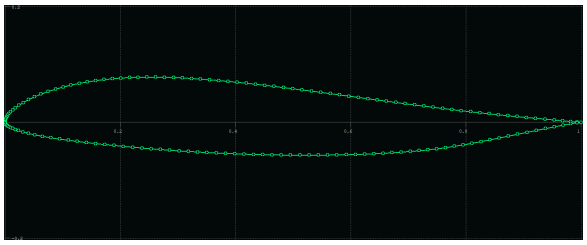

**Figure 6:** *The Eppler 325 airfoil used for the wing.*

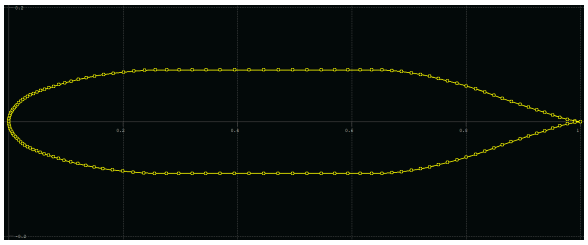

**Figure 7:** *The custom airfoil used for the fuselage.*

**Liquid Hydrogen Tank Design:** To carry the required fuel, a liquid hydrogen tank has to be made. Its design consists of three main steps: geometrical, mechanical, and thermal design. The first determines the geometry of the tank based on the amount of $LH_2$ it has to contain. The second determines the thickness of the wall based on the pressure differences on both sides. The last determines the required thickness of the insulation.

**Table 8:** *The final tank dimensions for the Lightning2 aircraft.*

| Parameter | Value |
|---|---|
| Contained $LH_2$ [kg] | 1753.7 |
| Diameter [m] | 2.9 |
| Length [m] | 6.0 |
| Inner wall thickness [mm] | 17.2 |
| Vacuum thickness [mm] | 5.0 |
| Outer wall thickness [mm] | 3.0 |
| Insulation thickness [mm] | 140.5 |
| Tank mass [kg] | 3455.6 |

A double-walled tank with a vacuum between the walls and insulation on the outside of the tank was designed. A trade-off had as result that aerogel would be used as the outside insulation. Several materials were considered to use for the inner and outer walls. As the design has to be finished within five years, it was not possible to implement composite tanks. It was concluded that the 2024 T81 alloy would be the best option for the inner wall due to increasing properties with decreasing temperature. The 2092 T81 alloy was chosen for the outer wall, as it is a lighter material than the 2024 alloy, with only a slight decrease in strength properties. The latter is not considered to be a crucial aspect, since the pressure difference the outer wall has to resist is lower compared to the inner wall. The final parameters are shown in Table 8. Additional mass due to the structural connection between the inner and outer tank and the required structure to minimise the sloshing, is included in the tank mass estimation.

**Wingbox & Fuselage Design:** To ensure nominal operating conditions in every flight regime, a wingbox shall be designed which shall endure all the different kind of loads with an ultimate safety factor of 3.75 without any failure, specifically yielding or buckling. The key design parameters of the wingbox and the complete stress distribution is shown in Table 9 and Figure 8, respectively.

**Table 9:** *Final design values of wingbox.*

| Name | Value |
|---|---|
| Stringer number top skin [-] | 9 |
| Stringer number bottom skin [-] | 9 |
| Stringer cross-section area [$mm^2$] | 200 |
| Skin thickness [mm] | 4.5 |
| Rib pitch [mm] | 500 |
| Total weight of wingbox [kg] | 2986 |

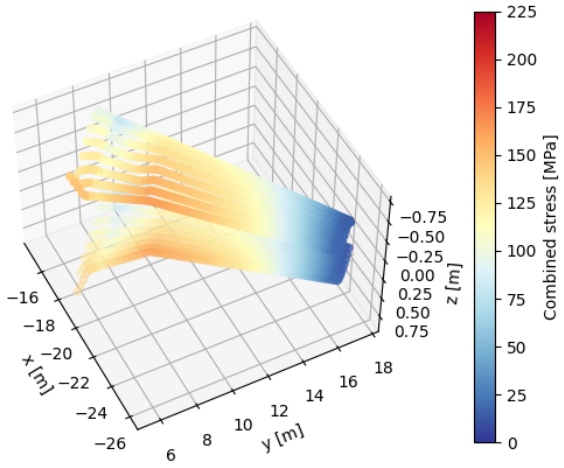


**Figure 8:** *Complete stress distribution of wingbox from side view.*

The fuselage should be able to withstand the nominal operating conditions as well as the loads introduced by the swept wing, as the wing box does not continue trough the fuselage. As the oval fuselage also has the need for pressurisation, additional loads are introduced in the trapezoidal fuselage structure. The final design parameters are shown in Table 10.

**Table 10:** *Final design values of fuselage.*

| Name | Value |
|---|---|
| Stringer cross-section area [$mm^2$] | 276 |
| Stringer spacing [mm] | 400 |
| Frame spacing [mm] | 1200 |
| Floor thickness [mm] | 7 |
| Ceiling thickness [mm] | 8 |
| Wall thickness [mm] | 8 |
| Skin thickness [mm] | 3 |
| Total weight of fuselage [kg] | 17388 |

**Table 11:** *Relevant values related to stability and control.*

| Name | Value |
|---|---|
| Minimum Aileron Area [$m^2$] | 34.05 |
| Total Vertical Stabiliser Area [$m^2$] | 30.74 |
| Vertical Tail Height [m] | 5.24 |
| Most Aft C.G. [m] | 14.136 |
| Most Forward C.G. [m] | 13.6 |
| Aerodynamic Centre Location [m] | 14.38 |

**Stability and Control Characteristics**: One of the main challenges in designing a blended wing body is stability and control. To ensure longitudinal stability, the moment at the aerodynamic centre must be positive and the centre of gravity must lie in front of it. The first condition was achieved by choosing a reflexed airfoil. For longitudinal stability, a vertical tail was sized on wingtips to account for engine inoperative cases and weather-wane stability. The control surfaces of the aircraft were limited by the take-off rotation phase, for which new innovative solutions, such as blown elevons [83] and a belly flap [105] were applied to improve the performance. Some results are highlighted in Table 11.

**Resource Allocation & Contingency Management**: Resource allocation and contingency management is used to keep track of all the important parameters during the design process, such that adjustments can be made to make sure that the parameters stay within the allocated range. In total, four essential parameters are chosen, being, $MTOW$, $W_F$, $T_{TO}$ and $L/D_{cruise}$. Table 12 shows the values for each of the four chosen parameters at different stages.

**Table 12:** *Essential parameters at different stages.*

| Stage | MTOW [kg] | $W_F$ [kg] | $T_{TO}$ [N] | $L/D_{cruise}$ [-] |
|---|---|---|---|---|
| Class I | 49422 | 6015 | 156976 | 17.91 |
| Class II | 62457 | 6015 | 156976 | 17.91 |

**Table 12 continued from previous page**

| Stage | MTOW [kg] | $W_F$ [kg] | $T_{TO}$ [N] | $L/D_{cruise}$ [-] |
|---|---|---|---|---|
| 1st Iteration | 87467 | 2863 | 177120 | 24.31 |
| 2nd Iteration | 96517 | 4518 | 195447 | 23.74 |
| 3rd Iteration | 103299 | 4643 | 209180 | 23.61 |
| 4th Iteration | 106473 | 5031 | 215606 | 23.51 |
| 5th Iteration | 108445 | 5198 | 219601 | 23.36 |
| 6th Iteration | 110251 | 5305 | 223256 | 23.29 |
| 1st corrected Iteration | 81399 | 1051 | 201790 | 21.40 |
| 2nd corrected Iteration | 86951 | 1552 | 200551 | 21.76 |
| Final value | 82267 | 1754 | 199997 | 21.97 |

**Aircraft Performance**: The aircraft noise is simulated by considering the propulsion system and landing gear as the two dominant sources. Table 13 tabulates the results and points to the fact that the aircraft is in-line with maximum values according to [107].

**Table 13:** *Total aircraft noise at certification points.*

| Certification Point | Aircraft Noise [dB] | Noise Requirement [dB] |
|---|---|---|
| **Approach** | 95.98 | 100.87 |
| **Lateral** | 94.25 | 97.16 |
| **Flyover** | 83.67 | 92.10 |

The design is subject to strict emission regulations that follow the ”Flightpath 2050” goals. As Lightning2 makes use of fuel cells to provide energy, the only emission of Lightning2 is water vapour. While Lightning2 produces 141% more water vapour compared to a A320, the effects of water vapour on global warming are 10 times less compared to $CO_2$. To be able to fly to all airports that the A320 is able to fly to, strict take-off and landing requirements need to be satisfied. The take-off distance of Lightning2 equals 1453 meters and the landing distance equals 1145 meters. Therefore, the Lightning2 is able to fly even the smallest airport an A320 can fly.

**Operational Framework**: The Lightning2 was analysed with respect to taxiing, turnaround time, and maintenance planning. Taxiing without greenhouse gas emissions proves to be infeasible, as production of water vapour is inevitable. However, this production can be offset elsewhere to effectively reach zero emissions. The turnaround time is expected to be slightly less than current aircraft, in the long run. The maintenance will be subject to difficulties with entry into service as a result of the radically different configuration, but will stabilise in due time.

**Sustainable Strategy**: Sustainability is implemented throughout the project. During the design phase, economic, social and environmental are the three aspects taken into consideration, as these form the key pillars for a sustainable design. For the operation phase, the *5M* technique is applied to optimise the maintainability and modernisation of the aircraft. Also, one of the client requirements is that the aircraft should be designed in such a manner that it can be upgraded to reduce the fuel consumption with an additional 10 % after 15 years in service. So, adjustability is another crucial aspect to consider. The MTOW is expected to be further decreased, since it is estimated that the hydrogen fuel cells efficiency will increase to 65% and a specific energy of 6 kW/kg before 2040. This results in a fuel consumption decrease of 12.3%. Finally, the End-of-Life Strategy & Recyclability Plan is made to ensure that every components of the BWB aircraft is either recyclable, degradable or reusable.

**Requirements Compliance**: At this stage of the project, the set of requirements can be checked in terms of compliance. A summary table is presented at the end of the report wherein each requirement is individually considered. Constrained by the scope of the Design Synthesis Exercise, not all requirements can be be verified at this stage. As the next step, the requirements that have not been fulfilled will be verified as the design progresses further, paying special attention to the avoidance of any conflict on interest within the requirements.

# Summary

The final report focused on the detailed design of the final chosen concept, which is a BWB aircraft with a distributed propulsion system powered by liquid hydrogen. Before doing the actual technical design part, a market analysis is made to investigate the future demand for this type of aircraft. To do so, the SWOT analysis, market characteristics, and competitor analysis are made. After that, an estimation of the market dynamics & trends, as well as the expected demand for the aircraft is made. In financial analysis, the financial forecast and strategies for the whole aircraft program are discussed, from which the unit cost, operational cost, return on investment and cost-breakdown structure can be found.

Next, a workflow diagram is included to show the high-level tasks in an interconnected and chronological manner, and a work breakdown structure segments these high-level tasks into smaller ones and allocates resources in the form of team members and manhours. An additional step that was taken is the technical risk analysis. This aims to identify risks in the design and production process so that they can be shifted or mitigated at an early stage. The technical risk analysis is based on four different steps. Risks were first identified and then given a risk score, after that they were ranked, and the corresponding mitigation strategies were introduced to minimise their effect.

The first subsystem in the technical part is propulsion. A Python script was made to calculate all the specification values of the distributed propulsion system, including total thrust, power, amount of fuel cells required, sizing, etc. To maintain a suitable operating temperature for the fuel cell, a cooling system is designed. To summarise for the whole propulsion system, 10 engines and 299 stacks of fuel cells are used, providing in total of 228 kN of thrust at sea level.

In aerodynamic design, the FLOPS method is used for the initial sizing of the cabin. After that, a NACA 6-series airfoil is selected due to the immense thickness required. However, there are some limitations to be considered. On the platform, there should be enough space for the distributed propulsion system to be implemented and since no HLDs will be used, a relatively high wing area is required. And once the final geometry of the design is done, the critical Mach number can be obtained from XFLR5. To summarise, the final exposed wing area is 390.9 $m^2$ with a wing loading of 1240 $N/m^2$, and the critical Mach number for the wing and body is 0.89 and 0.93 respectively.

After that is the structures & materials design. First of all, a load case study is made to identify all the critical loads. Then, a liquid hydrogen tank design is included, which consists of three main steps: the geometric, mechanical, and thermal design. Eventually, it is decided to use three tanks due to the available structural space. Next comes the wing box design. The axis systems are defined at first. After that, the cross-section is idealised with the use of boom idealisation and correspondingly the geometrical parameters are defined. Bending stress, shear stress and the failure mode is investigated afterwards. For fuselage design, a parametrisation of the oval fuselage is presented along with structural analysis based on a combination of pressurisation loads, steady state manoeuvre loads and aerodynamic loads.

For the stability part, the longitudinal stability & lateral stability and centre of gravity excursion are included. For the control part, the control surfaces for roll and pitch are determined. Undercarriage Sizing & Positioning are also discussed in the report.

After that, an iteration flow diagram is made to demonstrate the whole iterative process, thus showing how the final values are calculated. Next, resource allocation helps to keep track of all the design parameters throughout the design phases, if one parameter exceeds the specification value, some adjustments need to be made to ensure the parameter is within the constrain.

Performance analysis consists of three main parts, namely aircraft noise prediction & footprint, emissions, and take-off & landing performance. For noise prediction, it is analysed based on the propulsion and the landing gear noise since these are the two main sources that contribute to noise. Then, a LTO cycle emissions and

emissions per passenger kilometre table are made. Take-off and landing distance are one of the requirements set by clients, so calculations for both are included.

The robustness of the design is checked in a sensitivity analysis. It can be tested by changing major design parameters to see how the effects on the design are. Each key parameter is given a change of +/-10% to see if the design point still lies within the possible design space. If that is not the case, the design is no longer feasible.

The Hardware block diagram, software block diagram, aircraft characteristics block diagram, electrical block diagram, communication flow diagram and data handling block diagram is included in the report aiding in understanding various systems onboard. Other essential aspects to consider for the BWB aircraft are the operations & logistics. Taxiing between the gate and runway, operations at the gate and the maintenance of the aircraft are presented in the report. Next, RAMS analysis is performed based on the similar existing aircraft, the same method is then applied to the BWB design. In manufacturing, assembly, and integration plan of the BWB, firstly, the sustainability of the raw input materials and lean manufacturing considerations are included. Secondly, the key manufacturing techniques used during the manufacturing of aircraft components are discussed. Thirdly, the design considerations of the facility are presented and lastly, an intended aircraft assembly plan is made.

All parts need to be recycled at the end of life is another important client requirement. To achieve that, a sustainable strategic plan is made which contains a sustainability analysis for the design and operational phase, an adjustability plan for future upgrades and a full recyclability plan for the Lightning2 aircraft. Next, a requirement compliance matrix and feasibility analysis are created to make sure that all the requirements are met, and if they are not, certain modifications or mitigation strategy will be made.

Finally, the continuation of the Lightning2 program is discussed as well as a conclusion.

# Table of contents

# List of Symbols

**Abbreviations**

ADS-B Automatic Depended Surveillance-Broadcast

BLI Boundary Layer Ingestion

BWB Blended Wind Body

DME Distance Measuring Equipment

DP Distributed Propulsion

DSE Design Synthesis Exercise

FPR Fan Pressure Ratio

HLD High Lift Device

HSR High Speed Rail

ILS Instrument Landing System

ISA International Standard Atmosphere

LE Leading Edge

LHV Lower Heating Value

LTO Landing and Take-Off

MAC Mean Aerodynamic Chord

MTOW Maximum Take-Off Weight

OEW Operating Empty Weight

OPE Operational Expenses

PBT Profit Before Taxes

PNL Perceived Noise Level

PSR Primary Surveillance Radar

R&D Research and Development

RAMS Reliability, Availability, Maintainability, Safety

RoI Return on Investment

RPK Revenue Passenger Kilometer

SAF Sustainable Aviation Fuel

SGA Sales, General, and Administrative

SPL Sound Pressure Level

SSR Secondary Surveillance Radar

SWOT Strength, Weakness, Opportunity, Threat

TCAS Traffic Collision Avoidance System

VOR Very High Frequency Omni-Directional Range

YoY Year-over-Year

**Greek Symbols**

| | | |
|---|---|---|
| $\alpha$ | Angle of Attack | deg |
| $\delta$ | Boundary Layer Thickness | m |
| $\eta$ | Efficiency | - |
| $\Gamma$ | Dihedral Angle | deg |
| $\gamma$ | Ratio of Specific Heats | - |
| $\Lambda$ | Sweep Angle | deg |
| $\mu$ | Dynamic Viscosity | $N/m^2s$ |
| $\mu_{br}$ | Braking Friction Coefficient | - |
| $\nu$ | Poisson's Ratio | - |
| $\phi$ | Bank Angle | deg |
| $\Pi^*$ | Acoustic Power | W |
| $\rho$ | Density | $kg/m^3$ |
| $\sigma$ | Normal Stress | $N/m^2$ |
| $\tau$ | Shear Stress | $N/m^2$ |
| $\theta$ | Angle of Twist | deg |

**Latin Symbols**

| | | |
|---|---|---|
| $\dot{m}$ | Mass Flow | kg/s |
| $\dot{Q}$ | Heat Flux | W/m$^2$ |
| $A$ | Area | m$^2$ |
| $a$ | Speed of Sound | m/s |
| $AR$ | Aspect Ratio | - |
| $b$ | Wing Span | m |
| $c$ | Chord | m |
| $C_D$ | 3D Drag Coefficient | - |
| $C_d$ | 2D Drag Coefficient | - |
| $C_f$ | Skin Friction Coefficient | - |
| $C_L$ | 3D Lift Coefficient | - |
| $C_l$ | 2D Lift Coefficient | - |
| $C_m$ | Moment Coefficient | - |
| $C_p$ | Pressure Coefficient | - |
| $c_p$ | Specific Heat Capacity | J/kg/K |
| $C_{L_\alpha}$ | 3D Lift Slope | rad$^{-1}$ |
| $C_{l_P}$ | Aileron Roll Damping Derivative | rad$^{-1}$ |
| $C_{l_{\delta a}}$ | Aileron Control Derivative | rad$^{-1}$ |
| $D$ | Diameter | m |
| $D$ | Drag Force | N |
| $E$ | Elastic Modulus | GPa |
| $e$ | Oswald Efficiency Factor | - |
| $FF$ | Form Factor | - |
| $G$ | Shear Modulus | GPa |
| $g$ | Gravitational Acceleration | m/s$^2$ |
| $h$ | Height | m |
| $I$ | Moment of Inertia | m$^4$ |
| $IF$ | Interference Factor | - |
| $k$ | Surface Roughness Height | m |
| $k$ | Thermal Conductivity | W/mK |
| $L$ | Lift Force | N |
| $l$ | Length | m |
| $M$ | Mach Number | - |
| $M$ | Moment | Nm |
| $m$ | Mass | kg |
| $n$ | Load Factor | - |
| $P$ | Power | W |
| $P$ | Roll Rate | rad$^{-1}$ |
| $p$ | Pressure | N/m$^2$ |
| $q$ | Shear Flow | N/m |
| $R$ | Radius | m |
| $R$ | Specific Gas Constant | J/kg/K |
| $S$ | Surface Area | m$^2$ |
| $T$ | Temperature | K |
| $T$ | Thrust Force | N |
| $t$ | Thickness | mm |
| $t$ | Time | s |
| $t/c$ | Thickness-to-Chord Ratio | - |
| $V$ | Shear Force | N |
| $V$ | Velocity | m/s |
| $W$ | Weight | N |
| $w$ | Width | m |
| $y$ | Spanwise Coordinate | m |

# 1 Introduction

Commercial aviation has been a driving force behind the rapid increase in social and economic welfare around the globe and undoubtedly is an integral part of modern-day civilisation. Despite the abundance of positivity modern-day air travel has brought to society, it cannot (and should not) outpace the ominous cloud forming above it, the defining problem of the current generation: climate change. According to the International Energy Agency (IEA), the aviation sector is responsible 2.8% of global CO2 emissions from fossil fuel combustion[1] and growing every year. The requirements set by the client for this project are therefore in line with the road map put forth by the European Commission's visionary "Flightpath 2050" document. These ambitious goals are supplemented by a desire for a financially attractive investment to ensure a competitive, seamless entry into the currently A320/B737 dominated short-haul, single-aisle aircraft market segment.

This final report marks the end of the Design Synthesis Exercise, presenting the design of the innovative blended wing body aircraft: Lightning2. Over the course of the past 10 weeks, a team of 10 aspiring engineers worked towards producing a conceptual design of an aircraft that reduces emissions and noise considerably. This multidisciplinary challenge sits at the intersection between technical work and project management. The technical design is segmented between key aircraft systems, namely the propulsion, structures & materials, stability & control, and performance characteristics. The aircraft is detailed fully with regard to these systems. The final values are obtained through an iterative procedure, which converges to a final optimal design. Furthermore, the preliminary operational framework is established as entry into service of a feasible aircraft should be addressed early in the project phase. Being the final stage of the project, the aircraft design can and should be graded with respect to established criteria. This provides a metric for design success and paves the way to move forward.

The report commences with a Market & Financial Analysis, in Chapter 2 and Chapter 3, respectively. Therein, the existing and prospective commercial aviation sector is analysed to gain insight into existing or latent demand and the according financial picture. Next, the intended functionality of the aircraft is established in the Functional Analysis presented in Chapter 4. This reveals key required resources, which calls for a resource allocation projection in Chapter 11. Before any technical aspects of the design are revealed, the full risk assessment of the project is included in Chapter 5, whereby all identified risks and mitigation strategies are highlighted and deemed significant during the final phase of the Design Synthesis Exercise.

The proceeding chapters focus on the separate systems of the aircraft: Propulsion in Chapter 6, Aerodynamics in Chapter 7, Structures & Materials in Chapter 8, and Stability & Control in Chapter 9. Each chapter consists of an explanation of the methodology applied to the designing, verification, and validation procedures and a summary of the final results in the form of design parameters of the aircraft. Next, the iterative design process, including all final values, is presented in Chapter 10. With a final design established, the aircraft performance characteristics are included in Chapter 12. Following this, various aircraft block diagrams are included and the operational & logistics considerations are discussed in Chapter 15. This closely ties in with the Reliability, Availability, Maintainability, and Safety Analysis and the Manufacturing, Assembly, and Integration plan, in Chapter 16 and Chapter 17. As sustainability plays an integral role in the project, it is discussed separately in Chapter 18. The report continues with a review of compliance with all previously set requirements in Chapter 20. Finally the reader is informed of the project scope after the DSE, in Chapter 21. Lastly the report is concluded in Chapter 22 and the project up to this stage is reflected upon.

[1] `https://www.iea.org/reports/tracking-aviation-2020` - Accessed: 13-6-2022

# 2

# Market Analysis

In this chapter, the market analysis is presented. To this end, Section 2.1 first presents the SWOT analysis performed, identifying the market strengths, weaknesses, opportunities. Following this, the key stakeholders and their needs are identified in Section 2.2. Next, Section 2.3 presents characteristics of the commercial aviation market sector. Section 2.4 presents a market-based estimation of the design range for the aircraft. Section 2.5 presents a competitor analysis, after which Section 2.6 presents the market dynamics and trends. Section 2.7 presents the identified market gap. Finally, Section 2.8 presents the expected demand for the aircraft.

## 2.1. SWOT Analysis

To gain insight into the competitiveness of the blended wing body, a SWOT analysis was performed into the current and future market. The strengths and weaknesses pertain to the designed product and its position in the market, and are therefore internal, whereas the the opportunities and threats revolve around the competition in the sector, thus being external.

The SWOT analysis serves as a starting point to more detailed market analyses, which will be developed in subsequent sections. Despite SWOT analyses being widely used in industry, limitations exist. Certain elements can be considered both a strength and weakness or an opportunity and at the same time a threat. Additionally, basing corporate strategies too heavily on this assessment will ignore interrelations between factors. The items mentioned in the SWOT analysis are dynamic and subject to constant change. It is therefore emphasised that this assessment solely serves as a starting point.


**Figure 2.1:** *Market SWOT analysis.*

## 2.2. Stakeholder Identification

The key stakeholders for this project are the clients, governments, airports (and citizens around airports), aviation authorities, and the team members. The need of the client is directly expressed in the requirements which formed the basis for the project. Governments wish to subsidise efforts in green technology, as this benefits the population. The general population in the vicinity of the airport have a need for quiet aircraft to improve quality of living. If expectations are not met, protests and heavy resistance is to be expected, putting pressure on airports to take drastic measures. Aviation authorities are responsible for adjusting the framework to radically new aircraft configurations. Lastly, the team has a need for a safe working environment and job security.

## 2.3. Commercial Aviation Sector Market Characteristics

In this section, the commercial aviation sector market characteristics will be outlined, starting with the volume and growth.

### 2.3.1. Geographically Segmented Volume and Growth

The global commercial aviation sector can be segmented most naturally using a geographical distribution of passenger traffic. Table 2.1 presents figures on the geographic breakdown of commercial aviation aircraft traffic[1]. Data from 2019 has been chosen to be representative of the aviation market before the Covid-19 pandemic shock, which will be analysed separately. The metric used to quantify passenger traffic in this data is the total scheduled revenue passenger kilometres performed (RPKs).

As seen in the table, Europe, North America, and Asia & Pacific by far exceed the share of passenger traffic compared to the remaining regions, summing to more than 80%. Africa presents an untapped market, having a share of just over 2%, while experiencing growth in excess of that of North America. The greatest increase in traffic was observed in Europe, with close to 7% more traffic year over year.

**Table 2.1:** *Geographic breakdown of passenger traffic.*

| Region | % of Traffic | Growth (2018-2019) |
|---|---|---|
| Europe | 26.8% | 6.6% |
| Africa | 2.1% | 4.3% |
| Middle East | 9.1% | 1.9% |
| Asia & Pacific | 34.7% | 5.2% |
| North America | 22.2% | 4.1% |
| Latin America | 5.1% | 3.6% |

### 2.3.2. Covid-19 Pandemic Shock & Resilience

The Covid-19 pandemic severely affected civil aviation, with the effects being noticeable for years to come. This section aims to analyse the shock experienced in the market due to the outbreak, and forecast the magnitude of a potential bounce back based on preliminary data. The ICAO published a presentation on the economic effects of the Covid-19 pandemic on civil aviation [2]. The key figures for YoY (year-over-year) comparisons of 2020, 2021, ad 2022 with 2019 (pre-Covid) are summarised in Table 2.2.

**Table 2.2:** *Covid-19 Impact on Civil Aviation.*

| | 2020 / 2019 | 2021 / 2019 | 2022 (outlook) / 2019 |
|---|---|---|---|
| **Overall reduction of seats** | 50% | 40% | 21% - 24% |
| **Overall reduction of passengers** | 60% | 49% | 27% - 32% |
| **Loss - passenger operating revenues** | USD 372 billion | USD 324 billion | USD 188 - 216 billion |

Interesting data that can be extrapolated to this project is the assessment of how domestic and international flights seat capacity was reduced in lockdown times. A 150 seat A320 equivalent aircraft is more likely to be operational on shorter duration flights. In large nations (for example the United States of America), the shock to domestic flights was considerably less. Figure 2.2 and Figure 2.3 show the reduction in seating capacity on a YoY basis compared to 2019, for international and domestic flights, respectively.

[1] `https://www.icao.int/annual-report-2019/Pages/the-world-of-air-transport-in-2019.aspx` - Accessed: 26-4-2022

[2] `https://www.icao.int/sustainability/Pages/Economic-Impacts-of-COVID-19.aspx` - Accessed: 27-4-2022

Based on this assessment of the Covid-19 shock, the short-haul A320 equivalent market is more resilient to another wave of infections. This reinstates the justification of entering this market.

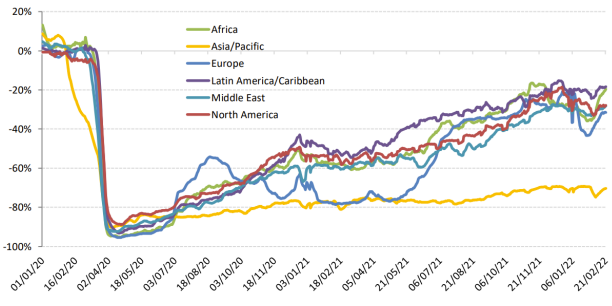


**Figure 2.2:** *International seat capacity reduction (7-day average, YoY compared to 2019).*

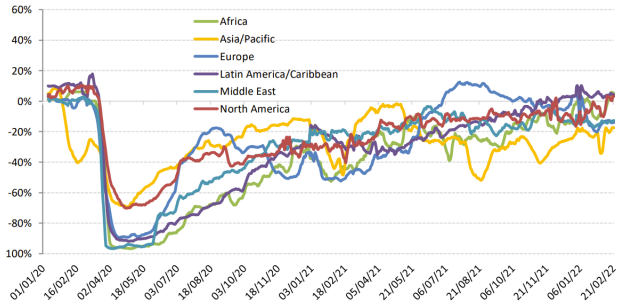


**Figure 2.3:** *Domestic seat capacity reduction (7-day average, YoY compared to 2019).*

### 2.3.3. Subsystem Suppliers

Not all components of an aircraft are made by the aircraft manufacturer, instead they are outsourced to reduce cost, save time and spread financial risk [63]. While outsourcing certain parts of the aircraft to third parties can be beneficial, it could also introduce problems. Extensive outsourcing could lead to communication, coordination, safety and quality issues, and cost increases. To reduce the risk of outsourcing, a very detailed cost and risk analysis is required to be performed in addition to clear collaboration agreements with partners.

### 2.3.4. Regulatory Framework

The commercial aviation sector is heavily regulated, underlining the relevancy of an analysis of the corresponding aviation regulatory agencies. The main regulatory agencies that are of importance for this project are EASA and the FAA, the agencies in Europe and the United States, respectively. These agencies have as mission to ensure safe air travel within their jurisdictions. The two agencies have consistent regulations between them, so for the design of the aircraft, the EASA CS-25 regulations will be used [3].

## 2.4. Range Determination: Airbus A320 and Boeing 737 Segment

The intended use of the aircraft is similar to that of an Airbus A320 or Boeing 737. It is a client requirement that the range of the aircraft should allow for adoption of most of the routes that these aircraft are currently operated on. To go from this qualitative description to a quantified value for the range, research on the current distribution of the range of the A320 and B737 is conducted. Figure 2.4 depicts the heat maps of the payload-range diagram of both types of aircraft [65].

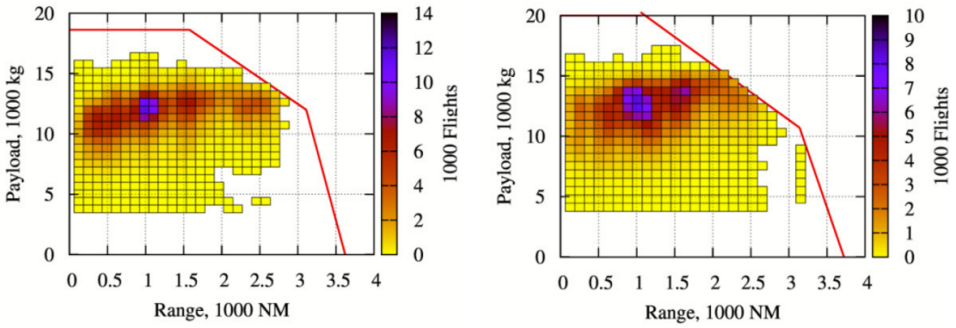


**Figure 2.4:** *Heat maps of payload-range diagram of the A320 (left) and the B737 (right) [65].*

It is important to note the wide range of the colour scale, purple signalling 14 times as many flights as yellow. To cover approximately 90% of the mapped flights, a design range of 3 700 kilometers is chosen. This range is visualised as a coverage circle with a radius of 3 700 km, projected onto a world map, as shown in Figure 2.5.

[3] `https://www.easa.europa.eu/the-agency/the-agency` - Accessed: 26-4-2022

The furthest that can be flown is from the midpoint to the circumference of each separate circle. It can be clearly seen that nearly all transcontinental flights fall within the feasible range area.

**Figure 2.5:** *Range coverage (radius of 3 700 km).*

## 2.5. Competitor Analysis

This section presents an analysis of the competitive playing field of short/medium-haul passenger transportation, not limited to aircraft. A distinction is made between the current competitive landscape, and what it is expected up to decades from now, given the current trends.

### 2.5.1. Current Competitive Playing Field

The competition that is established in today's day and age can be understood as the minimum competition that is expected. It is assumed that due to sustainability trends, alternatives continue to gain a market share. The medium-haul commercial aviation sector encompasses a global, oligopoly market-structure that contains the supply and demand of aircraft used for commercial purposes. For this reason, a natural starting point is the identification of key players in terms of manufacturers of these aircraft. The number of aircraft manufacturers is rather limited, and can be further reduced when focusing solely on 100-150 seat aircraft. The four main players in this category are: Airbus, Boeing, Bombardier, and Embraer[4]. Here, the former two occupy the vast majority of the market. The most popular narrow body aircraft are the Airbus A320 family, with a total of 16 106 sales and the Boeing 737 family with 14 982 sales[5,6]. Moreover, these aircraft are interesting to consider as their specifications are similar to those of the Lightning2. The range and speed are nearly identical, making them our direct, closest competitors. Additionally, the Chinese aircraft manufacturer Comac can be seen as a competitor. They are developing an A320-type aircraft called the C919 (range of 5 555 km) and are receiving considerable volumes of orders [7].

The orders and deliveries of the four aircraft families are stated in Table 2.3. It is clear that Airbus and Boeing currently posses the majority of the market share. The number of deliveries in the past five years are shown in Figure 2.6. A clear decrease in number of deliveries is seen in 2019. This can be traced back to the accidents involving the Boeing 737 MAX in October 2018 and March 2019 [8]. The deadly accidents grounded 400 operational 737 MAX aircraft from March 2019 till December 2020 [9]. The crashes also influenced the popularity of the 737 MAX with 448 orders cancelled and 782 orders dropped from the backlog. A decrease in number of delivered aircraft is also seen for the A320 family during the Covid-19 pandemic, but this is expected to increase in the coming years.

[4] `https://ri.embraer.com.br/Download.aspx?Arquivo=BQBSnssE6+eYgmmMRqIO5A==` - Accessed 26-4-2022

[5] `https://www.airbus.com/en/products-services/commercial-aircraft/market/orders-and-deliveries` - Accessed: 26-4-2022

[6] `https://www.boeing.com/commercial/#/orders-deliveries` - Accessed: 26-4-2022

[7] `https://edition.cnn.com/travel/article/comac-c919-china-airbus-boeing/index.html` - Accessed: 20-6-2022

[8] `https://edition.cnn.com/2020/11/17/business/boeing-737-max-grounding-cost/index.html` - Accessed: 26-4-2022

[9] `https://www.cnet.com/culture/entertainment/boeings-troubled-737-max-is-back-in-the-air-but-the-story-is-far-from-over/` - Accessed: 26-4-2022

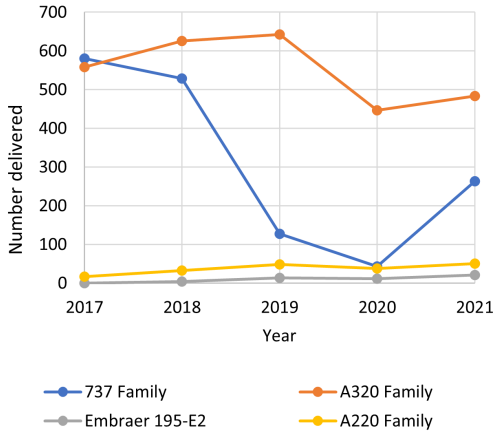


**Figure 2.6:** *Deliveries per aircraft family per year* [4,5,6].

**Table 2.3:** *Orders and deliveries of 150 seat aircraft* [4,5,6].

| Type | Orders | Deliveries |
|---|---|---|
| Embraer 195-E2 | 201 | 35 |
| A220-300 | 638 | 149 |
| A320 family | 16 106 | 10 285 |
| B737 family | 15 134 | 10 963 |

The A320neo replaced the old A320 variants in 2018. The unit cost for the A320 family ranges from 101.5 million dollar for the A319neo and 129.5 million dollar for the A321neo [10]. The Boeing 737 MAX price ranges between 99.7 million dollars for the 737 MAX-7 and 134.9 million dollars for the 737 MAX-10 [5]. The Embraer 195-E2 costs 60.4 million dollars and the A220-300 costs 91.5 million dollars [11,12].

### 2.5.2. Future Competitive Playing Field

**High-Speed Rail System**. As of October 2019, 47580 km of High-Speed Rail (HSR) is being used, with over 24000 km either under construction or planned. Downward pressure on air traffic is observed at all geographical locations, especially in the low and mid range. Although little impact is found on the long haul range, it is suggested that the Air-HSR competition will be stretched up to routes of 1300 km. This trend is already reflected in the average length of newly-introduced air routes weighted by seat capacity. This increased from 1080 km in 2008 to 1150 km in 2015. This suggest that airlines are inclined to expand the mid- to long-range markets when facing increasing competition [44]. This is especially true for low cost carriers, whom primarily increased their medium-haul, intra-EU flights [24].

A second suggestion in favour of air traffic, is the potential integration of the two modes, with airlines using railway services as additions in their network of services from a hub airport to complement and substitute for existing aircraft services [6]. Research shows that a large share of air routes tend to have an increase in air traffic after the introduction of HSR, except for routes under 500 km, which reduce in frequency [44].

The final part in the analysis of HSR is the public policy making. For example, the EU aims to complete a high-speed rail network in all member states, such that the majority of medium-distance passenger transport is performed by rail. This indicates that the market gap for aviation will only remain for longer range routes. On the other hand, the same policy also states: ”By 2050, connect all core network airports to the rail network, preferably high-speed”, which suggest that there may be an increase in demand for longer-range routes[13].

**Hyperloop**. With the release of the Hyperloop Alpha paper by Elon Musk [70], a major increase in research activity was observed. The hyperloop is a transportation method of high-speed and driver-less operations in which a vehicle is guided through a low-pressure tube or system of tubes, capable of achieving speeds up to 1200 $km/h$. Since 2013, multiple feasibility studies have been done for specific routes like: Helsinki-Stockholm, Amsterdam-Paris, Toronto-Montreal and Los Angeles-San Francisco. It is suggested that the same time-space compression of the HSR is expected for the hyperloop system. The case study of Los Angeles-San Francisco

[10] http://www.airbus.com/content/dam/corporate-topics/publications/backgrounders/Airbus-Commercial-Aircraft-list-prices-2018.pdf - Accessed: 26-4-2022

[11] https://web.archive.org/web/20140413154631/http://www.afm.aero/magazine/trading-legal-and-finance/item/907-the-e2-embraer-s-next-generation-of-ejets - Accessed: 26-4-2022

[12] https://www.aerospacemanufacturinganddesign.com/article/airbus-firms-orders-120-a220-aircraft-010819/ - Accessed: 26-4-2022

[13] https://eur-lex.europa.eu/legal-content/EN/TXT/PDF/?uri=CELEX:52011DC0144&from=EN - Accessed: 20-5-2022

considers the catchment area of multiple airports and the influence of integrating a hyperloop system. It concluded that leakage to the largest airport would occur, while a decrease in passenger demand was observed for the hyperloop route [113].

## 2.6. Market Dynamics and Trends

To investigate the demand for the designed aircraft, the market dynamics and trends need to be investigated. Firstly, the market for hydrogen and fuel cells are analysed in Subsection 2.6.1 and 2.6.2, respectively. Here, the former is split between usage in aircraft and integration in airport infrastructure. These two factors are critical to the design of the hydrogen BWB in this project. Subsequently, the key (and broader) themes of low-cost carriers and sustainability are touched upon, in Subsection 2.6.3 and Subsection 2.6.4, respectively.

### 2.6.1. Hydrogen

The blended wing body being designed in this project is powered by hydrogen, which is generates electricity through the usage of fuel cells. This section provides an analysis of its application in aircraft as well as the current/projected supporting infrastructure at airports.

**Hydrogen Powered Aircraft** Consultation with Raymond van der Meer, an external expert from NLR, shed light on the different sustainable fuel alternatives being considered in the industry. For short-haul, electric propulsion using batteries is deemed most effective. For medium-haul, most attention should be given to hydrogen. For long-haul, with the given technology, only SAF provides a feasible solution. The hydrogen used as a fuel source needs to be competitively priced to allow for adoption by companies. Figure 2.7 provides a cost projection of various types of liquid hydrogen up to 2050 [14]. A drastic price decrease is clearly expected.

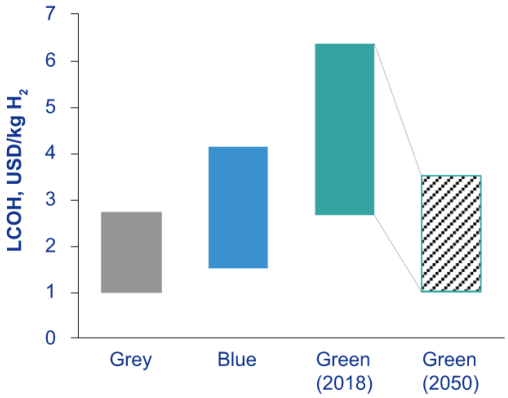


**Figure 2.7:** *Hydrogen price projection (Source: KPMG).*

This project seeks to outperform the A320 and obtain a market share. However, Airbus itself is not standing still. Hydrogen aircraft have been announced, including a similar BWB design [15]. The start-up ZeroAvia [16] is another example of a company that is working towards a hydrogen powered aircraft capable of flying routes that the A320neo currently operates on.

**Hydrogen Integration in Airport Infrastructure** Without the supporting operational infrastructure, a hydrogen-powered aircraft may not be integrated in the commercial aviation sector. In literature, evolving of the refuelling infrastructure is segmented between the early ramp-up years, before 2040, and the scale-up, after 2040 [23]. The former is expected to be manageable as liquid fuel trucks will be able to serve the traffic at most airports. Initially, small airports with ready accessibility to energy sources to produce green hydrogen would lead the way, meaning specific routes will be implementing hydrogen first [23]. Smaller airports also provide the opportunity to test the infrastructure. The demand for liquid hydrogen is projected to grow exponentially, and a substantial increase in infrastructure is required after 2040. The primary challenges that arise due to this scale-up are outlined hereafter.

Firstly, as aviation becomes a major source of demand of liquid hydrogen, the produced hydrogen needs to be liquefied, seeking the limits of the liquefaction capacity [23]. To serve large airports, hydrogen hydrant pipelines dedicated to hydrogen are the only long-term option of supplying enough [17]. For medium-haul aircraft, refuelling times remain manageable with predicted flow rates. The turn-around-times would remain same when

[14] `https://home.kpmg/xx/en/home/insights/2020/11/the-hydrogen-trajectory.html` - Accessed: 10-6-2022
[15] `https://www.airbus.com/en/innovation/zero-emission/hydrogen/zeroe` - Accessed: 23-5-2022
[16] `https://www.zeroavia.com/` - Accessed: 23-5-2022
[17] `https://www.kearney.com/transportation-travel/article/-/insights/aviations-hydrogen-the-airport-challenge` - Accessed: 23-5-2022

refuelling with hydrogen [23]. Airports will be required to revisit safety protocols[15], as handling hydrogen and its properties of reaction with water, asphyxiation, and vertical dispersion will pose new threats. The added length of hydrogen aircraft may require redesigning of ramps and gates where aircraft are parked. Lastly, re-optimisation of air traffic systems may be required to as aircraft alter in near-airport operations [23].

### 2.6.2. Fuel Cells

Fuel cell technology has advanced considerably over the past 15 years. Policy makers have included hydrogen and fuel cells on the map of future energy strategies. This area still has major challenges to overcome on the technical and commercial aspect.The proposed PEMFC fuel cell is a relatively new technology and shows a lot of potential. To date, only a small number of high-capacity installations are based on the PEMFC fuel cells. The cost of hydrogen fuel cells is still too high compared to electric batteries to be competitive. This is mainly the result of using Platinum which contributes about 30 % of the stack cost [80]. Research into different metal alloys is being performed to find a substitute. Expected is that further research and testing will drive the cost of hydrogen based fuel cells down [39].

### 2.6.3. Low-Cost Carriers

The largest A320 and B737 operators are low cost carriers, who are rapidly taking over the European market. In 2009, the market share for low-cost carriers was only 9%. In 2017, this has grown to 43% [14]. Not only in Europe the low-cost carriers are taking over the market, but also in South-East Asia, with a rapidly increasing share from 48% in 2019 to 54% in 2022 [18]. In South-Asia, passenger growth is estimated around 7% in the coming years [19]. The growth of low-cost carriers around the world also requires an increase of corresponding single aisle aircraft. In the next 20 years, the demand for 100-150 seat single aisle aircraft will be between 3 000 and 4 500 aircraft for the South-East Asia market[20].

### 2.6.4. Sustainability & Recycling

The reduction of the carbon footprint of the aerospace sector is of utter importance, with the ultimate goal of becoming emission free. Currently, the aviation sector is responsible for 3% of global carbon dioxide emission [21]. One of the largest challenges to achieve the sustainability goal is the fact that the aviation sector is a global sector. Regulations on emission set by the European commission do not apply in the United States of America. Still governments, airlines, aircraft manufactures, and airports made commitments to become net zero carbon [22]. The European Committee stated their zero emission goals in the ”Flightpath 2050” document [37]. The Royal Schiphol Group, an airport of interest for this project, is planning to reach the net zero carbon status by 2030 [23]. Besides zero emission, sustainability also focuses on efficient use of materials. In the past years, materials became scarce which boosted the prices but also availability of resources. Besides the fact that materials became more scarce, geopolitical (in)stability can also have effect on resource availability. This makes it more difficult to configure supply chain assets [24]. Evidently, all parties in the aviation sector aim to reduce emissions and become more sustainable. Sustainable aircraft can be achieved with different methods and design choices. Different options which are investigated at the moment are sustainable aviation fuels, electric aircraft, and green materials. Furthermore, for airlines to obtain zero emissions the old emission producing fleet has to be replaced by zero emission aircraft.

[18] https://www.reuters.com/article/boeing-new-aircraft-china-idINDEE88407U20120905 - Accessed: 26-4-2022

[19] https://www.businesstimes.com.sg/asean-business/south-east-asian-air-travel-boom-expected-on-low-cost-carrier-growth-boeing - Accessed 26-09-2022

[20] https://leehamnews.com/2018/01/24/boeing-aims-half-100-150-seat-sector-737-7/ - Accessed: 26-4-2022

[21] https://cen.acs.org/environment/sustainability/Airlines-want-make-flight-sustainable/99/i32 - Accessed on 26-04-2022

[22] https://www.iata.org/en/programs/environment/flynetzero/ - Accessed: 26-04-2022

[23] https://www.schiphol.nl/en/schiphol-group/page/a-co2-neutral-airport/ - Accessed: 26-04-2022

[24] https://www.iata.org/contentassets/690df4ddf39b47b5a075bb5dff30e1d8/iata-future-airline-industry-pdf.pdf - Accessed: 26-4-2022

## 2.7. Market Gap

Based on the market analysis performed in this chapter, a market gap can be identified. The commercial aviation sector is showing signs of a rebound after the Covid-19 shock, and the domestic (short-haul) flights are proving to be more resilient, reinstating the fact that a competitive A320 type aircraft will continue to be in demand. In terms of geographic location, Europe, North America, and Asia present established busy markets. Africa presents an untapped market and has the potential for many more international and domestic flights between the largest most populous countries.

Low-cost carriers are taking commercial aviation by a storm. These operating airlines are the last to switch to sustainable alternatives due to higher prices. The intersection of sustainability and low-cost carriers provides a gap in the market, if the aircraft list price remains competitive. Sustainability is the defining problem of the current generation, and the aerospace sector provides an opportunity to compensate huge amounts of pollutants. The regulations speak for themselves, sustainability is the future and entering the market earlier than the competition gives the project a competitive edge. Additionally, recyclability is an ever-growing theme and can save huge amounts of resources in the long run.

## 2.8. Expected Demand

To get a first estimate for the demand for the to be designed aircraft, its essential to get an overview of the total demand of the market. Airbus expects that the demand in the next 20 years will slowly shift from market growth to replacement of the less fuel efficient fleet [25]. The fleet replacement and market growth requires 29 700 new A220 and A320 like aircraft in the next 20 years. Boeing expects similar numbers and states that roughly 80% of the 2019 fleet will be replaced by 2040 [26]. Furthermore, the split for new aircraft will be 46% replacement and 54% growth. Of the 43 610 new aircraft forecast by Boeing, an expected 32 660 aircraft will be single aisle aircraft due to the high utilisation.

Boeing and Airbus currently dominate the 150 seat single aisle aircraft market. Embraer and Bombardier joint the market later which can be clearly seen in the market share of both brands. While the to be designed aircraft will have a large reduction in emission and noise, all other aircraft manufacturers will also evolve within this field in the coming years. This reduces the speciality of the design and therefore the possible market share. Entering the market will be very similar to the introduction of the Embraer 195-E2 and A220-300. While the demand for 100-150 passenger aircraft will increase in the coming years it is assumed that the majority of the demand will be satisfied by Boeing or Airbus. This is also concluded with the fact that all four aircraft manufacturers are heavily investing in sustainable aviation. From order history of both the Embraer and Bombardier an average of 60 orders per year is taken as first estimation for this project [4,5,6]. From statistical data it is concluded that the to be designed aircraft will be for sale for around 30 years [5,6]. This comes down to a total of 1 800 sold aircraft in the next 30 years.

[25] `https://www.airbus.com/en/products-services/commercial-aircraft/market/global-market-forecast` - Accessed: 26-4-2022

[26] `https://simpleflying.com/boeing-2021-commercial-market-outlook/amp/` - Accessed: 26-4-2022

# 3

# Financial Analysis

In this chapter, the financial analysis for the Lightning2 aircraft is outlined. First, Section 3.1 presents the cost breakdown structure. Next, Section 3.2 presents the unit cost analysis, after which Section 3.3 presents the operational costs. Finally, Section 3.4 presents the return on investment for the aircraft. In this chapter, all costs are rounded to the nearest 100,000 to account for uncertainties.

## 3.1. Cost Breakdown Structure

Before starting the financial analysis, the costs associated with bringing an aircraft to market need to be identified. The list price is comprised of the unit cost and the earnings. The costs are further elaborated using a cost breakdown structure as shown in Figure 3.1. The costs are divided in three categories: non-recurring costs, recurring costs, and operational cost.

The operating cost is used to assess the competitiveness of the aircraft within the market. Non-recurring costs are irregular expenses such as design and certification costs. The non-recurring costs are constant and do not change with the number of aircraft sold. Recurring cost are ongoing expenses. The recurring costs are split into two categories; overhead and manufacturing costs. The manufacturing costs apply for each identical aircraft sold and therefore vary with number of aircraft manufactured. Costs for quality control, manufacturing labour, and manufacturing materials are included in the component cost.

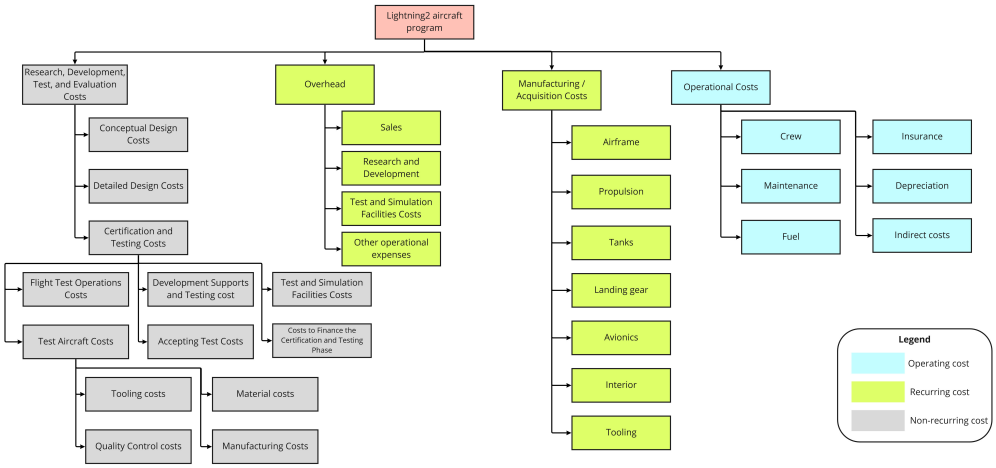


**Figure 3.1:** *Cost breakdown structure for the Lightning2 aircraft.*

## 3.2. Unit Cost Analysis

This section describes the unit cost of a single aircraft based on the Roskam method [90]. While this method is tailored to conventional aircraft, it is proven that it also works for blended wing body aircraft, with a margin of 30 % [43], which will be applied to the total required investment and the manufacturing costs. This means that the costs in this section might be overestimated. However, financially, it is better to overestimate costs than

underestimate.

The unit cost analysis consists of the total fixed costs and the manufacturing costs. The total fixed costs consist of the design, certification and testing costs. The latter can be split up in the manufacturing costs for the flight test aircraft, development support and testing, operational costs for the flight and other testing expenses.

The manufacturing costs can be split up in the costs for the airframe, propulsion system, tanks, avionics, and landing gear. All except the propulsion system and hydrogen tanks can be estimated with Roskam [90], because these are unconventional hydrogen components. The method uses cost rates for maintenance, manufacturing, tooling and design crews. They are assumed equal to 76, 67, 77 and 117 USD/h [40], respectively. The manufacturing costs of the tank were based on the amount of kWh hydrogen the tank contains. The estimated price for the hydrogen tanks is 35 USD/kWh [30].

The different components of the propulsion system are listed below in Table 3.1, including their cost relationship. Some prices are stated for the fiscal year 2012 which can be corrected for with the the consumer price index, $CPI = 1.28$. The power used in the cost relationships are in hp and the fan diameters are in feet.

**Table 3.1:** *Formulas for the propulsion system cost estimation [40, 98, 25, 120, 62, 109].*

| Component | Cost relationship |
|---|---|
| Electric motor | $174 \cdot N_{motor} \cdot P_{em,hp} * CPI$ |
| Inverter | 2.7 /kW |
| Fan | $210 \cdot N_{prop} \cdot D_p^2 \left(\frac{P_{em}}{D_p}\right)^{0.12}$ |
| Duct | $\frac{W_{duct} \cdot p_{al}}{0.07} N_{eng}$ |
| Fuel cells | 65 $/kW |
| Power management system | $150 \cdot P_{emto,hp} \cdot CPI$ |
| Compressor | $52 \cdot CPI$ /kW |
| Cooling system | 5 /kW |

Table 3.2 shows the estimated costs for the design phase, certification and testing, and manufacturing. The initial required investment for the Lightning2 program is equal to 19.7 billion USD. Based on the estimations, the unit cost is found from Eq. 3.1, where $n_{total}$ is equal to the number of sold aircraft within the entire aircraft program, giving a unit cost of 54.56 million USD, in compliance with requirement STH.CUS.1.

$$unit\ cost = \frac{total\ fixed\ cost}{n_{total}} + manufacturing\ cost \tag{3.1}$$

**Table 3.2:** *The unit cost analysis with a summary of the total fixed costs and the manufacturing costs. All numbers are expressed in FY2022 M$.*

| Parameter | Value | Parameter | Value |
|---|---|---|---|
| **Costs of design phase** | 6.42 | Airframe costs | 4.10 |
| Development support and testing costs | 161.0 | Propulsion costs | 24.71 |
| Flight test costs | 229.83 | Tank costs | 3.26 |
| Other testing costs | 5,826.83 | Landing gear costs | 1.76 |
| **Certification & Testing costs** | 19,694.7 | Avionics costs | 1.46 |
| | | Interior costs | 0.33 |
| | | Tooling costs | 2.28 |
| | | **Unit manufacturing cost** | 49.29 |
| **Unit cost** | 57.71 | **Market price (excl. VAT)** | 90.00 |

## 3.3. Operational Costs

To calculate the operational costs of a Lightning2 aircraft, several aspects need to be taken into account such as crew, fuel, depreciation, etc. All estimations were based on the Roskam method [90] with a 30 % margin, except the fuel cost estimation. For the crew cost, the salary of the pilot and copilot were assumed to equal 117,292 and 69,384 FY2022 USD per year, respectively. In addition, it was assumed that there is full depreciation of

the engines, fuel cells and tanks. Lastly, the fuel cost estimation was done based on the price of green LH2 of 5 USD per kg five years from now, which is assumed from Figure 2.7.

**Table 3.3:** *The operating cost estimation for the Lightning2 (All values are expressed in FY2022 USD per nautical mile).*

| **Parameter** | **Value** |
|---|---|
| Crew costs | 0.838 |
| Maintenance cost | 11.504 |
| Fuel cost | 3.911 |
| Insurance | 2.411 |
| Depreciation | 14.046 |
| Landing fees | 1.715 |
| Financing cost | 2.591 |
| Indirect costs | 25.912 |
| **Operating costs** | 62.929 |

## 3.4. Return on Investment

With the analysed cost breakdown, an estimate of the costs and cash balance of the production of the Lightning2 aircraft can be made. The start of the program was launched with the start of the DSE in spring 2022. This also marks the start of the design phase of Lightning2, which includes both the conceptual and the detailed design. In compliance with the STH.CUS.4 requirement, the end of the design phase is a milestone set five years from the start. As estimated in Table 3.2, the design phase will require an investment of five million USD. Next, the Lightning2 goes into the Certification and Testing phase to prove the safety and reliability of the aircraft in compliance with the CS25-requirements. According to the FAA, the certification of a new aircraft concept can take between five and nine years [1]. As an estimate, this milestone for the Lightning2 is set at seven years from the end of the design phase. The total required investment for the aircraft program sums up to 19 billion USD. This is in line with the expected development costs for a new aircraft in this category: 13 billion for the Airbus A320neo and 30 billion for the Boeing 737 MAX [73]. The cash balance throughout the two phases is shown in Table 3.4. The first units are expected to be sold in 2034, with a total number of 1800 units being sold over a time span of 30 years at a market price of 90 million, excluding VAT.

In the beginning of production, it is expected that the unit cost will be higher compared to the one estimated before due to the learning curve associated with the manufacturing of a new aircraft, especially since the Lightning2 is a blended wing body. It is expected that the manufacturing process will be optimised and the associated costs will go down to 95% of the first estimated number as time goes on, which is a conservative approach.

Other costs are associated with sales, general and administrative (SGA), research & development (R&D), and other operational expenses (OPE). From the 2018 financial report of Bombardier [13], these are 7%, 2 %, 0.6 % of the revenue, respectively. Profit taxes, equal to 24% in the Netherlands, can be subtracted from the profit before taxes (PBT) to generate the net profit. The total cash balance can then be calculated. Lastly, the return on investment (RoI) for that year can be determined by dividing the cash balance by the total investment at the end of the certification and testing phase. An entire overview is shown in Table 3.5. It can be seen that the RoI at the end of 30 years production is equal to 231.6 %.

Another measure that is commonly used in the aviation sector is the break-even point. This is the number of aircraft that have to be sold to offset the investments made in the design and certification & testing phase. In the case of the Lightning2 program, the break-even point is 554 aircraft.

[1] https://www.faa.gov/aircraft/air_cert/airworthiness_certification/#:~{}:text=The%5C%20certification%5C%20was%5C%20completed%5C%20in,between%5C%205%5C%20and%5C%209%5C%20years

**Table 3.4:** *The cash balance for the design and certification & testing phase of the Lightning2 aircraft. All numbers are expressed in FY2022 M$.*

| | **Design** | | | | | **Certification & Testing** | | | | | | |
|---|---|---|---|---|---|---|---|---|---|---|---|---|
| | 2022 | 2023 | 2024 | 2025 | 2026 | 2027 | 2028 | 2029 | 2030 | 2031 | 2032 | 2033 |
| Cash Balance | -1.28 | -2.57 | -3.85 | -5.14 | -6.42 | -2,819.95 | -5,633.48 | -8,447.01 | -11,260.53 | -14,074.06 | -16,887.59 | -19,701.12 |

**Table 3.5:** *The cash balance for the manufacturing phase of the Lightning2 aircraft. All numbers are expressed in FY2022 M$.*

| | **2034** | **2035** | **2036** | **2037** | **2038** | **2039** | **2040** | **2041** | **2042** | **2043** | **2044** | **2045** | **2046** | **2047** | **2048** |
|---|---|---|---|---|---|---|---|---|---|---|---|---|---|---|---|
| Units sold | 5 | 7 | 10 | 14 | 20 | 28 | 39 | 55 | 68 | 74 | 74 | 74 | 74 | 74 | 74 |
| MP (excl. VAT) | 90.0 | 90.0 | 90.0 | 90.0 | 90.0 | 90.0 | 90.0 | 90.0 | 90.0 | 90.0 | 90.0 | 90.0 | 90.0 | 90.0 | 90.0 |
| Unit cost | -69.3 | -67.8 | -66.4 | -64.9 | -63.5 | -62.0 | -60.6 | -59.2 | -57.7 | -57.1 | -56.6 | -56.0 | -55.4 | -54.8 | -54.8 |
| Revenue | 450.0 | 630.0 | 900.0 | 1,260.0 | 1,800.0 | 2,520.0 | 3,510.0 | 4,950.0 | 6,120.0 | 6,660.0 | 6,660.0 | 6,660.0 | 6,660.0 | 6,660.0 | 6,660.0 |
| SGA | -31.5 | -44.1 | -63.0 | -88.2 | -126.0 | -176.4 | -245.7 | -346.5 | -428.4 | -466.2 | -466.2 | -466.2 | -466.2 | -466.2 | -466.2 |
| R&D | -9.0 | -12.6 | -18.0 | -25.2 | -36.0 | -50.4 | -70.2 | -99.0 | -122.4 | -133.2 | -133.2 | -133.2 | -133.2 | -133.2 | -133.2 |
| OPE | -27.0 | -37.8 | -54.0 | -75.6 | -108.0 | -151.2 | -210.6 | -297.0 | -367.2 | -399.6 | -399.6 | -399.6 | -399.6 | -399.6 | -399.6 |
| PBT | 36.2 | 60.8 | 101.3 | 162.1 | 260.4 | 404.9 | 620.3 | 954.1 | 1,277.7 | 1,433.2 | 1,475.9 | 1,518.6 | 1,561.3 | 1,604.0 | 1,604.0 |
| Profit tax | -8.7 | -14.6 | -24.3 | -38.9 | -62.5 | -97.2 | -148.9 | -229.0 | -306.7 | -344.0 | -354.2 | -364.5 | -374.7 | -385.0 | -385.0 |
| Net profit | 27.5 | 107.1 | 178.3 | 285.2 | 458.3 | 712.7 | 1,091.7 | 1,679.2 | 2,248.8 | 2,522.4 | 2,597.5 | 2,672.7 | 2,747.9 | 2,823.0 | 2,823.0 |
| | 6.1% | 17.0% | 19.8% | 22.6% | 25.5% | 28.3% | 31.1% | 33.9% | 36.7% | 37.9% | 39.0% | 40.1% | 41.3% | 42.4% | 42.4% |
| Cash balance | -19,673.6 | -19,566.5 | -19,388.2 | -19,102.9 | -18,644.7 | -17,932.0 | -16,840.3 | -15,161.1 | -12,912.3 | -10,389.9 | -7,792.4 | -5,119.7 | -2,371.8 | 451.2 | 3,274.2 |
| RoI | -99.9% | -99.3% | -98.4% | -97.0% | -94.6% | -91.0% | -85.5% | -77.0% | -65.5% | -52.7% | -39.6% | -26.0% | -12.0% | 2.3% | 16.6% |

| | **2049** | **2050** | **2051** | **2052** | **2053** | **2054** | **2055** | **2056** | **2057** | **2058** | **2059** | **2060** | **2061** | **2062** | **2063** |
|---|---|---|---|---|---|---|---|---|---|---|---|---|---|---|---|
| Units sold | 74 | 74 | 74 | 74 | 74 | 74 | 74 | 74 | 74 | 74 | 74 | 74 | 74 | 74 | 74 |
| MP (excl. VAT) | 90.0 | 90.0 | 90.0 | 90.0 | 90.0 | 90.0 | 90.0 | 90.0 | 90.0 | 90.0 | 90.0 | 90.0 | 90.0 | 90.0 | 90.0 |
| Unit cost | -54.8 | -54.8 | -54.8 | -54.8 | -54.8 | -54.8 | -54.8 | -54.8 | -54.8 | -54.8 | -54.8 | -54.8 | -54.8 | -54.8 | -54.8 |
| Revenue | 6,660.0 | 6,660.0 | 6,660.0 | 6,660.0 | 6,660.0 | 6,660.0 | 6,660.0 | 6,660.0 | 6,660.0 | 6,660.0 | 6,660.0 | 6,660.0 | 6,660.0 | 6,660.0 | 6,660.0 |
| SGA | -466.2 | -466.2 | -466.2 | -466.2 | -466.2 | -466.2 | -466.2 | -466.2 | -466.2 | -466.2 | -466.2 | -466.2 | -466.2 | -466.2 | -466.2 |
| R&D | -133.2 | -133.2 | -133.2 | -133.2 | -133.2 | -133.2 | -133.2 | -133.2 | -133.2 | -133.2 | -133.2 | -133.2 | -133.2 | -133.2 | -133.2 |
| OPE | -399.6 | -399.6 | -399.6 | -399.6 | -399.6 | -399.6 | -399.6 | -399.6 | -399.6 | -399.6 | -399.6 | -399.6 | -399.6 | -399.6 | -399.6 |
| PBT | 1,604.0 | 1,604.0 | 1,604.0 | 1,604.0 | 1,604.0 | 1,604.0 | 1,604.0 | 1,604.0 | 1,604.0 | 1,604.0 | 1,604.0 | 1,604.0 | 1,604.0 | 1,604.0 | 1,604.0 |
| Profit tax | -385.0 | -385.0 | -385.0 | -385.0 | -385.0 | -385.0 | -385.0 | -385.0 | -385.0 | -385.0 | -385.0 | -385.0 | -385.0 | -385.0 | -385.0 |
| Net profit | 2,823.0 | 2,823.0 | 2,823.0 | 2,823.0 | 2,823.0 | 2,823.0 | 2,823.0 | 2,823.0 | 2,823.0 | 2,823.0 | 2,823.0 | 2,823.0 | 2,823.0 | 2,823.0 | 2,823.0 |
| | 42.4% | 42.4% | 42.4% | 42.4% | 42.4% | 42.4% | 42.4% | 42.4% | 42.4% | 42.4% | 42.4% | 42.4% | 42.4% | 42.4% | 42.4% |
| Cash balance | 6,097.2 | 8,920.2 | 11,743.2 | 14,566.3 | 17,389.3 | 20,212.3 | 23,035.3 | 25,858.3 | 28,681.4 | 31,504.4 | 34,327.4 | 37,150.4 | 39,973.4 | 42,796.4 | 45,619.5 |
| RoI | 30.9% | 45.3% | 59.6% | 73.9% | 88.3% | 102.6% | 116.9% | 131.3% | 145.6% | 159.9% | 174.2% | 188.6% | 202.9% | 217.2% | 231.6% |

# 4

# Functional Analysis

The functions which the system has to perform can be identified using a functional flow diagram and a functional breakdown structure. The first shows the chronological order of the functions which the system has to perform and the latter describes the hierarchy between those functions. Together, these form the functional analysis and will be used to aid in the requirements analysis later on.

First, Section 4.1 presents the functional flow diagram made for the aircraft being designed. Next, Section 4.2 presents the functional breakdown structure.

## 4.1. Functional Flow Diagram

The functional flow diagram shows the different functions the aircraft has to perform in chronological order: from the beginning of its lifetime in the design phase to the end in its end-of-life phase. The diagram is limited to the aircraft itself and its constituent parts.

The functional flow diagram follows the general operation of a commercial aircraft. AND/OR operators are included to illustrate different options. More elaborated deciders are used when discussing maintenance and verification of subsystems and assemblies. Together with feedback loops, these operators show the relationship between functions. The functional flow diagram is presented in Figure 4.1.

## 4.2. Functional Breakdown Structure

Next to the functional flow diagram, a functional breakdown structure was made. It hierarchically represents the functions that the product or system must perform in the form of an AND tree. The breakdown structure goes at least four levels deep and is further expanded for most of the functions in the operational part of its lifetime. This is done because a significant part of the requirements has a direct impact on the operational functions. Since the breakdown structure is a non-time-dependent representation of the aircraft, continuous processes are also included. The functional breakdown structure is represented in Figure 4.2.

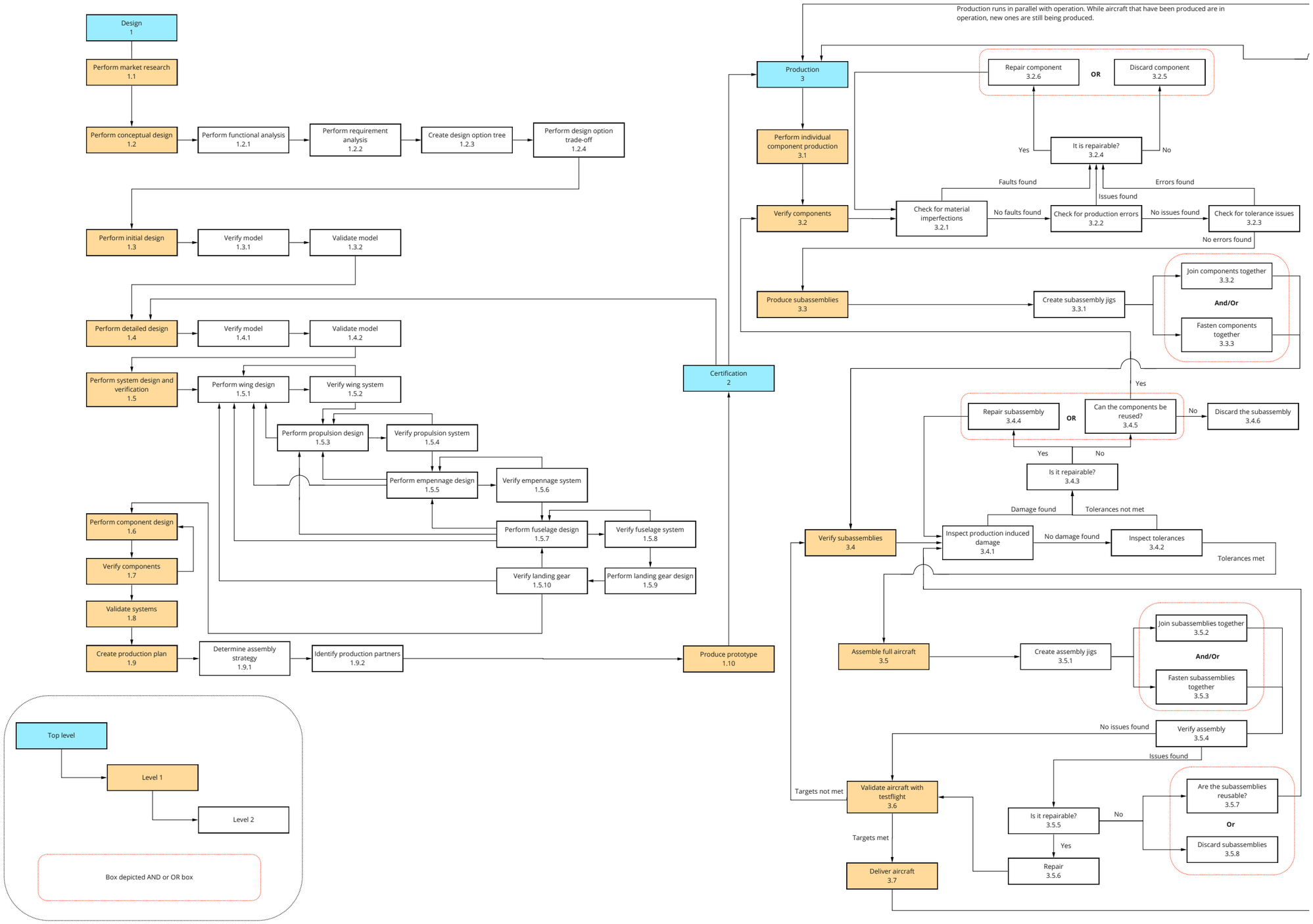


**Figure 4.1:** *Functional Flow Diagram for the design project.*

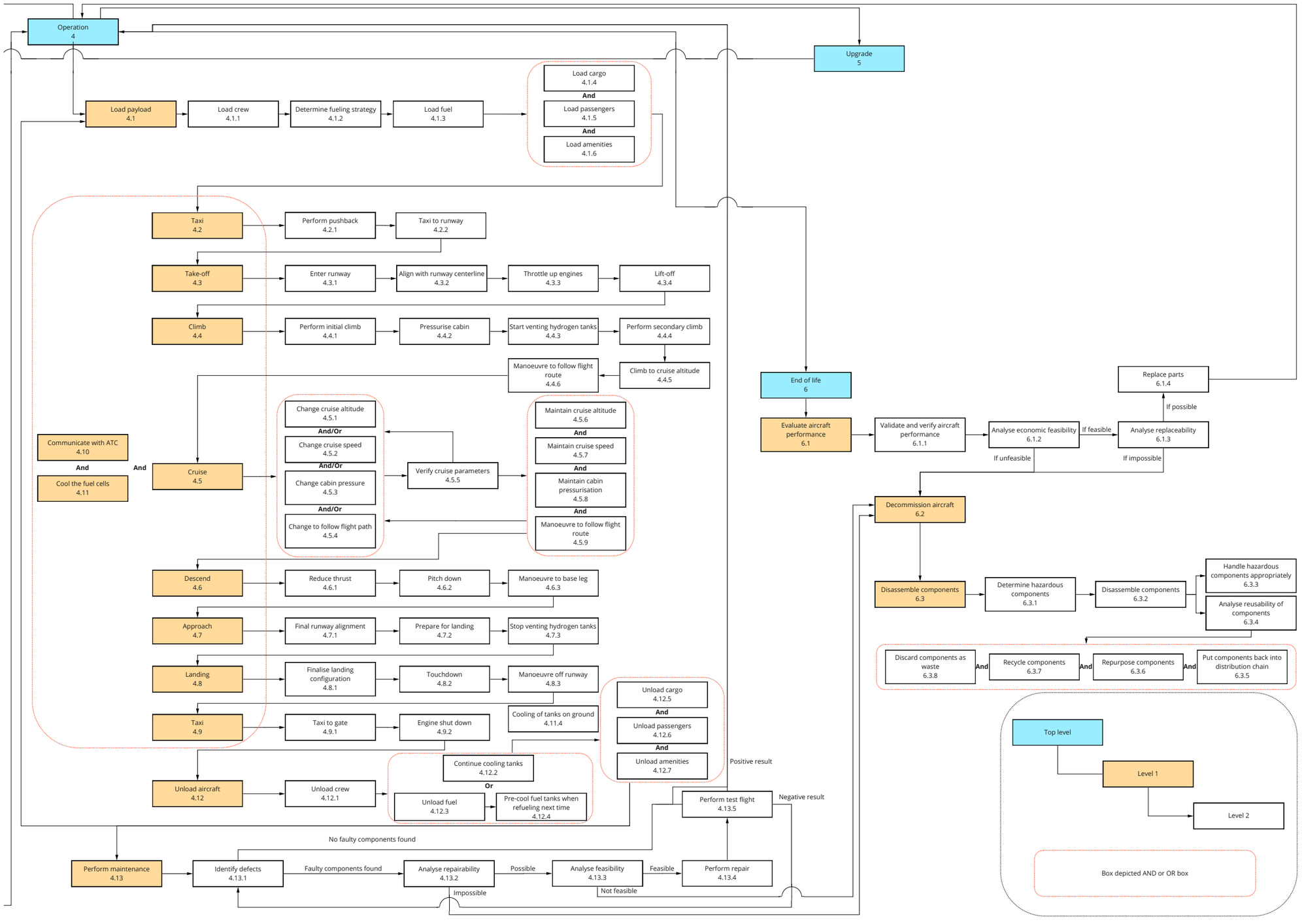


*Functional Flow Diagram for the design project.*

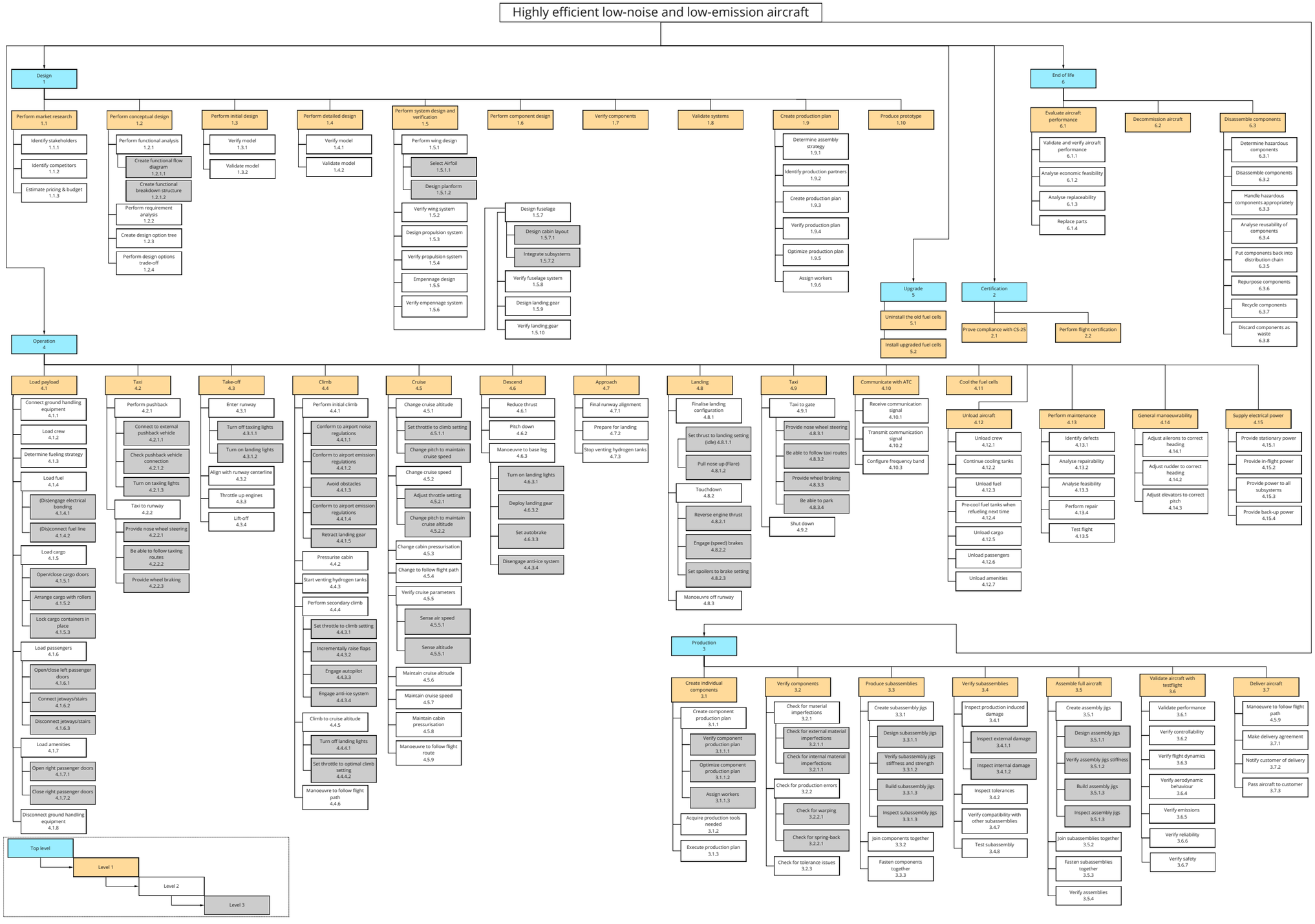


**Figure 4.2:** *Functional Breakdown Structure for the design project.*

# 5

# Technical Risk Assessment

The chapter starts with an explanation of how the risk analysis was performed in Section 5.1. After that, a strengths, weaknesses, opportunities, and threats (SWOT) analysis is performed. Then, technical risk identification, assessment, prioritisation, and mitigation strategies are presented in Section 5.3. The same approach is adopted for cost risks in Section 5.4, scheduling risks in Section 5.5, and programmatic risks in Section 5.6.

## 5.1. Introduction to Technical Risk

During the planning phase, an organisational risk analysis was performed to prevent the team from unexpected organisational obstacles. In the midterm report the focus shifted to more technical risks of the design. These risks were general and applicable to all three concepts. In the present report, a concept is chosen and risks concerning the blended wing body can be identified. In the previous phases of the design, the importance of the risk analysis was observed. Mitigation strategies had to be applied to keep the design within the designated time window of 10 weeks.

Technical risk encompasses all risks that are associated with the design and production that could influence the performance needed to satisfy the stakeholder requirements [1]. The technical risk analysis will be done in five steps but is an iterative and continuous process throughout the whole design. The steps that are taken in the risk analysis are shown in Figure 5.1.

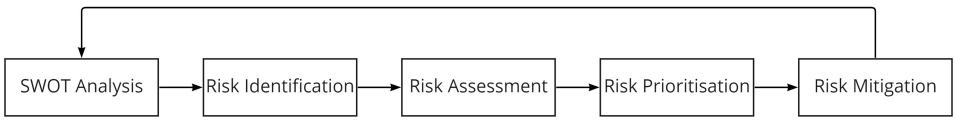


**Figure 5.1:** *Risk assessment flow chart.*

The SWOT analysis serves as a stepping stone for all further steps. For the risk analysis of the design, technical, cost, scheduling, and programmatic risks are assessed. For each category, all risks are identified, and collected in a table. Each risk receives a unique risk identifier, and a brief explanation of both the cause and the consequence. Some previously defined risks, do not apply anymore to the current design and are removed from the analysis. With a complete list of risks, each risk is assessed in terms of its probability of occurrence and severity to allow for a quantifiable risk metric, defined as the product of the two as stated in Eq. 5.1.

$$Risk = Probability \cdot Consequence \tag{5.1}$$

Eq. 5.1 is performed based on assigned metrics for assessing both of these quantities. The industry average assigns between three and six categories for each. The choice of categories for this technical risk assessment is

[1] `https://www.nasa.gov/seh/6-4-technical-risk-management` - Accessed: 25-04-2022

chosen to be identical to those used in the previously performed organisational and technical risk assessments, repeated in Table 5.1. Using these categories, all identified risks can be plotted on a risk map, which consists of three areas: low, medium, and high risk.

For risks that are positioned in the medium and high-risk regions of the risk map, mitigation strategies are presented to reduce the risk. After these mitigation strategies, an update of the risk map is provided depicting the effect of mitigation.

**Table 5.1:** *Categories for the consequences and probability of the risk analysis.*

| | Consequence | | Probability (PR) | |
|---|---|---|---|---|
| | **Category** | **Description** | **Category** | **Description** |
| **1.** | Catastrophic | - Failure of the project objective.<br>- Drastic underperformance. | Very high. | PR $\geq$ 70% |
| **2.** | Critical | - Questionable project success.<br>- Serious underperformance. | High. | 50% $\leq$ PR $<$ 70% |
| **3.** | Significant | - Impact on project success noticeable.<br>- Significant underperformance. | Moderate. | 30% $\leq$ PR $<$ 50% |
| **4.** | Marginal | - Alteration/cancelling of secondary objectives.<br>- Slight underperformance. | Low. | 1% $\leq$ PR $<$ 30% |
| **5.** | Negligible | - Solely minor impact on operation. | Very low. | PR $<$ 1% |

## 5.2. SWOT Analysis

The starting point for the technical risk assessment is a technical SWOT analysis such as the one performed in Section 2.1. Strengths and weaknesses are internal, whereas the opportunities and threats are external. The SWOT analysis can guide the team to successful strategies and raise awareness of possible weaknesses and threats.

The largest strength is the fact that the design starts with a blank piece of paper, such that the most innovative and outside the box design options and technologies can be applied. This strength is amplified by the opportunity of new cutting-edge technologies and materials which can be used in the design. While high-tech technologies can drive the design to the must cutting-edge of the spectrum, little literature will be available about these. This in combination with the limited knowledge on blended wing body designs and considerations can create a considerable risk for the project. The largest threats are the possible regulation changes towards hydrogen use and DP and the lack of influence in third party decisions. The technical SWOT analysis is shown in Figure 5.2.

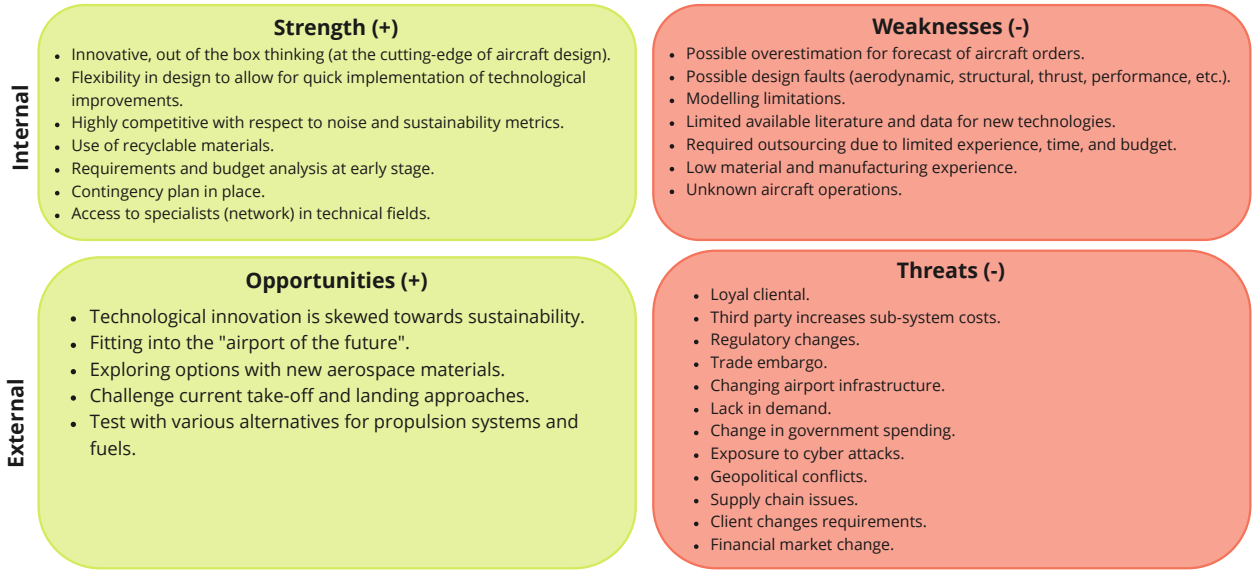


**Figure 5.2:** *Technical SWOT analysis.*

## 5.3. Technical Risk

First, the technical risks based on the technical aspect of the design have been identified. Technical risks arise when the ability of the product to achieve the performance requirements becomes compromised.

### 5.3.1. Risk Identification

The first step is to identify the possible technical risks that can occur during the design of the aircraft. Technical risks are identified with ”R.T.T” and stated in Table 5.2. For each risk the cause and consequence is stated.

**Table 5.2:** *Identified technical risks.*

| Risk ID | Risk | Cause/Situation | Consequence |
|---|---|---|---|
| **R.T.T.1** | Parts geometry too complex. | Lack of awareness in manufacturing process and material capabilities, faulty design process. | High costs, no possibility to produce the part. |
| **R.T.T.3** | Modelling limitations. | Limitation in software. | Inaccurate aircraft design. |
| **R.T.T.4** | Limited available literature & data. | New technology used, confidential reason. | Inaccurate aircraft design. |
| **R.T.T.5** | Unidentified killer requirement. | Lacking literature. | Not able to satisfy all client requirements. |
| **R.T.T.6** | Production inaccuracies. | Miscommunication between manufacturer and design team. Worn out tools. | Possible failure in aircraft structure, emergency situation, airframe loss. |
| **R.T.T.7** | Design fault (third party). | Miscommunication between two parties, negligence of third party. | Aircraft grounding, possible loss of airframe, redesign time needed. |
| **R.T.T.9** | Design calculation errors. | Lack of funding, rushed design process, lack of personnel. | Loss of airframe, sales, expensive redesigning, delayed deliveries. |
| **R.T.T.10** | Incomplete verification & validation. | Rushed design process, lack of funding. | Loss of air frame, high maintenance needs. |
| **R.T.T.13** | Over-complicated propulsion system. | A complex propulsion system can greatly complicate the system. | Can cause high design time compared to other systems, lower quality. |
| **R.T.T.14** | Incorrect reference data & information. | Use of inappropriate data & information during early design. | Point team in wrong design direction and hinder technical performance. |
| **R.T.T.15** | Incorrect noise and emission estimation. | Use of wrong methods or models. | Not satisfying the client requirements. |
| **R.T.T.16** | Improper weight prediction. | Inaccurate weight estimation for future technology. | Underestimating the weight of the aircraft requiring a redesign. |
| **R.T.T.17** | Oval pressure vessel weight penalty | Underestimated first preliminary pressure vessel weight. | Additional weight has to be added to the aircraft causing a snow ball effect. |
| **R.T.T.18** | Unstable aircraft. | Unstable characteristics of the blended wing body. | Aircraft is not able to fly within the CS-25 regulations. |

### 5.3.2. Risk Assessment and Prioritisation

The next step is to place the risks into a risk matrix. To do so, the risks need to be placed into a consequence and probability category as described in Section 5.1. The position of the risk within the risk matrix determines if it is a high, medium, or low risk. The risk matrix is shown in Table 5.3. It is clearly visible that almost all risks have a low probability of occurrence but a critical or catastrophic consequence. This implies that there are no high risks that have severe consequences for the project.

In the risk prioritisation, a score is assigned to each of the risk using Eq. 5.1, a lot of risks have the same risk score. This is because of the fact that almost all risks are located in the left upper corner of the risk matrix. Risks with the same score are classified as having the same impact on the project. The risk prioritisation is shown in Table 5.4.

**Table 5.3:** *Technical risk matrix.*

| | | | | | |
|---|---|---|---|---|---|
| **Catastrophic** | | R.T.T.10 | R.T.T.18 | | |
| **Critical** | R.T.T.7<br>R.T.T.9 | R.T.T.5<br>R.T.T.6<br>T.T.T.16 | R.T.T.15 | | |
| **Significant** | | R.T.T.1<br>R.T.T.14 | R.T.T.13 | R.T.T.17 | |
| **Marginal** | | R.T.T.3 | R.T.T.4 | | |
| **Negligible** | | | | | |
| **Consequence / probability** | **<1%** | **1-30%** | **30-50%** | **50-70%** | **>70%** |

**Table 5.4:** *Technical risk prioritisation table.*

| Rank | Risk ID | Score | Rank | Risk ID | Score |
|---|---|---|---|---|---|
| 1 | R.T.T.18 | 15 | 9 | R.T.T.4 | 6 |
| 2 | R.T.T.15 | 12 | 10 | R.T.T.14 | 6 |
| 3 | R.T.T.17 | 12 | 11 | R.T.T.1 | 6 |
| 4 | R.T.T.10 | 10 | 12 | R.T.T.3 | 4 |
| 5 | R.T.T.13 | 9 | 14 | R.T.T.7 | 4 |
| 6 | R.T.T.16 | 8 | 15 | R.T.T.9 | 4 |
| 7 | R.T.T.5 | 8 | | | |
| 8 | R.T.T.6 | 8 | | | |

### 5.3.3. Risk Mitigation

The possible mitigation strategies for medium or higher rated risks of Table 5.4 are stated in Table 5.5. The updated technical risk matrix is presented in Table 5.6. The new risk score after mitigation is shown in the last column.

**Table 5.5:** *Mitigation strategies for technical risks.*

| Risk ID | Strategy | Method | New / Old Score |
|---|---|---|---|
| **R.T.T.18** | Reduce | Use active stability control with the use of computer systems. | 6/15 |
| **R.T.T.15** | Reduce | Perform a very detailed verification and validation on the models used to prove accuracy. | 8/12 |
| **R.T.T.17** | Accept | In the iteration method used, an safety factor can be added in the weight estimation of the pressure vessel to account for the oval pressure vessel. | 9/12 |
| **R.T.T.10** | Reduce | Increase the development cost. Alter the schedule such that more time is available for verification and validation. | 4/10 |
| **R.T.T.13** | Reduce | Allocate more resources to this system. | 4/9 |
| **R.T.T.16** | Reduce | Use of multiple sources and estimations to get an accurate and representative weight estimation for future technology. Also a weight safety factor can be taken into account to reduce the consequence of a wrong estimation. | 6/8 |
| **R.T.T.5** | Reduce | Place more resources (man hours) on identifying the killer requirements. | 4/8 |
| **R.T.T.6** | Reduce | Ensure more strict quality control product and improve communication. | 4/8 |
| **R.T.T.1** | Reduce | Ensure requirements feasibility, so that components are not over-designed. | 6/6 |
| **R.T.T.4** | Accept | If not enough literature or data is available, a different design option must be chosen. | 6/6 |
| **R.T.T.14** | Reduce | Verify the sources used. | 3/6 |
| **R.T.T.7** | Reduce | Contractual agreements can be made between the two parties to reduce the probability of occurrence. | 4/4 |
| **R.T.T.9** | Reduce | Reduce severity of calculation mistakes by having more precise software and detailed verification and validation of the program. | 2/4 |

**Table 5.6:** *Mitigated technical risk matrix.*

| | | | | | |
|---|---|---|---|---|---|
| **Catastrophic** | | | | | |
| **Critical** | R.T.T.5<br>R.T.T.7<br>R.T.T.10 | R.T.T.15 | | | |
| **Significant** | R.T.T.14 | R.T.T.1<br>R.T.T.16 | R.T.T.17 | | |
| **Marginal** | R.T.T.2<br>R.T.T.9 | R.T.T.13 | R.T.T.4<br>R.T.T.18 | | |
| **Negligible** | | | | | |
| **Consequence / probability** | **<1%** | **1-30%** | **30-50%** | **50-70%** | **>70%** |

## 5.4. Cost Risk

Cost risk arises in the case of the project requiring more budget than was originally anticipated. In such an event, the project is required to invest more resources to realise the envisioned product which is highly undesirable.

### 5.4.1. Risk Identification

In Table 5.7, the identified cost risks are shown.

**Table 5.7:** *Identified cost risks.*

| Risk ID | Risk | Cause/Situation | Consequence |
|---|---|---|---|
| **R.T.C.1** | Excessive inflation. | A surge in demand can put inflationary pressure on the economy. | Reduces the effective available budget. |
| **R.T.C.2** | Expensive material. | Expensive materials might be needed to meet the requirements. | Reduces the margin between aircraft unit cost and list price, decreasing earnings. |
| **R.T.C.3** | Increase in raw material prices. | The price of raw materials such as aluminium are subject to change according to market dynamics. | This leads to an increase in the manufacturing costs, because raw materials are required. |
| **R.T.C.4** | Increased subsystem prices. | Suppliers may raise the price of their product. | Dependency of the project on a given supplier can lead to higher costs and lowered earnings margin. |
| **R.T.C.5** | FX-rate volatility. | The aerospace sector is international, which means the project is subject to changes in currencies when making transactions. | Making transactions at unfortunate market times decreases incomes. |
| **R.T.C.6** | Costly design changes. | The design might contain mistakes and (or) be infeasible. | Costs associated with changing a design increase with a given factor when the design matures. |
| **R.T.C.7** | Inaccurate cost estimate. | The preliminary cost estimate made at an early stage might contain fundamental mistakes and poor estimations. | This requires either compensation is required in other areas or a raise in the project budget. |
| **R.T.C.8** | Environmental factors. | Costs involved in offsetting carbon footprint and required investing in green technologies. | If emissions are to high, this will need to be offset, which will cost money. |
| **R.T.C.9** | Inefficient resource allocation. | Sub-optimal resource allocation can lead to due inexperienced management. | Misalignment in resource allocation will require more time and money to complete the same tasks. |
| **R.T.C.10** | Breakage during certification & testing. | Rigorous testing of components or the final product subjects it to breakage. | Performing limit tests or inappropriate testing can lead to component breakage break and require repairing or replacement. |
| **R.T.C.11** | Expensive software licenses. | The complex design of the blended wing body can require additional professional software. | The development cost can increase significantly because of expensive licenses. |

### 5.4.2. Risk Assessment and Prioritisation

To present the impact of risks, they are visualised in the risk matrix, as shown in Table 5.8. From Table 5.8, different risks are rated by multiplying the row and column category value of the risks. This gives them all a score, allowing them to be ranked in Table 5.9.

**Table 5.8:** *Cost risk matrix.*

| | | | | | |
|---|---|---|---|---|---|
| **Catastrophic** | | | R.T.C.7 | | |
| **Critical** | | R.T.C.2 | | R.T.C.6 | |
| **Significant** | | R.T.C.10 | R.T.C.9 | R.T.C.4 | |
| **Marginal** | | R.T.C.8 | | R.T.C.3<br>R.T.C.1 | |
| **Negligible** | | R.T.C.11 | R.T.C.5 | | |
| **Consequence / probability** | **<1%** | **1-30%** | **30-50%** | **50-70%** | **>70%** |

**Table 5.9:** *Cost risk prioritisation table.*

| Rank | Risk ID | Score | Rank | Risk ID | Score |
|---|---|---|---|---|---|
| 1 | R.T.C.6 | 16 | 7 | R.T.C.3 | 8 |
| 2 | R.T.C.7 | 15 | 8 | R.T.C.10 | 6 |
| 3 | R.T.C.4 | 12 | 9 | R.T.C.8 | 4 |
| 4 | R.T.C.9 | 9 | 10 | R.T.C.5 | 3 |
| 5 | R.T.C.1 | 8 | 11 | R.T.C.11 | 2 |
| 6 | R.T.C.2 | 8 | | | |

### 5.4.3. Risk Mitigation

For the cost risks that have been identified, 2 fall in to the high risk category and 6 fall into the medium risk category. These risks would be mitigated, with mitigation methods outlined in Table 5.10. The updated risk matrix is then shown in Table 5.11.

**Table 5.10:** *Mitigation strategies for cost risks.*

| Risk ID | Strategy | Method | New / Old Score |
|---|---|---|---|
| **R.T.C.6** | Reduce | Proper analyse of all the requirements set by the customer, and clearly and accurately define all the requirements the aircraft has to fulfil. This lowers the chance of this risk occurring. | 12/16 |
| **R.T.C.7** | Reduce | Implement some buffers in the financial estimate. This will save some financial resources that can be used to mitigate the effects of costs estimates being inaccurate, reducing the impact of that risk. | 12/15 |
| **R.T.C.4** | Reduce | Some financial resources can be set aside to incur these price increases. Furthermore, for some systems it might be possible to select a back-up system produced by a different manufacturer for if the product becomes to expensive. | 8/12 |
| **R.T.C.9** | Reduce | Continuously keep monitoring the use of the different resources. In the case some resources are being used less optimally than they could, they can immediately be reallocated removing the impact of the risk. | 6/9 |
| **R.T.C.1** | Accept | There is nothing that can be done against inflation in order to mitigate the risk. Close collaboration with the client is needed to change the unit price of the aircraft when necessary. | 8/8 |
| **R.T.C.2** | Reduce | The chance of having the use expensive materials is high, so setting aside financial resources for that is necessary. This will reduce the risk of going over the set budget. | 6/8 |
| **R.T.C.3** | Reduce | Set aside some financial resources to reduce the impact of price increases. It is also possible to look at different materials that also meet the requirements and are less expensive. That will bring down the impact of the risk. | 4/8 |
| **R.T.C.10** | Reduce | By applying appropriate safety margins during the design, and by ensuring the production quality of the aircraft is up to the standards set, the risk of failures during testing and certification is minimised. | 3/6 |

**Table 5.11:** *Mitigated cost risk matrix.*

| | | | | | |
|---|---|---|---|---|---|
| **Catastrophic** | | | | | |
| **Critical** | | | R.T.C.7<br>R.T.C.6 | | |
| **Significant** | R.T.C.10 | R.T.C.2 | | | |
| **Marginal** | | R.T.C.8 | R.T.C.9 | R.T.C.1<br>R.T.C.4 | |
| **Negligible** | | | R.T.C.5 | R.T.C.3 | |
| **Consequence / probability** | **<1%** | **1-30%** | **30-50%** | **50-70%** | **>70%** |

## 5.5. Schedule Risk

Risk with respect to the scheduling of the design process arises when certain processes take more time than initially planned. Delays usually accumulate, meaning having one delay at a given point in time, will lead to other delays later.

### 5.5.1. Risk Identification

The identified schedule risks are shown in Table 5.12.

**Table 5.12:** *Identified scheduling risks.*

| Risk ID | Risk | Cause/Situation | Consequence |
|---|---|---|---|
| **R.T.S.1** | Scarce materials & resources. | A rapid increase in demand for some resources can cause that materials become scarce. | If materials become scarce this can limit the availability and negatively influence the schedule. |
| **R.T.S.2** | Not passing airworthiness flight test. | It can occur that the aircraft does not satisfy all airworthiness requirements. | Alterations have to be made to the design which will negatively influence the schedule as this will take longer than initially planned. |
| **R.T.S.3** | Poor design changes management. | Incomplete considerations of impact that design changes have on the total design (lack of contingency planning). | The system or component has to be redesigned to satisfy the requirement. This can also influence other systems or components leading to a large increases in time scheduled. |
| **R.T.S.5** | Aircraft exceeding envisioned size. | Improper first estimate of aircraft size. | Resources are divided with an initial size in mind. If the size greatly differs from the initial estimation this can lead to extra iterations. This can change resource allocation and negatively influence the initial schedule. |
| **R.T.S.6** | Third party delivery delays. | The third party can have delivery problems or production issues. | A delay of a third party will cause an immediate delay for the delivery interval of the aircraft. |
| **R.T.S.7** | Lack of dedicated facilities. | Possibly facilities are need that do not yet exist. | This can cause huge delays as special dedicated facilities have to be build to manufacture the aircraft. |
| **R.T.S.8** | Additional testing required. | New technologies require possibly additional testing for airworthiness certification (ex. Hydrogen). | Applying for the test and testing itself can take a long time which extends the initial schedule. |
| **R.T.S.9** | Resource dependency. | A process whereby a bottleneck exists due to a required resource. | In the case many processes require a given resource to start, significant delays across all of them occur when this resource has a delay. This is an example of poor resource management. |
| **R.T.S.10** | Task dependency. | Improper initial scheduling making tasks highly depending on one another. | Process of finishing tasks is very slow and the schedule need to be extended to allow all tasks to be finished. |
| **R.T.S.11** | Ineffective communication between stakeholders. | Communication between various stakeholders always contains a risk of misalignment of information. | Misunderstandings can lead to required additional explanations and this per definition comes at the cost of extra time, together with mistakes that need to be redone. |
| **R.T.S.12** | Manufacturing mistakes. | Improper use of tooling or machines. | The component has to be made again which can take extra time. As components are produced in batches the consequences can be limiting. |

### 5.5.2. Risk Assessment and Prioritisation

To depict the risks and their impact visually, Table 5.13 was created. On its horizontal axis the probability of an event is shown in percentage (i.e. multiplied by 100) and the impact of the event on the vertical axis. Using Table 5.13, different risks could be ranked. This ranking is shown in Table 5.14.

**Table 5.13:** *Schedule risk matrix.*

| | | | | | |
|---|---|---|---|---|---|
| **Catastrophic** | R.T.S.5<br>R.T.S.7 | R.T.S.2 | | | |
| **Critical** | | R.T.S.3 | R.T.S.11 | R.T.S.1<br>R.T.S.6 | |
| **Significant** | | | | | |
| **Marginal** | R.T.S.10 | R.T.S.9 | | R.T.S.8 | |
| **Negligible** | | | R.T.S.12 | | |
| **Consequence / probability** | **<1%** | **1-30%** | **30-50%** | **50-70%** | **>70%** |

**Table 5.14:** *Schedule risk prioritisation table.*

| Rank | Risk ID | Score | Rank | Risk ID | Score |
|---|---|---|---|---|---|
| **1** | R.T.S.1 | 16 | **8** | R.T.S.5 | 5 |
| **2** | R.T.S.6 | 16 | **9** | R.T.S.7 | 5 |
| **3** | R.T.S.11 | 12 | **10** | R.T.S.9 | 4 |
| **4** | R.T.S.2 | 10 | **11** | R.T.S.12 | 3 |
| **6** | R.T.S.3 | 8 | **12** | R.T.S.10 | 2 |
| **7** | R.T.S.8 | 8 | | | |

### 5.5.3. Risk Mitigation

In Table 5.15, mitigation methods are presented for the high and medium risks. After mitigating those risks, their location in the risk matrix changes. Table 5.16 shows the new location, and thus their new probability of occurrence and their new impact.

**Table 5.15:** *Mitigation strategies for scheduling risks.*

| Risk ID | Strategy | Method | New / Old Score |
|---|---|---|---|
| **R.T.S.1** | Accept | Ways to mitigate this risk like having alternative materials for important components of the aircraft or storing some backup parts will dramatically increase the cost. | 16/16 |
| **R.T.S.6** | Accept | The only way to mitigate this risk would be to build a stock of the materials and products bought from third parties. This would however significantly increase the unit costs of the aircraft, making it indefeasibly. | 16/16 |
| **R.T.S.11** | Reduce | Setting up very clear and very accurate stakeholder requirements will reduce the chances of this risk occurring. This will enable the design to be in line with the views of the stakeholders from the very beginning, also reducing the need for communication with the stakeholders later in the design. | 8/12 |
| **R.T.S.4** | Reduce | Building in some safety margin into the production scheduling for the aircraft produced in the early phase will reduce the chance of the risk occurring. The risk of production delay is especially likely at the very beginning of production because the process is not yet optimised by then, increasing the chances of delays. | 6/9 |
| **R.T.S.3** | Reduce | Setting clear requirements for all the different subsystems, and by performing thorough verification of their function, the chance of the risk occurring is reduced. | 4/8 |
| **R.T.S.8** | Reduce | This risk can be mitigated by ensuring that already certified technologies are used when possible. This means the number of technologies that need to be tested is reduced to a minimum, also reducing the impact on the progress of the total design. | 4/8 |
| **R.T.S.5** | Reduce | By properly doing the initial class I and class II weight estimations, the rough size of the aircraft will be clear early in the design. By making sure that, if at that point the size of the aircraft exceeds expectations, and proper design choices are made to bring the size back down, the impact of the risk can be reduced. | 3/5 |
| **R.T.S.7** | Reduce | Again, this risk can be mitigated by using as many of the shelf options as possible. | 4/5 |

**Table 5.16:** *Mitigated schedule risk matrix.*

| | | | | | |
|---|---|---|---|---|---|
| **Catastrophic** | R.T.S.2 | | | | |
| **Critical** | R.T.S.7<br>R.T.S.3 | R.T.S.11 | | R.T.S.1<br>R.T.S.6 | |
| **Significant** | R.T.S.5 | R.T.S.4 | | | |
| **Marginal** | R.T.S.10 | R.T.S.9 | | | |
| **Negligible** | | | R.T.S.12 | R.T.S.8 | |
| **Consequence / probability** | **<1%** | **1-30%** | **30-50%** | **50-70%** | **>70%** |

## 5.6. Programmatic Risk

External factors could also be a source of considerable risk. These risks are referred to as programmatic risks. It is important to note that programmatic risks (external) ultimately feed into one of the other three risk categories (internal).

### 5.6.1. Risk Identification

The programmatic risk will be identified with ”R.T.P”. For each risk a small explanation of the cause and consequence is given which is stated in Table 5.17.

**Table 5.17:** *Identified programmatic risks.*

| Risk ID | Risk | Cause/Situation | Consequence |
|---|---|---|---|
| **R.T.P.1** | Regulatory changes. | EASA or the FAA can change the flight regulations for use of hydrogen and DP. | The aircraft could be grounded since it does not satisfy the regulations. Changes to the aircraft would be required, which can cost a lot of money. |
| **R.T.P.2** | Trade embargoes. | Trade embargoes can be used as economical sanctions because of geopolitical conflicts. | A trade embargo can limit the availability of a part or material, which causes problems in manufacturing. |
| **R.T.P.3** | Trade embargoes. | Trade embargoes can be used as economical sanctions because of geopolitical conflicts. | A trade embargo can limit the possibilities of selling an aircraft in a certain country, which would reduce the number of possible sales. This can cause the aircraft to be non-profitable. |
| **R.T.P.4** | Changing airport infrastructure. | The blended wing body will use pure hydrogen as fuel. | This will require the airport to change its fuelling infrastructure. Also the different shape needs possible alteration at the gate and hangars. |
| **R.T.P.5** | Lacking demand for aircraft. | Due to a lack of performance or strong competition there could occur a lack in demand. | This risk can cause the aircraft to not be profitable if the break-even point is not matched. |
| **R.T.P.6** | Government grants revoked. | Changes in government spending prioritisation can cause a lack of budget. | This could result in not having enough funding to complete the aircraft design. |
| **R.T.P.7** | Geopolitical conflicts. | Political indifference’s between governments. | Geopolitical conflicts can reduce the availability of resources, which can delay the production and reduce possible sales. |
| **R.T.P.8** | Supply chain issues. | This risk can be caused by scarce materials or productions issue at the third party. | Delayed components cause delayed manufacturing, which could result in fines. |
| **R.T.P.9** | Client changes requirements. | Developments within the aviation field may require different requirements. | Changing requirements require extra implementation time extending the schedule increasing cost. |
| **R.T.P.10** | New regulations for hydrogen and DP. | New aircraft designs for which no specific regulations are set up. | If regulations are changed this can may cause |

**Table 5.17 – continued from previous page**

| Risk ID | Risk | Cause/Situation | Consequence |
|---|---|---|---|
| **R.T.P.11** | Human factor | Passenger acceptability, vibrations, noise, etc. | New types of aircraft can ”scare” the passengers, reducing the acceptability of the aircraft. Also the comfort of the passenger can be jeopardised. |
| **R.T.P.12** | Future technology not ready on anticipated time. | Improper scheduling of third parties. | When future technology is not ready this can cause delays in the manufacturing of the aircraft. |

### 5.6.2. Risk Assessment and Prioritisation

A risk matrix can be created for the programmatic risk as for the previous two risk categories. The result is shown in Table 5.18.

The next step in the risk analysis is ordering the risks based on risk score to get a clear overview of the risks that could endanger the design of the aircraft. The risk score for each risk is shown in Table 5.19.

**Table 5.18:** *Programmatic risk matrix.*

| | | | | | |
|---|---|---|---|---|---|
| **Catastrophic** | R.T.P.3 | R.T.P.5 | | | |
| **Critical** | R.T.P.1 | R.T.P.7 | R.T.P.9<br>R.T.P.12 | | |
| **Significant** | | R.T.P.2<br>R.T.P.11 | | | |
| **Marginal** | | R.T.P.4 | | R.T.P.8<br>R.T.S.10 | |
| **Negligible** | R.T.P.6 | | | | |
| **Consequence / probability** | **<1%** | **1-30%** | **30-50%** | **50-70%** | **>70%** |

**Table 5.19:** *Programmatic risk prioritisation table.*

| Rank | Risk ID | Score | Rank | Risk ID | Score |
|---|---|---|---|---|---|
| 1 | R.T.P.9 | 12 | 7 | R.T.P.2 | 6 |
| 2 | R.T.P.12 | 12 | 8 | R.T.P.11 | 6 |
| 3 | R.T.P.5 | 10 | 9 | R.T.P.3 | 5 |
| 4 | R.T.P.7 | 8 | 10 | R.T.P.1 | 4 |
| 5 | R.T.P.8 | 8 | 11 | R.T.P.4 | 4 |
| 6 | R.T.P.10 | 8 | 12 | R.T.P.6 | 1 |

### 5.6.3. Risk Mitigation

While there are no programmatic risks that have devastating effects on the project, mitigation strategies still need to be applied. These mitigation strategies will be applied on risks classified as medium. As programmatic risks are risks created by third parties, internal (i.e. by the team) influence on those risks is limited. Most risks, however, could be mitigated with clear contractual agreements with third parties. Mitigation strategies are explained in Table 5.20. After mitigation, affected risks are moved within the risk matrix. This leads to a new risk matrix, which is shown in Table 5.21.

**Table 5.20:** *Mitigation strategies for programmatic risks.*

| Risk ID | Strategy | Method | New / Old Score |
|---|---|---|---|
| **R.T.P.9** | Reduce | Use a contract with the client to limit the probability of changing requirements. Also use meetings to inform the client on consequences of possible alterations of the design. | 8/12 |
| **R.T.P.12** | Accept | This has to be closely monitored by early on establishing relations with third parties. | 12/12 |
| **R.T.P.5** | Reduce | Performing a detailed market analysis of the demand and trends for the coming years the desired design can be constructed. This reduces the likelihood of occurrence. | 5/10 |
| **R.T.P.7** | Accept | As a team be aware of possible conflicts and are flexible in resources to change production locations if necessary. | 8/8 |
| **R.T.P.8** | Reduce | Create detailed contractual agreements on delivery intervals and consequences if the contract is not fulfilled. This reduces the probability of occurrence. | 6/8 |

**Table 5.20 – continued from previous page**

| Risk ID | Strategy | Method | New / Old Score |
|---|---|---|---|
| **R.T.P.10** | Reduce | Some regulations have to be assumed and safety factors have to be applied to these regulations to be safe in the future. | 4/8 |
| **R.T.P.2** | Reduce | Keeping in mind possible trade embargoes back up resources have to be researched to reduce the risk consequences. | 4/6 |
| **R.T.P.3** | Accept | If trade embargoes prevent the sale of the aircraft in certain countries it has to be accepted. | 5/5 |
| **R.T.P.1** | Reduce | Create a close collaboration with EASA and FAA to be aware of possible changes but also to gain control in regulatory changes. This reduces the probability as well as the magnitude of occurrence. | 3/4 |

**Table 5.21:** *Mitigated programmatic risk matrix.*

| | | | | | |
|---|---|---|---|---|---|
| **Catastrophic** | R.T.P.3<br>R.T.P.5 | | | | |
| **Critical** | | R.T.P.9<br>R.T.P.7 | R.T.P.12 | | |
| **Significant** | R.T.P.1 | | | | |
| **Marginal** | | R.T.P.2<br>R.T.P.4<br>R.T.P.10 | R.T.P.8 | | |
| **Negligible** | R.T.P.6 | | | | |
| **Consequence / probability** | **<1%** | **1-30%** | **30-50%** | **50-70%** | **>70%** |

## 5.7. Contingency

While most of the risks can be mitigated to reduce either the probability or consequence, some risks need to be accepted. Three of these risks; R.T.S.1, R.T.S.6, and R.T.P.12 are accepted but still have a to high risk score to neglect. Therefore, contingency plans have to be set up for these risks such that if they do materialise, a corresponding procedure is at bay. These procedures are explained in Table 5.22.

**Table 5.22:** *Mitigation strategies for programmatic risks.*

| Risk ID | Method |
|---|---|
| **R.T.S.1** | When the material becomes available, acquire additional stock to create a buffer. As a last resort, the components can be made out of a different material. |
| **R.T.S.6** | Introduce fines to the third party for late delivery. This gives the third party financial stimulation to deliver on time. Establish this in contractual agreements. |
| **R.T.P.12** | For all cutting edge technologies still under development or certification, a backup technology should be chosen. The effects of the backup technology on the design should be considered form the start, to avoid unpleasant surprises in the form of large design changes at the end of the design. |

# 6

# Propulsion

This chapter describes the design process of the propulsion subsystem. This includes sizing for the engines and the fuel cell as well as a weight and power estimation. Section 6.1 describes the engine design and Section 6.2 discusses BLI. In Section 6.3 the thrust for various operational phases are determined, while Section 6.4 describes the sizing method for the fuel cells. Section 6.5 includes an estimation for various additional electrical components. Next, Section 6.6 describes a method for a weight and power estimation. Finally, Section 6.7 and Section 6.8 include verification and validation procedures, respectively.

## 6.1. Engine Design for Distributed Propulsion

Distributed propulsion was chosen for the propulsion system of the Lightning2 aircraft [111]. Different possible engine configurations can be used such as turbofan engines, propellers, or ducted fans. In the case of Lightning2, it will generate power with the use of hydrogen fuel cells, which eliminates the turbofan option. In this case, ducted fans were chosen over propellers, because of the increase in static thrust and noise shielding [32].

Since the design should be finished within 5 years in compliance with STH.CUS.5, the best option is to buy most components off the shelf to satisfy the requirement. However, since distributed electric propulsion is a new concept within the aviation sector, it is not yet operational. Tests were done for electric propulsion on small aircraft such as the Sling 4, but not yet on large commercial aircraft. All designs for electric DP at the moment are still conceptual and only general data is available. After an extensive literature study not enough data was found for off-the-shelf electric ducted fans which could deliver the required thrust to size the propulsion system. However, since the propulsion system weight is required to create a weight estimation of the aircraft, an estimation had to be made for the propulsion system weight. Therefore, a preliminary sizing of the ducted fan was done on which an accurate weight estimation can be performed.

DP and BLI have many possible advantages but are all conceptual at the moment. Due to the limited resources, some parameters and assumptions were taken from literature. Since the design of the aircraft will be done using an iterative process, the DP was designed using a python script using multiple functions described below.

### 6.1.1. Aerodynamics

The first step in the design of the DP is establishing the aerodynamic properties of the ducted fans. Consequently, the ducted fan is simplified to the control volume shown in Figure 6.1. For the initial aerodynamic analysis, the effects of BLI are neglected but will be further investigated in Section 6.2. Due to the time constraint of the design, some assumptions are made to simplify the model:

- The inlet flow is assumed to be laminar, which results in a low Reynolds number.
- The reduction in the surface area because of the hub is neglected.
- The efficiencies are assumed to be constant with altitude.
- Air properties, such as the isotropic expansion factor and specific heat capacity, are assumed constant with altitude.
- The increase or decrease in inlet Mach number, because of the curvature of the airfoil, is neglected.

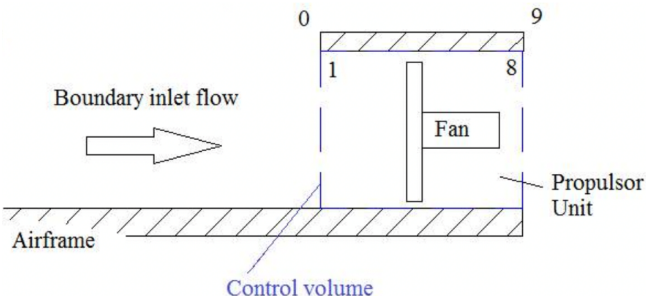


**Figure 6.1:** *The simplified control volume of the ducted fan [68].*

For the flow properties a standard python function called 'Atmosphere' is used. First, the total ambient pressure, temperature, and velocity need to be calculated using Eq. 6.1, Eq. 6.2, and Eq. 6.3, respectively [61].

$$p_{0,a} = p_a \left(1 + \frac{\gamma - 1}{2} M_a^2\right)^{\frac{\gamma}{\gamma - 1}} \tag{6.1}$$

$$T_{0,a} = T_a \left(1 + \frac{\gamma - 1}{2} M_a^2\right) \tag{6.2}$$

$$V_0 = M_a \sqrt{\gamma R T_a} \tag{6.3}$$

Next, the pressure and temperature in the inlet (location 1) are calculated. The total temperature at the inlet is equal to the total ambient temperature. However, the pressure changes and can be calculated with Eq. 6.4 [10]. The inlet efficiency $\eta_{in}$ is assumed to be 0.97 [61]. An additional correction factor has to be applied due to the duct pressure loss $\frac{\Delta P}{P}$, which is assumed to be 0.2 % [68, 66].

$$p_{01} = p_a \left[1 + \eta_{in} \left(\frac{T_{0,1}}{T_a}\right)\right]^{\frac{\gamma}{\gamma - 1}} \frac{\Delta P}{P} \tag{6.4}$$

The next location is location 8 in Figure 6.1, which is positioned behind the fan. To calculate the total pressure, a fan pressure ratio (FPR) has to be determined. A decrease in FPR results in a decrease in specific fuel consumption (SFC) [67]. A FPR below 1.25 is not interesting since this would result in possible severe inlet distortion which would affect the performance of the ducted fan [67]. Therefore, a FPR of 1.3 is chosen as the most optimum. It was assumed no inlet distortion has to be taken into account for the chosen FPR. The total pressure and total temperature can be calculated with Eq. 6.5 and Eq. 6.6, respectively [61]. The fan efficiency $\eta_{fan}$ is defined as how much power is translated into the air compared to the input power of the fan, which is assumed to be 97.5 % [38] and the isentropic efficiency is estimated to be 97.8 % [66].

$$p_{0,8} = p_{0,2} \cdot FPR \tag{6.5}$$

$$T_{0,8} = T_{0,2} \left(1 + \frac{1}{\eta_{fan}\eta_{fan,is}} \left[\left(\frac{p_{0,8}}{p_{0,2}}\right)^{\frac{\gamma - 1}{\gamma}} - 1\right]\right) \tag{6.6}$$

The power required by the fan can be calculated with Eq. 6.7.

$$P_{fan} = \dot{m} c_p (T_{0,8} - T_{0,1}) \tag{6.7}$$

Finally, the exit pressure, temperature, and velocity can be computed. First, it is required to determine whether the flow is chocked or not by calculating the critical pressure using Eq. 6.8. For a nozzle which is not choked, the exit pressure equals the ambient pressure ($p_e$=$p_a$) and temperature can be calculated with Eq. 6.9. The nozzle efficiency is determined from literature and assumed to be 0.97 [10]. The exit velocity can be calculated with Eq. 6.10. For a chocked nozzle the exit pressure equals the critical pressure ($p_e$=$p_{crit}$) and the temperature can be calculated with Eq. 6.11 and the exit velocity with Eq. 6.12.

$$p_{crit} = p_{0,8}\left[1 - \frac{1}{\eta_{nozzle}}\left(1 - \left(\frac{p_e}{p_{0,2}}\right)^{\frac{\gamma-1}{\gamma}}\right]\right) \tag{6.8}$$

$$T_e = T_{0,8}\left(1 + \eta_{nozzle}\left[1 - \left(\frac{p_{0,a}}{p_{0,8}}\right)^{\frac{\gamma-1}{\gamma}}\right]\right) \tag{6.9}$$

$$V_e = \sqrt{2c_{p,air}(T_{02} - T_e)} \tag{6.10}$$

$$T_e = T_{0,8}\left(\frac{2}{\gamma+1}\right) \tag{6.11}$$

$$V_e = \sqrt{\gamma R T_e} \tag{6.12}$$

### 6.1.2. Number of engines

Before sizing the ducted fans, the next step is determining the number of required engines. From literature, it was established that more than seven ducted fans do not reduce the noise of the propulsion system drastically [107]. However, there are a number of constraints that limit the lower and upper bound for the number of engines. First, there is a limited available wing span to place the ducted fans. In addition, current electric motors with limited available power have to be used. Lastly, fewer engines would increase the fan diameter and therefore decrease the possible beneficial effects of BLI. However, due to the other criteria, the overall objective is to minimise the number of ducted fans [67, 68, 38].

The number of engines is established using an integrative process starting at seven engines. Next, it is checked whether the thrust requirements for all flight phases can be satisfied. If not, the number of engines is increased until an engine configuration with satisfies the thrust requirements occurs.

### 6.1.3. Sizing

With the aerodynamic properties defined, the ducted fans could be sized to the most optimum shape. For simplicity it is decided that the ducted fans are sized individually first and later brought together in an array. From literature it was concluded that the top of climb will be the most demanding case for sizing. During this phase the velocity is 0.8 Mach with a rate of climb of 12.7 m/s at a cruising altitude of 10 952 m.

The maximum required thrust at sea level can be established from a loading diagram. Since the maximum required thrust is established at sea level, the thrust has to be corrected for altitude using Eq. 6.13.

$$T_h = T_0\left(\frac{\rho}{\rho_0}\right) \tag{6.13}$$

The most important parameter that should be taken into consideration during the sizing of the ducted fan is the mass flow as shown in Eq. 6.14 [2]. The required mass flow is depending on the required thrust and whether the nozzle is choked or not. If it is, an iterative process is needed to calculate the required nozzle area to satisfy the required mass flow. The nozzle area can be calculated using Eq. 6.15 [2].

$$\dot{m} = \frac{T_h - A_{noz}(p_8 - p_a)}{V_e - V_0} \tag{6.14}$$

$$A_{noz} = \frac{\dot{m}}{V_e \rho_e} \tag{6.15}$$

From the nozzle area, the required fan area can be calculated using Eq. 6.16 [1].

$$A_{fan} = \frac{\dot{m}}{p_8 M_8 A_e} \frac{1}{\left(1 + \frac{\gamma-1}{2}M_8^2\right)^{\frac{1+\gamma}{2(1-\gamma)}}} \sqrt{\frac{RT_{0,8}}{\gamma}} \tag{6.16}$$

From the fan area, the fan diameter can be established. While the sizing of the propulsion system is done to get an accurate weight estimation, the number of fans has to be established to evaluate the noise. From literature, it

was established that eight fan blades is optimal for the required thrust and to limit the noise [51]. With the fan diameter the rotational speed of the fan can be calculated with Eq. 6.17 [67]. The tip speed of the fan blades can be calculated with Eq. 6.18.

$$n = \frac{\sqrt{T_{0,a}}}{\pi D_{fan}}(2227.9\ FPR - 1941.2) \qquad (6.17)$$

$$V_{tip} = D_{fan}\pi\frac{n}{60} \qquad (6.18)$$

Finally, the duct can be sized using the fan size. For the inlet, it is assumed that the diameter of the inlet is equal to the diameter of the fan [115]. The length of the duct can be calculated with the assumption that the fan is located at $\beta = 35\%$ of the duct length [61] and that the hub should house the electric motor and inverter which are discussed in Section 6.5. A hub-to-tip ratio of 0.3 is taken [67]. For the length of the motor is assumed to be 1.75 the radius of the fan [101]. In Eq. 6.19 $D_i$ is the inlet width of the nacelle and $\phi$ is assumed to be 0.5 [115]. The inlet should be designed to diffuse the inlet flow to subsonic speeds. It should be taken into account that different FPRs result in different engine dimensions. A higher FPR will result in a smaller fan diameter and therefore a smaller nacelle.

$$D_n = D_i + 0.06\phi l_n + 0.03 \qquad (6.19)$$

## 6.2. Boundary Layer Ingestion

BLI refers to engine placement whereby the intake air consists of air from the boundary layer that develops over the aircraft. This air has a lower velocity due to surface drag. A lower entry velocity means that the engines have to work less to provide the same thrust. This is beneficial as it lowers fuel consumption. However, BLI has its share of associated difficulties. Most notably is the fact that airflow in the boundary layer is distorted. This distortion exerts stress on the fan blades requiring them to be tougher, therefore heavier and more expensive. This distortion effect can be slightly relieved through careful design of the engine intake[1].

A DP system compared to the conventional two engines on an A320 directly insinuates smaller engines. This suggests a larger portion of the engine intake area is placed into the boundary layer. Literature points to the fact that DP combined with BLI can lead to an increase in fuel consumption [57], which is the polar opposite of what the design strives to achieve. A plot of fuel consumption with N number of engines compared to the case of three engines non-BLI propulsion is shown in Figure 6.2.

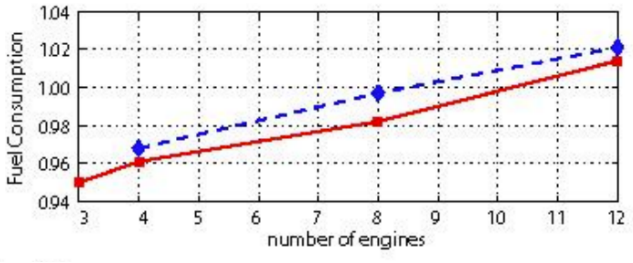


**Figure 6.2:** *Fuel consumption with BLI for varying number of engines [57].*

The red and blue lines indicate the optimistic and pessimistic intake total pressure losses, respectively [57]. Even when focusing on the optimistic estimate, the fuel consumption is higher for ten or more engines compared to the base case where three non-BLI engines are assumed.

In the same report, admittedly, the benefits of DP are reiterated, namely that it does provide lateral direction control (which is difficult to achieve otherwise in a blended wing body) [57]. For this design, a DP will remain the choice due to the strict noise requirements. To estimate the effect of BLI, a preliminary analysis is performed. The applicability of BLI is heavily dependent on whether the engine or a significant section is placed in the boundary layer.

[1] `https://www1.grc.nasa.gov/aeronautics/bli/` - Accessed: 28-05-2022

In the propulsion system simulation model, the thrust is quantified by taking the free-stream velocity as the air entering the engine at station 0 in Figure 6.1. This is an oversimplification since it neglects the viscous effects in the vicinity of the wing/body (boundary layer), but it is justified to make this estimation due to the preliminary status of the analysis at this point.

On the 25th of May, an expert, T. Sinnige, gave input on the considerations of BLI. The outcome of the discussion is discussed hereafter. The boundary layer can impact the actual velocity of the air that enters the engine and will be analysed here. Firstly, close to the surface of the aircraft the air is subject to viscous effects that slow down the airflow. To provide an initial indication of the viscosity effects of the boundary layer, an estimation of the size of the boundary layer at the engine position location must be made. Using XFLR with the wing airfoil, engine location, and airspeed as input, a preliminary estimation of the boundary layer development of the approximated wing can be generated. The boundary layer thickness at the engine location (Eq. 6.20) can be compared to the fan diameter to determine the portion of the engine that is placed in the boundary layer according to Eq. 6.21 [2] and Eq. 6.22.

$$BLI_h = \frac{\delta}{D_{engine}} = \frac{\delta}{2R_{engine}} \tag{6.20}$$

$$A_{BLI} = R^2 cos^{-}1(\frac{R-h}{R}) - (R-h)\sqrt{2Rh-h^2} \tag{6.21}$$

$$BLI_A = \frac{A_{BLI}}{A_{engine}} \tag{6.22}$$

If a 'significant' portion of the engine intake area is positioned in the boundary layer, the effects of BLI should be taken into account in the propulsion system design in terms of additional efficiency factors and weight penalties [68]. Using Eq. 6.22, it was determined that the area ratio is equal to 4.88 %. This means the effects of BLI can be neglected since they are insignificant.

## 6.3. Thrust During Various Operational Phases

As mentioned previously, the ducted fans are sized for the most demanding flight condition which is top of climb. However, the propulsion system should also be able to provide enough thrust during the other flight phases. Due to changes in atmospheric properties with altitude, the performance of the ducted fans can be negatively influenced. The thrust is checked for the take-off, climb, and cruise phases. The required thrust during each phase is obtained using a thrust setting which is shown in Table 6.1.

Since the atmospheric properties constantly change during climb a general average altitude has to be taken for which the climb thrust is evaluated. This is done by plotting the weighted density ($\rho/\rho_0$) against the altitude up to cruising altitude and establishing the altitude for which the area underneath the graph on both sides is equal. This altitude was determined to be 3 952 m.

**Table 6.1:** *Thrust setting and velocity during different flight phases.*

| Phase | Thrust setting [% of $T_{TO}$] | Mach [-] | Altitude [m] |
|---|---|---|---|
| Take-off | 100 | 0.25 [67] | 0 |
| Climb | 100 | 0.51 [3] | 3 952 |
| Cruise | $\frac{W_{cruise}}{L/D}\left(\frac{\rho_0}{\rho}\right)^{3/4}/T_{max}$ | 0.8 | 10 962 |

[2] `https://www.mathopenref.com/segmentareaht.html` - Accessed: 28-05-2022

[3] `https://abcnews.go.com/Travel/captain-fast-commercial-aircraft-climb/story?id=16886885` - Accessed: 28-05-2022

## 6.4. Fuel Cell Sizing

There are many different types of fuel cells available on market. Among them, there are the high-temperature proton exchange membrane fuel cells, low-temperature proton exchange membrane fuel cells, solid oxide fuel cells and phosphoric acid fuel cells that use hydrogen as fuel. A trade-off is made after collecting all the specifications for each type of the hydrogen fuel cells. It is found that the operating temperature for SOFC is between 500 °C to 1 000 °C [28] which is not suitable for aircraft. In addition, the unit cost for PAFC is around 3 000 US $/kW [96] because it does not yet have the possibility of massive reproduction. This leaves the option of proton exchange membrane fuel cells. Compared with PEMFC LT, the lifetime for PEMFC HT is only a quarter of it. The specification of each type of the fuel cell can be found in the following Table 6.2.

**Table 6.2:** *Fuel cell characteristics comparison.*

| | **PEMFC LT** | **PEMFC HT** | **SOFC** | **PAFC** |
|---|---|---|---|---|
| Operating temperature [°C] | 80 | 200 | 500-1 000 | 200 |
| Specific power [kW/kg] | 3 | 3 | 4 | 5 |
| Efficiency [%] | 45-60 | 40-50 | 45-60 | 40-45 |
| Price [USD$/kW] | 65 | 65 | 370 | 3 000 |
| Duration [h] | 20 000 | 5 000 | 40 000 | 40 000 |

Concluding from the trade-off, PowerCellution P Stack is selected as the final product for the fuel cell stack design. It has an output of up to 125 kW with only a mass of 42 kg. The product meets both stationary and mobile requirements and has also been validated by original equipment manufacturer (OEM). In addition, it is designed for low manufacturing costs and high volume production [4]. The specifications of PowerCellution P Stack are shown in Table 6.3.

**Table 6.3:** *Fuel cell specification from PowerCellution.*

| **MaX power [kW]** | **Cell count** | **Dimensions** | **Weight [kg]** | **Operational lifetime** | **Fuel quality** |
|---|---|---|---|---|---|
| 125 [5] | 455 | 420 x 582 x 156 mm | 42 | 20 000 h | Pure hydrogen |

The efficiency of the fuel cells is about 57 % [11] which can be calculated using Eq. 6.23. For the other 43 % of the energy, it is estimated about 30 % is converted into heat, 7 % is counted for the use of BoP global energy and the rest is H2 purge energy loss[6].

The fuel cells are sized for top of climb which requires the maximum power. The take-off and climb phase only takes 14.4 minutes while the cruise phase takes 261 minutes. Therefore, during the majority of the flight not all fuel cell stacks have to deliver power. A certain number of fuel cells can be turned off during the cruise phase such that the fuel cells can deliver the required power with optimum efficiency. By changing which stacks are turned on during cruise the operational lifetime of the fuel cell stacks can be extended significantly. A fuel cell stack only needed to be used during cruise around one every three flights.

Finally, the number of stacks is determined using the power required during take-off, which is derived for the thrust required during climb. This creates a redundancy which is further explained in Subsection 12.3.1.

$$\text{Hydrogen amount [kg]} = \frac{P \cdot t}{\eta_{FC} \cdot LHV} \tag{6.23}$$

## 6.5. Other Propulsion Components

Besides the ducted fans and the fuel cells, other components have to be taken into consideration to design the propulsion system. This system will require electric power and add weight to the propulsion system. The most

[4] `https://powercellution.com/p-stack/` - Accessed: 28-05-2022

[6] `https://blogs.sw.siemens.com/simcenter/evaluate-the-energetic-performance-of-a-fuel-cell-electric-vehicle-with-system-simulation/` - Accessed: 28-05-2022

important components that should be taken into consideration are discussed in this section. Hydrogen feeding system is for now neglected because of the high complexity of the system.

### 6.5.1. Electric Motor

One of the most important components for the propulsion system and a limiting factor for sizing the ducted fans is the electric motor which drives the fan. It is beneficial to have a very powerful motor since this reduces the number of required fans and decreases the propulsion system weight. Currently, the most promising electric motor is the Wright Electric Motor which can produce 2 MW of power with a power density of 10 kW/kg and an efficiency of 96 % [7]. The two motors can be connected in series to create an electric motor with a total power of 4 MW. Each 4 MW motor combination drives one fan. The motor requires a high-frequency input and therefore an inverter has to be added. The electric motor can be purchased with an optimised inverter to obtain the required voltage input for the motor which has a power density of 30 kW/kg and an efficiency of 99.5 % [8].

The electric motor as well as the inverter are in their final stages of development and are planned to go through flight certification within the next two years. Wright is planning to implement the electric motor in their own Wright Spirit in 2026 [9].

### 6.5.2. Compressor

The PEM fuel cells use oxygen for the chemical reaction. The required oxygen can be delivered to the fuel cell using an air feeding system. For optimum efficiency of the fuel cell, the air has to be at 1 bar when entering the fuel cell [10]. During cruise, this requires the inlet air to be compressed using a compressor. The compression will be done using an electrical-driven centrifugal compressor. The air mass flow required for the fuel cell is calculated for the top of climb (TOC) power requirement at cruising altitude with Eq. 6.24, where pd is the power density and $\eta_{comp}$ is the compressor efficiency which was set to 0.7 [108]. From the mass flow the power required by the compressor can be calculated with Eq. 6.25 [108].

$$\dot{m}_{air} = \frac{P_{tot,TC}}{\frac{pd_{hyd}}{9} - \frac{c_p T_h}{\eta_{comp}} \left( \left( \frac{p_{FC}}{p_h} \right)^{\frac{\gamma-1}{\gamma}} - 1 \right)} \tag{6.24}$$

$$P_{comp} = \frac{\dot{m}_{air} c_p T_h}{\eta_{comp}} \left( \left( \frac{p_{FC}}{p_h} \right)^{\frac{\gamma-1}{\gamma}} - 1 \right) \tag{6.25}$$

### 6.5.3. Cooling System

Since about 30 % of the total energy produced will be converted to thermal energy as discussed in the previous section, the fuel cell will generate a tremendous amount of heat. The operational temperature for the selected PEMFC is 80 °C. If the temperature reaches the design limit, the stack components will be damaged [92]. So it is crucial to find a feasible cooling strategy to maintain the stack temperature at a certain level. An air cooling system is suitable for low power generation, however, a parasitic drain is introduced for high power generation, so liquid cooling should be applied [92]. A schematic diagram is made to demonstrate the cooling process for the hydrogen fuel cell in Figure 6.3.

[7] https://techcrunch.com/2021/09/07/wright-tests-its-2-megawatt-electric-engines-for-passenger-planes/?guce_referrhttps://medium.com/@jeff_60994/wright-has-begun-testing-our-2-mw-aviation-grade-motor-for-transport-category-zero-emissions-79cb01c2cfc6 - Accessed: 02-06-2022

[8] https://www.electrive.com/2021/05/10/wright-electric-presents-inverter-system-for-electric-aircraft/ - Accessed: 02-06-2022

[9] https://www.weflywright.com - Accessed: 02-06-2022

[10] https://www.datocms-assets.com/36080/1636022110-p-stack-v-221.pdf - Accessed: 02-06-2022

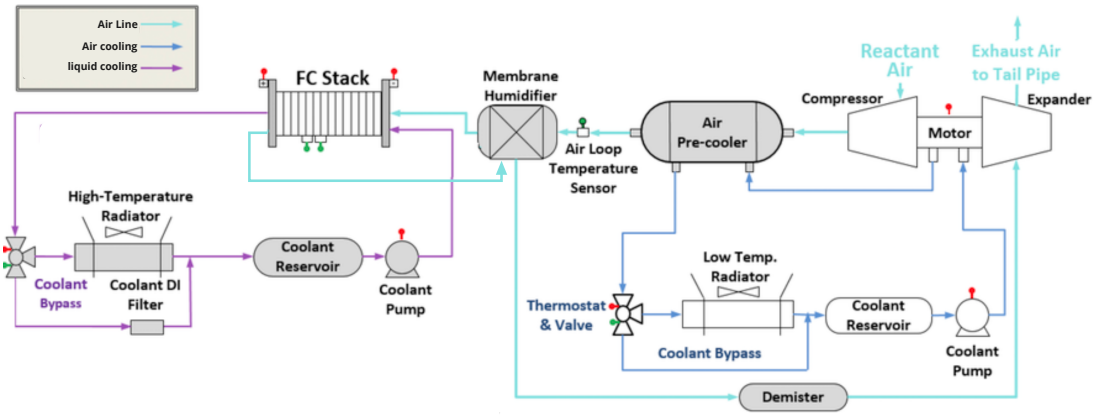


**Figure 6.3:** *The fuel cell stack and balance of plant, including liquid cooling and air cooling systems [110].*

Liquid cooling and an air cooling system are implemented for the design. Ethylene glycol, with a specific heat capacity of 2.433 J/g °C, is chosen as the coolant for the liquid cooling system. A deionizer is added to deionize the water produced by the fuel cell, which can then be reused to mix with the coolant for corrosion protection. The rest of the produced water will be exhausted through a tailpipe. The coolant will be pumped from the tank to circulate the cooling process.

An air cooling system is also implemented for the design. Apart from some same components used in the liquid cooling system, it also consists of a membrane humidifier, air pre-cooler, expander, motor, compressor, and a demister. Air that comes from the engine first passes through a compressor to circulate the air in the system under pressure and an air pre-cooler to further decrease the temperature before going through the membrane humidifier, which is used to provide humidity to the incoming oxidant, preventing the fuel cell membrane becomes too dry, resulting in poor fuel cell function or even failure[11]. Then air looped out of the fuel cell will go through a demister, which is used to separate droplets of liquid from flowing gaseous media before passing an expander and exhaust from the tailpipe.

### 6.5.4. Batteries

While batteries have a very low specific energy and add a weight penalty to the aircraft, they are needed for emergency power. During the loss of electrical power, the batteries should be able to provide DC power to back up the avionics and lighting system [116]. To get an initial weight estimation for the batteries the main batteries of an A320 are considered which weigh 31 kg [116]. For the A320 batteries with a specific energy of 250 Wh/kg where used [116]. The specific energy of lithium-ion batteries are expected to increase to 400 Wh/kg in the coming 5 years [71]. The additional weight of the batteries can be neglected compared to the overall weight of the propulsion system.

## 6.6. Weight and Power Estimation

For the weight estimation of the ducted fans, a weight relationship between the duct geometry and weight is used [94]. It is assumed that the ducts are both made of aluminium. Aluminium is chosen since it has a relatively low density, is cheap, and is easily recyclable at the end of life. For the fans, it is chosen to use graphite epoxy composite as this reduces the weight by around 75% compared to an aluminium fan [4].

An additional 500 kW is added to the required power of the fans to account for the power of the other subsystems in the aircraft [71]. Multiplying all the efficiencies of the propulsion components will give an efficiency of 40.7 %. After the iteration has been performed the required power per propulsion system component and the corresponding component weight can be calculated. The total required power that needs to be generated by the fuel cells is during take-off and equals 37.4 MW. The total power during each phase is shown in Table 6.4 Summing all the weights of the propulsion system gives a total propulsion weight of 23.0 tons.

[11] `https://www.fuelcellstore.com/fuel-cell-testing/fuel-cell-humidifiers` - Accessed: 02-06-2022

**Table 6.4:** *Total power required during different flight phases.*

| Component | Weight relation | Total weight [tons] | Efficiency [-] |
|---|---|---|---|
| Electric motor | 10 [kW/kg][12] | 4.00 | 0.96 [119] |
| Electric inverter | 30 [kW/kg][13] | 1.33 | 0.995 [13] |
| Cables | 0.007 [kg/m][22] | 1.74 | 0.996 [119] |
| Compressor | 0.6 $W_{cooling}$[108] | 0.62 | 0.75 [62] |
| Fuel cell | 3 [kW/kg] [13] | 12.55 | 0.57 [11] |
| Cooling system | 0.124 $\cdot W_{FC}$ [108] | 1.02 | n/a |
| Fan | [94] | 1.72 | n/a |

**Table 6.5:** *The total power required for the different flight phases.*

| Phase | Total power [MW] |
|---|---|
| Take-off | 37.4 |
| Climb | 31.9 |
| TOC | 34.2 |
| Cruise | 4.9 |
| Descent | 8.4 |
| Loiter | 5.5 |

## 6.7. Verification of the Propulsion Subsystem

Before the propulsion system code could be used for the iteration, a verification of the code had to be done. The first performed verification test is unit testing. During unit testing, the code is split up into smaller parts, on which different tests are applied as shown in Table 6.6. During the hand calculation unit test, a mistake in the simulation was found. The altitude input for the function ”altitudeThrustChecker” was incorrect which influenced the output of the simulation. After the alteration, all the unit tests passed.

**Table 6.6:** *Unit tests propulsion system.*

| Identifier | Test | Final result |
|---|---|---|
| V.PS.U.1 | Visual inspection | Pass |
| V.PS.U.2 | Hand calculations | Pass |
| V.PS.U.3 | Unit decomposition | Pass |

With the unit testing complete, subsystem tests could be performed on the simulation. This is done with the use of benchmark testing. For the sensitivity test, a design parameter was altered to check if the change in outcome makes sense. For example, an increase in required thrust would require more ducted fans, which was indeed the case. For the extreme value test, negative and very large values are fed into the simulation to see its behaviour. Finally, a sanity check was performed on the outputs of the simulation. The simulation passed all benchmark tests.

**Table 6.7:** *Subsystem verification tests.*

| Identifier | Test | Final result |
|---|---|---|
| V.PS.B.1 | Sensitivity test - Altitude | Pass |
| V.PS.B.2 | Sensitivity test - Thrust required | Pass |
| V.PS.B.3 | Sensitivity test - FPR | Pass |
| V.PS.B.4 | Extreme value test - Thrust required | Pass |
| V.PS.B.5 | Sanity Check | Pass |

## 6.8. Validation of the Propulsion Subsystem

While the simulation passed all verification tests, it should be checked if the model is correct and accurate. The method and level of detail in the simulation were deemed correct by Tomas Sinnige (personal communication, 25th of May 2022), an expert within the field of DP, considering the amount of time available. As currently no blended wing bodies exist with hydrogen power DP, results of the simulation are checked with literature.

[12] `https://medium.com/@jeff_60994/wright-has-begun-testing-our-2-mw-aviation-grade-motor-for-transport-category-zero-emissions-79cb01c2cfc6` - Accessed: 03-06-2022

[13] `https://www.datocms-assets.com/36080/1636022110-p-stack-v-221.pdf` - Accessed: 03-06-2022

NASA's N3-X is a blended wing body with DP for which sufficient data is available to perform validation with [68].

The ducted fans are sized for the aerodynamic design point chosen to be at an altitude of 30 000 ft [68]. To compare the simulation result with the paper, some input parameters such as MTOW, design altitude, and Thrust had to be changed accordingly. During the validation of the model, a large difference between the model's fan diameter and the N3-X fan diameter was observed ($\approx$ +30%). This difference could be traced back to the required thrust calculation per ducted fan. An assumption was made, which neglected the thrust contribution of a choked nozzle. However, during the validation, it was established that the contribution of the choked nozzle could not be neglected. The model was altered, after which it gave more similar results compared to the N3-X, as shown in Table 6.8.

While there are some signification deviations in the power required per fan and the mass flow, the results are deemed accurate enough for this stage of the design and the available resources. These deviations can be partly attributed to assumed parameters such as the efficiencies and assumptions. To increase the accuracy of the result a detailed flow simulation has to be performed in combination with a more elaborate engine performance analysis. For the weight and power estimation, the relationships are cross-referenced with other literature. By comparing the relationships, ambitious values could be identified and changed accordingly. After an extensive literature study, all parameters used in the simulation are deemed appropriate and accurate.

**Table 6.8:** *Validation of propulsion parameters [38].*

| **Parameter** | **Lightning2** | **N3-X** | **Difference [%]** |
|---|---|---|---|
| Number of engines [-] | 15 | 15 | 0.0 |
| Exit velocity [m/s] | 308.0 | 306.6 | 0.5 |
| Power per fan [MW] | 1.61 | 1.83 | -12.2 |
| Diameter fan [m] | 0.98 | 1.08 | -9.2 |
| Mass flow [kg/s] | 73.12 | 84.37 | -13.3 |

# 7

# Aerodynamic Design and Performance

In this chapter, the aerodynamic design and analysis of the Lightning2 aircraft are presented. Section 7.1 describes the general design philosophy and reasoning behind the design, then Section 7.2 outlines the planform design, evolution, and the main challenges during each step of the process. Section 7.3 presents the selection procedure for the wing and body airfoils. Section 7.4 presents the analysis procedure for the previously sized planform. Then, Section 7.5 explains the critical Mach number calculation method and Section 7.6 presents the method for calculation of aerodynamic loads. Then Section 7.7 and Section 7.8 describe verification and validation of the used methods and finally, Section 7.9 presents a summary of the final design and recommendations for further improvement.

## 7.1. Design Approach

The main challenge to be tackled when designing a blended wing body is the fact that both the ”blended fuselage” (later referred to as the body) and the wing produce a non-negligible amount of lift. This differs from the conventional design process where the lift generated by the fuselage is neglected in the conceptional design phase. In the case of a blended wing body, the fuselage has to be analysed as a lifting surface as well. Furthermore, as this specific design does not include a dedicated empennage for longitudinal stabilisation, more emphasis is placed on stability and control. Due to the unconventionality of the blended wing body, it might seem like a very opportunity-rich concept. In reality, however, this is not the case. Due to many contradicting requirements and constraints, the design space is much more limiting compared to a conventional tube-and-wing concept and each choice comes with penalties. The initial goal is to fit the payload and systems within the body. This is a challenge due to the limitations posed on the shape of the body. Once optimal accommodation of systems and internal volume utilisation is ensured, the aerodynamic properties of the body are analysed and added to the contribution of the main exposed wing area.

The body area was initially fixed by the cabin design and subsequently by other systems as well. On the other hand, a first estimate of the wing planform was generated with conventional methods [91, 85] from the Class I weight estimation. Features of this initial planform include a chosen aspect ratio, surface area, wingspan, taper ratio, sweep angles, thickness-to-chord ratio, etc. In the preliminary sizing of the planform, the defining parameters are the wing loading as chosen from the design point and the cruise Mach number. XFLR5 was used for the analysis of different airfoils as well as for an indication of the aerodynamic performance of the total aircraft. Since XFLR5 is primarily suited for low-speed simulations, all simulations were run at speeds of 100 m/s or below and the results were then converted to the appropriate speeds. It should be noted that XFLR5 results from the Wing and Plane Design module were used as an indication of trends and orders of magnitude. The actual performance of the planform was estimated using the DATCOM method [85].

Both the body and the reference wing evolved over the project following the design of other systems (i.e. optimised cabin, propulsion system, hydrogen tanks, etc.). Once all systems were accommodated within the body and the geometry was locked, this final planform was used as an input to the main design iteration such that a more efficient design could be obtained and all systems along with the corresponding parameters are taken into account properly.

## 7.2. Planform design

After the initial design point was chosen, the reference wing was generated using Class I sizing methods as described in Section 7.1. At this stage, the first challenge had already arisen: the surface area required for the body already exceeded the reference wing area. This implies that only the body by itself could produce more than sufficient lift to balance the aircraft's weight. This result is unreasonable due to the severe limitations on the geometry of the body. An additional challenge is that the high subsonic cruise Mach number requires low profile thickness but on the other hand, the fitment of systems and payload requires immense thickness.

As a solution to the former, an assumption was made that 35% of the cruise lift would be produced by the body and the remainder being left to the exposed wing. This initial assumption of the body producing the minority of the lift is deemed reasonable due to the limited geometry and aerodynamic properties of the body.[69]

Next, the body and reference wing were imposed on each other to create a new planform. Unfortunately, this planform is not feasible because the overlap between the body and the wing is large: 36.75 $m^2$ or 20.9% of the reference wing area. This would lead to a large reduction in the initially estimated lift. Since the wing is finite (and tapered), a 20.9% reduction of the surface does not mean a 20.9% loss of the lift but the majority of the lift will be lost. The situation is illustrated in Figure 7.1 where the blue indicates the body area and the green the overlap of area of the wing planform.

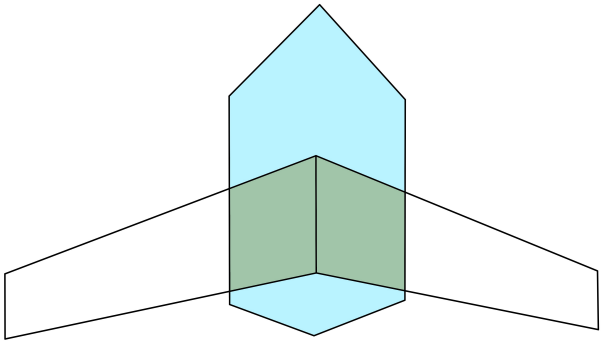

**Figure 7.1:** *Initial A/C configuration, not to scale.*

In addition, once the hydrogen tank was designed and the cabin cross-section was optimised, the fuselage volume had to be adjusted to accommodate these subsystems. This lead to an increase in fuselage area from 204.5 $m^2$ to 237.3 $m^2$. Furthermore, another design choice was made that it shall have no HLDs due to the lack of empennage to counter the resulting pitching moment arising from HLDs. Another consequence of the lack of empennage is the fact that pitch control surfaces have to be placed on the wing, thus having a lower moment arm.

All these considerations meant the general planform needed to be redesigned compared to the one made based on Class I. The wingspan and the total surface area were increased from 35.2 m to 44 m and from 304.8 $m^2$ to 519 $^2$, respectively. In addition, a kink was added to the wing to provide even more surface area. The quarter chord sweep was increased substantially from 32.3°to 47.1°to increase the moment arm for control surfaces. The resizing was done using XFLR5's Plane and Wing Design module. For the redesign to be executed in a structured manner, a few key parameters were tracked after each parameter was changed. Those parameters, among others, include the $C_M - \alpha$ curve, cruise and maximum L/D ratio as well as the spanwise lift and centre of pressure position distributions.

It should be noted that this planform is also suboptimal. The total surface area amounts to 519 $m^2$. This results in a very low wing loading, 906 $N/m^2$ which means an inefficient design. While it is true that blended wing bodies have generally twice as low wing loading compared to a conventional aircraft due to the larger lifting area [75]. However, a wing loading this low was deemed unacceptable.

With the previous discussion in mind as well as the fact that some system parameters were updated, a third, updated and optimised version of the planform was necessary. As stated, the main issue with that last design

version is the very high wing area and the resulting low wing loading. In order to further lower the total wing area, which also includes the body area, the body area was further optimised. By lowering the chord of the body and by increasing the thickness-to-chord to maintain the required internal cabin height, the area of the body was decreased from 237.5 $m^2$ to 211.3 $m^2$. Furthermore, the exposed wing area was also reduced in order to increase wing loading. However, there are limits to how far this area could be reduced. This limit is primarily imposed by the fact that there has to be enough space for the distributed propulsion system to be implemented. Also, since no HLDs shall be used, a relatively large wing area is required. In conclusion, these requirements were translated into a exposed wing area of 179.6 $m^2$, a total area of 390.9 $m^2$ and a span of 36 m. With that value, the wing loading reached a more reasonable value of 1240 $N/m^2$. After this decrease in area and increase in wing loading, the design was deemed optimised enough for it to be used as the starting point for the overall design iteration. The final platform, that is, after general design iteration convergence is shown in Figure 7.2 and Figure 7.3.

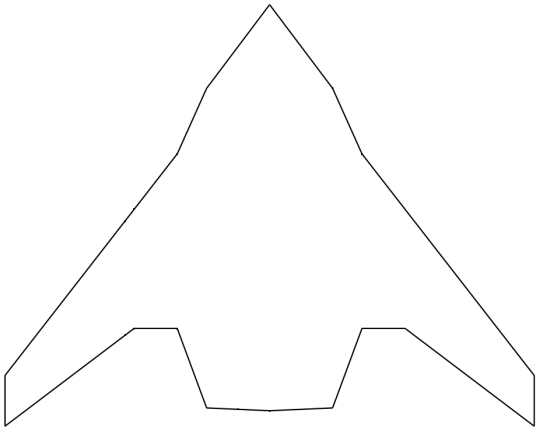

**Figure 7.2:** *Top view of the planform.*

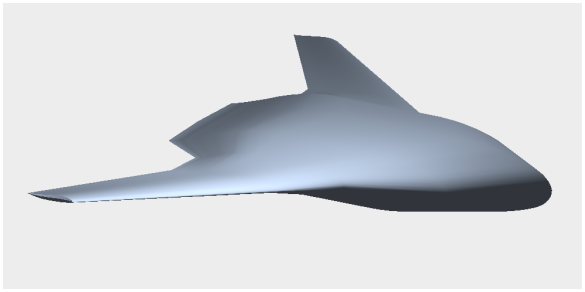

**Figure 7.3:** *Isometric view of the planform.*

The parameters which are relevant for the aerodynamic analysis of the planform are presented in Table 7.1.

**Table 7.1:** *Planform parameters, relevant for aerodynamic analysis.*

| **Parameter [Units]** | **Value** | **Note** |
|---|---|---|
| Aircraft Wing Loading [$N/m^2$] | 2133 | Cruise weight divided by $S_{ref}$ |
| $C_{L_{des}}$ [-] | 0.21 | Cruise lift coefficient |
| $C_{l_{des_{body}}}$ [-] | 0.10 | Body section design lift coefficient |
| $C_{l_{des_{wing}}}$ [-] | 0.29 | Wing section design lift coefficient |
| Body Lift [%] | 30% | Fraction of total cruise lift |
| $S_{ref}$ [$m^2$] | 373.58 | Aircraft surface area without the blending |
| Blow Factor [-] | 1.83 | Estimate of lift increase due to engine blow |

A few important notes must be made on the values of Table 7.1. Firstly, the wing loadings are calculated from cruise and maximum take-off weights and w.r.t. reference area. Secondly, the assumption on body-to-wing lift distribution is revised here: the lift required of the body is only 30% of the cruise lift instead of the initial 35%. This reduction is explained by the fact that a modified airfoil with unknown real-world performance is used for the body. Further, by reducing body wing loading, the cruise angle of attack could be reduced. A lower angle of attack of the body means a lower angle of attack for the cabin which improves passenger comfort [19]. Further, an alleviating factor for the wing design is the placement of engines above the wing. 50.3% of the wingspan is blown over by fan exhaust flow. Further, the lower pressure in front of the inlet of the motors increases the lift produced by the wing substantially and delays separation [56]. To account for that the lift produced by the wing is multiplied by a blow factor of 1.83. This means that in reality only 54.5% of the lift needs to come from the actual wing planform and the rest is taken care of by the propulsion system. This factor is a conservative estimate based on [1] and [27].

For subsequent analysis, especially for the airfoil selection and critical Mach number checks, a distinction between body and wing is necessary. More specifically, it is important that separate values for section design lift coefficients with respective angles of attack are calculated. Evidently, Table 7.1 presents $C_{l_{des}}$ for the body and the wing but an explanation of how these values were calculated is necessary. Once average cruise wing loading and reference surface area are calculated, average cruise weight may be obtained. Under the assumption that in cruise lift equals weight, cruise lift may be obtained as well.

$$W_{cruise} = (W/S_{ref})_{cruise} S_{ref} \quad (7.1) \qquad L_{cruise} = W_{cruise} \quad (7.2)$$

$L_{cruise}$ is the total lift required to balance the weight during cruise. Fortunately, the actual lift to be produced by the wing planform is substantially lower due to the previously introduced blow factor. In fact, lift produced by the wing needs to be only $L_{cruise}$/1.83. Now, with the assumption that 30% percent of this lift comes from the body, wing loadings for the body and the wing can be defined, namely:

$$(W/S)_{body} = \frac{0.30 L_{cruise}}{1.83 S_{ref}} \quad (7.3) \qquad (W/S)_{wing} = \frac{(1-0.30) L_{cruise}}{1.83 S_{ref}} \quad (7.4)$$

With these wing loadings, design lift coefficients can be defined for the two lifting surfaces separately:

$$C_{L_{des_{body}}} = \frac{(W/S)_{body}}{1/2 \rho V^2} \quad (7.5) \qquad C_{L_{des_{wing}}} = \frac{(W/S)_{wing}}{1/2 \rho V^2} \quad (7.6)$$

Where $\rho$ and $V$ are the cruise density and speed. In order for the low speed airfoil coefficients to be obtained, sweep and Mach number need to be accounted for. Eq. 7.5 and Eq. 7.6 could be modified:

$$C_{L_{des_{body}}} = \frac{(W/S)_{body}}{1/2 \rho (V cos(\Lambda_{LE_{body}})^2 \sqrt{1-M^2}} \quad (7.7)$$

$$C_{L_{des_{body}}} = \frac{(W/S)_{body}}{1/2 \rho (V cos(\Lambda_{LE_{body}})^2 \sqrt{1-M^2}} \quad (7.8)$$

From these Mach- and sweep- corrected coefficients and $C_l - \alpha$ curves from XFLR5, design angles of attack for the body and the wing could be estimated. With these values, airfoil and planform analysis could be conducted.

It should be noted that the presented procedure is a continuous process. After each planform change or design iteration the previously defined parameters are reevaluated and performance of the planform at hand as well as airfoil requirements are revised. The final values are presented in Table 7.2.

**Table 7.2:** *Body and Wing Design parameters.*

| Parameter | Body | Wing |
|---|---|---|
| Leading Edge Sweep [deg] | 53 | 52.12 |
| Cruise Mach Number [-] | 0.8 | 0.8 |
| Wing Loading [N/m2] | 617 | 1874 |
| $C_{L_{des}}$ [-] | 0.06 | 0.18 |
| $C_{l_{des}}$ [-] | 0.10 | 0.29 |
| AoA [deg] | 2.96 | 3.03 |

## 7.3. Airfoil Selection

Once an initial planform was generated it was time for proper sections to be chosen for the body and the outboard wing. The general procedure is the following: a few requirements for each section were identified, candidates that satisfy these requirements were identified, and after each design change or iteration compliance with these requirements was revised. These requirements include:

- For the body:

1. The section shall have thickness-to-chord ratio such that optimal fitment of cabin and hydrogen tanks is ensured.
2. The section shall have a design lift coefficient as close as possible to the one identified in Table 7.1.

- For the wing:
  1. The section shall be self-stabilising. More specifically, it shall provide the highest possible $C_m$ between an angle of attack of 0 and 15 degrees.
  2. The section shall have a design lift coefficient as close as possible to the one identified in Table 7.1.

It should be noted that this procedure significantly deviates from the conventional one, since no requirements have been set on section $C_d$ and $C_{l_{max}}$. The reason behind this is the fact that the requirements set were already severely limiting the pool of sections and therefore. If candidates satisfy these requirements, they are considered good enough for the present design.

Here, again the main challenge is the body. A thin airfoil would be ideal for the high cruise Mach number but it would result in an enormous chord in order to provide the required thickness which would result in high skin friction drag. As a result of this reasoning, a thicker airfoil with reasonable drag characteristics was sought. This leads to the NACA 6-series sections due to the presence of the so-called drag bucket in their drag polar. 6-series airfoils are also referred to as laminar airfoils as they encourage a laminar boundary layer over their surface which lowers skin friction drag and explains the drag bucket. Experimental drag polar of a laminar airfoil is presented in Figure 7.4.

The lowered, flat bottoms of the $C_d - C_l$ graphs in Figure 7.4 represent the aforementioned drag bucket. With the requirements of a wide drag bucket, maximum possible thickness-to-chord ratio, and a design lift coefficient that satisfies the cruise requirement for the body, the NACA $64_4$-221 airfoil was selected. However, in order to accommodate the cabin, this airfoil would still result in an excessive thickness and large underutilised volume due to its camber and top side curvature. The section as well as the resulting situation due to cabin fitment is illustrated in Figure 7.5.

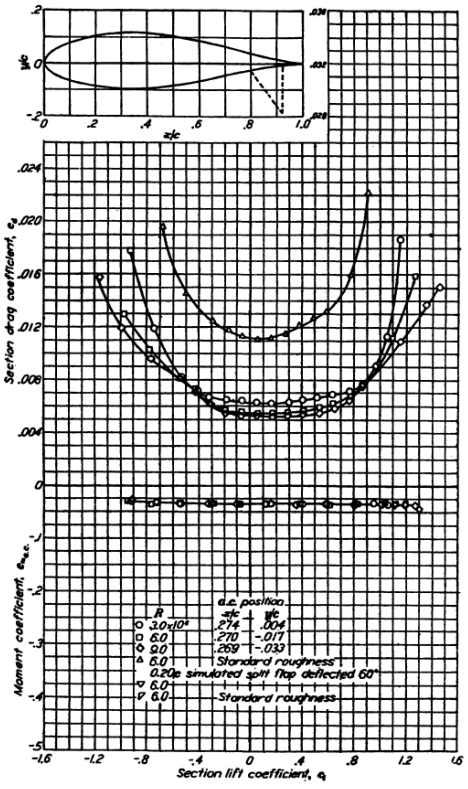


**Figure 7.4:** *Experimental plots of the NACA $63_4 - 221$ airfoil.[3]*

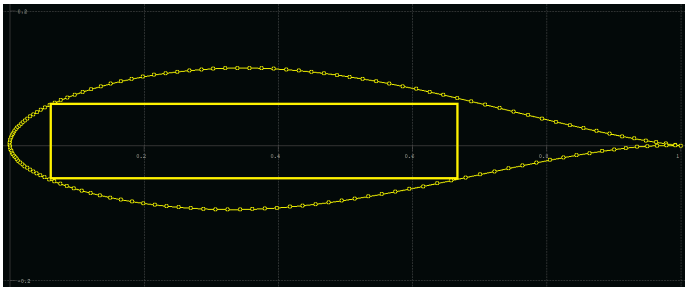

**Figure 7.5:** *NACA $63_4 - 221$ airfoil with cabin longitudinal cross-section fitted.*

The solution is a modification of the section such that volume is utilised optimally. This evidently, comes at the expense of aerodynamic performance but the approach was deemed worthwhile due to the relatively low

amount of lift required for this section. [69] The modifications were mainly reduction of camber and flattening of both top and bottom sides. Initially, only the top side was flattened and the camber was reduced slightly but further modifications were necessary, so the bottom was also flattened and thus, the camber was removed. As a by-product of this process, the thickness-to-chord was reduced from 21% to 18.1% which is beneficial. The final section is presented in Figure 7.6.

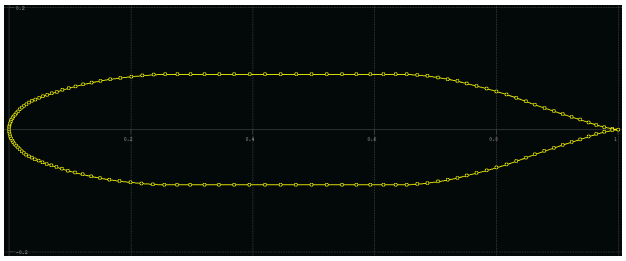

**Figure 7.6:** *NACA* $63_4 - 221$ *airfoil after modifications.*

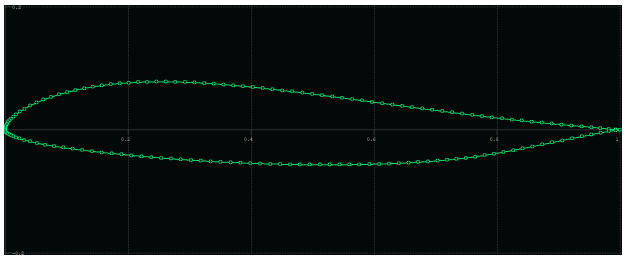

**Figure 7.7:** *Eppler 325 airfoil.*

It should be noted that the flattening of the top is only feasible due to the fact that engines are placed on top of the body. This configuration increases the lift produced by the wing substantially. Further, due to the lower pressure over the top surface created by the fans, separation is delayed[1, 56]. Thus, if engines were placed elsewhere, this manipulation would not have been possible.

For the outboard wing, the situation is different. No airfoil modifications have been made there, since the majority of the lift is to be produced by this wing, so a section with verified and reliable properties is sought. Further, a design choice was made not to design an empennage and therefore, a wing that is statically stable by itself is required. This limits the section pool to reflexed airfoils. The Eppler airfoils were found to be suitable. The selected candidates range from Eppler 325 to Eppler 343.[89], [41]. The final choice is shown in Figure 7.7.

This is the Eppler 325 airfoil. It has a thickness-to-chord of 12.65% and a moderate camber of 1.77%. All of the selected candidates have satisfactory performance in terms of lift, drag, and stall properties. The winner was chosen based on its superior stability characteristics, namely, it has the most positive $C_m - \alpha$ curve and therefore, the largest stability margin.

**Recommendations**

Even though the body section is expected to work in theory, further research on this subject is recommended. Ideally, a physical model of the airfoil and the whole configuration should be built such that the previously discussed features could be validated in a wind tunnel. If it turns out that the proposed body section does not work as intended, the use of a generic elliptical section is advised such that it provides optimal available volume utilisation. If a net lift deficit is introduced by changing the body section, wing twist distribution (or higher incidence angle w.r.t. body) could be introduced such that the outboard wing compensates for this deficit.

## 7.4. Aerodynamic Performance Analysis

Each planform needs to be analysed in terms of lift and drag generation such that it is certain that requirements are met. This section presents methods for lift and drag estimation, and critical Mach numbers calculation.

### 7.4.1. Wing Lift Estimation

There are few parameters of interest with respect to wing lift - namely wing lift curve slope, maximum lift coefficient, $C_{L_{max}}$, with its corresponding AoA, $\alpha_{max}$, as well as maximum and cruise L/D ratios. Unfortunately, $C_{L_{max}}$, with its corresponding AoA, $\alpha_{max}$ are possibly the two least reliable parameters of the whole design. The values are provided only for the sake of completeness and to provide an order of magnitude. In reality, not even windtunnel experiments are reliable enough and those values are most reliably obtained during test flights with real aircraft.[85] L/D on the other hand, is a measure of aerodynamic efficiency and as such can be used for estimation of the aerodynamic performance of a design.

For the analysis the DATCOM method is used as outlined in [85] and [76]. Firstly, the wing lift slopes are calculated by:

$$C_{L_\alpha} = \frac{2\pi AR_{eff}}{2 + \sqrt{4 + \frac{A_{eff}^2 \beta^2}{\eta^2}(1 + \frac{tan^2(\Lambda_{0.5c})}{\beta^2})}} \tag{7.9}$$

$$\beta = \sqrt{1 - M^2} \tag{7.10}$$

$$\eta = 0.95 \tag{7.11}$$

It should be noted that effective aspect ratio is used in Eq. 7.9 which is increased by the fact that vertical fins on the tips of the wing act as large winglets. Effective aspect ratio is related to geometric aspect ratio by:

$$AR_{eff} = AR + AR(1 + 1.9 * h/b) \tag{7.12}$$

where h is the height of the vertical fins and b is the aircraft wingspan.[85] An important distinction has to be made here, namely between high- and low-aspect-ratio wings. It is important as there are two different methods for estimation of $C_{L_{max}}$ and $\alpha_{C_{L_{max}}}$ depending on the aspect ratio of the wing. More specifically, a wing is considered to have a low aspect ratio if its aspect ratio obeys the following inequality:

$$AR_{eff} \leq \frac{3}{(C_1 + 1)(cos(\Lambda_{LE}))} \tag{7.13}$$

where $C_1$ is a parameter depending on taper ratio and is obtained graphically from [85]. The body, with an aspect ratio of 0.34 falls in the low-aspect-ratio wings category, so it is analysed as per Eq. 7.16 and Eq. 7.17. The wing, however, falls within the high-aspect-ratio category with an aspect ratio of 7.5.

Maximum lift coefficient as well as maximum angle of attack for high aspect ratio wings are estimated as follows.

$$C_{L_{max}} = C_{l_{max}}(\frac{C_{L_{max}}}{C_{l_{max}}}) + \Delta C_{L_{max}} \tag{7.14}$$

$$\alpha_{C_{L_{max}}} = \frac{C_{l_{max}}}{C_{L_\alpha}} + \alpha_{0L} + \Delta\alpha_{C_{L_{max}}} \tag{7.15}$$

In Eq. 7.14 and Eq. 7.15 $\frac{C_{L_{max}}}{C_{l_{max}}}$, $\Delta C_{L_{max}}$, and $\Delta\alpha_{C_{l_{max}}}$ depend on airfoil sharpness parameter, $\Lambda_{LE}$, and Mach number and are obtained graphically from [85]. $C_{l_{max}}$ and $\alpha_{0L}$ are properties of the airfoil and are output by XFLR5. Conversely, $C_{L_{max}}$ and $\alpha_{C_{L_{max}}}$ for low aspect ratio wings are calculated as follows.

$$C_{L_{max}} = (C_{L_{max}})_{base} + \Delta C_{L_{max}} \tag{7.16}$$

$$\alpha_{C_{L_{max}}} = (\alpha_{C_{L_{max}}})_{base} + \Delta\alpha_{C_{L_{max}}} \tag{7.17}$$

In Eq. 7.16 and Eq. 7.17 the variables are obtained graphically from [85].

The previously outlined method, when put into a Python script, produces the linear part of the $C_L - \alpha$ graph of the wing and the body separately as well as $C_{L_{max}}$ and $\alpha_{C_{L_{max}}}$. Those are presented in figure and table

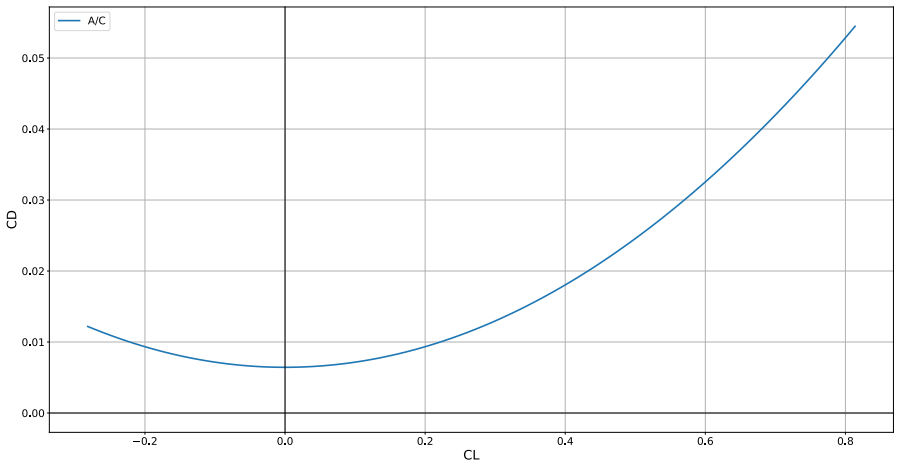


**Figure 7.8:** *Linear part of the lift curves of the body, wing, and whole aircraft.*

**Table 7.3:** *Maximum lift coefficients and respective angles of attack.*

| Parameter | Wing | Body | A/C |
|---|---|---|---|
| $C_{L_{max}}$ | 0.93 | 0.36 | 0.93 |
| $\alpha_{max}$ | 9.99 | 42.5 | 13.67 |

As previously stated, these values are possibly the least reliable (or realistic) values of the whole design. They are simply an output of a statistical estimation method, so they are not expected to be accurate. The most relevant parameter Table 7.3 of these is the maximum lift coefficient for the whole aircraft. When multiplied with the blow factor it must match $C_{L_{max}} = 1.7$ a required by the design point and indeed it does.

### 7.4.2. Drag Polar Estimation

One of the main benefits of the blended wing body is the increased aerodynamic efficiency compared to a conventional tube-and-wing aircraft [95]. To accurately quantify this aerodynamic efficiency, which is expressed in the Lift-to-Drag ratio ($L/D$), an updated drag estimation is required. From experiments, drag is found to vary quadratically with lift [76]:

$$C_D = C_{D_0} + KC_L^2 \qquad (7.18)$$

$$K = \frac{1}{\pi A R_{eff} e} \qquad (7.19)$$

The missing values from Eq. 7.18 and Eq. 7.19 are the zero-lift drag and the Oswald efficiency factor (i.e. $C_{D_0}$ and $e$) To estimate the zero-lift drag, the component drag build-up method is used. In this method, the parasite drag of each of the aircraft components is estimated using the flat plate skin friction coefficient, component form factor and interference factor, as well as a miscellaneous drag factor to account for features like wave drag or the landing gear. The total zero-lift drag coefficient can then be estimated using Eq. 7.20 [76]. The different parameters needed to estimate the parasite drag will be outlined in the following subsections.

$$C_{D_0} = \frac{1}{S_{ref}} \sum_c C_{f_c} \cdot FF_c \cdot IF_c \cdot S_{wet_c} + \sum_c C_{D_{misc}} \qquad (7.20)$$

#### Flat Plate Skin Friction Coefficient Estimation

The flat plate skin friction coefficient is used in Eq. 7.20 to estimate the component friction drag. It is a function of the Reynolds number and the type of boundary layer. Two types of boundary layers exist: laminar and turbulent boundary layers. A laminar boundary layer is thinner, has lower friction, but is more prone to separation compared to a turbulent boundary layer.

At this stage of the design, an estimate has to be made of the fraction of laminar flow over the aircraft surfaces. Here, the assumption is made that the body can be modelled as a wing. This is a valid assumption, as the body (sub)-systems are fitted within an airfoil, resulting in a wing-shaped fuselage, as was described in Section 7.3.

From literature, it is found that the fraction of laminar flow, depending on the aircraft surface finish, can differ between 30-50% for newer aircraft. As such, a laminar flow fraction of 30% is taken [76], as to remain conservative in the design assumptions.

As said earlier, the skin friction coefficient is a function of Reynolds number. For the high subsonic flow regime of interest for the design of the Lightning2, the Reynolds number is determined from Eq. 7.21, which is equal to the minimum between the actual and cutoff Reynolds number. The cutoff Reynolds number determines the effect of surface roughness on transition [76]. In this equation, $k = 0.052 \times 10^{-4}$ m, which is taken to be a representative surface roughness for modern materials and surface finishes.

$$Re = min\left(\frac{\rho V MAC}{\mu}, 44.62\left(\frac{MAC}{k}\right)^{1.053} M^{1.16}\right) \tag{7.21}$$

From the Reynolds number, the laminar and turbulent skin friction coefficients can be determined using Eq. 7.22 and 7.23, respectively. The overall skin friction coefficient can then be determined from the weighted average between the two using the laminar flow fraction.

$$C_{f_{laminar}} = \frac{1.328}{\sqrt{Re}} \tag{7.22}$$

$$C_{f_{turbulent}} = \frac{0.455}{(\log_{10} Re)^{2.58}\,(1 + 0.144M^2)^{0.65}} \tag{7.23}$$

**Component Form Factors**

The next step in the zero-lift drag estimation is the determination of the component form factors, which estimate the pressure drag due to viscous separation.

For the fuselage, wing, empennage and pylons, the component form factor is given by Eq. 7.24 [76]. In this equation, $(x/c)_m$ is the position of maximum thickness, and $\Lambda_m$ is the sweep angle at the position of maximum thickness. For the engine nacelles, the form factor is given by Eq. 7.25 and 7.26, where $l$ is the length of the nacelle and $d$ is the maximum nacelle diameter.

$$FF = \left[1 + \frac{0.6}{(x/c)_m}\left(\frac{t}{c}\right) + 100\left(\frac{t}{c}\right)^4\right]\left[1.34M^{0.18}(\cos\Lambda_m)^{0.28}\right] \tag{7.24}$$

$$FF = 1 + \frac{0.35}{f} \tag{7.25}$$

$$f = \frac{l}{d} \tag{7.26}$$

**Component Interference Factors**

The component interference factors account for the interference drag due to boundary layer interactions between the different components. For the design, the used component interference factors are shown in Table 7.4 [76].

**Table 7.4:** *Used interference factors for the considered components.*

| Component | IF | Component | IF |
|---|---|---|---|
| Fuselage | 1.0 | Vertical Tail | 1.04 |
| Wing | 1.0 | Nacelle | 1.3 |
| Horizontal Tail | 1.04 | Pylon | 1.05 |

**Wetted Areas**

The final parameter needed to estimate the contribution of each component is the wetted area. This is the total area exposed to the flow. For the fuselage and wing, the wetted area is given by Eq. 7.27, while the empennage wetted area is given by Eq. 7.28 [76].

$$S_{wet_w} = 1.07 \cdot 2 \cdot S_{exp_w} \tag{7.27}$$

$$S_{wet_T} = 1.05 \cdot 2 \cdot S_{exp_T} \tag{7.28}$$

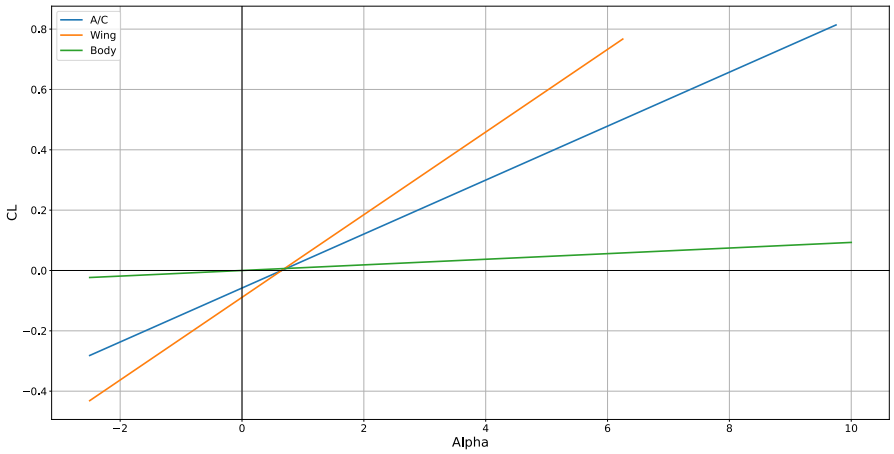


**Figure 7.9:** *Drag polars for the body, wing, and whole aircraft, based on Eq. 7.18.*

**Miscellaneous Drag**

In subsequent Section 7.5 it is mentioned that the Lightning2 aircraft operates below its critical Mach number. As such, no wave drag is present. For the landing gear, the contribution to $C_{D_0}$ is given by Eq. 7.29, where $\Delta C_{D_s} = 0.7$, and $S_s = 0.2554$ m$^2$ [76]. Finally, an excrescence and leakage drag factor of 2% is added to account for the effects of air intakes, lights, antennas and sensors.

$$\Delta C_{D_{ref}} = \Delta C_{D_s} \frac{S_s}{S_{ref}} \tag{7.29}$$

**Oswald Efficiency Factor**

The final parameter that needs to be estimated before the aircraft drag and aerodynamic efficiency can be determined is the Oswald efficiency factor. To estimate this factor for the Lightning2 aircraft, the Frost and Rutherford method is used [72], given in Eq. 7.30. The suction factor $R$ is a function of $A\lambda/\cos(\Lambda)$, defined within the method to take values $0.86 \leq R \leq 0.97$.

$$e = \frac{1.1 C_{L_\alpha}/AR_{eff}}{RC_{L_\alpha}/AR_{eff} + (1-R)\pi} \tag{7.30}$$

Once obtained, $C_{D_0}$ and $e$ could be plugged back in Eq. 7.18 and the resulting $C_D$ could be plotted as a function of $C_L$. Further, the aforementioned measure for aerodynamic efficiency could be plotted in the form of $C_L/C_D$ against $\alpha$. These plots are presented in .

Once lift and drag estimations are done, $L/D$ ratio could be plotted against $\alpha$ and then compared to competitor designs. This plot is shown in Figure 7.10.

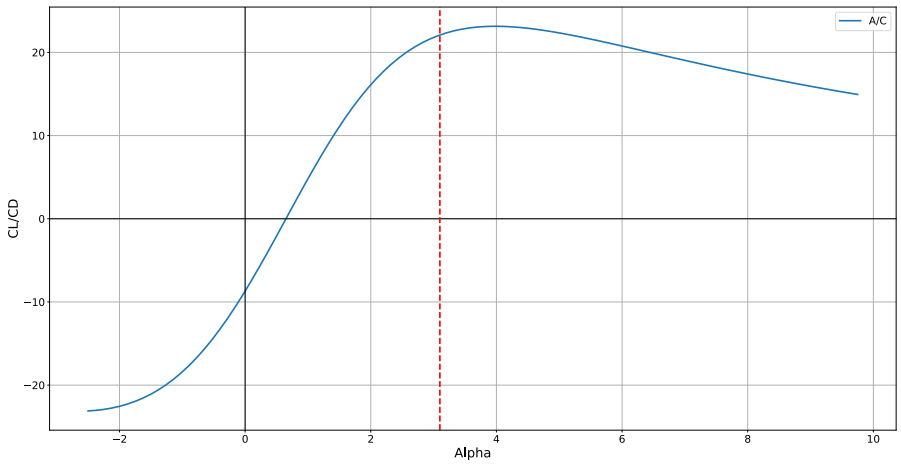


**Figure 7.10:** *$L/D$ ratio as a function of angle of attack.*

## 7.5. Critical Mach Number

Once the final geometry of the design is locked, the critical Mach numbers of the wing and the body at cruise conditions need be evaluated. The methodology is taken from [7] and is outlined as follows.

Firstly, the low-speed minimum pressure coefficient $C_{p,0}$ at the design cruise angle of attack for both airfoils is obtained from XFLR5. Then, the high-speed pressure coefficient, $C_p$ is plotted against freestream Mach number using the Karman-Tsien compressibility correction:

$$C_p = \frac{C_{p,0}}{\sqrt{1-M_\infty^2} + [M_\infty^2/(1+\sqrt{1-M_\infty^2})]C_{p,0}/2} \tag{7.31}$$

After that, the critical pressure coefficient (i.e. the pressure coefficient when the local Mach number reaches unity) is plotted against critical Mach number, $M_{cr}$, using the following relation:

$$C_{p,cr} = \frac{2}{\gamma * M_{cr}^2}\left[\left(\frac{1+[(\gamma-1)/2]M_{cr}^2}{1+(\gamma-1)/2}\right)^{\frac{\gamma}{\gamma-1}} - 1\right] \tag{7.32}$$

When Eq. 7.31 and Eq. 7.32 are plotted on the same graph, their intersection point is the critical Mach number of the given section, at a specified angle of attack. Plots for the wing and the body are presented in Figure 7.11.

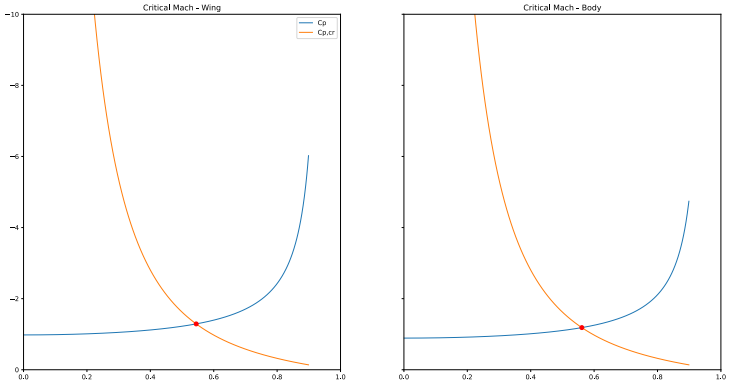


**Figure 7.11:** *Critical pressure coefficients, wing and body.*

It should be noted that these values are the critical Mach numbers of the sections. Critical Mach numbers for the finite wing and body themselves could be obtained by dividing the section critical Mach numbers by the cosine

of the leading-edge sweep of each part (e.g. wing or body). From Figure 7.11 it could be deduced that airfoil critical Mach numbers for the wing and body are 0.56 and 0.52, respectively. These, divided by the cosines of wing and body leading-edge sweep angles result in $M_{cr_{wing}} = 0.89$ and $M_{cr_{body}} = 0.93$. It is evident that these provide a more-than-reasonable margin when compared to the cruise Mach number of 0.8.

## 7.6. Generation of loads

The main results from the aerodynamic analysis that are needed for other subsystems are the loads and moments generated by the wing and fuselage. These are produced from XLFR5, and have to be edited somewhat so that they can be used for designing the wingbox. The outputs of XLFR5 that are used are the following. Lift and drag XFLR produces as a spanwise distribution of their coefficients, that are normalised by multiplying them by the local chord than dividing them by the mean aerodynamic chord. For the moment it simply outputs the total moment coefficient of the total span.

In order to transform the lift and drag coefficients into a distributed loading that can be used to produce the wingbox. The lift and drag coefficients are converted using the following formula.

$$L_i = 0.5\rho V^2 C_{L_i} MAC \tag{7.33}$$

This formula closely resembles the formula to calculate the lift produced by a wing, with the only difference being that it is not multiplied by an area but with only a length. This thus generated a results that has the unit of $N/m$ instead of $N$. The multiplication with MAC is done to cancel out the fact that XFLR divides by it before exported the results. For the drag the same exact formula is used, but $L_i$ and $C_{L_i}$ are substituted by $D_i$ and $C_{D_i}$ respectively.

Converting the moment coefficient to a distributed moment takes one extra step. Where XLFR already multiplies the lift and drag coefficients with the local chords, is does not do that for the moment coefficient. The local chords of the wing are known for a spanwise locations, so it can simply be included as a term in the following formula.

$$M_i = 0.5\rho V^2 C_{M_i} c_i^2 \tag{7.34}$$

## 7.7. Verification of the Programs for Aerodynamics

With the provided lift, drag, and critical Mach number estimation methods implemented into Python scripts, verification was performed. This was done through both visual inspection, hand calculation and unit decomposition, as described in the verification plan of the Midterm report [111]. During the hand calculations, a sign error was found in the skin friction coefficient for the fuselage. After correction of this error, all unit tests were passed.

**Table 7.5:** *Unit tests*

| Identifier | Test | Final result |
|---|---|---|
| V.AER.U.1 | Visual inspection | Pass |
| V.AER.U.2 | Hand calculations | Pass |
| V.AER.U.3 | Unit decomposition | Pass |

After the unit tests, order of magnitude tests were performed on the different subsystems, evaluating the magnitudes of the different contributions to the drag. Finally, sensitivity tests were performed to see if a change in input causes a corresponding change in output. For example, an increase in exposed wing surface area should correspond to an increased wing contribution, while a decrease in stream-wise thickness to chord ratio should correspond to a decrease. The implemented estimation method passed all these tests.

## 7.8. Validation of the Programs for Aerodynamics

The general method outlined in Section 7.1 was presented to Mr. G. Palma of Roma Tre University, (i.e. an external expert) and the feedback received is considered validation. According to this feedback, the sizing method is suitable for this stage of the design. Further, the use of the XFLR5 solver provides sufficient accuracy for a conceptual design. Further validation could be obtained by testing a physical model as explained in Section 7.9.

For the validation of the drag polar, a remark should be made. As the zero-lift drag of an aircraft is highly dependent on its design, it is difficult to make useful conclusions from comparisons between aircraft. As previously mentioned, it is common for $L/D$ to be used as a comparison factor. For the Lightning2 blended wing body, $L/D_{cruise} = 21.97$, which lies exactly in the estimated range for blended wing bodies [95]. Therefore, the drag polar estimation is considered validated. However, during further design stages, these results should be further validated using CFD models as discussed in Section 7.9.

## 7.9. Summary and Further Recommendations

In conclusion, it should be noted that the method used for lift and drag estimation relies on statistics. The data points in these statistics consist primarily of conventional aircraft. This means that the results of this method when applied to an unconventional concept are approximate at best. Further, the bending area is neglected in these analyses due to the resource constraints of this project. Therefore, it is recommended that further, more detailed research and analysis are done on the aerodynamic properties of this planform. More advanced tools should be used for the evaluation of the aerodynamic properties of this design. Finally, if the design proves its capabilities, a physical scaled model should be built such that it could be tested in actual flow conditions.

# 8

# Structures & Materials

The following chapter focuses on the general structural design of the Lightning2 aircraft with special focus on the most critical load cases experienced during the entire flight profile and the corresponding analysis in Section 8.1, followed by Section 8.2 with the liquid hydrogen tank design. Section 8.3 and Section 8.4 pivots around the complete design of wingbox and fuselage including the analysis of different failure modes. Closing with the verification and validation of all the above mentioned design and analysis in Section 8.5.

## 8.1. Critical Load Cases

Before being able to perform the structural design, it is important to identify the critical load cases. This is done by evaluating the different load cases during flight, and identifying the most critical positive and negative load cases, which are shown in Table 8.1. This also includes the climb requirements set by CS-25 [36]. For each of the load cases mentioned above, a manoeuvre and gust diagram was generated, from which the maximum and minimum load factors were found. These diagrams are shown in Figure 8.1 to 8.4.

**Table 8.1:** *Assessed load cases.*

| Case Identifier | Description | Speed | Weight | Altitude | $n_{max}$ |
|---|---|---|---|---|---|
| **LC-1** | Takeoff + | $V_{TO}$ | $MTOW$ | Sea level | 1.92 |
| **LC-2** | Takeoff - | $V_{TO}$ | $MTOW$ | Sea level | -1 |
| **LC-3** | Landing + | $V_{land}$ | $W_{max,landing}$ | Sea level | 1.95 |
| **LC-4** | Landing - | $V_{land}$ | $W_{max,landing}$ | Sea level | -1 |
| **LC-5** | Cruise 1 + | $V_{cr}$ | $W_{start\ cruise}$ | 36000 [ft] | 2.5 |
| **LC-6** | Cruise 1 - | $V_{cr}$ | $W_{start\ cruise}$ | 36000 [ft] | -1 |
| **LC-7** | Approach + | 250 [kts] | $W_{max,landing}$ | 5000 [ft] | 2.5 |
| **LC-8** | Approach - | 250 [kts] | $W_{max,landing}$ | 5000 [ft] | -1 |

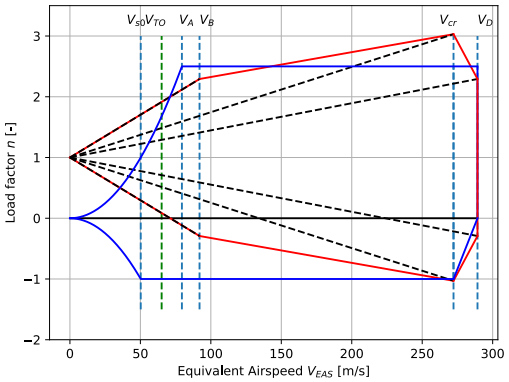


**Figure 8.1:** *Manoeuvre and Gust Diagram for LC-1 and LC-2.*

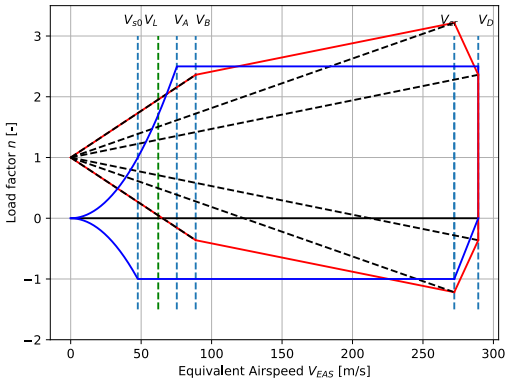


**Figure 8.2:** *Manoeuvre and Gust Diagram for LC-3 and LC-4.*

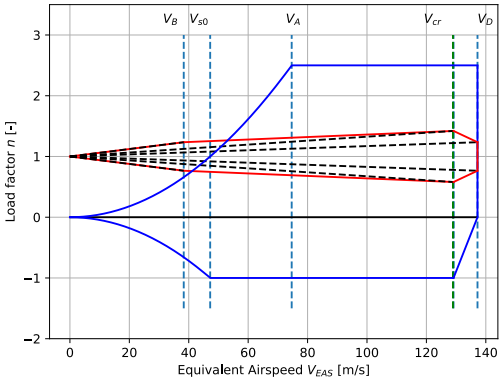


**Figure 8.3:** *Manoeuvre and Gust Diagram for LC-5 and LC-6.*

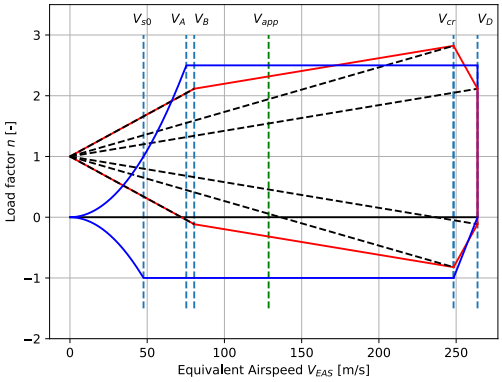


**Figure 8.4:** *Manoeuvre and Gust Diagram for LC-7 and LC-8.*

The evaluation of the shear, bending and torque loading for each load cases in order to determine the most critical scenario will be presented in Subsection 8.3.2.

## 8.2. Liquid Hydrogen Tank Design

The tank design consists of three main steps: the geometric, mechanical, and thermal design. Each step consists of the necessary trade-offs and calculations.

Before the design shall be started, conditions of the liquid hydrogen have to be specified. Since aircraft flies on liquid hydrogen, cryogenic conditions apply. To minimise the hydrogen lost during flight, the hydrogen storage shall be pressurised. It was recommended on the 25th of May by J. van Campen, who is an assistant professor at the TU Delft and works on hydrogen tanks, to use a pressure of 30 bars. Next, a temperature of -250 °C was chosen, which is beyond the critical temperature of hydrogen. Density is a consequence from above mentioned two state variables and equals 71.21 kg/m$^3$ [1].

Another aspect required to be specified before the start of the design is the general lay-out of the tank. More specifically, the trade-off between integral and non-integral tanks as well as the insulation type. For the first trade-off, an integral tank means that it would be an integral component of the aircraft structure and therefore also carry the fuselage skin loading. The second option is a non-integral tank that only shall withstand the loads associated with the fuel storage. Even though the integral tank is beneficial in terms of weight saving and volumetric efficiency [121], the non-integral option was chosen because of the time and resource constraints of this project.

In addition, the second trade-off for the insulation type is summarised in Table 8.2. Overall, four options were considered: multi-layer insulation (MLI), vacuum, foams, and aerogels. The latter are a open micro-structures that consist of interconnected particles with a high porosity and low density [112]. From the trade-off, the conclusion leads to a double-walled tank with vacuum in between and aerogel insulation on the outside as the most optimal combination. The properties of the latter are shown in Table 8.3.

[1] `https://cmb.tech/hydrogen-tools` - Accessed: 25-05-2022

**Table 8.2:** *The trade-off for the insulation type to be used for the tank according to [112].*

| | Weight | Volume | Cost | Thermal Conductivity | Safety Concerns | TRL |
|---|---|---|---|---|---|---|
| **MLI** | High, since heavier tank walls are required. | High if only MLI is used. | High. | Very low. | Decrease in range if vacuum is lost. | High. |
| **Vacuum** | High, since heavier tank walls are required. | Low. | Dependence on the chosen materials. | Near zero. | Decrease in range if vacuum is lost. | High. |
| **Foams** | Low. | High. | Low. | Relatively high. | Potential damage from environment. | High. |
| **Aerogels** | Low. | High | Medium | Very low. | Potential damage from environment. | Medium. |

### 8.2.1. Geometric Design of the Liquid Hydrogen Tank

The first step in the geometric design, is the design of the tank shape. To simplify the concept, a cylinder with spherical caps was assumed for the tank shape which is the most optimal shape for pressure vessels and simplifies the calculations.

To determine the geometry of the tank, the required liquid hydrogen mass shall be converted into volume by dividing by the density. An additional excess volume of 10% was used to account for the portion of gaseous hydrogen that will still occur at cryogenic temperatures. Next, the radius of the tank can be found by the summation of the volume equations for a cylinder and a sphere. The length can be derived from the available space in a 3D model of the aircraft and can be used as an input.

This approach can be used to determine the radius of the inner tank. Furthermore, adding the thickness of the vacuum to the radius, the overall radius of the outer tank can be computed. In the design, a vacuum thickness of 5 mm was chosen. In addition, a minimum thickness of 3 mm was chosen for the wall in order to account for manufacturing constrains.

### 8.2.2. Mechanical Design of the Liquid Hydrogen Tank

The next step is the mechanical design of the tank, which gives the thicknesses of the inner and outer wall as outputs. The thickness calculations are based on the maximum pressure difference the walls shall withstand. The inner wall shall withstand the difference between the pressurised hydrogen and vacuum. The outer wall shall withstand the difference between vacuum and the pressure of the ambient air at the minimum operating altitude in the tank compartment of the aircraft. The minimum operating altitude is equal to the altitude of the lowest airport in the world, which is the Bar Yehuda Airfield in Israel at -400 m [2].

The maximum pressure or burst pressure within the tank is defined by Eq. 8.1 [18], where the design pressure is set at 30 bars as previously discussed.

$$p_{burst} = 2.00 p_{des} \tag{8.1}$$

The minimum thickness of the walls for the cylindrical part of the tank can be determined by Eq. 8.2 and 8.3. Eq. 8.2 is valid for spheres as well. For a uniform thickness, it can be seen from the formulas that the hoop stress of the cylindrical part will be leading since this requires the largest thickness to withstand the same pressure difference.

It is important to calculate the minimum thickness for both the yield and ultimate stress of the wall material. Both stresses also have a corresponding safety factor (SA): 1.15 for yield and 1.3 for ultimate. The one for ultimate is higher because if the loads go over the ultimate stress, it would lead to catastrophic failure. Using

[2] `https://en.wikipedia.org/wiki/List_of_lowest_airports` - Accessed: 25-05-2022

the found thickness and the density of the materials, the mass of the inner and outer tank can be calculated using the volume equation for a cylinder and a sphere.

$$t = \Delta p \; SA \; R/2\sigma_{axial} \qquad (8.2) \qquad\qquad t = \Delta p \; SA \; R/\sigma_{hoop} \qquad (8.3)$$

To complete this step, it is required to know the materials for the inner and outer wall. The most common materials used for tanks is aluminium or one of its alloys. For this design, composites were also considered. Since the design should be ready to be implemented within five year (requirement ST.CUS.4), this was not an option due to the current low TRL of composite tanks at cryogenic temperatures. However, it should be kept in mind that future updates can contribute to weight saving. When looking at alloys for the inner tank, the aluminium-copper alloy ,AL2024-T81, is proved to be the best option as the properties of the material increase with decreasing temperature and has a relatively low density [8]. In addition, the aluminium and copper molecules do not react with hydrogen. The outer tank material was chosen to be the aluminium-lithium alloy, AL2090-T86. This material was chosen because of the lower density, but still good stress characteristics. AL2090-T86 was not chosen for the inner wall because lithium reacts with hydrogen and the corresponding lower stress properties would require more material thus overall make the tank heavier. The properties of both materials are reported in Table 8.3. Other alloys such as the 7-series were also considered, but the magnesium in some of these alloys would react with the hydrogen thus can not be used. Others in 7-series can not handle cold temperature and would become brittle.

**Table 8.3:** *Properties of materials used in the tank where the properties of the inner wall are taken at 23 K and the others at room temperature [8]* [3] [4].

| Name | Type | Yield Stress [MPa] | Ultimate Stress [MPa] | Density [kg/m$^3$] | Thermal Conductivity [W/mK] |
|---|---|---|---|---|---|
| AL 2024 T81 | Inner wall material. | 538 | 586 | 2780.0 | 151. |
| AL 2090 T86 | Outer wall material. | 520 | 550 | 2590.0 | 88.0 |
| Aerogel | Insulation material. | - | - | 100.0 | $10^{-5}$ |

### 8.2.3. Thermal Design of the Liquid Hydrogen Tank

The thermal design of the tank will determine the insulation thickness on the outside of the tank. Several heat transfer types are considered: convection, conduction and radiation. After careful consideration, it was assumed that the liquid hydrogen in the tank would have a quasi uniform temperature. This means that internal convection can be neglected. External convection can also be neglected, since it is a function of the airflow outside the tank and it was decided that the tank is non-integral. Conduction will be considered for the inner and outer wall as well as for the insulation. Radiation will be considered for the vacuum layer.

The first step is to determine the heat flux that is allowed to flow into the tank to minimise the boil-off. For this tank, it is assumed that 15% of the total LH2 mass will be lost during flight due to a change in state from liquid to gaseous hydrogen in terms of temperature. The allowed heat flux can be determined using Eq. 8.4 [42]. The heat flux can then be divided over the different layers of the tank, where the insulation will lose the largest amount of heat relative to the vacuum layer.

[1] https://www.matweb.com/search/DataSheet.aspx?MatGUID=6441f805a3bb42758ab5b15752343138 - Accessed: 25-05-2022

[2] https://www.matweb.com/search/datasheet.aspx?MatGUID=8243b6cbf091445ea11bd651e9009200 - Accessed: 25-05-2022

[3] https://www.matweb.com/search/DataSheet.aspx?MatGUID=6441f805a3bb42758ab5b15752343138 - Accessed: 25-05-2022

[4] https://www.matweb.com/search/datasheet.aspx?MatGUID=8243b6cbf091445ea11bd651e9009200 - Accessed: 25-05-2022

$$\dot{Q} = \frac{m_{boil-off}\, c_{LH2}\, \Delta T}{t_{flight}} \tag{8.4}$$

$$\Delta T = \frac{l}{kA}\dot{Q} \tag{8.5}$$

Next, by computing the temperature increments throughout the different layers, the allowed temperature increase through the insulation can be established, which can then be used to determine the thickness of the insulation. The temperature increase due to conduction in the inner wall can be determined using Eq. 8.5, where $A$ stands for the surface area and $l$ stands for the thickness of the layer in question [42]. For the vacuum layer, Eq. 8.6 can be used in which $\sigma$ is the Stefan-Boltzmann constant and equals to $5.67 \cdot 10^{-8}$ W/m$^2$ K$^4$. Furthermore, the temperature change in the outer wall can be determined in the same way as the inner wall.

$$T_2 = \left( \frac{\dot{Q}}{e\sigma A {T_1}^4} \right)^{0.25} \tag{8.6}$$

The last step is to determine the thickness of the insulation by rewriting Eq. 8.5, where $\Delta T$ is equal to the difference between the temperature at the outer wall and the ambient temperature at minimum operating altitude of -400 m as mentioned before.

### 8.2.4. Summary and Recommendations of the Tank Design

After the iterations, the final mass of the hydrogen is determined, which is 1753.7 kg. In combination with the finalisation of the Lightning2 aircraft's internal lay-out, the tank design can be finalised. Due to the available structural space, it was decided to use one tank in the back. A summary of all dimensions and thicknesses are reported in Table 8.4.

Finally, there are some additional aspects to discuss. First, since the tank contains liquid, sloshing is expected. To limit the loads due to these movements, an additional structure shall be included inside the tank. One way to do this, is to split the tank into different closed compartments. A second consideration is the connection between the inner and outer tank through the vacuum layer. It was recommended on the 25th of May by J. van Campen to use three-point connections at intervals made out of the same alloy as the inner tank. To account for both these aspects, a 2% increase in the tank mass is taken into account.

Next, the fuel cell does not operate with LH2 at a pressure of 30 bar. The most optimal state of the hydrogen is in gaseous state at a pressure of 1 bar. This means that in the pipe lining to the fuel cell, pressure valves are required. By lowering the pressure, the hydrogen will change to a gaseous state.

Lastly, it is important to consider how the tank will be operated. In the case of this design, it is most optimal to always keep an amount of LH2 in the tank. This way the cryogenic temperature and the high pressure can be maintained. If this would not be the case, the tank would experience fatigue loads due to the many pressure changes and the temperature inside the tank would increase. The increase in temperature has as a consequence that the tank has to be cycled when tanking. Cycling of the tank means that the tank has to be cooled down to cryogenic temperatures by first circulating cold gaseous LH2 or another cold gas. Otherwise during tanking, the LH2 would warm up and immediately transfer to gaseous state, which could lead to catastrophic failure of the tank. The downside of cycling the tank is that it takes time, which increases the turn-around time of the aircraft. In addition, when another gas is used, it needs to be removed completely since the fuel cells will fail if another gas enters the system. A complete removal of this gas is very hard to accomplish.

**Table 8.4:** *The final tank dimensions for the Lightning2 aircraft.*

| Parameter | Value |
|---|---|
| Contained LH2 [kg] | 1753.7 |
| Diameter [m] | 2.9 |
| Length [m] | 6.0 |
| Inner wall thickness [mm] | 17.2 |
| Vacuum thickness [mm] | 5.0 |
| Outer wall thickness [mm] | 3.0 |
| Insulation thickness [mm] | 140.5 |
| Tank mass [kg] | 3455.6 |

## 8.3. Design of the Wingbox

The following sub-sections present the detailed design of the wingbox with the focus on the bending and shear stresses in addition to yielding an buckling failure.

### 8.3.1. Axis systems of the Aircraft

Three different axis systems will be differentiated, namely the aerodynamic axis system, the body axis system and the wingbox axis system. The aerodynamic axis system is used to determine the aerodynamic loads resulting from XFLR5 from which the loads are translated to tangential and normal forces to align with the body axis system. Next, the transformation from body axis system to the wingbox axis system is required to ensure that the analysed cross-section lies in plane. The direction of the wingbox axis system is mainly constrained by the so called elastic axis as the bending of the wingbox always follows the elastic axis, thus the to be analysed cross-sections shall be taken normal to the above mentioned axis. In case of an un-swept wing, the elastic axis is horizontal as can be seen in Figure 8.5a marked with red, therefore the cross-sections (marked with light green) can be taken stream wise, but in case of a swept wing, the elastic axis is not horizontal, but instead approximately follows the quarter chord sweep angle line as can be seen in Figure 8.5b. Therefore, the cross-sections (marked with dark green) shall be taken normal to the quarter chord sweep angle line. Taking the cross-sections stream wise in case of a swept wing might result in an overestimation of the cross sectional properties such as the moment of inertia which ultimately leads to an incorrect design.

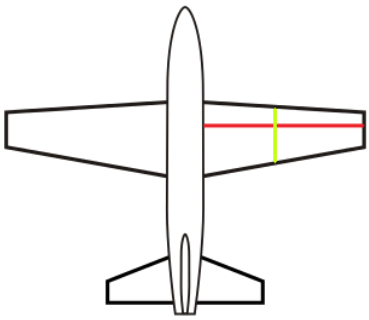

**(a)** *Un-swept wing elastic axis and cross-section.*

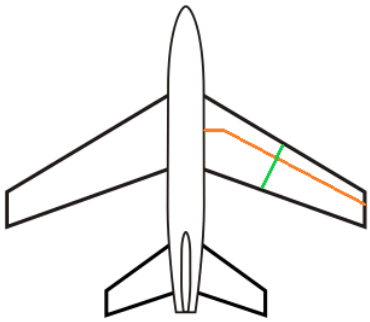

**(b)** *Swept wing elastic axis and cross-section.*

**Figure 8.5:** *Difference in elastic axis for swept and un-swept wing.*

In addition, one extra observation shall be made. In case of a swept wing, the elastic axis takes a turn, which is approximated by a kink on Figure 8.5b. The above mentioned turn implies, that the to be analysed cross-section shall be rotated right after the kink to ensure its perpendicular alignment with respect to the elastic axis. Due to the limited available time for the design, the kink in the elastic axis will be neglected, thus the elastic axis shall follow the quarter chord sweep angle line without any disruption. The above mentioned assumption results in an underestimation of strength of the structure at the root chord but as the connection at the fuselage requires extensive analysis and does not directly influence the remaining part of the wingbox analysis, thus the assumption is deemed acceptable.

A summation of the different axis systems and the corresponding relations can be found in Figure 8.6 in which, green represent the aerodynamic axis system, orange represents the body axis system and blue represent the wingbox axis system.

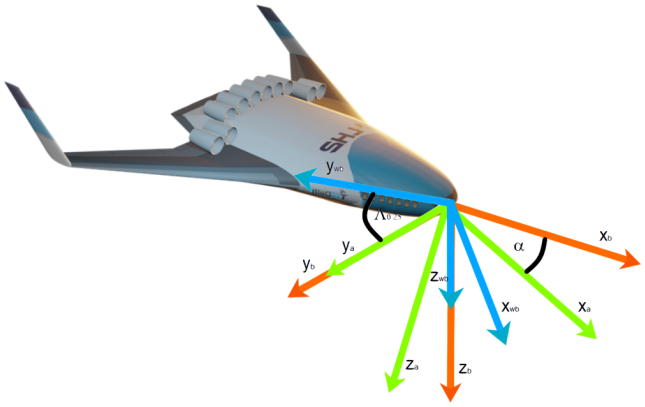


**Figure 8.6:** *Three different axis system.*

### 8.3.2. Loading

To determine the lay-out of the wingbox, it is crucial to know what loads it should sustain. Several can be identified in the body axis system in the x- and z-direction as defined in Figure 8.6.

In the x-direction there is the aerodynamic tangential force ($T_{aer}$) that can be derived from the lift and drag distributions and the thrust provided by the engines ($T_{eng}$). The latter can be simulated as a constant distributed load over the length of the engines due to the distributed propulsion. The forces are shown in the free body diagram in Figure 8.7.

In the z-direction, the following distributed forces can be identified: the aerodynamic normal force ($N_{aer}$) and the engine weight ($W_{eng}$). In addition, there are also point forces due to the landing gear weight ($W_{MLG}$) and the vertical wings at the tips ($W_{vw}$). These are shown in the free body diagram in Figure 8.8.

At the cross-section of the wingbox, there will be shear forces acting on the skin and spars. These can be determined by integrating the distributed force from each spanwise location to the tip of the wing. The point forces can be added to this function as a Heaviside function. This is shown in Eq. 8.7. In the same fashion, the moment distribution can be calculated using Eq. 8.20.

$$S(y) = \int_{y}^{b/2} w(x)\, dx + P\, u_{x1}(y) \qquad (8.7) \qquad M(y) = \int_{y}^{b/2} S(y)\, dx + M\, u_{x1}(y) \qquad (8.8)$$

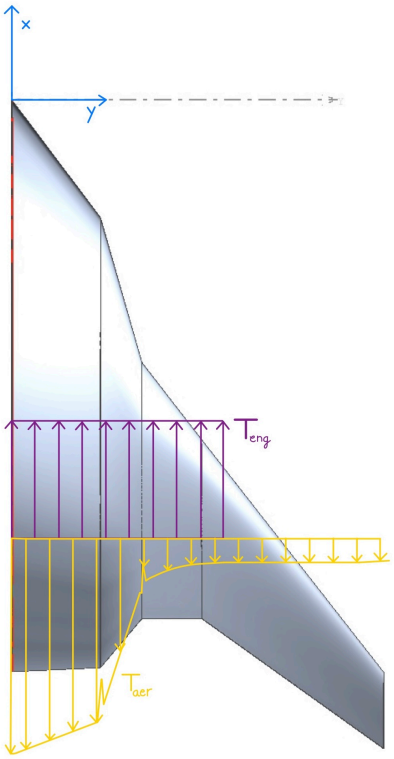


**Figure 8.7:** *The free body diagram for half of the aircraft viewed from the top.*

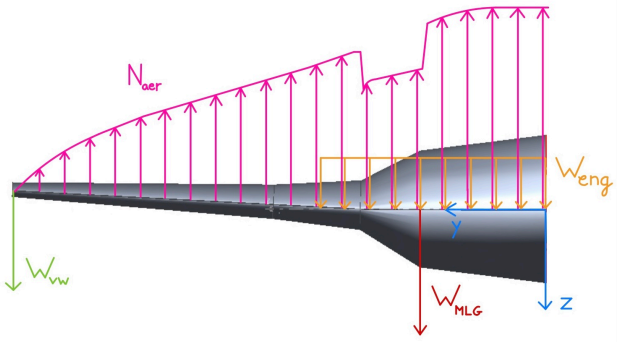


**Figure 8.8:** *The free body diagram for half of the aircraft viewed from the front.*

One aspect to be aware of is the difference in axis systems as explained in Subsection 8.3.1. To use the shear and bending loadings in the design of the wingbox, the transformation to the wingbox axis system is required. This can be done by a rotation around the z-axis by the quarter chord sweep angle using Eq. 8.9 and Eq. 8.10. Here *b* stands for the body axis system and *wb* stands for the wingbox axis system.

$$\begin{bmatrix} S_{x_{wb}}(y) \\ S_{y_{wb}}(y) \\ S_{z_{wb}}(y) \end{bmatrix} = \begin{bmatrix} cos\Lambda_{0.25c} & sin\Lambda_{0.25c} & 0 \\ -sin\Lambda_{0.25c} & cos\Lambda_{0.25c} & 0 \\ 0 & 0 & 1 \end{bmatrix} \begin{bmatrix} S_{x_b}(y) \\ 0 \\ S_{z_b}(y) \end{bmatrix} \tag{8.9}$$

$$\begin{bmatrix} M_{x_{wb}}(y) \\ M_{y_{wb}}(y) \\ M_{z_{wb}}(y) \end{bmatrix} = \begin{bmatrix} cos\Lambda_{0.25c} & sin\Lambda_{0.25c} & 0 \\ -sin\Lambda_{0.25c} & cos\Lambda_{0.25c} & 0 \\ 0 & 0 & 1 \end{bmatrix} \begin{bmatrix} M_{x_b}(y) \\ 0 \\ M_{z_b}(y) \end{bmatrix} \tag{8.10}$$

### 8.3.3. Cross-section design

As the axes systems have been defined in Subsection 8.3.1, the cross-section shall be initialised. Due to the cross-section being aligned normal to the elastic axis, a convenient point shall be chosen which serves as a reference point for the location of the cross-section along the span in the global axis system. The point in name is the location at which the vertical span location intersects the quarter chord sweep angle line. Therefore, when the cross-section is analysed, for example at a span of 15 metres, it corresponds to the cross section which is normal to the elastic axis and its centre line passes through the intersection point mentioned above. Figure 8.9 shows an example cross-section in top view in which the red line indicates the elastic axis, the green line indicates the spanwise location, the purple cross indicates the intersection point at the given spanwise location, and the yellow line the cross-section.

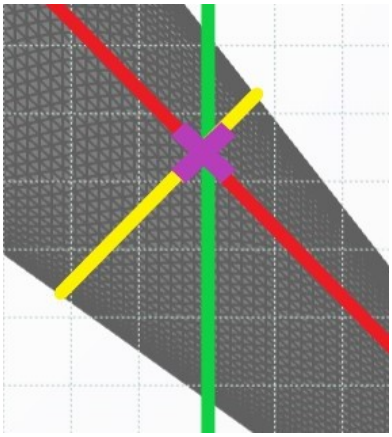

**Figure 8.9:** *Example of a cross section in top view.*

As the cross-section location convention has been defined, the actual cross-section design shall be started. The cross-section is idealised with the use of boom idealisation in which it is assumed that the skin may carry a portion of the bending loads and each boom corresponds to a stringer. Furthermore, the aforementioned assumption was coupled to a new key assumption that the shape of the wingbox shall follow the shape of the aerofoil to ensure that the wasted space between the actual wing skin and the wingbox is minimised as well as the trailing edge control surfaces have appropriate connection to the wingbox. Overall, the above mentioned assumptions result in a total deviation of 1-2% [84] compared to the non-idealised scenario, thus the assumption is deemed acceptable. In addition, a front spar and aft spar location of 0.1 and 0.7 as a fraction of the chord was determined, respectively. The value of 0.7 was determined to ensure the avoidance of a possible interference with the trailing edge control surfaces and the value of 0.1 to utilise the major portion of the wing in case fuel tanks shall be placed in the wing.

Due to the fact that the skin carries a portion of the bending stress, the boom areas shall be corrected for this affect. The correction requires several different equations as no symmetry property can be used due to the reflexed aerofoil used for the design. The required equations can be seen below.

$$I_{ZZ} = \sum_{i=1}^{n} B_i x_i^2 \quad (8.11) \qquad I_{XX} = \sum_{i=1}^{n} B_i z_i^2 \quad (8.12) \qquad I_{XZ} = \sum_{i=1}^{n} B_i x_i z_i \quad (8.13)$$

$$x_c = \frac{\sum_{i=1}^{n} B_i x_i}{\sum_{i=1}^{n} B_i} \quad (8.14) \qquad z_c = \frac{\sum_{i=1}^{n} B_i z_i}{\sum_{i=1}^{n} B_i} \quad (8.15)$$

$$B_i = \frac{t_i b_i}{6} \cdot \left(2 + \frac{\sigma_{i+1}}{\sigma_i}\right) + A_i \quad (8.16)$$

$$\sigma_i = \frac{(M_x I_{ZZ} - M_z I_{XZ})\, z + (M_z I_{XX} - M_x I_{XZ})\, x}{I_{XX} I_{ZZ} - I_{XZ}^2} \quad (8.17)$$

In order to aid the understanding of the boom area correction process, the process is shown as a flow diagram in Figure 8.10.

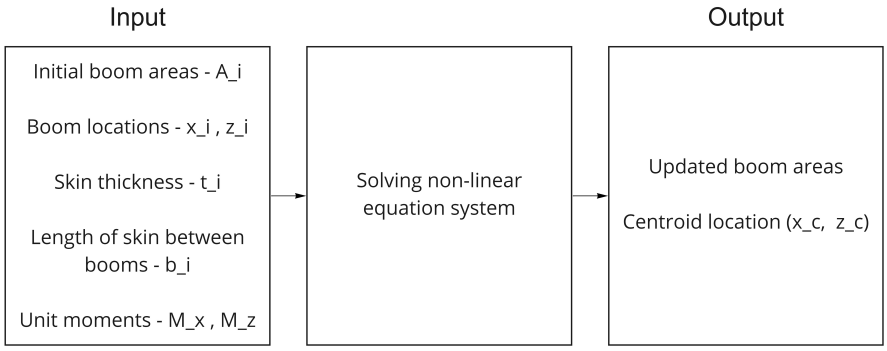


**Figure 8.10:** *Flow diagram of boom area correction.*

An example of a cross-section at span location of 15 metres is shown in Figure 8.11a in the wingbox axis system before the correction and after the correction.

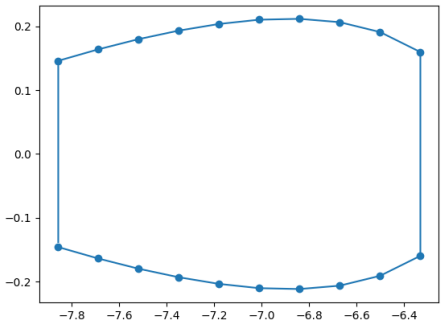


**(a)** *Cross section example at span location of 15 metres in wingbox axis system before correction.*

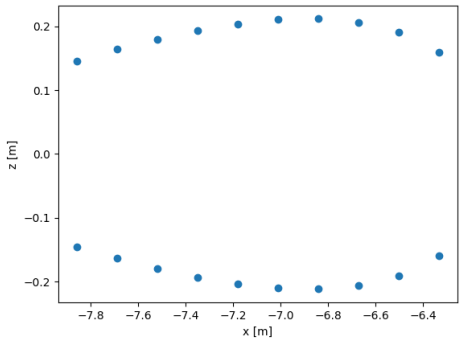


**(b)** *Cross section example at span location of 15 metres in wingbox axis system after correction.*

**Figure 8.11:** *Boom area correction due to presence of skin.*

### 8.3.4. Wingbox material selection

As the geometrical parameters have completed be defined, the last step before the analysis can be performed is the material selection. Non / quasi isotropic materials are excluded from the selection procedure due to complexity and time constraints, thus only isotropic materials are being considered.

On account of the expected high stresses and large size of the wingbox, the material with highest yield stress to density ratio shall be chosen in addition to the CS25 regulations regarding materials certified for use in aerospace industry.

Based on the above mentioned criteria, the chosen material is special alloy of aluminium, namely the AL2024-T81, the same material that is being used for the hydrogen tank design. The key proprieties of the wingbox material can be seen in Table 8.5.

**Table 8.5:** *Wingbox material with properties listed at room temperature.*

| **AL 2024-T81** | | |
|---|---|---|
| **Name** | **Sign** | **Value** |
| Density $[kg/m^3]$ | $\rho$ | 2780 |
| Poisson ratio [-] | $\nu$ | 0.33 |
| Yield strength [MPa] | $\sigma_{yield}$ | 450 |
| Shear modulus [GPa] | G | 28 |
| Elastic modulus [GPa] | E | 72.4 |

As the cross section is fully defined as a function of the span in the wingbox axis system and the material is chosen, the stress analysis can be started.

### 8.3.5. Bending stress

Since all the geometrical parameters were already defined in Subsection 8.3.3, the bending stress can straightforwardly be computed at every boom location as a function of the span with the use of Eq. 8.17 and with the use of the bending loads determined in Subsection 8.3.2.

An example of the bending stress distribution can be seen in Figure 8.12. Important to note that for illustrational purposes, the absolute value was taken of the bending stress distribution, thus the more red the colour of the boom, the higher the bending stress. The actual sign of each bending stress is still stored to account for compression or tension but only for computational and verificational purposes.

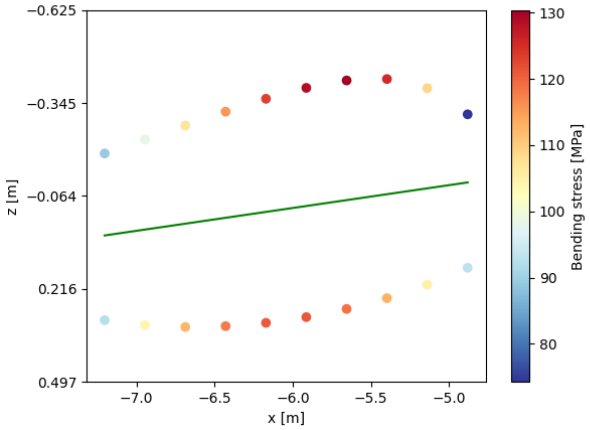


**Figure 8.12:** *Bending stress distribution at an arbitrary span location in wingbox coordinate system.*

### 8.3.6. Shear stress

The shear stress calculation is split into two distinct categories, namely, the shear stress induced by pure shear loads and shear stress induced by pure torsion. With the use of superposition, the two cases can be combined to obtain the final shear distribution. Important to note that the boom idealisation still holds thus the booms carry the normal stresses due to bending and the skin carry the shear flows. Furthermore, in order to make use of the above mentioned superposition, the shear forces are relocated to the shear centre [5] to ensure that only pure shear stresses are produced, thus the corresponding induced torsion due to the relocation is considered as pure torsion.

#### Category I - Pure shear load

In case of a pure shear load, the driving equation is described in Eq. 8.18, in which $q_b$ denotes the basic shear flow which is a change is shear flow across the booms and $q_{s0}$ which is the constant shear flow.

$$q_s = q_b + q_{s0} = -\frac{V_z I_{ZZ} - V_x I_{XZ}}{I_{XX} I_{ZZ} - I_{XZ}^2} \sum_{i=1}^{n} B_i z_i - \frac{V_x I_{XX} - V_z I_{XZ}}{I_{XX} I_{ZZ} - I_{XZ}^2} \sum_{i=1}^{n} B_i x_i \tag{8.18}$$

In order to determine the the basic shear flow, the cross-section shall be cut which is done at the aft spar for convenience. Next, the angle of twist is being calculated with the use of Eq. 8.19.

$$\frac{d\theta}{dy} = \frac{1}{2A} \oint \frac{q_s ds}{tG} \tag{8.19}$$

[5] The shear centre is a point at which the loads applied do not generate any torsion.

One additional equation is required to ensure the system is determined which is the moment equivalence. The moments caused by the shear force $V_x$ and $V_z$ shall be equal to the moment induced by the shear flows around the same point. The corresponding equation can be seen in Eq. 8.20 in which $p_i$ denotes the moment arm of each basic shear flow, $\eta$ and $\xi$ the moment arms of the shear loads and $A$ the area of the cross-section.

$$V_x\eta - V_z\xi = \sum_{i=1}^{n} \oint p_i q_{b_i} ds + \sum_{i=1}^{n} 2A_i q_{s0_i} \tag{8.20}$$

**Category II - Pure torsional load**

In case of a pure torsional load, the shear distribution can straightforwardly be computed with Eq. 8.21, in which $t$ denotes the skin thickness and $A$ the cross-section area of the wingbox.

$$\tau = \frac{T}{2tA} \tag{8.21}$$

### 8.3.7. Failure modes

Two major failure modes are considered for the wingbox, namely, yielding failure and buckling which will be further detailed below.

**Yielding**

The yielding criteria is driven by the Tresca yield criterion. In order to examine if the overall combined stress distribution satisfies the criterion, first, the different stresses shall be combined with the use of the Mohr circle. Before the Mohr circle can be constructed, a stress element of the wingbox shall be analysed, which can be seen in Figure 8.13.

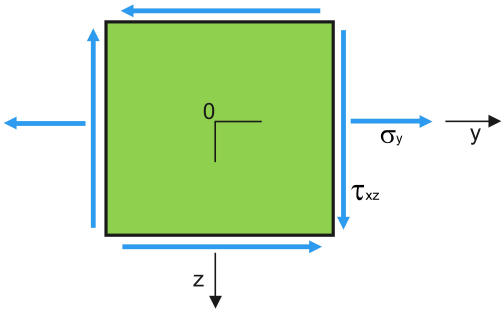


**Figure 8.13:** *Stress element of wingbox.*

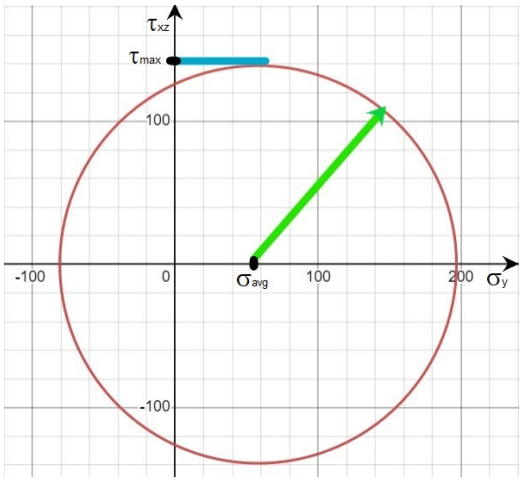


**Figure 8.14:** *Constructed Mohr circle with the use of stress distribution at an arbitrary span location.*

As the bending stress, shear stress distribution and the stress element are known, an example Mohr circle can be constructed which can be seen in Figure 8.14. For the construction of the Mohr circle, Eq. 8.22 and Eq. 8.23 were used.

$$\sigma_{avg} = \frac{\sigma_y}{2} \tag{8.22}$$

$$\tau_{max} = R = \sqrt{\sigma_{avg}^2 + \tau_{xz}} \tag{8.23}$$

As the stress distribution varies along the span and along the cross section, the Mohr circle shall be reconstructed each time taking the most demanding stress location, resulting in a spanwise distribution which represents the maximum combined stress as a result of the combined loading. In addition, in order to satisfy the Tresca yield criterion, the maximum shear stress,$\tau_{max}$, shall not exceed 50% of the maximum yield stress of the material at any location along span. Furthermore, according to CS25 regulations [36], an extra safety factor of 3.75 shall be

used, therefore, the yield criterion shifts upwards, making the overall yield criterion more limiting. The stress distribution with the Tresca yield criterion is shown on Figure 8.15.

A few remarks shall be made regrading Figure 8.15. First, as can be seen, the current wingbox design satisfies the requirement. The maximum stress, in general increases towards the root up till a location 11.5 metres, indicated with red on Figure 8.16, after which the the aft spar changes direction thus making the overall cross-sectional area significantly larger which results in a decrease in combined stress, thus a decreasing stress can be observed in Figure 8.15 up till a spanwise location of 9.2 metres (indicated with yellow in Figure 8.16 at which a discontinuity can be seen. The observed discontinuity is the result of the direction change of the elastic axis (indicated with green in Figure 8.16). As the elastic axis direction changes, the cross-section direction changes as well (yellow to orange in Figure 8.16), which ultimately results in two different wingbox reference frames. In order to close the gap in the graph, one of the reference frames hall be rotated to match the other, in other words, the stress tensor shall be rotated. Unfortunately, this falls out of the scope of the analysis and requires a more complicated analysis, thus will be ignored.

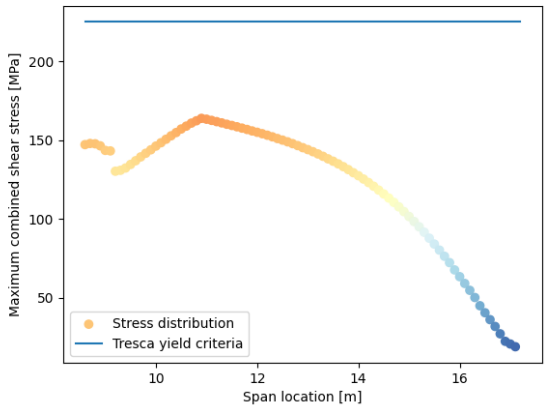


**Figure 8.15:** *Stress distribution with Tresca yield criteria.*

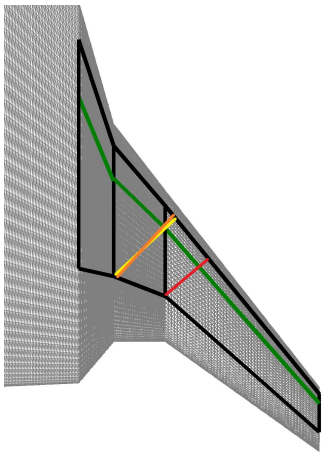

**Figure 8.16:** *Top view of wingbox structure in which the black line indicates the outline of structure and green line indicates the elastic axis.*

In addition, the complete stress distribution of the wingbox can be seen in Figure 8.17 in which the more red the colour, the higher the stress. As can be seen, the highest stresses occur around a span location of 10 metres which is the direct cause of the largest combination of loads at that location and also the presence of the kink.

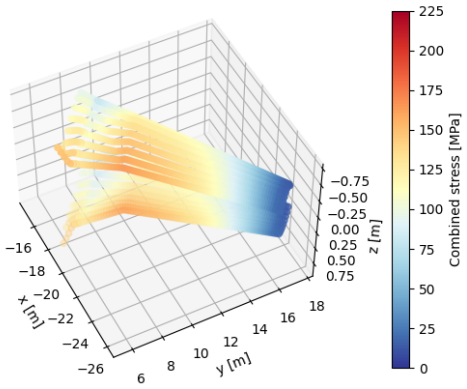


**(a)** *Complete stress distribution of wingbox from side view.*

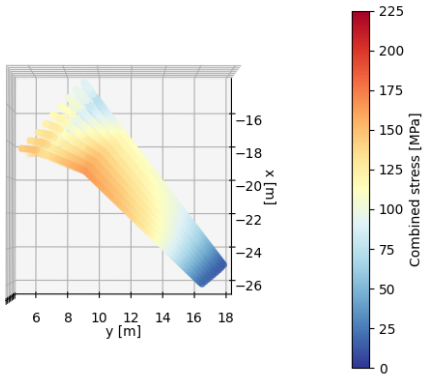


**(b)** *Complete stress distribution of wingbox from top view.*

**Figure 8.17:** *Complete stress distribution of wingbox in 3D.*

### Buckling

Buckling in general, is a sudden deformation of a structural component under compressive load, therefore, the main focus is directed towards the upper half of the wingbox skin at which the largest compressive stresses occur. Buckling of the skin can occur during normal operations but does not lead to failure thus buckling failures is considered only if the panel including the stringers are buckled under the compressive load, which therefore creates the buckling criteria for the analysis of the wingbox.

The analysis of the buckling behaviour closely follows the method presented in Subsection 8.4.4 with slight modifications in the constants due to the use of different geometries.

At first, the partial skin sections in between the boom areas (or stringers for that matter) are analysed as thin plates without stiffening. The sections mentioned above buckle before even reaching the maximum compressive stress, therefore, the affect of the stringers shall be factored in as the presence of stringers increase the critical buckling stress significantly. As expected, the presence of stringers increased the critical buckling stress considerably but in order to meet the criteria, the rib pitch was decreased to 50 cm. With the strengthened panel and decreased rib pitch, the criteria is fulfilled.

### 8.3.8. Final design values

The final design parameters regarding the wingbox can be seen in Table 8.6. Important to note, that there exists different combination of values which satisfy the failure criteria mentioned in Subsection 8.3.7 and the buckling criteria mentioned in Figure 8.3.7, but the combination for lightest structure is considered.

**Table 8.6:** *Final design values of wingbox.*

| Name | Value |
|---|---|
| Stringer number top skin [-] | 9 |
| Stringer number bottom skin [-] | 9 |
| Stringer cross-section area [$mm^2$] | 200 |
| Skin thickness [mm] | 4.5 |
| Rib pitch [mm] | 500 |
| Total weight of wingbox [kg] | 2986 |

### 8.3.9. Future recommendation

Due to the limited available time, the design could not be fully optimised for the specific load cases, therefore future recommendation shall be given in order to ensure, the wingbox can reach its fullest potential. The recommendations can be seen below with the corresponding explanation.

1. Computation of deflection for positive and negative load case.
    - The deflection of the wingbox (or the entire wing for that matter) in general is important during ground operations as it constrains the landing gear height and can alter the previous design if certain deflection requirements are not fulfilled.
2. Redesign for multi-cell structure.
    - Due to the large vertical shear forces, a multi-cell structure is advisable to reduce the pure shear stresses in the spars and in the overall structure. Furthermore, stresses induced by torsion will be reduced as the overall stress is subdivided into the different cells.
3. Use of different skin thickness and stinger number along the span and cross-section.
    - In order to further minimise the weight of the overall structure and reduce the stresses at certain locations, the thickness and the number of stringers shall be changed along the span and within the cross-section.
4. Detailed analysis of wingbox-fuselage and wingbox-wingtip connection
    - Due to the time constrains of the project, the analysis of the wingbox-fuselage and wingbox-wingtip junction was outside of the scope of the project but as the above mentioned connections are crucial in terms of load transfer between the sub-systems, detailed analysis in the future is highly recommended.
5. Use of quasi-isotropic carbon fibre.

- In order to further reduce the weight of the wingbox, consideration of quasi isotropic carbon fibres is advisable due to its extremely high stiffness to weight ratio. Important to note that only quasi isotropic layups are considered as using non-symmetric layups require even more in depth analysis and certain structural idealisations are no longer valid.

## 8.4. Fuselage Design

The following section describes the design of the oval fuselage of the Lightning2. A parametrisation of the oval fuselage is presented along with structural analysis based on a combination of pressurisation loads, steady state manoeuvre loads and aerodynamic loads. Each inner structural member is sized in order to satisfy the requirements on bi-axial strength and buckling. The outer structure is sized based on global and local buckling criteria.

The oval fuselage enables a large unobstructed cabin and cargo area, which eases the emergency egress and gives airliners flexibility for seating configuration and cargo placement. Due to presence of a structural box passing trough the cabin this can be integrated with the carry trough wingbox.

### 8.4.1. Parametrization

The oval fuselage is modelled to consist of the trapezoidal box over which the oval fuselage is fitted. The width of the cabin floor is sized to fit ten passengers abreast and conform with aisle width regulations set by CS-25[36]. Together with the height of the trapezoidal box this provides the framework. The oval fuselage is then fitted over the corners of the trapezoidal minimising the area at the sides and ensuring room for the cargo floor and possible other components. An example layout can be seen in Figure 8.18.

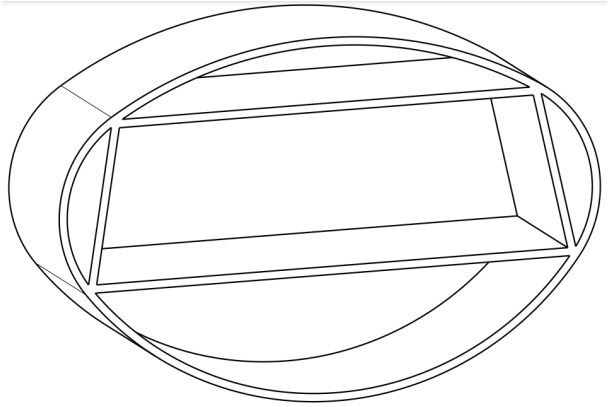

**Figure 8.18:** *Oval fuselage layout [99].*

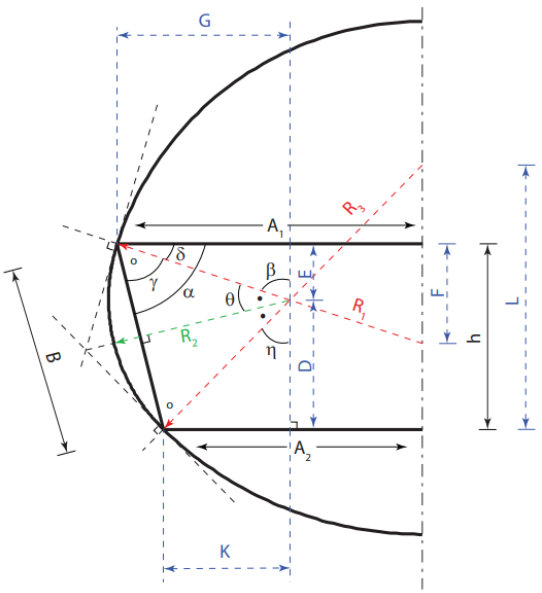


**Figure 8.19:** *Oval fuselage dimensions [99].*

To be able to analyse this cross-section, the ellipse over the arc is assumed to consist of 4 arcs between the connection points. Following the requirements for payload the dimensions for the trapezoidal box can be found. These are then used to compute the dimensions of the remaining arcs. The geometrical relations are illustrated in Figure 8.19 and in Eq. 8.24 to Eq. 8.32. The needed inputs for these relations are the width of the ceiling ($2A_1$) and floor ($2A_2$), height ($h$) and the radius of the arcs at the side ($R_2$).

$$\alpha = arctan\frac{h}{A_1 - A_2} \quad (8.24) \qquad \theta = arcsin\,\frac{B}{2R_2} \quad (8.25) \qquad B = \sqrt{h^2 + (A_1 - A_2)} \quad (8.26)$$

$$\gamma = arccos\frac{B}{2R_2} \quad (8.27) \qquad \delta = \alpha - \gamma \quad (8.28) \qquad \beta = \frac{\pi}{2} - \delta \quad (8.29)$$

$$\eta = \pi - 2\theta - \beta \quad (8.30) \qquad R_1 = A_1/cos(\delta) \quad (8.31) \qquad R_3 = A_2/sin\,\eta \quad (8.32)$$

### 8.4.2. Loading & Fuselage Beam

The load cases presented in 8.1 are used in sizing of the fuselage. The loads that are considered are presented below and its corresponding stresses are numerically solved for the fuselage.

- Tensile stresses in the shell due to pressurisation
- Axial stresses in the members of the trapezoidal structure due to pressurisation and bending moment induced by the wing.
- Longitudinal stresses in the shell and the trapezoidal structure due to the (distributed) inertial loads of the aircraft components.
- Axial and shear stresses in the horizontal members of the trapezoidal structure due to distributed transverse load of furnishing, passengers, cargo and others.

**Fuselage beam**

All the loads acting on the fuselage structure are projected on a one dimensional beam along the longitudinal axis of the aircraft. All loads are directly projected on this beam enabling structural analysis at every point in the fuselage. The loads of the wing are transferred through the wing box and distributed over the whole connection with the fuselage structure. This method is retrieved from [99]. In 8.20 a load distribution can be seen for a load factor of one.

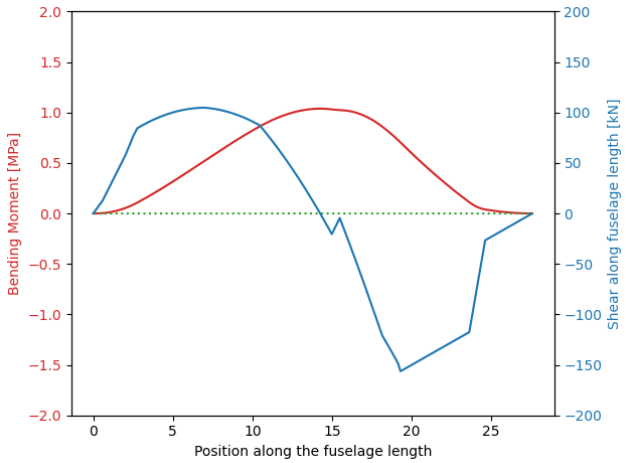


**Figure 8.20:** *Shear and bending moment over the fuselage length.*

The longitudinal bending of the fuselage is introduced in the fuselage beam by replacing them with an equivalent line load. This is calculated by Eq. 8.33 where $\bar{t}$ is the smeared thickness of the cross section, $M$ is the longitudinal moment, $I_{section}$ is the moment of inertia of the idealised cross section. In the horizontal members this line load will lead to a constant stress. In the vertical members this stress will vary over the fuselage height.

$$N_b = \frac{M \Delta z_{max}}{I_{section}} \bar{t} \quad (8.33)$$

The shear in the fuselage is introduced by the inertial loads of the aircraft components and the aerodynamic loads. The shear flow problem is simplified by assuming the floor and the ceiling of the trapezoidal box have a small contribution to the shear flow. By then combining the vertical wall of the trapezoid with the side arc to a smeared thickness, the structure can be analysed.

The shear flow over this arc can be quantified with Eq. 8.34 where $r$ is the radius of the arc and $\alpha$ is the angle between the vertical symmetry axis and the point the arc. Due to the symmetry the shear flow at the top and bottom is known ($q_0 = 0$) and the shear flow can be determined leading to the shear stress in the section by using Eq. 8.35.

$$q = q_0 - \frac{V}{I_{shear}} \int r^2 \, \bar{t} \, cos\alpha \, d\alpha \qquad (8.34) \qquad \tau = \frac{q}{\bar{t}} \qquad (8.35)$$

**Axial forces**

The tensile stresses in the skin are governed by Eq. 8.36 and Eq. 8.37 where $\Delta p$ is the pressure differential induced by the pressurisation of the oval fuselage and $r$ is the radius of the fitted arcs. The pressure differential is set between sea level and a cruising altitude of 11 $km$.

$$N_{p,long} = \frac{\Delta p \, r}{2} \qquad (8.36) \qquad N_{p,lat} = \Delta p \, r \qquad (8.37)$$

Due to the unsymmetrical pressurisation of the fuselage axial forces are introduced in the trapezoidal members. These are derived by utilising node analysis illustrated in Figure 8.21 and are governed by Eq. 8.38, Eq. 8.39 and Eq. 8.40.

$$N_{p,ceiling,inplane} = -\Delta p(r_1 - r_2)(cos\alpha_1 + sin\alpha_1 tan(-\beta)) \qquad (8.38)$$

$$N_{p,wall} = \Delta p(r_1 - r_2)\frac{sin\alpha_1}{cos\beta} \qquad (8.39)$$

$$N_{p,floor,inplane} = -\Delta p(r_3 - r_2)(cos\alpha_3 + sin\alpha_3 \, tan\beta) \qquad (8.40)$$

The axial forces induced by the bending of the wings are introduced as a force couple trough the ceiling and the floor of the trapezoidal box. For positive load factors this is illustrated by Figure 8.22.

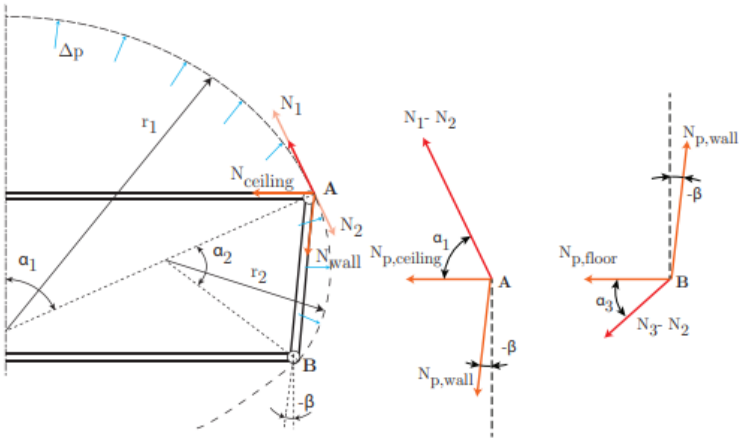


**Figure 8.21:** *Node analysis for the oval fuselage [99].*

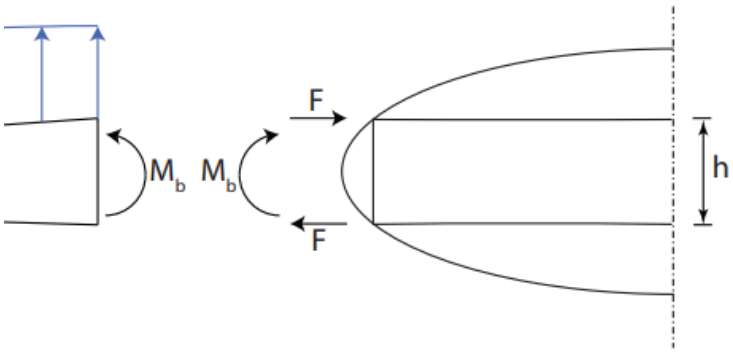


**Figure 8.22:** *Example wing bending for positive load factors.*

### 8.4.3. Inner structure sizing

The trapezoidal structure is loaded in both axial tension or compression and bending loads. A conservative assumption is made to assume this behaves as simply supported. Depending on the detailed design this needs to be reconsidered.

A visual representation of the load over the lateral direction can be seen in Figure 8.23. Here $N_lat$ is the sum of the forces introduced by the pressurisation and the bending of the wing, $q$ is the distributed load introduced by all weight components connected to the floor and $N_{long}$ is the longitudinal force introduced by the fuselage bending.

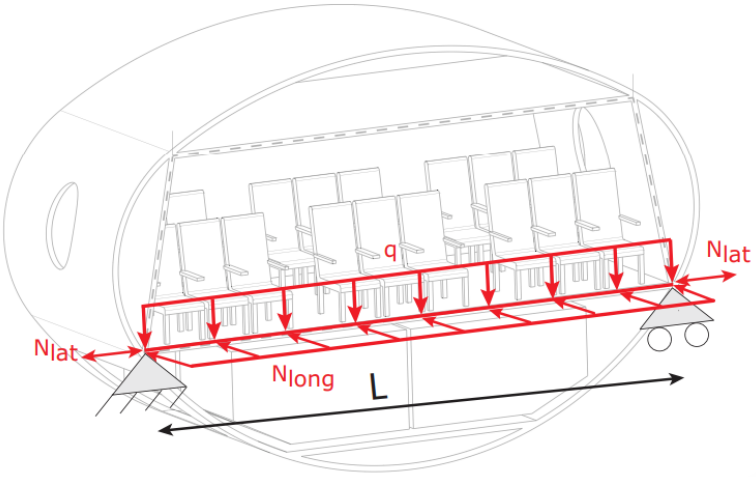


**Figure 8.23:** *Visual representation of floor loading [99].*

The stress in lateral direction can then be determined by Eq. 8.41.

where $I_{beam}$ is the moment of inertia of the beam and the Moment ($M$) is found to be maximum at the symmetry axis and is equal to $\frac{qL}{8}$.

The longitudinal stress, $\sigma_{lon}$ is then found from the line load (Eq. 8.33).

$$\sigma_{lat} = \frac{N_{lat}}{t_{floor}} + \frac{Mz}{I_{beam}} \tag{8.41}$$

$$\sigma_{lon} = \frac{N_b}{t_{floor}} \tag{8.42}$$

The inner structure is sized based on the same method described in Subsection 8.3.7. Instead of checking it on the Tresca yield criterion, which is rather conservative, it is checked on the Von Mises yield criteria Eq. 8.43.

$$\sigma_v = \sqrt{\frac{1}{2}\left[(\sigma_{11}-\sigma_{22})^2 + (\sigma_{22}-\sigma_{33})^2 + (\sigma_{33}-\sigma_{11})^2 + 6(\sigma_{12}^2+\sigma_{23}^2+\sigma_{31}^2)\right]} \tag{8.43}$$

### 8.4.4. Skin & Outer structure sizing

The outer skin is stiffened by frames and hat-stiffeners. For the calculation of the local buckling between the frames and the stringers of the local stiffened panel, the fuselage skin is modelled as rectangular skin sections having a length equal to the frame length $L_{frame}$ and a width constrained by the stiffener spacing $b$. The curvature of the skin is neglected in the local buckling analysis.

The critical buckling stress of the individual panel can then be analysed using Eq. 8.44 in which C can be estimated depending on the support of the sheet [26] with the use of the ratio between parameters "a" and "b" which are indicated in Figure 8.24.

$$\sigma_{cr} = C\frac{\pi^2 E}{12(1-\nu^2)}\left(\frac{t_{shell}}{b}\right)^2 \tag{8.44}$$

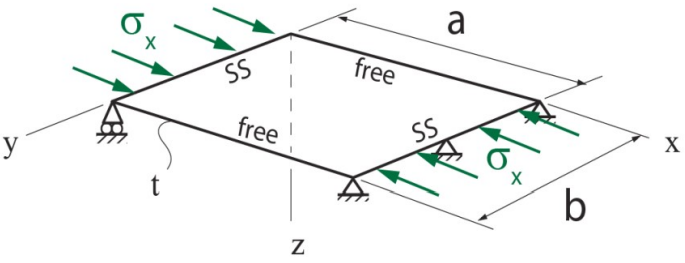


**Figure 8.24:** *Clean thin sheet buckling free body diagram [26].*

A conservative approach is assuming a simply supported constraint all around. For the hat stiffener the crippling stress is determined using Eq. 8.45.

$$\sigma_{cc} = \alpha\left[\frac{C}{\sigma_{yield}}\frac{\pi^2 E}{12(1-\nu^2)}\left(\frac{t}{b}\right)^2\right]^{1-n} \tag{8.45}$$

The skin section supported by the stiffener would now be able to carry the same stress as the stiffener. The effective sheet width $w_e$ can now be calculated using Eq. 8.46.

$$w_e = \frac{t}{2}\sqrt{\frac{C\,\pi^2}{12(1-\nu^2)}}\sqrt{\frac{E}{\sigma_{cc_{stiffener}}}} \tag{8.46}$$

Finally the buckling stress of the stiffened panel can be found using Eq. 8.47.

$$(\sigma_{cc})_{panel} = \frac{\sum \sigma_{cc}^{(i)} A_i}{\sum A_i} \tag{8.47}$$

### 8.4.5. Design parameters & Recommendations

The final design parameters regarding the fuselage box can be seen in table Table 8.7. These are the needed dimensions with the usage of Aluminium-2024-T4 for all structural components. For now this material was chosen as it is widely used in the aircraft industry and will give a accurate comparison between the output of the FLOPS method and the first analysis of the structure.

Further material selection for the structure heavily influences the needed combination of stringers, frames and sheet thicknesses. A trade-off should be done between the performance of the structure and its associated cost.

**Table 8.7:** *Final design values of fuselage.*

| Name | Value |
|---|---|
| Stringer cross-section area [mm$^2$] | 276 |
| Stringer spacing [mm] | 400 |
| Frame spacing [mm] | 1200 |
| Floor thickness [mm] | 7 |
| Ceiling thickness [mm] | 8 |
| Wall thickness [mm] | 8 |
| Skin thickness [mm] | 3 |
| Total weight of fuselage [kg] | 17388 |

In the same manner as for the wingbox discussed in Section 8.3 some future recommendations are presented. Due to limitations in available time and deep understanding of lightweight structures, conservative approaches were made.

For the inner trapezoidal fuselage structure the usage of sandwich panels was considered but not implemented. The increased properties of sandwich structures against bending reduce the longitudinal stresses and will lead to a reduction in structural weight. This can be further reduced by utilisation of composites in the face material of the sandwich structure as the shear stresses could be carried by the core material. Unfortunately the combination of different buckling modes illustrated in Figure 8.25 of the sandwich panel make this a rather complicated subject.

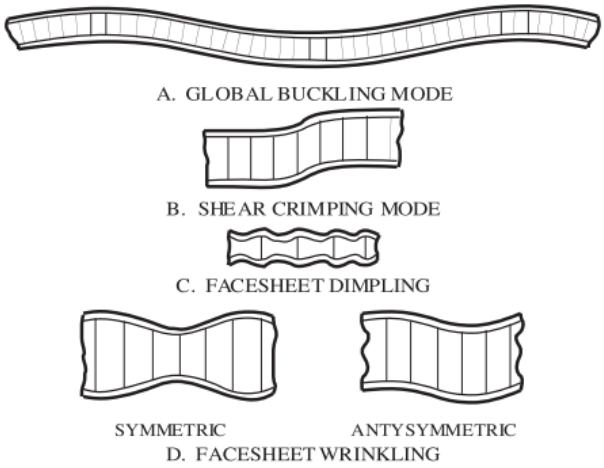


**Figure 8.25:** *Failure modes of a sandwich panel [52].*

In the same manner one major aspect that is not yet considered is the sizing of the frames. As these should be sized, independently of the stiffened skin, to prevent general instability of the fuselage due to compressive forces. A second sizing parameter can be considered in varying the thickness of the structural members along the fuselage length.

## 8.5. Verification of the Programs for Structures

Before the structures of the Lightning2 aircraft can be finalised, a verification has to be performed on the programs used.

The first test is the visual inspection of the code. This includes, for example, identifying and resolving any occurring errors. Visual inspection is complemented by plotting loads and stresses over the cross sections and identifying abnormalities. For example, the shear distribution should increase when moving to the root, because the shear at one point includes the summation of all shears from that point to the tip. Furthermore, in the wingbox

design a discontinuity was observed located at the kink of the wing plan-form. The discontinuity observed is an expected behaviour due to a change in direction of the elastic axis.

The second test is to check the outcomes of the code by comparing it to hand calculations. For example, the total force distribution can be determined by hand by superimposing the aerodynamic tangential force and the engine thrust. The same procedure can be used by calculating stresses for a particular cross section.

The third step is to do a unit decomposition on the used formulas to ensure that the inputs are implemented in the correct units since it is crucial to avoid mixing imperial and metric units. The results of the tests are described in Table 8.8.

**Table 8.8:** *Benchmark tests for the structure.*

| Identifier | Test | Final result |
|---|---|---|
| V.STR.B.1 | Visual inspection | Pass |
| V.STR.B.2 | Hand calculations | Pass |
| V.STR.B.3 | Unit decomposition | Pass |

## 8.6. Validation of the Programs for Structures

In order to validate the simulations, the technique of proof of match shall be used in which the experimental scenarios are recreated and compared to the simulation results. In terms of the structural validation, first, simple geometries shall be manufactured after which the specimens shall be tested under unit loads. As the simulations are completely parameterised, adapting to different shapes can straightforwardly be done, thus modifying the simulations with the exact same geometry and loads as the above mentioned test specimen shall results in comparable numbers (stresses and/or deflection) which serve as the basis of the validation. For example, off the shelf pressurised hydrogen tanks for the hydrogen tank, small scale pressurised cylinder for the fuselage or a swept rectangular beam for the wingbox.

# 9

# Stability & Control

In this chapter, the stability and control of the aircraft will be addressed. Section 9.1 first presents the sizing of the vertical tails, after which the centre of gravity margins and longitudinal stability is presented in Section 9.2. The control surfaces are sized in Section 9.3, after which the undercarriage sizing and positioning is presented in Section 9.4.

## 9.1. Vertical Tail Sizing

The key element of lateral stability and control is the vertical tail. Due to the spacial interference with the distributed propulsion, and the longer moment arm, the vertical tail is positioned on the wingtips of the aircraft. Another reason why the vertical tail was chosen to be split in two was to reduce the later-directional coupling, which long vertical tails are more prone to. By positioning the vertical tail on the wingtips, dynamic instabilities are reduced. This section aims to describe the sizing method of these vertical tails and the results. The sizing is based on the DATCOM1982 method [100].

This method sizes the vertical tail based on both control and stability. These two yield two required tail surface areas, for which the biggest is the most critical and will be used for sizing. Since the vertical tails are connected to the wingtips, its root chord should be equal to the tip chord of the aircraft. It was assumed for the critical moment arm that a quarter of the engines would malfunction on the same side. Following the method outlined in [100], the required tail area then follows straightforwardly. For the Lightning2 aircraft, the control criteria is the most critical. This is because stability yields a very small surface area, since the aircraft does not have a distinctive fuselage. The taper ratio was assumed to be 0.7, with a quarter chord sweep angle equal to the quarter chord sweep angle of the main wing plus three degrees. Other required variables for this method were assumed according to the corresponding notes made in [100]. The resulting tail planform parameters are shown in Table 9.1. Note that $S_{vertical\ tails}$ here refers to the total tail surface area of both tails combined, whereas the other parameters pertain to a singular vertical tail.

**Table 9.1:** *The dimensions of both vertical tails at the wingtips of the aircraft.*

| Parameter | Value |
|---|---|
| $S_{vertical\ tails}$ [m$^2$] | 30.74 |
| $b_{vt}$ [m] | 5.24 |
| $\Lambda_{0.25c}$ [deg] | 52.34 |
| $c_{r_{vt}}$ [m] | 3.45 |
| $c_{t_{vt}}$ [m] | 2.41 |
| $MAC_{vt}$ [m] | 2.96 |
| $YMAC_{vt}$ [m] | 1.23 |

## 9.2. Stability

All operational aircraft (there are few exceptions) are designed to be stable. Stability ensures that the aircraft will go back to its initial state after any type of disturbance, such as gusts or sideslip. A stable aircraft also ensures safety of the passengers. Special care has to be given when designing the blended wing body aircraft,

because the lack of a horizontal tail can introduce major instability issues. In this section a process and design choices will be presented that are tailored to ensure the static stability of the Lightning2.

### 9.2.1. Longitudinal stability

The blended wing body falls in a category of tailless aircraft, which tend to have stability issues due to the lack of a horizontal stabiliser, which counteracts the pitching moment introduced by a wing. In order to achieve longitudinal static stability, two conditions need to be satisfied: $C_{m_\alpha} < 0$ and $C_{m0} > 0$ [78]. For a tailless aircraft, the $C_{m0} = C_{m_{ac}}$, the aerodynamic centre becomes a neutral point, and the equation for longitudinal stability is given by Eq. 9.1. Since $C_{m_{ac}}$ does not change with angle of attack, taking the derivative with respect to $\alpha$ gives Eq. 9.2.

$$C_m = C_{m_{a.c.}} + C_L \frac{(x_{cg} - x_{ac})}{\bar{c}} \tag{9.1}$$

$$\frac{dC_m}{d\alpha} = \frac{dC_L}{d\alpha} \frac{(x_{cg} - x_{ac})}{\bar{c}} \tag{9.2}$$

To satisfy the first equation, the centre of gravity must be in front of the aerodynamic centre. To satisfy the later condition, it is required that $C_{m_{ac}} > 0$. Airfoils used by conventional aircraft typically have $C_{m_{ac}} < 0$. Hence, for this design, an airfoil with reflexed camber line was used. The downside of a reflexed airfoil is that it provides less lift than a conventional airfoil at the same angle of attack. This proved not to be an issue due to large lifting surface area of the design.

While theoretically $C_{m0} < 0$ can provide stability, $C_{L_{trim}} < 0$, making the aircraft uncontrollable in normal flight conditions [78]. It is also possible for a tailless aircraft to have a conventional airfoil with $C_{m_{ac}} < 0$ if the moment is compensated for with wing sweep and twist for washout. However, $C_{m_{ac}}$ still has to be very close to 0, and the washout angle might impose structural complications in the wingbox design for a high wingspan. Just as the reflexed airfoil, the washout produces drag. For these reasons, along with the reasons outlined in Chapter 7, a reflexed airfoil was chosen.

### 9.2.2. Loading diagram Centre of Gravity Excursion

To ensure longitudinal stability, the centre of gravity must be in front of aerodynamic centre. In order to ensure that the aircraft is stable in all flight conditions, a loading diagram and c.g. excursion need to be constructed. First a class I c.g. excursion is made for different loading cases: operational empty mass (OEM), OEM and full fuel tanks, OEM and full payload, and both combined. Figure 9.1 displays the c.g. as fraction of MAC for each of these loading cases. For this figure, $MAC = 14.39$ m, with $LEMAC = 10.56$ m, and the aerodynamic centre located at $0.25MAC$.

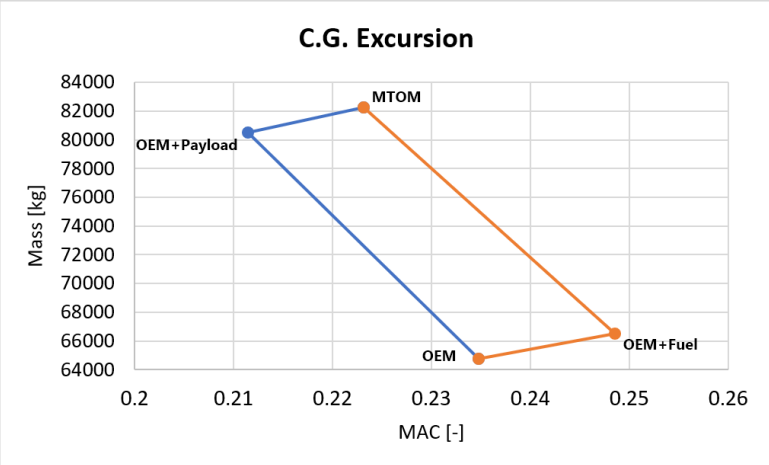


**Figure 9.1:** *Class I c.g. excursion.*

After positioning of the landing gear and vertical tail sizing has been performed, a loading diagram is constructed for a more accurate c.g. excursion prediction, which can be seen in Figure 9.2. The diagram shows how the c.g. of the aircraft shifts when loading cargo, passengers and fuel. This provides a better insight into how the c.g. can change throughout different phases of flight. Figure 9.3 shows how the bubbles in the loading correspond to a way of boarding passengers (colours match with the loading diagram). The average passenger and carry-on luggage mass was assumed to be 90.7 kg. The c.g. location shift is very minimal. This is because the aircraft has only 15 rows, so the moment arm to shift the c.g. when boarding passengers is minimal. A 1% margin was also added to the c.g. shift, for which the upper bound exceeds the location of the aerodynamic centre. To account for this, it is advised to implement certain procedures to avoid overloading the aft part of the aircraft.

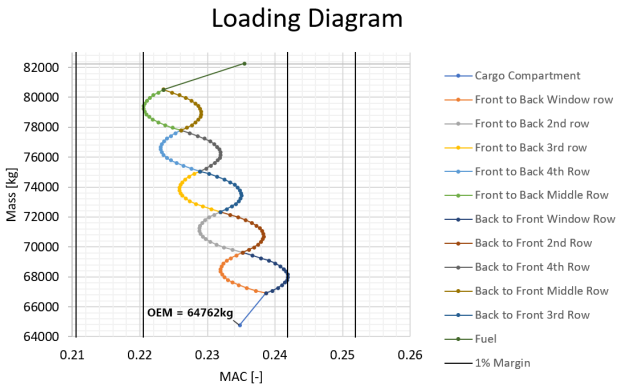


**Figure 9.2:** *Loading diagram showing the position of the c.g. during loading of the Lightning2 aircraft.*

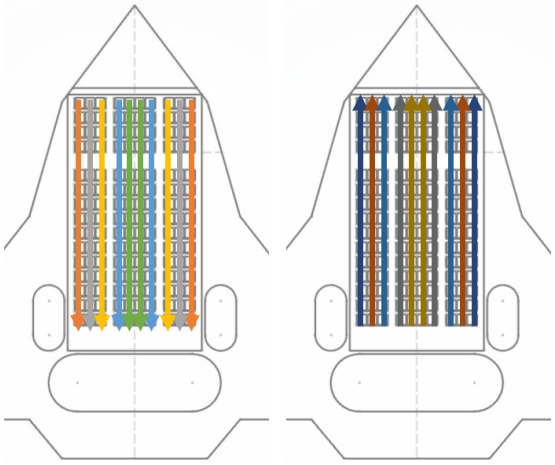

**Figure 9.3:** *Two methods of loading passengers: front to back and back to front.*

The roll stability that keeps the wings level is provided by the dihedral angle of 3 degrees on the outer wing, which is a common angle transport aircraft[82]. The restoring roll moment application is no different than from a conventional aircraft.

## 9.3. Control

All control surfaces located on the wing can provide both pitch and roll control. Such control surfaces are called elevons, a combination of elevator and aileron. One of the disadvantages of a blended wing body is that it has a very low moment arm, thus requiring large elevons which need strong and heavy actuators to operate. In this section, the control surfaces design is outlined, starting with the roll control surfaces.

### 9.3.1. Roll control surfaces

First, the required surface area for a roll manoeuvre was sized. The blended wing body design falls under the class II aircraft classification as a low to medium manoeuvrability aircraft. This means that the aircraft must roll 45 deg in 1.4 s. The roll time and roll rate are given by Eq. 9.3 and 9.4, respectively [77].

$$\Delta t = \frac{\Delta \phi}{P} \tag{9.3}$$

$$P = -\frac{C_{l_{\delta a}}}{C_{l_P}} \delta a \left(\frac{2V}{b}\right) \tag{9.4}$$

In Eq. 9.4, $C_{l_{\delta a}}$ is the aileron control derivative and $C_{l_P}$ is the roll damping coefficient. The aileron derivative depends more on aileron shape and location, while the roll damping coefficient depends more on wing geometry and aerodynamic characteristics. For best roll performance, the control surfaces were placed in the area that is not affected by engines, which starts at 9.864 m from the centre line of the fuselage, extending to the wingtip. The control surfaces must also lie behind the wingbox, implying the ailerons start at $0.7x/c$. This location maximises the aileron effectiveness coefficient, such that $\tau = 0.8$. The aileron effectiveness is used in calculating the roll control derivative, given by Eq. 9.5. For the roll damping coefficient, given by Eq. 9.6, the aerodynamic properties $C_{l_\alpha}$ and $C_{d_0}$ were taken from the aerodynamic analysis of the wing [77]. The effective deflection angle is set as 30 deg [29], which is a typical value for a blended wing body. To account for adverse yaw, differential ailerons are preferred. The deflection ratio is taken as 0.75 [77], such that the down going aileron

will deflect 25.7 degrees and upward going by 34.3 degrees. Finally, since the most critical case occurs when the speed is lowest, $V$ is taken equal to the stall speed at MTOW, such that $V = V_{stall}$. In the equations for the aileron control derivative and roll damping coefficient, $c(y)$ is the function describing the chord as a function of spanwise location, given by Eq. 9.7.

$$C_{l_{\delta a}} = \frac{2c_{l_\alpha}\tau}{S_{ref}b}\int_{b1}^{b2} c(y)ydy \tag{9.5}$$

$$C_{l_P} = -\frac{4(c_{l_\alpha} + c_{d_0})}{S_{ref}b^2}\int_0^{b/2} c(y)y^2dy \tag{9.6}$$

$$c(y) = c_r - c_r(1 - \frac{c_t}{c_r})\left(\frac{y}{b/2}\right) \tag{9.7}$$

For the critical case identified above, it was found that the entire spanwise length from $9.864$ m to $18$ m is required for the ailerons. However, if these deflections were applied during cruise conditions, the bending moment will be too high and could cause the wing structure to fail. For this reason, the wing was split at $13.2$ m, which allowed just enough aileron surface area to satisfy the roll requirement for cruise speed. Figure 9.4a illustrates the aileron allocation. Finally, these ”ailerons” can also act as pitch control surfaces if required.

### 9.3.2. Pitch control surfaces

In the introduction to this section, it was mentioned that BWB designs tend to have difficulties when it comes to sizing and placing control surfaces. The most limiting case for pitch control sizing is the rotation during the take-off. Low speed combined with a pitch down moment from the engine thrust and low moment arm calls for very large and quick acting elevons. Usually, the wing area available for control surfaces is also limited by the engine placement to avoid hot engine exhaust. However, the Lightning2 aircraft is driven by electric distributed propulsion removing this limitation. In fact, the engine exhaust can be used to increase the effectiveness of the pitch control surfaces. This would result in a lower surface area required for the elevons. The blown flaps can also be used in flight by applying different thrust settings between engines when certain control surfaces are deflected. It has been shown that such external control surface blowing can increase their effectiveness by 26% at idle and 44% at full thrust [83]. The trim deflection of the surface is also reduced. Shortly after landing, blown flaps can be extended at high angles to reduce velocity on the runway. During take-off, the exhaust velocity is $M = 0.66$, which is lower than the freestream during cruise, so no additionally strengthened elevon actuators are necessary. A disadvantage of blown flaps is the additional drag generated and loss of pitch moment capability in case of major engine loss.

Another way to improve the pitch-up moment during take-off is a belly flap [105]. This is a flap located at the bottom of the fuselage, at the centre of gravity. By deflecting it 90 degrees, the static pressure increases in front of it and decreased behind it, resulting a pitch-up moment. From experimental data, it is shown that a belly flap may increase $C_L$ by 35% and the pitching moment 10% together with other pitching surfaces. The main disadvantage is once again drag, as well as possible structural damage from runway debris. This flap is implemented in the design as a redundancy feature on the aircraft, the hinge location is at the centre of gravity of the aircraft with a surface area of $6m^2$ and spanning entire fuselage width (8.86m).

### 9.3.3. Resulting control surface configuration

The proposed configuration of control surfaces can be seen in Figure 9.4b. The blown over surface area resulted in around $22m^2$ by sizing to maximum possible area that would not interfere with engines or hydrogen tank. The roll dominant area (blue coloured) is $75.36m^2$, which was sized by aileron method mention before. All control surfaces are coupled, which means that the pilot cannot directly deflect only outboard or inboard surfaces. Hence, a fly-by-wire system has to be implemented. A thrust augmentation system should also be implemented, to provide trim or pitch moment. For example, during landing, when engine thrust is lower, certain engines can be chosen to to provide more thrust than others, to increase effectiveness of the elevators behind them. The locations of the ailerons on the wing, including the split, are also shown in Figure 9.4a. The key values can be seen it Table 9.2.

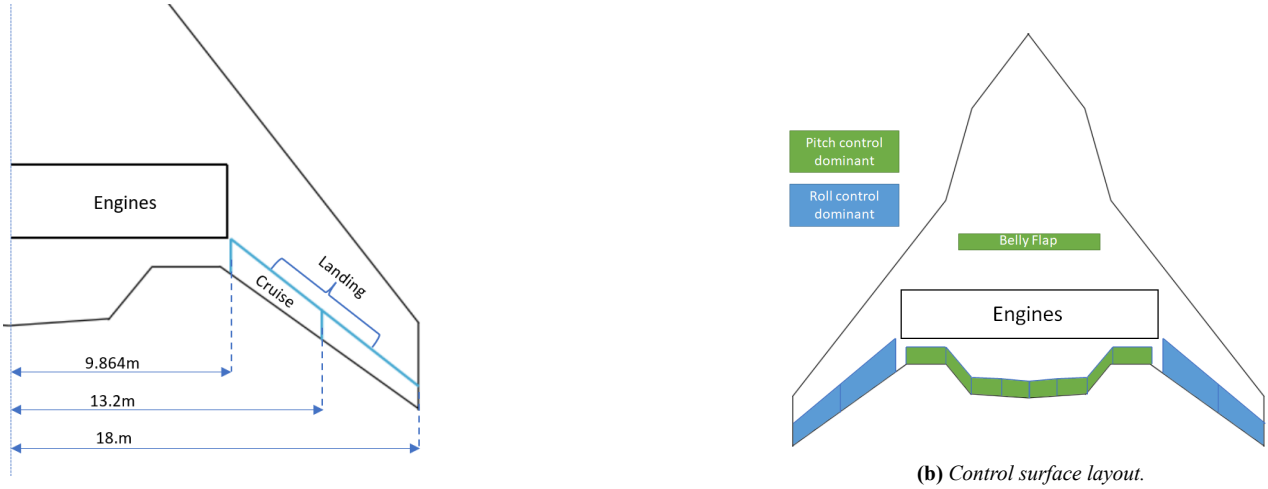


**(a)** *Aileron locations on a wing.*

**(b)** *Control surface layout.*

**Figure 9.4:** *Placement of control surfaces on the Lightning2 aircraft.*

**Table 9.2:** *Key values of the control surface sizing.*

| Name | Value |
|---|---|
| Minimum Aileron Area [$m^2$] | 34.05 |
| Total Trailing Edge Surface Area[$m^2$] | 97.36 |
| Belly Flap Area [$m^2$] | 6 |
| Total Vertical Stabiliser Area [$m^2$] | 30.74 |
| Vertical Tail Height [m] | 5.24 |
| Most Aft C.G. [m] | 14.136 |
| Most Forward C.G. [m] | 13.6 |
| Aerodynamic Centre Location [m] | 14.38 |

## 9.4. Undercarriage Sizing & Positioning

This section discussed the undercarriage design of the Lightning2 aircraft. The wheel sizing is performed in Subsection 9.4.1, after which the positioning is outlined in Subsection 9.4.2.

### 9.4.1. Sizing of Landing Gear

The sizing of the wheels of the landing gear consists of determining the diameter and width [114]. These values of will differ for the nose gear wheels and the main landing gear wheels. Additionally, the sizing of the landing gear wheels is an input to the zero-lift drag estimation during the iteration.

Based on the weight of the aircraft, the nose gear is chosen to have two wheels (one on either side of the strut). The main landing gear follows a similar configuration, however, consists of a two struts for a total of four wheels. The tire pressure is dependent on the intended surface the aircraft will be operational on. To determine a adequate tire pressure, equivalent values to the A320 are assumed, resulting in a tire pressure of approximately 200 psi[1] . At this stage, the nose and main landing gear are assumed to have the same tire pressure. With the pressure and static load distribution amongst nose and main landing gear, specific tire dimensions (diameter and width) can be selected according to methods presented in [114]. It is important to note that at this stage, the ultimate load cases resulting in failure are not taken into account in the design. Table 9.3 includes the diameter and width dimensions for either type of landing gear.

$$P_{\text{mw}} = 0.92 W_{\text{TO}} / N_{\text{mw}} \qquad P_{\text{nw}} = 0.08 W_{\text{TO}} / N_{\text{nw}} \tag{9.8}$$

[1] `https://www.boeing.com/commercial/aeromagazine/aero_05/textonly/m03txt.html` - Accessed: 8-6-2022

**Table 9.3:** *Landing gear wheel sizing.*

| | Nose gear wheels | Main landing gear wheels |
|---|---|---|
| **Diameter** [m] | 0.762 | 1.270 |
| **Width** [m] | 0.196 | 0.508 |

### 9.4.2. Positioning of Landing Gear

The longitudinal position of the nose and main landing gear is determined using the most aft centre of gravity location of the aircraft and the fact that 10% of the load is carried by the nose gear to ensure adequate ground steering and ample braking during landing. Additionally, the distance between the centre of gravity and the main landing gear must be large as this is the moment arm for the upward pitching moment during take-off, and the scrape angle criteria must be met.

$$P_{\text{n}} > 0.10W \tag{9.9}$$

The lateral positioning of the main landing gear is performed through adherence to various criteria, being the lateral tip-over criterion, Eq. 9.10, wing tip clearance, Eq. 9.11, and engine clearance [114]. The critical lateral position is taken from the set of equations. The engine clearance can be disregarded as for the Lightning2 design, the engines are not located under the wing.

$$y_{\text{MLG}} > \frac{l_{\text{n}} + l_{\text{m}}}{\sqrt{\frac{l_{\text{n}}^2 \tan^2 \psi}{z^2}} - 1} \tag{9.10}$$

$$y_{\text{MLG}} > \frac{b}{2} - \frac{z_{\text{t}}}{\tan \varphi} \tag{9.11}$$

Table 9.4 presents the longitudinal and lateral positioning of all nose and main landing gear. The longitudinal distance is measured from the nose of the aircraft. The lateral distance is measured from the centerline outwards. A minimum lateral position of the main landing gear is found to be 3.20 m, however, a further outward position is chosen to incorporate the main landing gear in the wing of the aircraft.

**Table 9.4:** *Landing gear longitudinal & lateral positioning.*

| | Nose gear | Main landing gear |
|---|---|---|
| **Longitudinal** [m] | 5.15 | 15.39 |
| **Lateral** [m] | 0 | +/- 5.00 |

## 9.5. Verification of Stability and Control

The code was written for aileron sizing, c.g. excursion, landing gear placement and vertical tail sizing in forms of smaller functions. The unit testing was based on the same method that was applied in previous sections: visual inspection, comparing to hand calculations, and unit decomposition. For example in visual inspection, the output of the landing gear was replicated in 3D Experience and measured to check whether combination of scrape and main landing gear position actually did not interfere with aircraft it self. In addition to hand calculations, an equivalent model in Excel was used for certain programs. When testing the c.g. excursion, a program was compared against already verified excel program when conventional aircraft was being sized for trade-off. It allowed to find a mistake in mixed up signs. In during unit decomposition, a mistake was found in angle units of aileron sizing.

After the unit testing, a sensitivity analysis was done together with a sanity check. The sensitivity testing included checking whether increased aileron size yields lower roll rate or if changing c.g.location of certain component does make the c.g. of the aircraft change towards the required direction. Similar test was done for vertical tail sizing program, to see whether the c.g. shift in c.g. excursion affects the size of vertical tail. Some examples of sanity checks include checking whether aileron area does not exceed wing area for given range or if the vertical shape and area corresponds with the constrained root chord. All types of unit tests have passed the check.

## 9.6. Validation of Stability and Control

After passing all verification tests, the results should be validated. At this stage, the validation of the control surfaces and the control derivatives with propulsion system effect is not possible yet. For this, wind tunnel tests need to be performed and compared with more in depth analysis tools, such as Computational Fluid Dynamics.

## 9.7. Recommendations for Further Design

The stability and control aspects of the aircraft are very difficult to predict and the blended wing body design is very difficult to make stable. For better understanding, very complex analysis tools, such as CFD simulation, need to be used. For full accuracy, the wind tunnel tests need to be completed to measure the effect of the fuselage and engine exhaust on the elevators, the functionality of the belly flap. A dynamic stability analysis, which is out of the scope of this project, also needs to be conducted to find all control derivative values. If further analysis proves the aircraft to be unstable, a possible solution is to implement relaxed stability with active control.

# 10

# The Final Design

In this chapter, the iterative process used to obtain the final converged design is outlined. Section 10.1 presents the iteration flow diagram. Next, Section 10.2 presents the iterative behaviour of the iteration framework, demonstrating convergence and the behaviour of the design during the iteration process. Finally, Section 10.3 presents the iterated Lightning2 aircraft design.

## 10.1. Iteration Flow Diagram

Design iteration is performed after each subsystem calculation is done. Iteration is needed to ensure a converged final aircraft design that meets all the set requirements. To do so, an iteration framework was setup, as is shown below in Figure 10.1. In this framework, the FLOPS weight estimation method used was outlined in the Midterm report [111]. For the iteration process, a convergence requirement was set for a 0.5% difference between the $MTOW$ of two subsequent iterations.

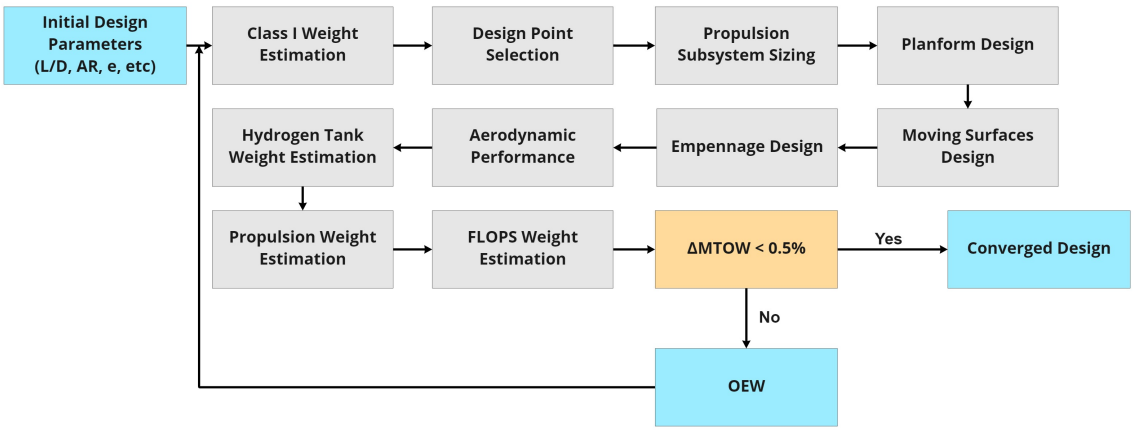


**Figure 10.1:** *Flow diagram of the iteration framework.*

Before continuing to the converged design after the iteration, the design point is presented. The design point is a function of parameters like the zero-lift drag coefficient, and $MTOW$ amongst others. As such, the design point is also part of the performed iterations. The final design point is shown in Figure 10.2, corresponding to a wing loading of $W/S = 2150$ N/m$^2$ and a thrust loading of $T/W = 0.249$. As seen in the loading diagram, this is not the most optimal design point possible. However, the space required to integrate the engines and control subsystems onto the wing require a higher surface area, and therefore a lower wing loading.

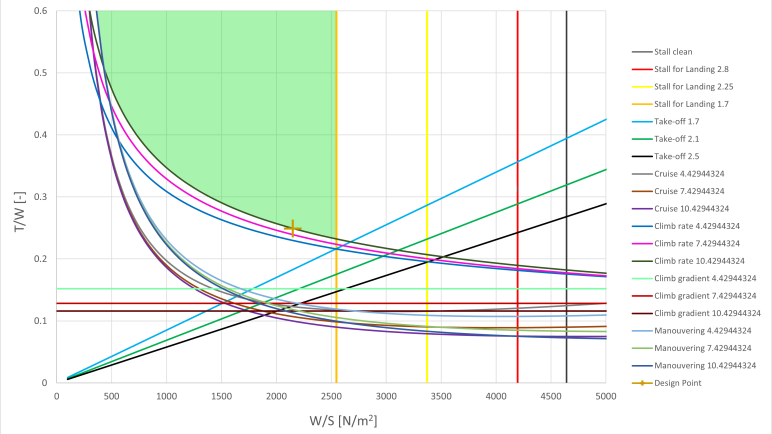


**Figure 10.2:** *Iterated thrust and wing loading diagram indicating the feasible design space in green. The final design point is indicated by a plus.*

## 10.2. Iterative Behaviour

During the iteration, the design parameters change as the design converges. The iterative behaviour of the $MTOW$ is shown in Figure 10.3. This plot demonstrates the convergence of the iteration, with the difference in $MTOW$ tending to zero as the iteration progresses. Plots are also provided for the reference surface area and take-off thrust in Figure 10.4, giving an overview of how the design changes with iterations. Looking at these plots, an increase in area and thrust can be seen after the first iteration. Due to the statistical nature of iteration zero, the aircraft parameters are underestimated. After this statistical phase, these underestimations get corrected, resulting in these increases.

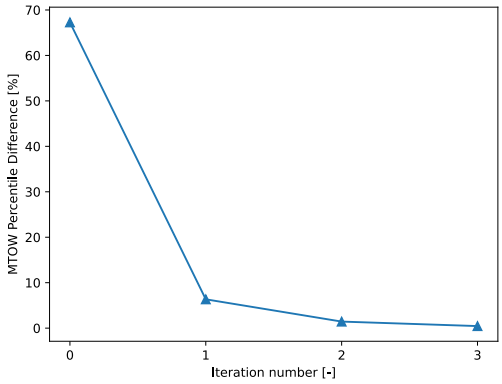


**Figure 10.3:** *Percentage change in $MTOW$ between iterations, showing the convergence of the iteration framework.*

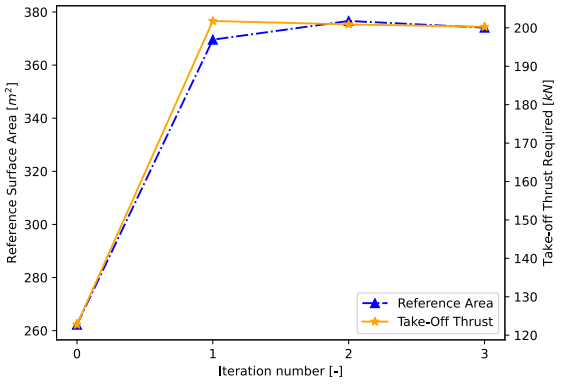


**Figure 10.4:** *Change in reference surface area and take-off thrust required with iterations.*

## 10.3. Summary of the Final Design

With the iteration outlined in the previous sections, a converged design was obtained. For this design, the resulting parameters are shown in Table 10.1, below. The parameters are grouped into the same categories as those used in Figure 10.1.

**Table 10.1:** *Overview of design parameters for the iterated design.*

| Variable | Description | Value |
|---|---|---|
| **Class I Weight Estimation** | | |
| $W_{TO}$ [N] | Maximum Take-off Weight | 806 759 |
| $W_{OE}$ [N] | Operating Empty Weight | 635 100 |
| $W_F$ [N] | Fuel Weight, including allowed boil off | 17 203 |
| **Design Point** | | |

**Table 10.1 continued from previous page**

| Variable | Description | Value |
|---|---|---|
| $S_{ref}$ [m$^2$] | Reference Surface Area | 373.6 |
| $T_{TO}$ [N] | Total Take-Off Thrust Required | 199 996 |
| $W/S$ [N/m$^2$] | Wing Loading | 2 150 |
| $T/W$ [-] | Thrust Loading | 0.243 |
| **Propulsion Subsystem Sizing** | | |
| $N_{eng}$ [-] | Number of Engines | 10 |
| $D_{fan}$ [m] | Fan Diameter | 1.649 |
| $D_{inlet}$ [m] | Inlet Diameter | 1.649 |
| $D_{exhaust}$ [m] | Exhaust Diameter | 1.345 |
| $L_{nacelle}$ [m] | Nacelle Length | 2.729 |
| $D_{nacelle}$ [m] | Maximum Diameter | 1.761 |
| $N_{eng_{fuselage}}$ [-] | Number of Engines Positioned on the Aft Fuselage | 4.732 |
| $N_{eng_{wing}}$ [-] | Number of Engines Positioned on the Wing | 5.268 |
| $b_{DP}$ [m] | Span of Distributed Propulsion | 17.953 |
| $N_b$ [-] | Number of Blades | 8 |
| $N_{FCS}$ [-] | Number of Fuel Cell Stacks | 299 |
| $V_{FC}$ [m$^3$] | Fuel cell volume | 11.4 |
| **Planform Design** | | |
| Fuselage Airfoil | Modified NACA $63_4$-221 | - |
| $S_{cabin}$ [m$^2$] | Cabin Area | 147.9 |
| $S_{fuselage}$ [m$^2$] | Fuselage Area | 211.3 |
| $C_{r_{fuselage}}$ [m] | Fuselage Root Chord | 27.6 |
| $C_{t_{fuselage}}$ [m] | Fuselage Tip Chord | 21.724 |
| $w_{fuselage}$ [m] | Fuselage Width | 8.568 |
| $h_{fuselage}$ [m] | Fuselage Height | 4.200 |
| $MAC_{fuselage}$ [m] | Fuselage Mean Aerodynamic Chord | 24.779 |
| $\Lambda_{LE_{fuselage}}$ [deg] | Fuselage Sweep LE | 53.00 |
| Wing Airfoil | Eppler 325 | - |
| $\Gamma$ [deg] | Dihedral Angle | 3.00 |
| $i$ [deg] | Wing Incidence Angle | 0.57 |
| $x/c_{front\ spar}$ [-] | Front Spar Location | 0.1 |
| $x/c_{aft\ spar}$ [-] | Rear Spar Location | 0.7 |
| $S_{wing}$ [m$^2$] | Exposed Wing Area | 162.277 |
| $C_{r_{wing}}$ [m] | Root Chord | 12.686 |
| $C_{k_{wing}}$ [m] | Kink Chord | 8.094 |
| $C_{t_{wing}}$ [m] | Tip Chord | 3.448 |
| $y_k$ [m] | Spanwise Location of Kink | 9.213 |
| $MAC_{wing}$ [m] | Mean Aerodynamic Chord of the Wing | 7.761 |
| $b$ [m] | Wing span | 36 |
| $\Lambda_{LE_{wing}}$ [deg] | Wing Leading Edge Sweep | 52.12 |
| $\Lambda_{C/4_{wing}}$ [deg] | Wing C/4 Sweep | 47.13 |
| $\Lambda_{C/4_{wing}}$ [deg] | Wing C/2 Sweep | 40.56 |
| **Empennage Design** | | |
| $S_{tails}$ [m$^2$] | Total Surface Areas of Vertical Tails | 30.743 |
| $b_{tail}$ [m] | Span of Each Vertical Tail | 5.245 |
| $\Lambda_{LE_{tail}}$ [deg] | Vertical Tail Leading Edge Sweep | 52.34 |
| $C_{r_{tail}}$ [deg] | Root Chord of Each Vertical Tail | 3.448 |
| $C_{t_{tail}}$ [deg] | Tip Chord of Each Vertical Tail | 2.414 |
| $MAC_{tail}$ [deg] | Mean Aerodynamic Chord of Each Vertical Tail | 2.961 |
| $y_{MAC_{tail}}$ [deg] | Spanwise Location of MAC of Each Vertical Tail | 1.234 |

**Table 10.1 continued from previous page**

| Variable | Description | Value |
|---|---|---|
| **Aerodynamics** | | |
| $C_{L_\alpha}$ [deg$^{-1}$] | Wing Lift Slope | 0.088 |
| $C_{L_{max}}$ [-] | Wing Maximum Lift Coefficient | 1.7 |
| $\alpha_{stall}$ [deg] | Stall Angle of Attack | 13.64 |
| $V_{stall}$ [m/s] | Sea Level Stall Speed | 45.44 |
| $AR_{eff}$ [-] | Effective Aspect Ratio | 4.429 |
| $e$ [-] | Oswald Efficiency Factor | 0.997 |
| $C_{L_{cruise}}$ [-] | Cruise Lift Coefficient | 0.209 |
| $\alpha_{cruise}$ [deg] | Cruise Angle of Attack | 3.1 |
| $C_{D_{0_{clean}}}$ [-] | Zero-Lift Drag Coefficient in Clean Configuration | 0.00636 |
| $C_{D_{0_{landing}}}$ [-] | Zero-Lift Drag Coefficient in Landing Configuration | 0.00939 |
| $L/D_{cruise}$ [-] | Cruise Lift-to-Drag Ratio | 21.97 |
| $L/D_{loiter}$ [-] | Loiter Lift-to-Drag Ratio | 22.54 |
| **Moving Surfaces Design** | | |
| $S_{aileron}$ [m$^2$] | Aileron Surface Area | 70.99 |
| $t_{roll}$ [s] | Roll Time | 1.22 |
| **Hydrogen Tank Design** | | |
| $D_{tank}$ [m] | Tank Diameter | 2.90 |
| $L_{tank}$ [m] | Tank Length | 6.00 |
| $t_{wall,inner}$ [mm] | Inner Tank Thickness | 17.20 |
| $t_{vacuum}$ [mm] | Vacuum Thickness | 5.00 |
| $t_{wall,outer}$ [mm] | Outer Tank Thickness | 3.00 |
| $t_{insulation}$ [mm] | Insulation Thickness | 140.5 |
| **C.G. Excursion** | | |
| $c.g._{aft}$ [m] | Most Aft C.G. | 14.1 |
| $c.g._{fwd}$ [m] | Most Forward C.G. | 13.6 |
| $c.g._{OE}$ [m] | Operating Empty C.G. | 13.9 |
| **Undercarriage Design** | | |
| $D_{nw}$ [m] | Diameter of Nose Wheels | 0.762 |
| $D_{mw}$ [m] | Diameter of Main Wheels | 1.270 |
| $w_{nw}$ [m] | Width of Nose Wheels | 0.196 |
| $w_{mw}$ [m] | Width of Main Wheels | 0.508 |
| $n_{nw}$ [-] | Number of Nose Wheels | 2 |
| $n_{mw}$ [-] | Number of Main Wheels per Landing Gear | 2 |
| $l_{nw}$ [m] | Longitudinal Position of Nose Gear | 5.15 |
| $l_{mw}$ [m] | Longitudinal Position of Main Gear | 15.39 |
| $y_{nw}$ [m] | Lateral Position of Nose Gear | 0.00 |
| $y_{mw}$ [m] | Lateral Position of Main Gear | 5.00 |
| **Class II Weight Estimation** | | |
| $W_{FUS}$ [kg] | Fuselage Weight | 15271.823 |
| $W_{WING}$ [kg] | Wing Weight | 9029.11 |
| $W_{VT}$ [kg] | Vertical Tail Weight | 821.47 |
| $W_{LG}$ [kg] | Landing Gear Weight | 3325.44 |
| $W_{PNT}$ [kg] | Paint Weight | 282.45 |
| $W_{SYSEQUIPMENT}$ [kg] | Systems and Equipment Weight | 9031.88 |
| $W_{OPERATINGITEMS}$ [kg] | Operating Items Weight | 555.65 |
| $W_{PROPULSION}$ [kg] | Propulsion Weight | 22989.03 |
| $W_{HYDROGENTANKS}$ [kg] | Total Hydrogen Tank Mass | 3455.6 |

Furthermore, the complete final Payload-Range diagram can be seen in Figure 10.5, in which an extra 10% of the design payload can be carried with a maximum range of approximately 2 000 km, defining the harmonic range. In addition, if the complete payload is omitted, a ferry range of approximately 9 200 km can be reached.

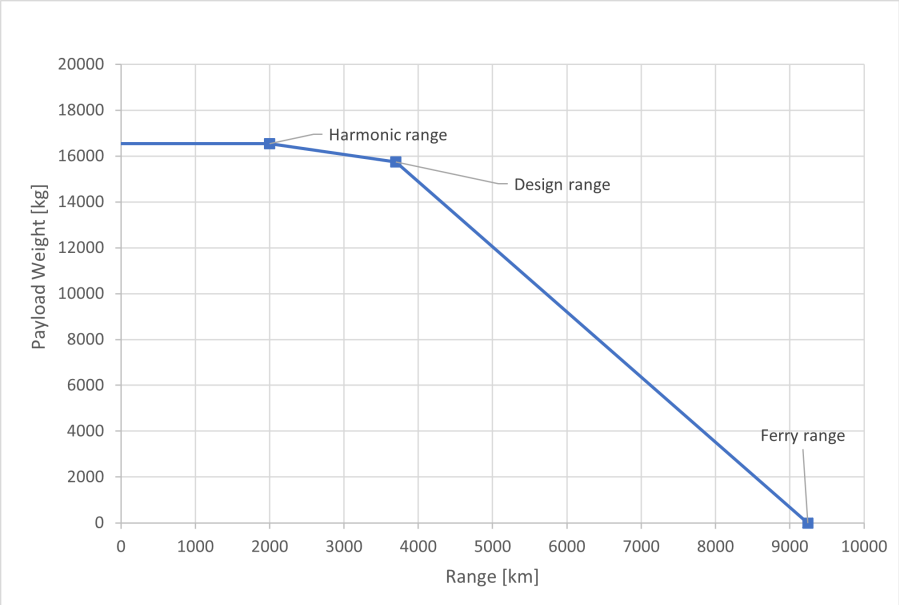


**Figure 10.5:** *Payload-range diagram for the iterated final design of the Lightning2 aircraft.*

## 10.4. Validation of Iterated Design

As a final step in the iteration process of the Lightning2 aircraft, the design is validated against literature. As a fist step, the design point is checked against literature. It is found that for a blended wing body of 150 passengers, a wing loading of $W/S = 2200$ and thrust loading of $T/W = 0.29$ are common [19]. For the Lightning2, the thrust loading is 14.1% lower, which at this conceptual stage is considered validated, especially considering that the reference thrust loading is based of off a conventional turbofan propulsion system.

Another design parameter that was validated is the effective aspect ratio. Due to the inclusion of the fuselage area in the aspect ratio, this parameter is usually much lower for a blended wing body compared to a conventional aircraft. For the iterated design, $AR_{eff} = 4.429$, which matches with the value given in [19], thereby validating the planform design.

# 11

# Resource Allocation

To make sure that the final design achieves the given requirements with acceptable consumption of resources, Technical Performance Measurement (TPM) is applied. This methodology checks whether the discrepancies between actual and required values are within an acceptable margin. If the actual values exceed the limit, it is desired that this is identified in an early stage so that certain measurement can be applied to keep the value within the range. Section 11.1 first presents the technical resource allocation, after which Section 11.2 presents the resource budgets contingencies.

## 11.1. Technical Resource Allocation

The specification values were set in the baseline report during a very early design phase. At that stage, most technical resources are difficult to predict since the aircraft configuration is still unknown. Therefore, these specifications were set based on the Airbus A320neo, as this is an aircraft comparable in size and mission to the Lightning2 aircraft. After the midterm report, the design has been finalised, being a blended wing body with a hydrogen propulsion system, so the specification values can be filled in.

The technical resource allocation can be seen in Table 11.1. The specification values are determined after performing the Class I weight estimation. Regarding the noise levels, from the Flightpath 2050 document it states that the perceived noise reduction should be at least 65% with respect to aircraft that entered service in 2000 [37]. To achieve this, 100.87 EPNdB is set for the approach specification value.

Since it is impossible to keep track of all the parameters and plot the corresponding graphs for each of them at each stage during the design, several key parameters are recorded: MTOW, $W_F$, $T_{TO}$, and $L/D_{cruise}$. The maximum take-off weight is the most top-level parameter to track, as it gives an overall view of the design. The design fuel weight in this case is the amount of hydrogen used for the mission, which directly relates to the design of the hydrogen tank. Total thrust is another parameter that will be monitored since that affects the number of fuel cells as well as the engines. $L/D_{cruise}$ plays an important role in the airfoil selection and aircraft aerodynamics.

**Table 11.1:** *Technical performance table.*

| | **Aircraft Technical Resources\Budget** | **Specification** | **Target** |
|---|---|---|---|
| General resources | $MTOW$ [kg] | 49 422.0 | 37 066.5 |
| | Cruise specific fuel consumption [kg/kNs] | 1.42E-05 | 1.07E-05 |
| | Usable Fuel Weight [kg] | 24 240.0 | 18 180.0 |
| | Aircraft dispatch reliability [%] | 99.7 | 99.7 |
| | Aircraft trun around time [min] | 45.0 | 33.8 |
| | Max Take-Off Thrust [kN] | 320.0 | 240.0 |
| | Cruise L/D [-] | 16.1 | 12.1 |
| Resources from customer requirements | Series production cost [Mil $] | 110.0 | 82.5 |
| | development time [years] | 5.0 | 3.8 |
| | Take off distance [m, sea level] | 2 000.0 | 1 500.0 |
| | Landing distance [m, sea level] | 1 400.0 | 1 050.0 |
| | Life time [year] | 30.0 | 22.5 |

**Table 11.1 continued from previous page**

| | Aircraft Technical Resources\Budget | Specification | Target |
|---|---|---|---|
| | Part recycability [%] | 100.0 | 75.0 |
| | Gas emissions of on ground operations [kg] | 0.0 | 0.0 |
| | Range [km] | 5 317.0 | 3 987.8 |
| | Reduction in NOx emissions [%] | 50.0 | 37.5 |
| | Reduction in CO2 emissions [%] | 75.0 | 56.3 |
| | Noise levels approach [dB] | 100.87 | 99.62 |
| | Noise levels lateral [dB] | 97.16 | 95.91 |
| | Noise level during flyover [dB] | 92.10 | 90.85 |

Table 11.2 shows the values for each of the four chosen parameters at different stages. Correspondingly, four graphs are made to keep track of these values, Figure 11.1 demonstrates how the MTOW changes throughout the design phase. The orange curve represents the actual value of the parameter and the grey curve shows the current value is equal to the actual value including a contingency, reflecting the actual status of the design. The target value in blue equals specification values, represented by the yellow curve, but with contingency subtracted. If actual values exceed the specification values, certain adjustment measures need to be taken. In this case, whenever the current value is lower than specification values, a 10% margin will be added to the current value based on the previous maximum current value reached in iteration. Same method is applied to $W_F$, $T_{TO}$, and $L/D_{cruise}$ which are demonstrated in Figure 11.2, 11.3 and 11.4, respectively.

**Table 11.2:** *Essential parameters at different stages.*

| Stage | MTOW [kg] | $W_F$ [kg] | $T_{TO}$ [N] | $L/D_{cruise}$ [-] |
|---|---|---|---|---|
| Class I | 49 422 | 6 015 | 156 976 | 17.91 |
| Class II | 62 457 | 6 015 | 156 976 | 17.91 |
| 1st Iteration | 87 467 | 2 863 | 177 120 | 24.31 |
| 2nd Iteration | 96 517 | 4 518 | 195 447 | 23.74 |
| 3rd Iteration | 103 299 | 4 643 | 209 180 | 23.61 |
| 4th Iteration | 106 473 | 5 031 | 215 606 | 23.51 |
| 5th Iteration | 108 445 | 5 198 | 219 601 | 23.36 |
| 6th Iteration | 110 251 | 5 305 | 223 256 | 23.29 |
| 1st corrected Iteration | 81 399 | 1 051 | 201 790 | 21.40 |
| 2nd corrected Iteration | 86 951 | 1 552 | 200 551 | 21.76 |
| Final value | 82 267 | 1 754 | 199 997 | 21.97 |

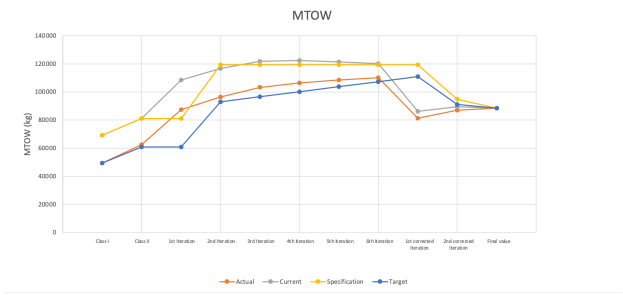


**Figure 11.1:** *Technical Performance Measurement for maximum take-off weight.*

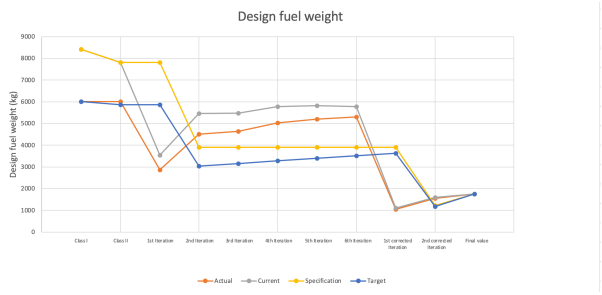


**Figure 11.2:** *Technical Performance Measurement for design fuel weight.*

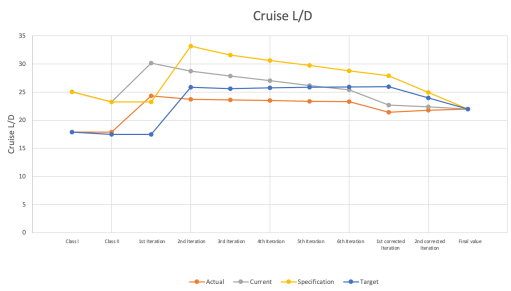


**Figure 11.3:** *Technical Performance Measurement for cruise L/D.*

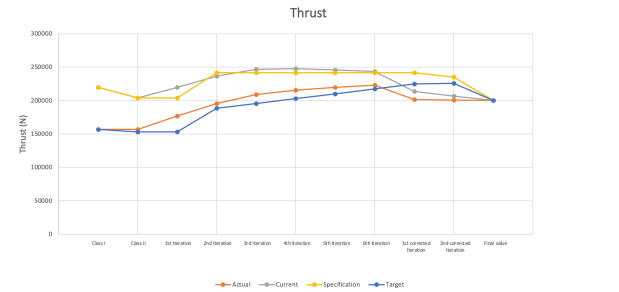


**Figure 11.4:** *Technical Performance Measurement for total thrust.*

## 11.2. Resource Budget Contingencies

Table 11.3 lists out the contingency required for each parameter at the different design phases. This ensures that the actual values for these parameters do not exceed the specification. If it does, it is detected at an early stage. The contingency is initially set at 40% at the Class I design phase since the Class I weight estimation is based on existing aircraft, which have a similar size compared to the A320, so the contingency is set high at the first stage. This decreases with the development of the design. For the Class II weight estimation, the contingency is decreased to 30%, and after each iteration made will decrease by a further 3%, converging to 0% for the final product.

**Table 11.3:** *Resource budgets contingencies table.*

| | **Contingency (%)** | | | |
|---|---|---|---|---|
| **Design maturity**: | **MTOW** | **$W_F$** | **$T_{TO}$** | **$L/D_{cruise}$** |
| Class I weight estimation | 40 | 40 | 40 | 40 |
| Class II weight estimation | 30 | 30 | 30 | 30 |
| 1st Iteration | 24 | 24 | 24 | 24 |
| 2nd Iteration | 21 | 21 | 21 | 21 |
| 3rd Iteration | 18 | 18 | 18 | 18 |
| 4th Iteration | 15 | 15 | 15 | 15 |
| 5th Iteration | 12 | 12 | 12 | 12 |
| 6th Iteration | 9 | 9 | 9 | 9 |
| 1st corrected Iteration | 6 | 6 | 6 | 6 |
| 2nd corrected Iteration | 3 | 3 | 3 | 3 |
| Final value | 0 | 0 | 0 | 0 |

# 12

# Performance Analysis

This chapter contains the analyses regarding the performance characteristics of the aircraft. It commences with the aircraft noise prediction & footprint in Section 12.1. Next, the emissions are quantified in Section 12.2. Subsequently, the take-off and landing performance is discussed in Section 12.3.

## 12.1. Aircraft Noise Prediction & Footprint

Compliance with new noise regulation and targets is a strict requirement of the BWB aircraft design. Before commencement of the noise prediction methodology, the noise footprint definitions as established by the ICAO are depicted in Figure 12.1 [33]. The approach, fly-over, and lateral certification points are well-defined and each must be complied with.

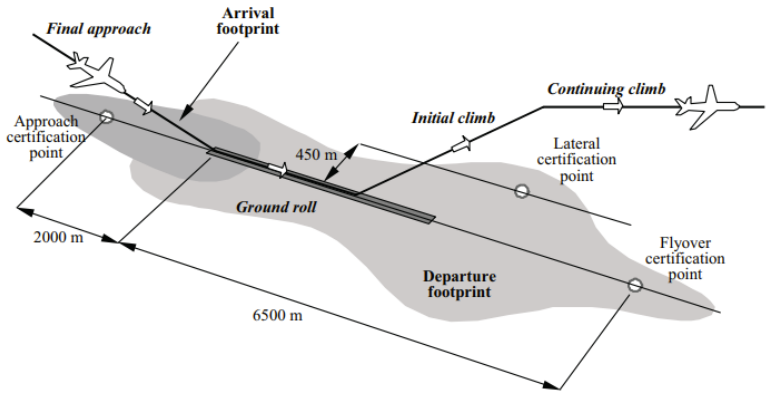


**Figure 12.1:** *Noise footprint definitions for approach, fly-over, and lateral certification points [33].*

For the typical mission profile, the distance and angle between the aircraft and observer at the various certification locations are summarised in table Table 12.1.

**Table 12.1:** *Certification points aircraft location.*

| Certification Point | Distance [m] | Angle [degrees] |
|---|---|---|
| Approach | 101.56 | 90 (below) |
| Lateral | 450.00 | 90 (side) |
| Flyover | 1 429.42 | 90 (below) |

To make an estimate of the emitted noise of the aircraft, the most important sources of noise are considered for near-airport operations, being the engines and the landing gear. The estimation of their individual contributions are detailed in the following subsections: propulsion noise in Subsection 12.1.1 and landing gear noise in Subsection 12.1.2 [118]. The airframe noise is limited to consideration of the landing gear, as experimental data suggests that this is the primary noise source for the very similar Airbus A321 [102]. For this reason, the combination of these sources is expected to give a reliable estimate of the total noise.

### 12.1.1. Propulsion Noise

During take-off, the propulsion system is the main source of noise of the aircraft. Additionally, the ducted fan contributes significantly to the perceived noise in the passenger cabin. These combined reasons render the propulsion system as a quintessential part of the noise prediction analysis.

The methodology outlined in this section concerns the estimation of propeller noise, focusing on the far-field method presented in [45]. A factor representing the benefits of noise shielding from the duct and engine positioning on top of the aircraft is applied to the final obtained value, based on literature. The total sound pressure level is primarily composed of three partial levels, denoted by $FL_1$, $FL_2$, and $FL_3$. The first level consists of the loudness of noise emitted by the propellers, depending on the Mach number of the blade tip ($M_{tip}$) and the horsepower power input of the propeller ($P_{HP}$). [45] has compiled the results of multiple curves into the single parametric formula, Eq. 12.1.

$$FL_1 = 17.237 + 36.886M_{tip} + 6.88ln(P_{hp}) \tag{12.1}$$

This propeller noise is subsequently adjusted based on the number of blades in a single propeller and the diameter thereof, according to Eq. 12.2.

$$FL_2 = 32.551 - 8.312ln(N_B) - 8.642ln(D_p) \tag{12.2}$$

The value is also corrected for damping effects of the atmosphere and the spherical noise propagation from the source. A segmentation is made between very close and further distances from the source, with the cut-off distance being 100 ft, as shown in Eq. 12.3.

$$FL_3 = \begin{cases} 16.29 - 0.5ln(x_{ft}), & \text{if } x_{ft} < 100ft \\ 56 - 9.1202ln(x_{ft}), & \text{if } x_{ft} > 100ft \end{cases} \tag{12.3}$$

To obtain the total sound pressure level, two additional factors are taken into account. Firstly, the directivity of perceived noise ($DI$) is simulated by correcting for the angular position between the source and observer. This distribution is symmetric along the propeller axis, defined as horizontal forward as zero degrees. Secondly, a correction factor ($NC$), depending on the number of propellers (engines), is introduced. [45] provides this factor up to four engines. However, extrapolation using a fitting logarithmic interpolation function reveals this value to be 10 in the case of ten engines. The sum of previously calculated components and correction factors reveals the total sound pressure level ($SPL$) at a specific distance and angle, according to Eq. 12.4.

$$SPL = FL_1 + FL_2 + FL_3 + DI + NC \tag{12.4}$$

The perceived noise level ($PNL$) can be computed by adding a corrective factor computed based on the number of blades of each propeller. The number of blades is chosen to be eight. With that number, the $PNL$ for the propulsion system can be computed. This can be combined with other noise generating components of the aircraft to compute the $PNL$ of the entire aircraft, which can in turn be used to verify compliance with set requirements.

### 12.1.2. Landing Gear Noise

During take-off and landing, the landing gear also greatly contributes to the noise. To estimate the noise generated by the nose and main landing gear, the assumption is made that the main contributors to the noise are the wheels and the struts. This allows for NASA's ANOPPS method to be used [124]. In this method, the polar and azimuthal directivity of the landing gear noise are also taken into account, giving a more accurate result when evaluating the noise at different locations around the aircraft.

To evaluate the noise contributions, the Strouhal number is needed. This number normally depends on the vortex shedding frequency. However an estimate for the Strouhal number such that the noise contribution is maximal was made as $S_{nlg} = S_{mlg} = 10^{0.5}$ and $S_{strut} = 1$.

To find the noise contributed by the landing gear, the acoustic power for the wheels and struts of both the nose and main landing gears are calculated. The mean-square acoustic pressure for the wheels and the struts can then be computed using Eq. 12.5, which is summed to obtain the total mean-square acoustic pressure for the nose and main landing gear, respectively. The perceived noise level for each landing gear can then be found using Eq. 12.6 [124].

$$< p^2 >^* = \frac{\Pi^*}{4\pi(r_s^*)^2} \frac{D(\theta,\phi)F(S)}{(1 - M_\infty \cos(\theta))^4} \tag{12.5}$$

$$PNL = 10 \log_{10} < p^2 >^* + 20 \log_{10} \frac{\rho_\infty a_\infty^2}{p_{ref}} \tag{12.6}$$

### 12.1.3. Total Noise at Certification Points

This section presents the total noise produced by the aircraft at the three certification points. A noise correction factor of 20 dB is deducted for the shielding effects of the wing body and the ducts. This value is taken from [118], taking the lower bound to be conservative. The values at all points result in compliance with the noise requirements set for the project. Note that the requirements at certification points set by [48] are functions of the MTOW of the aircraft, and are specified for the Lightning2 in Table 12.2.

**Table 12.2:** *Total aircraft noise at certification points.*

| Certification Point | Aircraft Noise [dB] | Noise Requirement [dB] |
|---|---|---|
| Approach | 95.98 dB | 100.87 dB |
| Lateral | 94.25 dB | 97.16 dB |
| Flyover | 83.67 dB | 92.10 dB |

### 12.1.4. Verification & Validation

The verification of the noise model consists of performing unit tests analogous to other systems. Subsequently, subsystem checks could be performed on each of the noise components (within the propulsion system and between propulsion and landing gear). Each noise source values are subject to a sanity check. The checks and outcome are summarised in Table 12.3.

**Table 12.3:** *Benchmark tests for the noise.*

| Identifier | Test | Final result |
|---|---|---|
| V.NOI.B.1 | Visual inspection | Pass |
| V.NOI.B.2 | Hand calculations | Pass |
| V.NOI.B.3 | Unit decomposition | Pass |

The validation of the model is difficult at this stage. However, the outcome values are close to the expected results according to regulations [48]. The values are lower than for the A320 which is expected due to the noise shielding in the given aircraft configuration. The noise shielding factor of the ducted fans and their positioning is quoted using [118].

### 12.1.5. Cabin Noise

Although no set requirement concerns cabin noise, it should be equivalent to noise levels experienced by passengers in current fleets, most notably the Airbus A320 and Boeing 737. Excessive cabin noise is not only uncomfortable, but will place the aircraft at a competitive disadvantage as consumers would favour other aircraft. Furthermore, noise above certain levels for prolonged periods at a time can lead to irreversible hearing damage, which clearly is to be avoided. Within the scope of the Design Synthesis Exercise and the current design phase, a detailed vibration/noise simulation of the cabin is infeasible. Nonetheless, it is discussed from a more qualitative perspective and remains a next step of project.

The engine placement on the top-side of the aircraft leads to considerable benefits for noise reduction by shielding due to the airframe. However, naturally, one may wonder about the implications of said positioning for the cabin. First and foremost, the distributed propulsion system is located behind the most aft cabin location. Engines will not be directly above any passenger, for obvious reasons. This makes a considerable difference in vibrations and perceived noise. Secondly, research is conducted on noise absorbent materials that could be used to line the top of the cabin. A leading expert in this field is Luminary Air Group. This company has over 20 years of experience in cabin noise reduction and more importantly, has certification for aircraft applications [1]. The lightweight solutions can be easily installed at minimal cost and have been proven to be adaptable to different aircraft configurations. Testing of noise absorption in the audible ranges of humans will be done before commencing operations with the aircraft in further stages of the project.

## 12.2. Emissions

In the requirements it is stated that the aircraft shall have a 45 % reduction in $CO_2$ and 75 % reduction in $NO_x$ emissions per passenger kilometer [60]. The emissions are evaluated based on the Landing Take-off (LTO) cycle and emissions per passenger kilometer. While emissions per passenger kilometer is mainly focused on the emissions during cruise, a LTO cycle focuses more on the power demanding phases. The emissions of the blended wing body will be compared to that of an A320ceo and an A319neo, as both can transport around the same number of passengers.

### 12.2.1. LTO cycle

A LTO cycle consist of 4 phases; take-off, climb, approach, and taxi/ground idle as shown in Figure 12.2. Each phase has a certain duration and power setting prescribed by ICAO. For the Lightning2 aircraft, used hydrogen can be calculated with the required power during each phase and the duration thereof. As the maximum altitude of the LTO cycle is only 3 000 ft, ISA conditions are assumed during the entire LTO cycle.

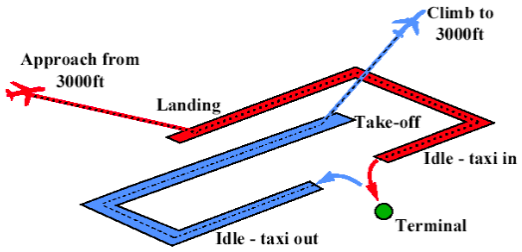


**Figure 12.2:** *LTO cycle [88].*

**Table 12.4:** *LTO cycle [88].*

| Operating mode | Power setting [% of $P_{motor}$] | Time in mode [s] |
|---|---|---|
| Take-off | 100 | 42 |
| Climb | 85 | 132 |
| Approach | 30 | 240 |
| Taxi/ground idle | 7 | 1560 |

For the reference aircraft the LTO emissions for a CFM56-5B4/2P and CFM LEAP-1A26 turbofan engines ,which are used by the the A320ceo and A319neo, respectively. The CFM56-5B4/2P burns 442 kg of fuel during one LTO cycle, while the CFM LEAP-1A26 only uses 324 kg of fuel. Using the required power of the Lightning2, the total hydrogen used during one LTO cycle is 538 kg. This corresponds to a total of 4841 kg of produced water vapour. As shown in Table 12.5, this is a major increase compared to the turbofan engines. However, the effects of water vapour on the environment bellow 25 000 ft are small [50].

**Table 12.5:** *LTO cycle emissions.*

| Emissions | Lightning2 | A320ceo | A319neo |
|---|---|---|---|
| $CO_2$ [kg] | 0 | 2 793.44 | 2 047.68 |
| $NO_x$ [kg] | 0 | 7.75 | 7.07 |
| $H_2O$ [kg] | 1 855.55 | 1 087.32 | 797.04 |

### 12.2.2. Emissions per Passenger Kilometer

The emissions per passenger kilometer can be calculated using the fuel burned and the emission index. The most important emissions to take into account are $CO_2$, $NO_x$, and $H_2O$. The $CO_2$ emission index for a gas turbine

[1] `https://luminary.aero/cabin-comfort-systems/` - Accessed: 02-06-2022

engine equals 3.16 kg/kg of fuel, for $NO_x$ it equals 0.017 g/kg of fuel, and for $H_2O$ it equals 1.23 kg/kg of fuel [47]. It should be taken into account that the emission index of $NO_x$ is highly depending on altitude.

The A320ceo burns on average 2.91 kg/km of fuel for a medium-haul flight (3984 km) [58]. Assuming a 100% load factor the A320ceo can transport 150 passengers resulting in a fuel consumption of 0.0194 kg / km pax. The fuel consumption of an A319neo is equal to 2.4 kg/km for the 136 passenger configuration, which is equal to 0.0176 kg / km pax[2]. For the given design range of 3 700 kilometers, the Lightning2 uses 4908 kg of hydrogen. The used amount of hydrogen corresponds with 79.59 g/km pax of water vapour emissions. Comparing the total amount of energy used by the Lightning2 and the A320ceo, the Lighning2 requires 78.4% less energy for the given design range. An overview of the emissions are given in Table 12.6.

**Table 12.6:** *Emissions produced per passenger kilometer.*

| Emissions | BWB | A320ceo | A319neo |
|---|---|---|---|
| $CO_2$ [g/km/pax] | 0 | 61.30 | 55.76 |
| $NO_x$ [g/km/pax] | 0 | $3.30 \cdot 10^{-4}$ | $3.00 \cdot 10^{-4}$ |
| $H_2$ [g/km/pax] | 26.12 | 23.86 | 21.76 |

While a hydrogen propulsion system eliminates almost all emissions, it is clear that during cruise a lot more water vapour is procured compared to a turbofan engine. However, while water vapour still has a negative effect on the environment if contrails are formed, the effects on the environment are around 10 times less compared to $CO_2$ [23]. This is as the residence time of water vapour is only a couple of weeks while that of $CO_2$ is 100 years [46]. With the hydrogen propulsion, the Lightning 2 satisfies the requirements MIS.SUS.4.1 and MIS.SUS.4.3.

## 12.3. Take-off and Landing

In the client requirements it is stated that the aircraft shall have a maximum take-off distance of 2 km and a maximum landing distance of 1.4 km [111]. The take-off and landing distance are depending on the performance of the aircraft. The design space in the loading diagram is already restricted by the maximum take-off and landing distance but it should be double checked if the aircraft indeed satisfies these requirements. Both the take-off and landing distance are calculated for normal operations at sea level conditions.

### 12.3.1. Take-off

The take-off consists of two parts; the ground run and airborne phase. The airborne phase is the distance the aircraft covers until it clears a height of 15.2 meters. A method taught in [86] is used to calculate the take-off distance with assumptions made to simply the calculations, namely: no ground effect, no runway slope, and no wind. The lift and drag during take-off are calculated using an average velocity, which is calculated using Eq. 12.7 and Eq. 12.8. The method takes into account the take-off thrust, average drag, and the average ground (friction) drag. From the aircraft iteration a $C_{L,max,TO}$ of 1.7 and a climb gradient of 1.37 degree were established and a friction drag of 1.5 % is assumed [55]. This gives a total take-off distance of 1307 meters, which is below the maximum take-off distance stated in requirement MIS.FLI.2 [111].

There is a 700 meter margin between the actual take-off distance and the requirement. This margin can be used for engine inoperative or fuel cell failure operations. If some of the fuel cell stacks fail during take-off, less power can be delivered to the electric ducted fans, resulting in less thrust. Because less thrust is available, more runway distance is necessary. With the large runway distance margin it is safe to say, the Lightning2 can still take-off in most failure situations. However, further research should be done in how much power can be lost or how many engines can be inoperative to still be able to take-off.

$$\bar{V} = \frac{V_{LOF}}{\sqrt{2}} \tag{12.7}$$

$$V_{LOF} = 1.05\sqrt{\frac{2W/S}{\rho C_{L,max,TO}}} \tag{12.8}$$

[2] `http://leehamnews.com/2015/02/25/cs300-first-flight-wednesday-direct-challenge-to-737-7-and-a319neo/` - Accessed: 02-06-2022

### 12.3.2. Landing

The ground run distance consists of the reaction time of the pilot and the braking distance. The landing distance is also calculated by the method taught in [86]. Analogous to take-off, some assumptions are made to simplify the calculations: no ground effect, no runway slope, no wind, and constant braking performance. The approach speed is 1.23 times the stall speed during approach which is calculated with Eq. 12.9 [36], where $C_{L,max.app}$ equals 1.7. Finally a braking friction coefficient of 0.5 was assumed [31]. The total landing distance can be calculated using Eq. 12.10. This gives a total landing distance of 828 meters, which is bellow the maximum landing distance stated by requirement MIS.FL.2 [111].

$$V_{app} = 1.23\sqrt{\frac{2(W/S)_{app}}{\rho C_{L,max,app}}} \tag{12.9}$$

$$x_{landing} = V_{app}^2 \frac{W_{app}}{g} \frac{1}{-\bar{D} - \mu_{br}(W - \bar{L})} \tag{12.10}$$

# 13

# Sensitivity Analysis

With the conceptual design of Lightning2 completed, the robustness of the design should be established. The robustness of the design can be tested by changing major design parameters and assumptions to see the effects on the design. If a certain design parameter has major influences on the design, this parameter should be closely monitored throughout the design. This way, required changes to the design can be identified as soon as possible, to keep the design within the required five years.

The sensitivity analysis is performed by changing an input value, in the iteration with -10% and +10% of its original value. The effect of the change on the original design values is monitored for the most critical parameters for the propulsion system, aerodynamics, and tank design. Critical parameters are defined as parameters which are assumed in the design but can have major effects on the design, such as efficiencies and values can change throughout the design. For the sensitivity analysis it is determined to keep the design point fixed, as otherwise the comparison between the output variables to the original values is no longer objective.

## 13.1. Propulsion System

For the propulsion system sensitivity analysis only the most important results are shown in Table 13.1. It is clear from this sensitivity analysis that a change in fuel cell efficiency can have major consequences for the design. The effects for a reduction in fuel cell efficiency are more severe compared to an increase in efficiency. This is as a 10% decrease in fuel cell efficiency will relatively add more weight to the fuel cell weight, compared to the reduction in fuel cell weight because of an increase in fuel cell efficiency. The fuel cell efficiency should be determined as soon as possible to fix the design and reduce the risk of design alterations in a latter stage.

Two other parameters which are worth mentioning in the sensitivity analysis are the cooling system weight and fan positioning. A change in the cooling system weight estimation, has a small effect on the design. But, the effects on the design seem to be linear with changing cooling system weight. It is also visible in Table 13.1 that changing the fan position within the duct causes a change in weight. This is as the nacelle length is depending on hub length which is dependent on fan positioning. Placing the fan more forward decreases the nacelle length and therefore reduces the duct weight and wetted surface area and vice versa. Finally, all changes to the propulsion system input parameters do not change the number of required engines. From it can be concluded that the final design will most likely have 10 engines.

**Table 13.1:** *Sensitivity analysis for propulsion system parameters.*

| | **Original value** | **FC efficiency** | | **Cooling system weight** | | **Fan position** | |
|---|---|---|---|---|---|---|---|
| | | -10% | +10% | -10% | +10% | -10% | +10% |
| MTOW [N] | 807 984.0024 | 1.29% | -0.79% | -0.35% | 0.35% | -0.15% | 0.16% |
| Fuel weight [N] | 17 188.00556 | 12.16% | -9.42% | -0.28% | 0.28% | -0.60% | 0.66% |
| OEW [N] | 636 341.2593 | 1.31% | -0.75% | -0.44% | 0.43% | -0.18% | 0.19% |
| Max Power [W] | 37 412 935.18 | 1.43% | -0.64% | -0.32% | 0.31% | -0.13% | 0.14% |
| Number of engines | 10 | 0.00% | 0.00% | 0.00% | 0.00% | 0.00% | 0.00% |

## 13.2. Aerodynamics

For the aerodynamic sensitivity analysis almost all parameters inside the drag estimation and planform creation are depended variables. For this reason only the wing interference factor and turbulance fraction could be changed for the analysis. Both parameters have major influences on $C_{D,0}$ and therefore also the fuel weight. However, the effects on MTOW and OEW are relatively small.

The parameters are currently assumed from literature and are assumed to provide accurate first estimations for the conceptual design. To increase the accuracy of the parameters, wind tunnel test need to be performed.

**Table 13.2:** *Sensitivity analysis for aerodynamic parameters.*

| Parameter | Original value | Wing interference | | Turbulence fraction | |
|---|---|---|---|---|---|
| | | -10% | +10% | -10% | +10% |
| MTOW [N] | 807 984 | -0.16% | 0.39% | -0.46% | 0.71% |
| Fuel weight [N] | 17 188 | -2.09% | 2.29% | -5.61% | 5.73% |
| OEW [N] | 636 341 | -0.15% | 0.43% | -0.44% | 0.74% |
| Cd0 | 0.006415 | -3.41% | 3.40% | -8.80% | 8.75% |

## 13.3. Tank design

No major assumptions are made in the design of the tank, but the tank weight is a substantial part of the operational empty weight. The tank design is depended on the amount of fuel that needs to be stored inside the tanks. It is not possible to change the fuel weight in the iteration code, as this would change the entire design causing a snowball effect. This will conceal the real response of the tank weight. The tank weight function is therefore ran separately to see the sensitivity of the design. The results are shown in Table 13.3.

**Table 13.3:** *Sensitivity analysis for tank design.*

| Parameter | Original value | Fuel weight | |
|---|---|---|---|
| | | -10% | +10% |
| Tank weight [kg] | 3 456 | -8.08% | 8.31% |
| Tank diameter [m] | 2.917 | -4.53% | 4.46% |

## 13.4. Results of the Sensitivity Analysis

While the effects of changing multiple key parameters are outlined in this chapter, the most critical parameter is identified to be the fuel cell efficiency. A wrong estimation of the fuel cell efficiency can have major consequences on not only the fuel weight but also the overall MTOW. This can cause a snow ball effect as a decrease in efficiency can lead to an increasing in fuel weight, which increases the tank weight as described in Section 13.3. This can lead to an significant change in the design, which if identified to late, can cause dramatic effects on the schedule.

Other key parameters which are used in the sensitivity analysis all have little influence on the MTOW. From this it can be concluded that the design is robust and is unlikely to change significantly throughout the next design phases.

# 14

# Aircraft Block Diagrams

This chapter contains a compilation of tools that aid in understanding various systems onboard the aircraft. A total of six diagrams are included, namely: Hardware Block Diagram, Software Block Diagram, Aircraft System Characteristics Block Diagram, Electrical Block Diagram, Communication Flow Diagram, and the Data Handling Block Diagram. Each diagram is accompanied with brief explanatory text for the reader.

## 14.1. Hardware Block Diagram

Figure 14.1a shows the hardware block diagram. This figure shows the different physical systems in the aircraft and how they interact with one another. Note that the systems included in the diagram is not exhaustive, rather, the focus lies on the key systems.

## 14.2. Software Block Diagram

The software block diagram is shown in Figure 14.1b. This serves as an overview of the different software systems that are used in the aircraft, and their interaction. The blue blocks are the software system, orange blocks indicate the input and the yellow ones represent the output.

## 14.3. Aircraft System Characteristics Block Diagram

Aircraft System Characteristics Block Diagram is shown in Figure 14.2a. This serves as an overview of the system characteristics of the Lightning2 aircraft. It combines the hardware and software block diagram together and shows their interaction.

## 14.4. Electrical Block Diagram

The electrical block diagram represents several electrical components such as batteries, switching lines and the interaction between the blocks for example conversions. The diagram can be seen in Figure 14.2b, in which the focus lies on the fact that the fuel cells generate direct current (DC), thus the batteries can straightforwardly be charged but as he remaining part of the electrical system requires alternating current (AC), several inverters are required. Furthermore, the electrical sub-systems are grouped based on the importance such as the consumers below the essential bus. In addition, a DC of 28V and AC of 115V was chosen to ensure the aircraft can be handled at most airports [5]. [1] Furthermore, the use of switches ensure backup power from batteries in case of the loss of primary energy sources.

## 14.5. Communication Flow Diagram

The communication flow diagram is used to portray data flow between the aircraft, ground other aircraft and satellites. The main use of communication for airline transport is to safely direct the aircraft from A to B (pilot to air traffic control communication (ATC)), traffic location awareness and avoidance (automatic dependent surveillance–broadcast (ADS-B), traffic collision avoidance system (TCAS)) and approach guidance operations (very high frequency omni-directional range (VOR), distance measuring equipment (DME), instrument landing system (ILS)).

[1] `https://www.schiphol.nl/en/schiphol-group/page/electricity-for-aircraft/` - Accessed: 03-06-2022

**Ground-to-Aircraft and Aircraft-to-Ground:**

The communication between air traffic control (ATC) and pilots is done through radio. VHF (very high frequency) bandwidth is used for short distance communication and HF (high frequency) is used for longer distance communication (for example, when the aircraft is flying above the ocean) [15].

To display the position of the aircraft to ATC, multiple ways of tracking are used, which are synchronised for better accuracy. The on ground radars consist of primary surveillance radar and (PSR) and secondary surveillance radar (SSR), and, for additional measure, an on ground ADS-B station is used. The PSR only sends an interrogation signal and measures the distance where aircraft is from the reflection. The SSR sends an interrogation signal, to which aircraft responds with it's identity [17]. Finally the ADS-B ground station collects positional and identity information from the aircraft [2].

Lastly, several means of one way ground-to-aircraft communication allow a guided approach that a pilot can follow. The VOR and DME show the location of the aircraft with respect to these antennas. They are often placed near the runway to allow pilots position themselves correctly during the approach. VOR antennas also deliver weather and airport information, such as Meteorological Aerodrome Report (METAR). The ILS provides an approach path that aircraft automatically can follow with an autopilot. It consists of a localizer to provide lateral guidance and glide slope to provides vertical guidance [16].

**Aircraft-to-Aircraft and Aircraft-to-Satellite:**

The aircraft-to-aircraft communication is used for anti-collision and traffic management. It allows pilots to visualise where surrounding traffic is located. First, if the radio is on the same frequency, the pilots of different aircraft can communicate with each other. For anti-collision, the TCAS is used, which receives positional data of surrounding aircraft and sends audio warnings to pilots in case action needs to be taken [17]. Additional information of aircraft positional data to TCAS processors can be achieved by means of ADS-B, which acquires positional data from the satellite communication. Satellite communication can also be used to have internet on board [1].

## 14.6. Data Handling Block Diagram

Fuelled by the onset of the era of 'Big Data', aircraft are becoming increasingly data-driven[3]. The potential benefits in operational efficiency and safety are significant, however, an increasingly elaborate data handling system requires careful design. Adequately named, the data handling block diagram depicted in Figure 14.4 shows the how data is handled by the aircraft. The main components of the system are included in combination with the flows of the data themselves. The diagram is inspired by a combination of [49] and [21].

[2] `https://en.wikipedia.org/wiki/Automatic_Dependent_Surveillance%E2%80%93Broadcast` - Accessed: 16-06-2022

[3] `https://www.sita.aero/pressroom/blog/aircraft-data-management-for-the-future/` - Accessed: 14-06-2022

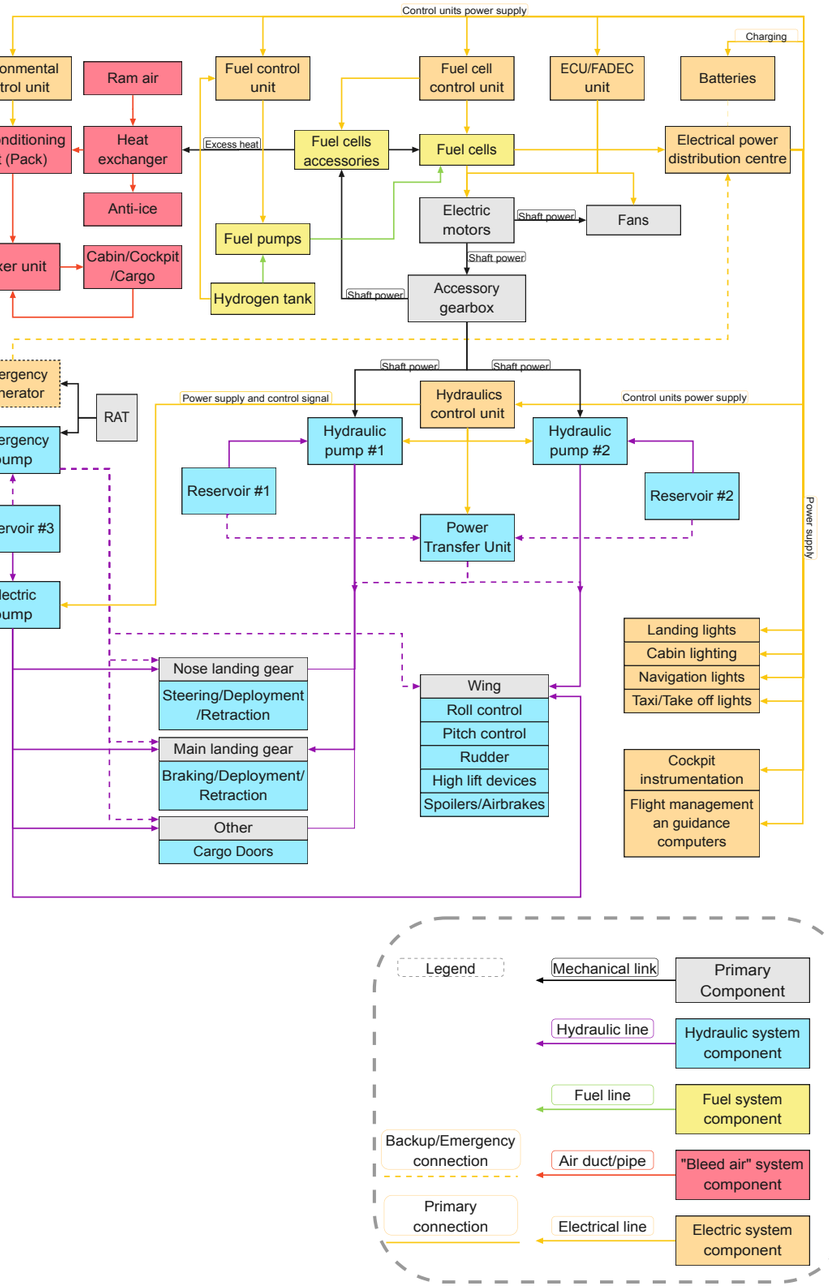


**(a)** *Hardware Block Diagram.*

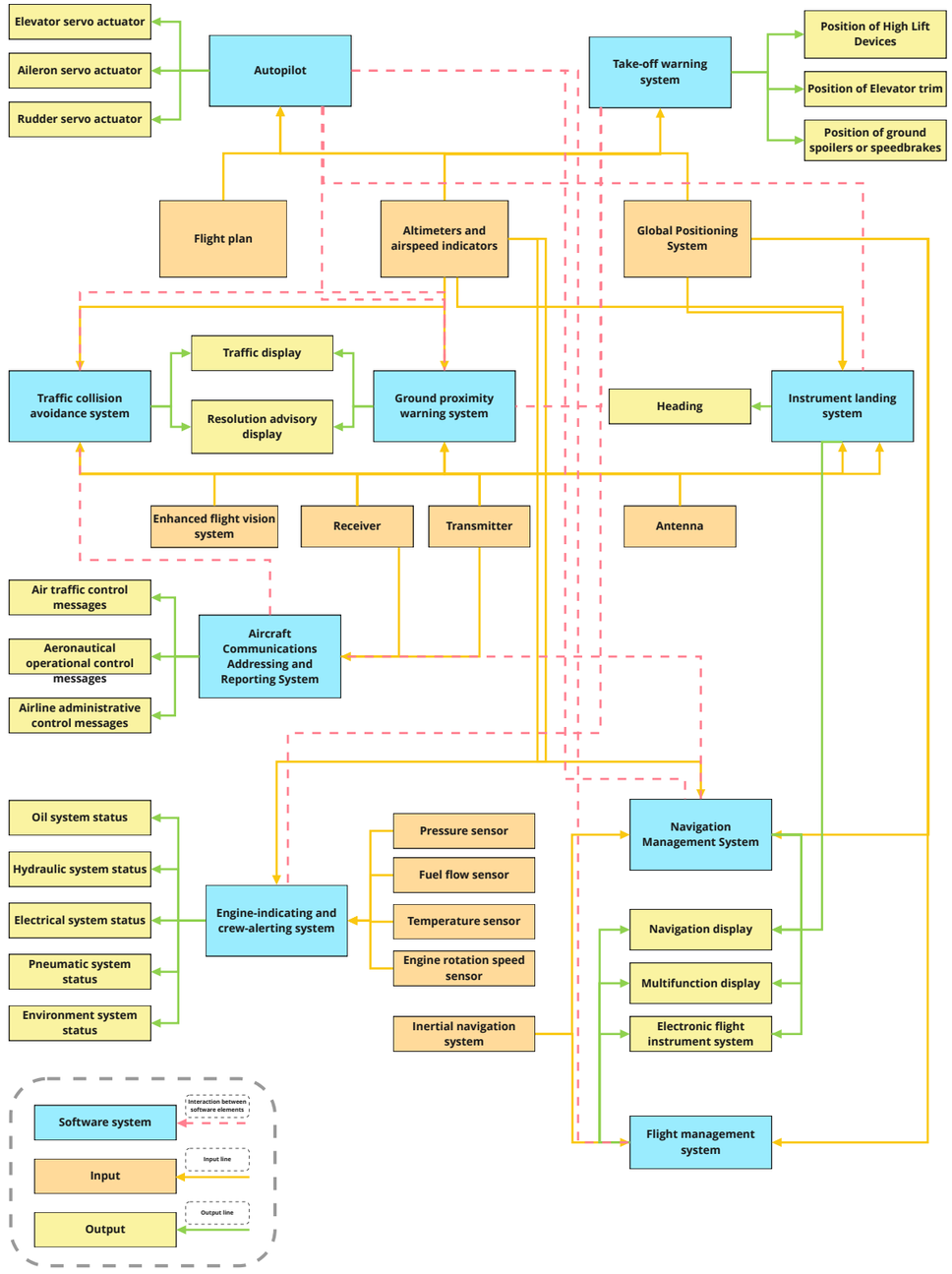


**(b)** *Software Block Diagram.*

**Figure 14.1:** *Hardware and Software Block Diagrams.*

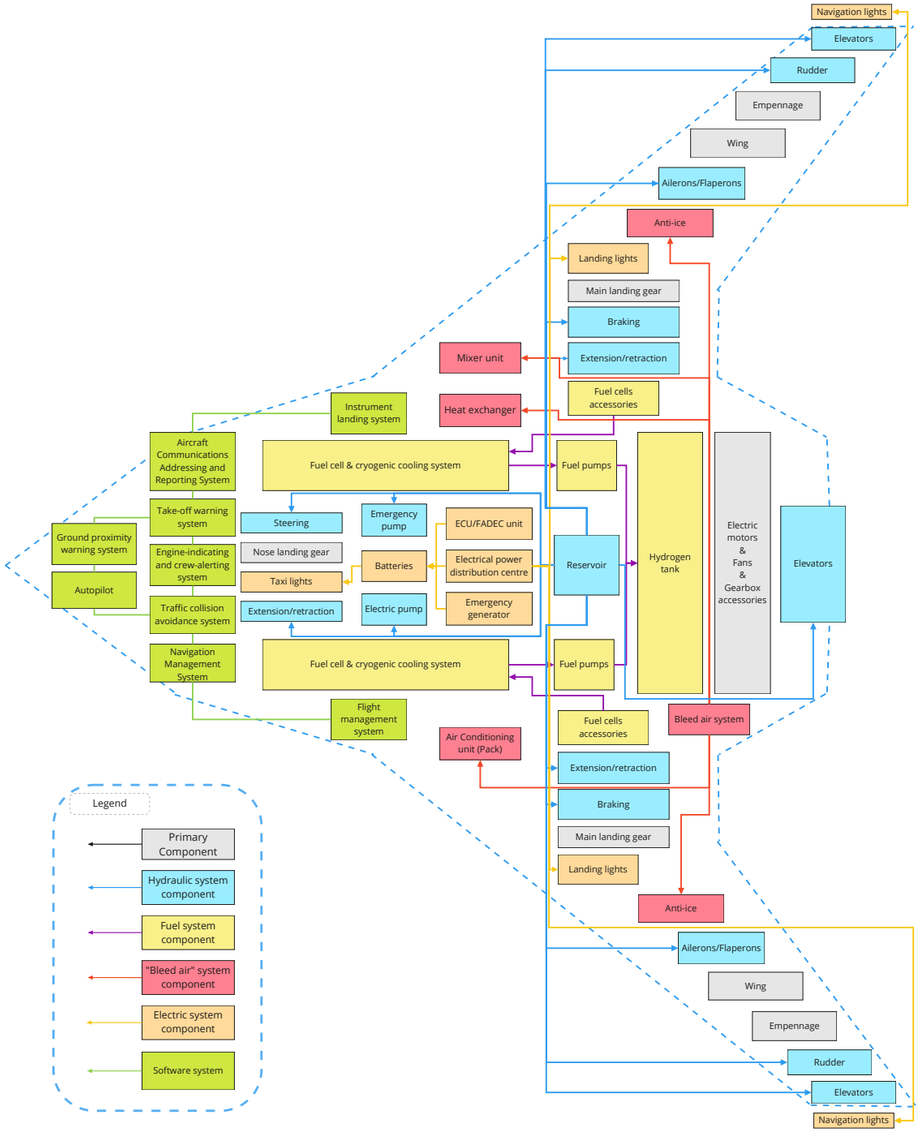


**(a)** *Aircraft System Characteristics Diagram.*

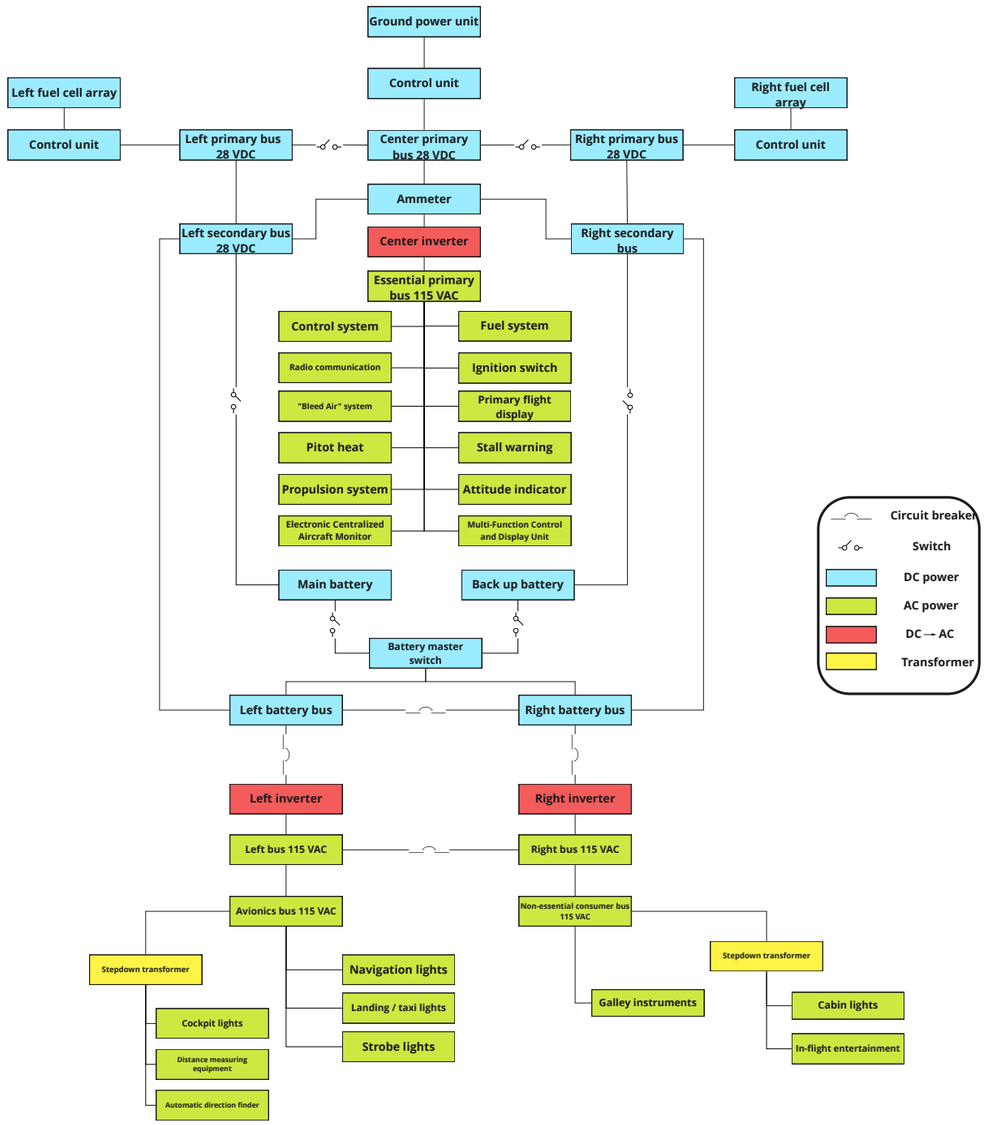


**(b)** *Electrical Block Diagram.*

**Figure 14.2:** *Aircraft System Characteristics and Electrical Block Diagram.*

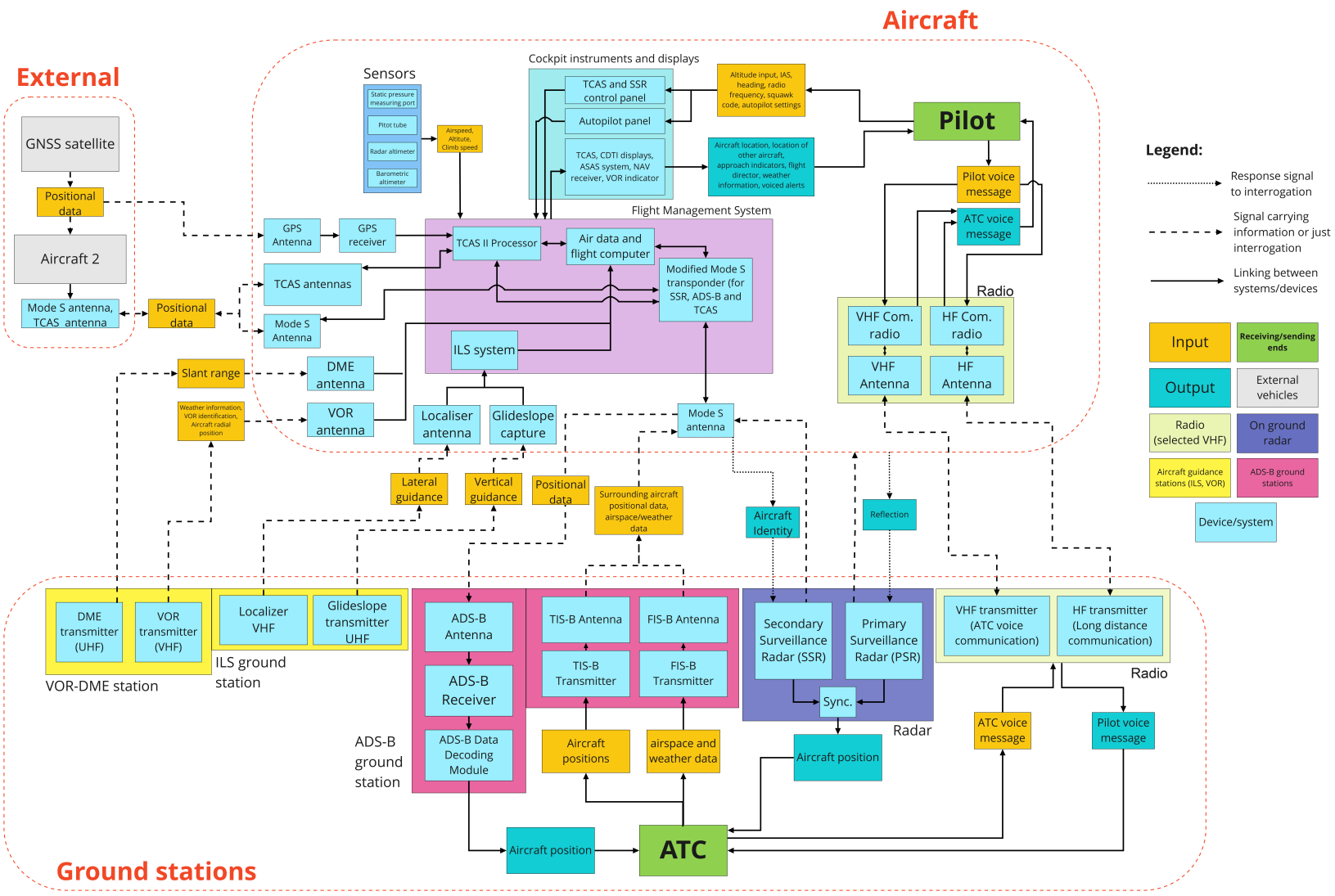


**Figure 14.3:** *Communication Flow Diagram.*

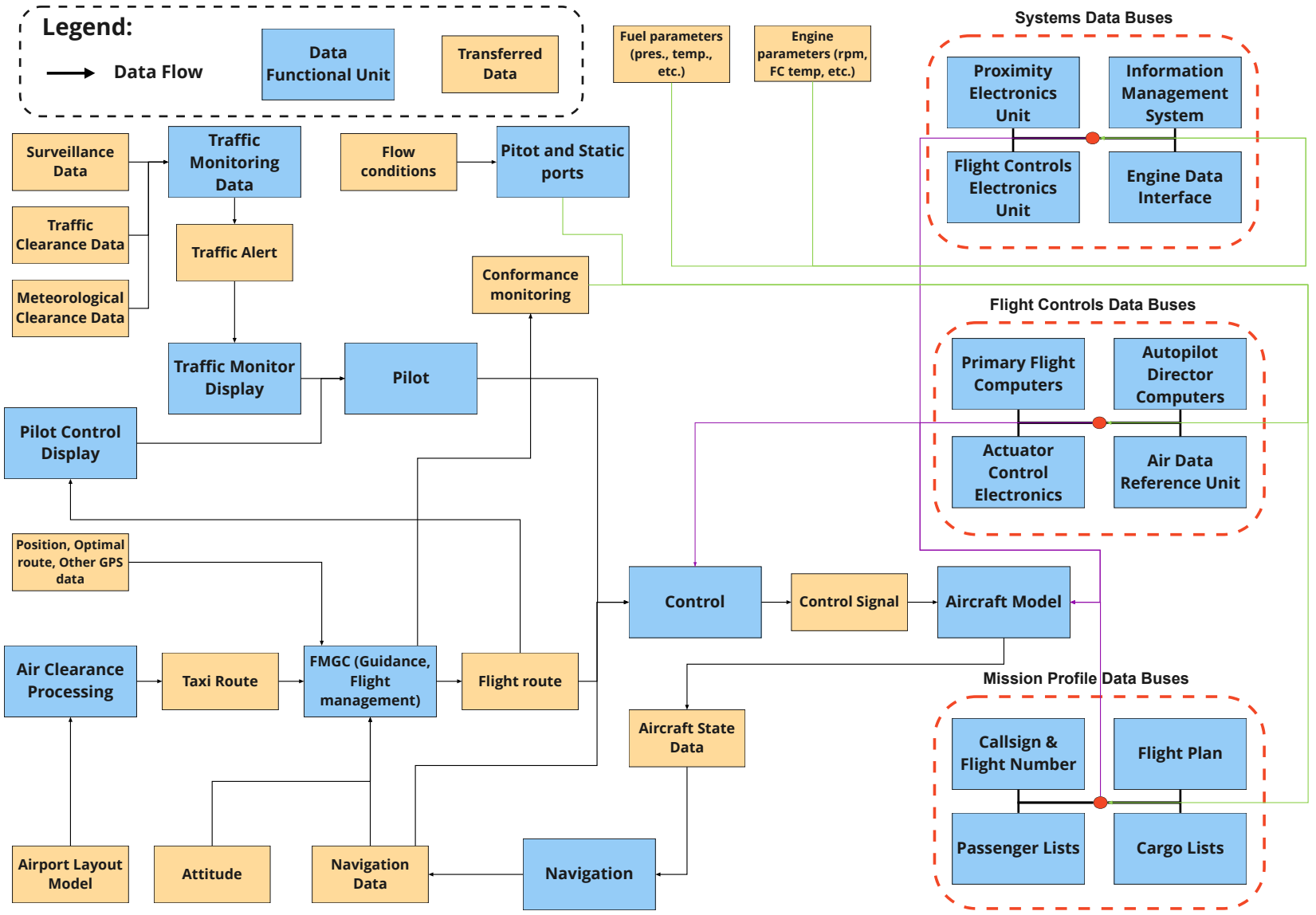


**Figure 14.4:** *Data Handling Block Diagram.*

# 15

# Operations & Logistics

This chapter presents the operational and logistical framework in which the Lightning2 aircraft will operate, limited to on-ground aspects. In-flight operations are largely equivalent to that of current aircraft and are implicitly addressed throughout this report. The chapter commences with a dedicated section on taxiing between the gate and runway in Section 15.1. Next, operations at the gate are discussed with regard to the crucial turnaround time of the aircraft, in Section 15.2. The maintenance of the aircraft is discussed with emphasis on operations regarding maintenance planning and types of maintenance checks, in Section 15.3.

## 15.1. Taxiing

One of the most important requirements is that during ground operations no emissions can be produced. Current aircraft have the turbofan engines set to idle to provide the necessary thrust to taxi around the airport. A ground speed between 25 and 30 kts is necessary to provide the necessary flow around the airport and to avoid congestion [87]. Because of the constant thrust setting, the pilot controls the ground speed with braking, which creates additional wear on the brakes and unnecessary fuel burn. For short haul flights, taxiing accounts for 6% of the entire fuel burned during the trip [123]. At larger airports, the large amount of taxiing aircraft cause a high concentration of pollutant gas, which influences the area around the airport.

To reduce the emissions around the airport, different approaches are being investigated. A company called WheelTug is currently certifying their electric motor which drives the nose landing gear [1]. The power required for the electric motor will have to be provided by the APU or onboard batteries, creating a weight penalty. Another idea is the use of Taxibot. This is a hybrid electric cart which drives the aircraft from the gate to the runway without the need of engines [2]. However, according to Yanniek Huisman (personal communication, May 25, 2022, Programma coördinator Fieldlab Next Aviation & Urban Air Mobility), Taxibot is not feasible at smaller airport as the taxi time from the gate to the runway is the time needed for the turbofans to warm up.

The big advantage of the blended wing body design is that it uses hydrogen, in combination with fuel cells instead of kerosene with turbofan engines. Fuel cells only produce water vapour during the chemical process, eliminating the production of $CO_2$, $NO_x$, and particulate matter. However, water vapour is seen as a green house gas and is therefore classified as an emission. In discussions with Yanniek Huisman (personal communication, May 25, 2022, Programma coördinator Fieldlab Next Aviation & Urban Air Mobility), Ivan Langella (personal communication, May 23, 2022), and Julien van Campen (personal communication, May 25, 2022), experts within the field of hydrogen, they all stated that the effects of water vapour on the environment at ground level can be neglected. Water vapour is harmful for the environment when contrails are formed. This only happens at high altitudes and not at sea level [50].

The client has stated its ambition to be emission neutral during ground operations. Therefore, the option of using batteries is investigated to achieve this. Taking the longest taxi time in Europe, which is the 14 minute taxi at Amsterdam Schiphol Airport from the Polderbaan to the gate, would require around 8.5 tons of batteries, which is too large a weight penalty to be implemented [93]. Capturing the produced water vapour during taxiing and emitting it at cruise altitude, has much more severe consequences on the environment compared to emitting

[1] https://www.forbes.com/sites/michaelgoldstein/2020/09/11/can-wheeltug-a-driveable-aircraft-nosewheel-save-airlines-money/ - Accessed on 10-05-2022

[2] https://www.schiphol.nl/en/innovation/page/sustainable-taxiing-taxibot-trial/ - Accessed on 10-05-2022

water vapour at ground level. This is therefore also not a option. An alternative solution is to cool down the water vapour to water and emit it on the taxiway or towards the sides. However, during taxiing around 0.7 $m^3$ of water would be produced, while this is not a problem if one aircraft does this as the amount of water can be emitted over five kilometres, when more hydrogen aircraft drive the same taxiway, this can become a problem. Therefore, the only possible solution to become emission neutral during taxiing is to offset the water vapour emitted. This can be done using the European Union Emission Trading scheme, where airlines are required to monitor their emissions and pay allowances to offset these emissions.

## 15.2. Turnaround Time

Turnaround time refers to the required time to fully unload and prepare an arrived aircraft for a subsequent departure. Within this dedicated time-slot, a multitude of functions are performed. The goal here is minimisation of the turnaround time, as time is money. An aircraft on the ground as opposed to in the air is not generating revenue, but is consuming financial resources. Ensuring financial viability and seamless entry into service at existing airports is of the essence. The turnaround time of the radically different BWB-type aircraft requires review and prediction of various factors, to assess the competitiveness with respect to current fleets. The analysis of the turnaround time is limited to three key factors, particularly where differences between the conventional and the BWB lie, namely passenger deboarding/boarding, cargo offloading/loading, and refuelling.

### 15.2.1. Passenger Deboarding & Boarding

The turnaround of the aircraft simultaneously marks the start and end of the onboard experience of travellers. Deboarding and boarding of passengers needs to be efficient and comfortable, as airlines are often judged harshly on this by travellers. As such, the aircraft can be (de-)boarded using either a jet bridge or stairs. Figure 15.1 plots the boarding time for for various types of aircraft as a function of single class configuration passenger capacity [122]. Increasing number of seats abreast (with adequate number of aisles), decreases boarding time, which is highly favoured. Regarding the boarding strategy, several options exist. Figure 15.2 depicts the boarding times for random, outside-in, and rear to front strategies for varying percentages of seats filled (x-axis) [122]. This simulation is based on a BWB with a 400 passengers capacity and two front doors used for boarding. The optimal strategy, surprisingly, is a random order of boarding. The results of this simulation are assumed to be valid when extrapolated to 150 passengers. It can be concluded that the cabin layout of a BWB type aircraft is favourable with regard to turnaround time.

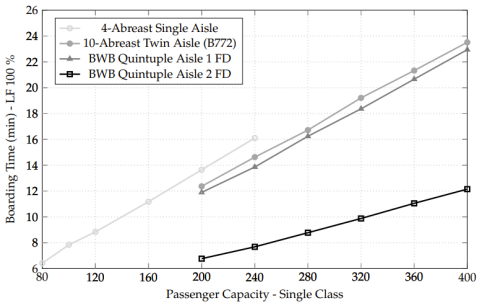


**Figure 15.1:** *Boarding time of various aircraft as a function of passenger capacity (single class) [122].*

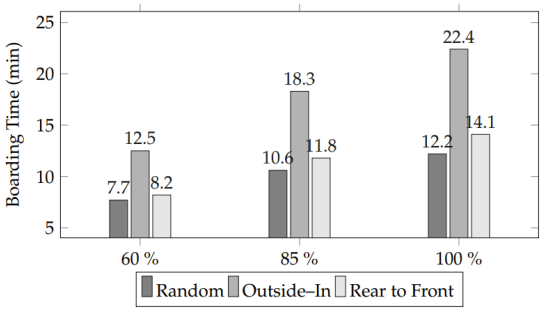


**Figure 15.2:** *BWB boarding strategies for various seats-filled percentages [122].*

### 15.2.2. Cargo Offloading & Loading

Analogous to passengers, cargo is required to be offloaded and loaded onto the aircraft during the turnaround time. The cargo bay of the BWB is designed to equip LD3-45 containers, which are widely used in industry. Compared to a custom container, a known type facilitates the cargo procedures. The Airbus A320 carries the same LD3-45 containers[3], so the Lightning2 can follow the same/similar (un-)loading procedures as for the A320. The loading of the cargo bay will not require radically different procedures or machinery. The time required to perform cargo handling is expected to be similar to the A320 and is not hindered by simultaneous refuelling and (de-)boarding of passengers.

[3] `https://www.nordisk-aviation.com/en/ld-containers/akh-ld3-45/nordisk-akh-/` - Accessed: 09-06-2022

### 15.2.3. Refuelling

If required, the aircraft is refuelled during the turnaround time. In some cases, depending on the airline, an aircraft will carry enough fuel for both the in- and outbound flights. Instead of kerosene jet fuel, the Lightning2 is powered by hydrogen. The refuelling of the aircraft refers to the refilling of the cryogenic hydrogen fuel tanks.

Refuelling of a hydrogen-powered aircraft was previously discussed in the market analysis in Chapter 2. In this section, the focus lies on refuelling in reference with the turnaround time. For short-range aircraft, the turnaround is expected to remain unaffected to changes in fuel type to hydrogen. Flow rates of liquid hydrogen are able to attain similar values compared to the current kerosene counterparts (approximately 900 l/min) [23]. To achieve this, investments will be required to counteract the adverse characteristics of hydrogen hoses, being heavy weight and low manoeuvrability [23]. With this in mind, it must be emphasised that upon entry into service, the infrastructure will not be at its final capacity and a slower refuelling process could result. Ultimately, the turnaround time with regard to refuelling will remain competitive.

## 15.3. Maintenance

Naturally, the BWB will undergo maintenance throughout its operational lifetime. This section starts with a presentation of an overview of the maintenance framework in Figure 15.3. This provides the general overview of the maintenance program, inspired by [54].

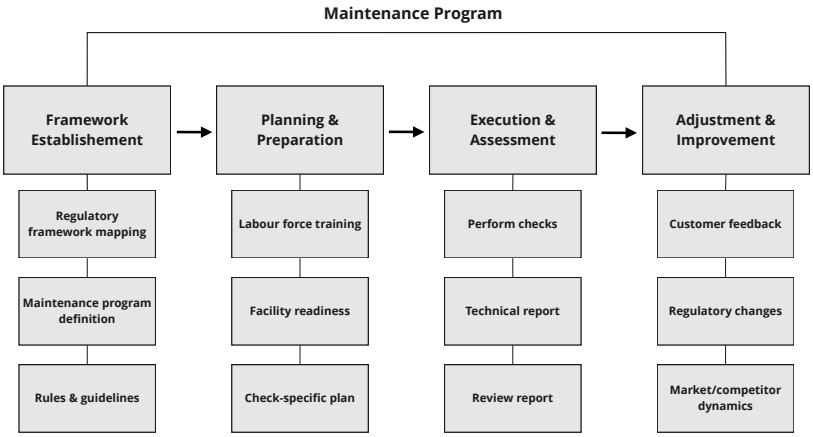


**Figure 15.3:** *Maintenance Program Framework [54].*

Figure 15.3 is seen to start with the framework establishment through adherence to regulatory guidelines. The program for the BWB is defined and the rules and important notes are documented. With a program in place, planning and preparation is performed for each specific check. This consists of forming a trained workforce and gaining access to a dedicated facility. The maintenance work itself speaks for itself, with as output a technical and review report. Maintenance is a dynamic field, therefore periodic adjustments/improvements are required based on customer feedback, regulatory changes, and market/competitor dynamics.

Depending on the aircraft age, the concentration of full flight cycles, and total flight hours, a given test is required. The majority of the industry follows the ABCD-check system or a variation thereof. The designed BWB will adhere to a similar framework, briefly outlined in Table 15.1. Input for this table was compiled from [20] and Studyflying website[4]. It is important to note that checks of increasing granularity are cumulative, meaning that a B-check encompasses everything from an A-check plus additional factors. The maintenance costs (financial and time) are incorporated in the financial analysis of the project, in Chapter 3. The exact maintenance details are subject to refinement based on decisions made by the operator. At this stage, values serve an indicative purpose.

[4] `https://studyflying.com/a-b-c-d-check-airline-maintenance/` - Accessed: 09-06-2022

**Table 15.1:** *Outline of ABCD-Checks.*

| **Type** | **A-Check** | **B-Check** | **C-Check** | **D-Check** |
|---|---|---|---|---|
| **Description** | Primarily visual inspection, assessment of general condition. | A-Check + Fluid replacement and lubrication. LH2 tank test | B-Check + Detailed component inspection and corrosion prevention program. | C-Check + Complete strip of the aircraft to shell. Checking of structural integrity. |
| **Frequency** | Every 7 - 9 days | Several months | Every 2 years | Every 6-10 years |
| **Duration** | 10 - 20 m.h. (overnight) | 100 - 300 m.h. (several days) | 10 000 - 30 000 m.h. (2 - 4 weeks) | 50 000 m.h. (2 months) |

*m.h.: man-hours

# 16

# RAMS Analysis

The acronym RAMS analysis refers to a tool frequently implemented when engineering a product or system, that concerns the reliability, availability, maintainability, and safety characteristics. In earlier phases of this project, the RAMS analysis was based on similar existing aircraft and served the purpose of providing input for the design trade-off. At this final stage, the focus shifts solely to the BWB design and its RAMS characteristics. The chapter commences with analysis of the reliability in section Section 16.1. Following, the availability, maintainability, and safety characteristics are analysed in Section 16.2, Section 16.3, and Section 16.4, respectively.

## 16.1. Reliability

Reliability is the probability that a system will perform its required function, which is a function of the complexity of the system [12, 81]. The hydrogen-powered blended wing body with the distributed propulsion and advanced control characteristics is inherently complex. To limit the scope, reliability of the design is discussed with regard to three critical components where reliability plays a pressing role, namely the distributed engines, the fuel cell, and the wingbox.

In a certain sense, the distributed engines simultaneously contribute and compromise the reliability of the aircraft. A given engine has a set reliability, however with multiple engines, the probability that a failure occurs in one of them is greater. Nonetheless, the impact of a engine failing is far less significant in the case of distributed propulsion. One out of eleven engines is merely a 9% reduction in thrust. Also the maximum thrust for which the engines are designed, take into account an one engine inoperative case. This way even with one engine inoperative, it still satisfies the CS.121 requirement. Additionally, the yawing moment generated in this case is much smaller compared to the case of a twin-engine aircraft losing one engine. Overall, the distributed engine positively impacts the reliability of the aircraft. The cooling of the fuel cell is a critical part of the propulsion system. It is performed by a combination of liquid and incoming air cooling. Two separate systems increases the reliability. When either one of the cooling sources fails, the fuel cell can still be maintained at an acceptable temperature. Nonetheless, the throttle does have to be decreased immediately and the landing should be anticipated. Lastly, the wingbox is designed to be extremely reliable. All required safety factors are taken into account in the design, and fatigue-loading allows for many more load cycles than the aircraft is expected to face in its operational lifetime.

## 16.2. Availability

Availability can most aptly be understood to be the intersection of reliability and maintainability of the aircraft [81]. The more time an aircraft spends on the ground, the less revenue it generates and the higher the costs incurred. For an aircraft with a commercial intended use, the turnaround time is a key factor, which was analysed in Chapter 15. This will not be reiterated here, rather, the availability with respect to adaptability to traffic fluctuations and meteorological resilience will be discussed.

Traffic fluctuations can call upon the loiter and divert capabilities of the aircraft. During the design phases, these factors have been taken into account with a fuel buffer, meaning that the BWB will not become unavailable when traffic issues arise. Failure of loitering and immediate diversion implies further routes are cancelled, reducing availability of the aircraft for its intended use. Meteorological resilience of the aircraft refers to the performance during adverse weather conditions. The Lightning2 aircraft has a comparatively low static stability margin due

to the absence of an empennage [117]. This makes it less efficient during take-off in high winds. The decreased lift and increased drag as a result of heavy rain presents added difficulties as well [117]. The cruise altitude however, is far above the height where weather threats are most common. For the majority of the mission profile the aircraft does not fly at compromised efficiency due to weather.

Furthermore, availability is a function of duration of maintenance checks and repairing of critical failures. The former is improved by well-defined maintenance schedules and procedures for various periodic checks. A network of spare parts and trained crew in the vicinity of operational hubs can prevent long waiting times. Deviation from conventional designs tends to elongate the process of maintenance work, especially at the start of operation. The latter is inherently dependent on the reliability of the aircraft, as a small chance of failures (high reliability) automatically reduces the expected time required for resolving failures.

## 16.3. Maintainability

The radically different configuration of the Lightning2 poses challenges with regard to maintainability as dedicated facilities are largely optimised for conventional aircraft. The maintenance program and types of checks that will be performed are explained in Chapter 15, this section focuses on the glaring issue when maintaining the BWB: access to the distributed propulsion.

Engines are a critical part that must be inspected during maintenance, even just a small check while parked at the gate. The positioning on-top of the body requires a new method for inspecting these, which are still in development [74]. One can think of usage of drones or specially designed platforms that grant access. Naturally, these radically new concepts will call upon additional training for operational maintenance crews. Having established that maintenance will be possible for the aircraft, the procedure should be compared to current methods. Upon entry into service of BWB-type aircraft, the time-slots for maintenance will admittedly be lengthier than for existing fleet. However, the duration is expected to be a monotonously decreasing function of time due to specialisation and adaptability of the sector.

## 16.4. Safety

Arguably, safety is the most important pillar of a RAMS analysis. It comprises a broad term that encompasses the mitigation of processes that can cause damage to people, material, and the broader environment/surroundings during operation. Fundamentally, operational safety should be segmented between safety during nominal operation and safety during abnormal operation [12]. The latter essentially refers to technical safety, which comprises the familiar steps of risk identification, classification, and mitigation. This aspect of safety receives a dedicated Technical Risk Assessment, presented in Chapter 5.

For the purpose of this RAMS analysis, the focus lies on safety considerations during nominal operation of the aircraft, primarily cabin safety. The required safety characteristics fall within the monitoring framework set by overarching organisations. The positioning of fuel tanks and inherent blended shape of the wing-fuselage combination requires different positioning of emergency exits for passengers. Positioning over the wing (sides of cabin) is simply not possible. Due to regulations in CS-25, at least a combination of Type-II and Type-A [36] emergency/access doors should be present. The implementation can be found in Chapter 19, in which the cabin layout is discussed.

# 17

# Manufacturing, Assembly & Integration

This chapter sheds light on the manufacturing, assembly, and integration plan of the blended wing body aircraft, and is segmented into four sections. First, the sustainability of the raw input materials and lean manufacturing considerations are discussed in Section 17.1. Secondly, the key manufacturing techniques used during the manufacturing of aircraft components is discussed in Section 17.2. Thirdly, the design considerations of the facility are presented in Section 17.3. Lastly, the intended aircraft assembly plan is included in Section 17.4. This schematically depicts the final integration of all aircraft parts into a single product. In general, at this stage, the plan is limited in granularity, as the design is not detailed enough to truly account for all possible manufacturing/assembly issues. Nonetheless, it provides a good starting point and ensures that the ultimate production framework is not neglected during the design phase.

## 17.1. Sustainable Raw Input Materials & Lean Manufacturing

To achieve sustainability during manufacturing it is important to take into account recycled materials. As the first Lightning2 will retire in 30 years, a partnership, with for example Aircraft End-of-Life Solutions, to provide the recycled materials. The big disadvantage of using recycled materials such as aluminium and composites, is that because of regulations it is not possible to use recycled material in load bearing structures of the aircraft [9]. This should be taken into account when designing the supply chain as the recycled material has to be separated from primary material. A big advantage is that the energy needed to produce aluminium is 95% less compared to primary aluminium [106].

The simplest definition of lean manufacturing is manufacturing without waste [103]. From a sustainability perspective, eliminating waste is key component of the bigger picture. Waste is a broad term and can be subdivided into various forms: overproduction, waiting time, work in progress inventory, processing waste, transportation, movement or motion, rework, and under-utilisation of people [103]. To embody lean manufacturing, the 5S method (Sort, Simplify, Scrub, Standardise, and Sustain) will be implemented in the manufacturing process. This method consist of five steps briefly discussed below, for which [103] was extensively used.

**1. Sort:** A complete revision of the workplace is conducted, distinguishing between necessary and unnecessary items. The latter are to be removed from the process entirely.

**2. Simplify:** Items without a specified location are categorised into a designated area. This is documented to constantly keep the overview.

**3. Scrub:** This step refers to frequent cleaning of the manufacturing facility, including the general floor-plan as well as individual machines and tools.

**4. Standardise:** The steps undertaken must be documented clearly to create a standardised method that all workers can follow. A guide is required to ensure the organisation as a whole follows the lean methodology.

**5. Sustain:** Finally, the last step consists of reviewing the 5S method efforts and identifying places where additional positive results can be obtained. This highlights to 'philosophy' behind lean manufacturing. It is a *dynamic* to *continuously eliminate waste*.

## 17.2. Manufacturing Techniques

To cover all manufacturing aspects of the aircraft promises to be a Herculean task, rather, a selection of the two key techniques is made that are both applied to critical systems and are employed frequently throughout the design process: Riveting and Adhesive Bonding. These methods are widely used in the commercial aviation sector. For each manufacturing technique, a description is provided including key pitfalls. Furthermore, the application of the technique to specific components is elaborated upon. It is important to note that the manufacturing techniques discussed hereafter are solely for assembly purposes. The manufacturing of individual components will be outsourced to specialised third-parties and are assumed to be delivered to the dedicated assembly facility.

**Riveting**

Aluminium is extensively used throughout the structure of the aircraft due to its excellent material properties, low-cost, and re-purposing capabilities. Riveting will be the primary technique used to combine individual parts. The rivet spacing is carefully considered as shear failure, bearing failure, and plastic deformation are ever-present dangers when not manufactured properly [104]. Furthermore, riveting is often a loud process and this affects the design of the manufacturing facility Section 17.3[1].

**Adhesive Bonding**

Adhesive bonding has been deemed a viable technique to combine aircraft parts for many years now. It primarily applied in combination with metals, such as aluminium. Current trends in commercial aviation are shifting to composite aircraft, where adhesive bonding research is lagging to optimally be utilised in practice.[2] In the case of Lightning2, large structures including the wing box and fuselage are in fact made out of aluminium, allowing for adhesive bonding to be used.

## 17.3. Assembly Facility

The line assembly of the aircraft will occur in a dedicated facility, which will be located in the Zeeland province in the Netherlands. Choice for this location is a combination of vicinity to the Delft University of Technology (for specialists) and proximity to waterways allowing for efficient transport of components and materials. Furthermore, the location is not in a densely populated area and grants enough space to build a runway. The facility will be built to precisely tailor to a blended wing body design, whereby many utility considerations must be accounted for, the key ones briefly outlined hereafter. These considerations are inspired by a two employees from The Austin Company, a recognised expert in this field [3]. This source is used extensively throughout this section.

**Assembly method:** The choice of assembly style is a line assembly, requiring the facility to accommodate a 'flow' throughout the building.

**Production rate:** Naturally, the size of the facility is heavily dependent on the predicted production rate of the aircraft. And the value is reflected on the return on investment table in financial analysis.

**Manufacturing techniques:** The key manufacturing techniques laid out in Section 17.2 must be possible within the facility.

**Dimensions of aircraft (systems):** Simply put, the facility needs to be large enough to accommodate the aircraft in its final configuration. Once assembled, the aircraft has leave the building, requiring careful thought of the doors (and mechanisms) of the facility.

**Tooling & jig requirements:** The appropriate tooling must be available within the facility and be granted extra storage space when not in use. Accessibility of key components such as the distributed propulsion system on

[1] https://www.areadevelopment.com/Aerospace/q3-2018-auto-aero-site-guide/designing-the-aircraft-manufacturing-facility.shtml - Accessed: 05-06-2022

[2] https://www.tudelft.nl/en/ae/current/spotlight/one-way-to-make-composite-aircraft-lighter-stop-riveting-and-start-bonding - Accessed: 05-06-2022

[3] https://www.areadevelopment.com/Aerospace/q3-2018-auto-aero-site-guide/designing-the-aircraft-manufacturing-facility.shtml - Acessed 05-06-2022

top of the wing/body can pose an issue. Jigs to grant workers access to these parts of the aircraft are essential, and must be transportable throughout the facility.

**System & material intra-facility conveyance:** More generally, transportation of materials, components, tools, etc. is required throughout the facility and entire assembly procedure. This is to be accounted for when establishing the space dimension requirements.

**Material storage requirements:** Aircraft materials can place requirements on the facility setting. Aluminium is widely used throughout the aircraft and due to its coefficient of expansion requires stable temperatures. Significant fluctuations in facility temperatures can lead to inaccuracies during assembly. In general, sunlight exposure, humidity, and ventilation should be kept as consistent as possible.

**Utility requirements:** The facility should be kept clean at all times, requiring an abundance of clean compressed air. There should be multiple redundant sources of this to ensure the integrity of the aircraft is never compromised irreversibly.

**Aircraft grounding:** The aircraft should be grounded in the facility as static electricity can adversely affect various electronic components. Additionally, it can protects staff from harm by electrocution.

**Utility intra-facility distribution:** Distribution of utilities to the required departments within the facility can be realised in multiple ways. To maximise the use of space in the facility, a network of cranes on ceiling rails will be utilised. This network is intended to transport items, with the exception of significant heavy components.

**Foreign object debris (FOD) protection:** What is not intended to enter the facility should be kept out. This is encompasses a broad range of items including scrap waste, paint chips, faulty components. The risk of damaging components entering the manufacturing process is of utmost importance and should be fully mitigated.

**Emergency exiting for staff:** The facility should be safe for all staff. This requires proper emergency protocols, particularly with regard to emergency exits. Building exit doors will be clearly marked and accompanied with exit path lighting in case of smoke.

**Noise insulation:** Noise limitation is primarily an issue in reference to hearing protection of workers. Riveting is a key manufacturing process and often times is very loud. To minimise damage (hearing loss) these processes can be conducted in separate, insulated area or performed outside the peak-hours.

**Fire/explosive protection:** In general, aircraft assembly occurs without any fuel reducing the chance of fires and/or explosions. Nonetheless, the facility will be equipped with a an extensive sprinkler system to limit the risks.

## 17.4. Aircraft Assembly Line

Now with the design ready, a first preliminary assembly and manufacturing line can be made, which is shown in Figure 17.1. The order of the assembly is important as sufficient space is needed to install other subsystems such as the fuel cells and the hydrogen tank. Some components such as the wing box are assembled separately from the aircraft and added later to the airframe to allow parallel assembly and increase the efficiency.

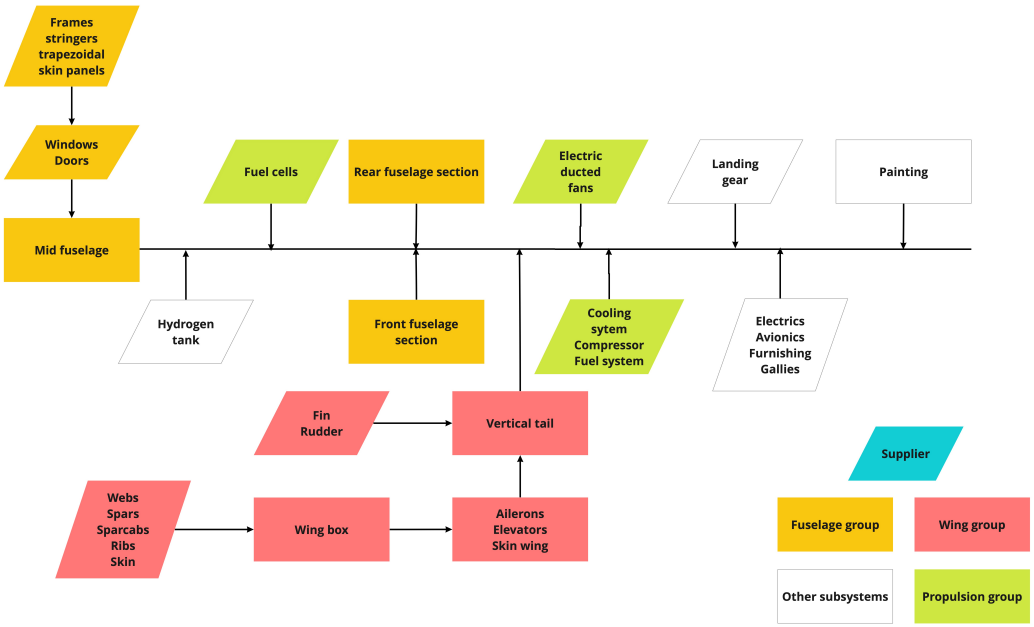


**Figure 17.1:** *Assembly line for Lightning2.*

It is not possible to manufacture all parts of Lightning2 in-house. This is due to certain subsystem requiring a lot of knowledge, but also to reduce cost, save time, and spread financial risk [63]. For these reasons subsystems need to be outsourced to third parties. It is decided to develop all blended wing body specific parts in house as few companies have the expertise to make the process more efficient. Subsystems that can also be found in conventional aircraft are outsourced if possible. In Table 17.1 the most important subsystems/components that will be outsourced are listed. When choosing a supplier it should be taken into account where the parts are manufactured. If long distances have to be covered between the manufacturing location of the subsystem and the assembly location, this requires difficult logistics and shipping cost which is undesirable. It is very important to collaborate with suppliers early in the design stage to optimise the design and minimise the design time.

**Table 17.1:** *Subsystem suppliers.*

| Component | Supplier | HQ location |
|---|---|---|
| Electric ducted fans | General Electric | Ohio, U.S. |
| Hydrogen tank | Cryoworld | Netherlands |
| Fuel cells | PowerCellution | Sweden |
| Landing gear | Safran | France |
| Doors | Latécoère | France |
| Ailerons | Saab | Sweden |
| Seats | Safran | France |

# 18

# Sustainable Strategy

This chapter presents the sustainable strategy through various phases of the project. The chapter starts with sustainability during the design phase in Section 18.1. Next, the operational phase is discussed in Section 18.2. As specified in the requirements, the design should be adjustable to allow for further improvements with regard to fuel consumption. This closely ties in with the sustainability strategy and is therefore included here, in Section 18.3. To conclude, the end-of-life strategy and recyclability plan are presented in Section 18.4.

## 18.1. Design Phase

During the design phase the three pillars of sustainable development are taken into consideration. These are economic, social and environmental. Keeping the correct balance of these three pillars is key to achieve a truly sustainable design.

Starting with the most obvious of the three, the environmental impact on the world. During the design phase considering the impact of used materials, fuel and assembly methods can drastically increase the sustainability in this section. As the requirements already include reduction in emissions and complete recyclability of the aircraft, this aspect will surely be accounted for. A second consideration is that historically the aviation sector uses relatively large amount of physical tests. The use of digital twins can further reduce the environmental impact during the design phase. This testing environment can be on component level, all the way up to the system level.

The second aspect of sustainability is the economic pillar. Considering most environmental improvements are based on newer technologies, the infrastructure and availability can be limited. An increase in demand for these technologies can create localised jobs around airports and in the supply chain.

Finally the social aspect relates to the community aspect of things. It looks at the benefits and detriments on the community. This is closely related to design choices made and the requirements on environmental impact. The reduction in(near) ground emissions can have a positive impact. This also holds for an increase in jobs previously stated or the increased mobility introduced by a cost efficient aircraft.

## 18.2. Operational Phase

Optimising the maintainability and modernisation of the aircraft during its operational phase is key to improving the economic sustainability. To attain this, the aircraft operator should use its resources efficiently and responsibly so that it can operate in a sustainable manner to consistently produce an operational profit. The team decided to implement the *5M* technique throughout the design and future operations. The technique stands for Measuring, Monitoring, Modelling, Maintenance, Modernisation [1]. The *5M* technique will be further explained below.

1. **Measuring:** Measurements can be established with the use of test panels and prototypes in laboratory conditions to predict crack propagation and strains, and therefore predict preliminary maintenance locations.

[1] `https://www.swri.org/technology-today/5-ms-aircraft-life-extension` - Accessed: 10-05-2022

2. **Monitoring:** After the production of the aircraft, monitoring devices can be placed at several predetermined critical locations (based on initial measurement data) across the whole aircraft to measure strain, stresses and possible crack propagation, thus providing key real life data.
3. **Modelling:** After the monitoring data has been collected and processed, the data can be combined with the measurement data to establish accurate numerical models to predict future failure locations. This can be used to establish key maintenance strategies with which the operational efficiency is maintained.
4. **Maintenance:** The maintenance procedure and the corresponding strategy are key aspects in maintaining operational efficiency since regular accurate maintenance ensure nominal operating conditions. However, the maintenance is carried out by the responsible airline and its corresponding maintenance team, advice can be given on maintenance intervals, and predicted maintenance locations to ensure the repair conducted at the right time and at the right location.
5. **Modernisation:** Certain aircraft parts can be changed or upgraded to decrease the noise emission, fuel consumption and increase the overall efficiency of the aircraft, thus maintaining its attractiveness to the airline after several years into service. Such change or upgrade can easily be implemented on the wingtips, resulting in lower noise levels and fuel consumption thus making it and effective upgrade to extend the operational lifetime of the aircraft. This is already part of the requirements but is included for complicity of the *5M* technique.

## 18.3. Adjustability

While already taking a giant leap forward towards sustainable aviation, the next step in the aircraft design should be considered. One of the client requirements is that the aircraft should be designed in such a manner that it can be upgraded to reduce the fuel consumption with an additional 10 % after 15 years in service. As new concepts such as distributed propulsion and hydrogen are used in the design, major advancements are expected in the coming years.

While upgrades to the aircraft can be very beneficial for the aircraft performances, it should be taken into account that it requires re-certification. Re-certification of the aircraft is a lengthy and costly process which should be avoided as much as possible. While the A320neo was largely based on the A320ceo with newer more fuel efficient engines, it took 14 months to re-certify the aircraft [2]. While the engines could be certified independently of the aircraft, testing had to be done on the effects of the loads induced by the new engine on the airframe. This lengthy certification process of the aircraft aircraft can cost up to 100 million dollar[3].

After a consultation with the client, it became clear that a lengthy and costly re-certification of the aircraft to achieve the required 10% reduction in fuel consumption was not an option. It is therefore chosen to not update the engines after 15 years in services. The impact of this is limited, as the current engine designed already uses cutting edge components which have a slightly less performance (mostly in efficiency) compared to the projected performance over 15 years [71]. However, the fuel system which have no significant influence on the aircraft aerodynamic performance and loading of the airframe, can be certified independently of the aircraft reducing the required time for re-certification. The 2040 goal of the European commission is to increase the efficiency of PEMFC from 57% to 65% [11, 34]. Also, the specific energy of fuel cells is expected to increase to 6 kW/kg, which will cause a signification decrease in fuel cell weight [35, 53]. Other components such as the compressor and cooling system are already cutting edge when it comes to efficiencies and performance. While the required fuel decreases because of the increase in FC efficiency, the tank design is not changed as this will require major changes to the manufacturing process.

Because of the increases in efficiencies of the fuel cell, the fuel system weight reduces. This causes a small snowball effects as the MTOW decreases as well. Iterating this effect reduces the required fuel for the design mission range form 1.58 tons to 1.37 tons. This is a fuel reduction of 12.31 %. This satisfied the required 10% reduction stated by requirement MIS.SUS.4.2.

[2] `https://aviationsourcenews.com/manufacturer/the-airbus-a320neo-has-been-in-service-for-five-years-an-exploration/` Accessed: 01-06-2022

[3] `https://www.plm.automation.siemens.com/global/pl/our-story/customers/tlg-aerospace/51461/` - Accessed: 30-05-2022

## 18.4. End-of-Life Strategy & Recyclability Plan

Despite being 30 years away and seeming like a worry for later, end-of-life considerations of the aircraft are required to be addressed even before entry into service as it largely impacts design choices. Sustainability and recyclability are ever-growing themes in the aerospace sector and are an integral part of the requirements. This section provides the plan for retirement of Lightning2.

The whole process of aircraft decommissioning is divided into two main parts as shown in Figure 18.1. During the first phase, some valuable components are removed from the aircraft and then inspected. Depending on their conditions, they are either sold to the airliners directly, or are inspected and repaired before returning to the aviation market[4]. For example, the engines are one of the most lucrative parts. Satair, which is an aircraft component and service company revealed that 70% of the second-hand aviation market is for engines and engine parts.[5]

In the second phase, the rest part of the aircraft are dismantled and recycled. Some parts will enter the non-aerospace market after implementing some changes. While the left part is considered as waste and thus requires further treatment. Recyclable wastes will be processed, and the non-recyclable wastes will be disposed for conventional aircraft.

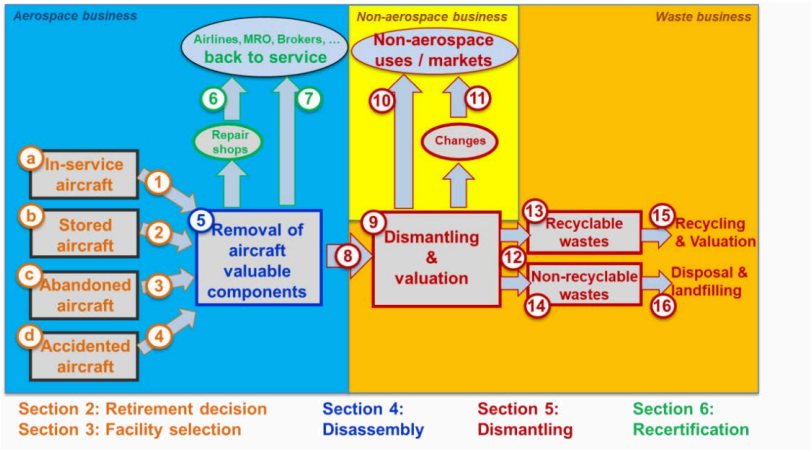


**Figure 18.1:** *Process of aircraft decommissioning* [6].

The majority part of the Lightning2 aircraft can be recycled using the process discussed above following the same procedure. The valuable parts like engines, landing gears and seats will be removed, repaired and sold as second-hand. These components will go back to aviation industry and be implemented on low-cost airliners. The wingbox and the fuselage is made of AL 2024-T81 which can be dismantled and recycled completely afterwards.

However, there are some extra considerations need to be taken into account for the hydrogen powered Lightning2 aircraft. First of all, the decommissioning of fuel cell stack is an essential part in the whole recycling process. A refurbishment program is now offered by Ballard, a fuel cell company, they replace the membrane electrode assemblies while reusing the existing hardware and plates. The used membrane electrode assemblies will be sent to a third-party for recovery of the platinum and other precious metals. Because of this, the cost of purchasing a new fuel cell stack will reduce by 30%. Normally, around 95% of the metals in the membrane electrode assemblies are reclaimed during the recycling process[7]. And the rest of the components in a fuel cell stack can be recycled by using ordinary recycling processes.

[4] https://www.icao.int/environmental-protection/Documents/EnvironmentalReports/2019/ENVReport2019-pg279-284 - Accessed 07-06-2022

[5] https://simpleflying.com/what-happens-when-an-aircraft-is-scrapped - Accessed: 07-06-2022

[6] https://www.icao.int/environmental-protection/Documents/EnvironmentalReports/2019/ENVReport2019-pg279-284 - Accessed 07-06-2022

[7] https://www.ballard.com/docs/default-source/web-pdf's/recycling-technical-note_final - Accessed: 07-06-2022

Another important aspect to take into account is the flame retardant material such as Phos-Chek, they play an important role in preventing the development of ignition by a variety of different chemical methods. They are widely used for cabin interior components such as: insulation blankets, carpets, seat cushions, sidewalls, and ceiling panels, however, safety regulations preclude them from recycling. Thus, an alternative material need to be implemented. In this case, recyclable epoxy resin (REP) composites are considered as the substitute for the flame retardant material, they are proved to have a good flame retardancy and are fully recyclable [64]. Besides that, silica aerogel is used as the insulation material for the hydrogen fuel tank. And the material is proved to be recycable by applying MCS gel process which is a reversible gel process based on changes in the binding ability of the hydrophilic and hydrophobic segments in water without additional crosslinking agents [59].

Lastly, the recycling of composite material is also an important part to look into. Composites are used in the fan blades but also in the seats, cabinets, and overhead bins. Take carbon fiber as an example, there are currently two ways to recycle it, either to dissolve the resin using chemicals or use high temperature to melt it before extract the carbon [79], article shows that recycling of composite materials can be up to 70% cheaper while maintaining 90% of its original strength, at the same time, leading to a 90-95% reduction in CO2 emissions compared to standard manufacturing[8]. As recycled composites lose part of its original strength, they can still be re-used in the cabin interior part. The recycling process also heavily depend on the type of the polymer and matrix. For thermoplastic matrix, it can be re-melted, re-shaped and re-moulded to manufacture new products as described above. However, for thermoset composite, a large amount of them cannot be re-processed or recycled because of their cross-link structure [79]. So, repurposing of the thermoset composite material is necessary. For example, they can be used for educational purpose in universities.

[8] `https://www.sydney.edu.au/news-opinion/news/2021/03/08/researchers-develop-improved-recycling-process-for-carbon-fibres.html` - Accessed: 07-06-2022

# 19

# Internal & External Configuration

After the initial fuselage cross section design, iterations were performed to optimise for minimal lost area in the lateral direction. Various seating configurations were selected and compared to each other from which the 3-4-3 configuration yielded the best result, having the smallest lost area in lateral direction while maintaining the ability to store a standard sized cargo container. In addition, the fuselage shall comply with requirement MIS.STR.2 to house the required payload volume.

The final optimised fuselage cross section design can be seen in Figure 19.1. Here, the layout with respect to seating, cargo storage and fuel cell placement is illustrated. Due to the trapezoidal area there is some side space that can be utilised depending on further needs, for example extra carry-on bins. In the centre, on the bottom, the unit load devices are fitted which are of the LD3-45 type. [1]

In Figure 19.2, the top view of the cabin can be seen. With the needed seating arrangement, the galley should be fitted in the aft of the fuselage, where there is also space for lavatories. Arrangement of the fuel tanks is determined on the basis of the required centre of gravity balance during loading of the aircraft. The cabin exits are located in the front of the passenger cabin as above-wing emergency exits are infeasible due to the blending area of the body. In case of emergency, the aircraft should be able to be evacuated within 90 seconds. A combination of a Type-II and Type-A exits on both sides of the plane is required to satisfy the regulations set by CS-25 [36]. As the Type-A exit has the biggest dimensions this is also used as the loading entrance in the centre of the aircraft. The cabin is designed using materials that are not toxic to passengers and crew, and the temperature is kept between 17 and 24 degrees Celsius.

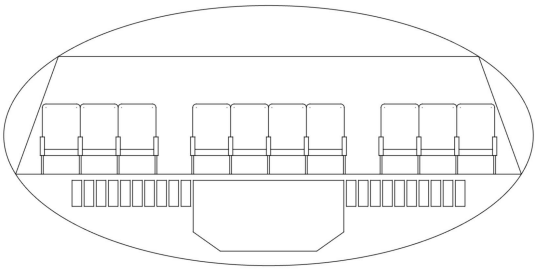

**Figure 19.1:** *Fuselage cross section design.*

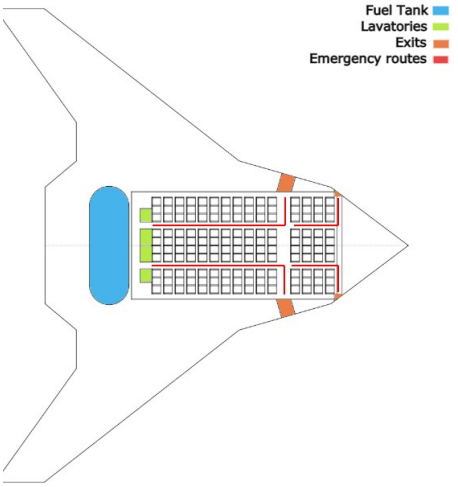


**Figure 19.2:** *Fuselage top view layout.*

[1] https://www.nordisk-aviation.com/en/ld-containers/akh-ld3-45/nordisk-akh-/- Accessed: 15-06-2022

Looking externally at the plane in Figure 19.3, the configuration of the propulsive system and initial placement of windows can be identified. Six out of ten engines are placed over the aft of the fuselage structure where the fuel tank is located. The remainder of the engines are placed on the blending area of the plane. Furthermore, it is ensured that no debris is released into the environment during normal operation. Doors are not yet rendered in Figure 19.3, but should be located right after the last cabin window.

The lack of windows in the blending area of the aircraft is inherent to the blended wing body concept. From a structural analysis perspective, this can be seen as beneficial, however acceptance from the public could pose present difficulties. As described in [97] a solution based on OLED technology can be utilised to improve passenger comfort avoiding claustrophobic effects that can arise from the exclusion of windows over the blending area. Their survey showed that despite the concerns of the claustrophobic effects, most passengers would consider flying in a windowless plane with the additional functions suggested below.

1. Take pictures with the outboard cameras and stream them to personal digital devices
2. Receive superimposed information about the places flown by
3. Enable the crew to get live images to monitor external system, for example, in case of engine failure

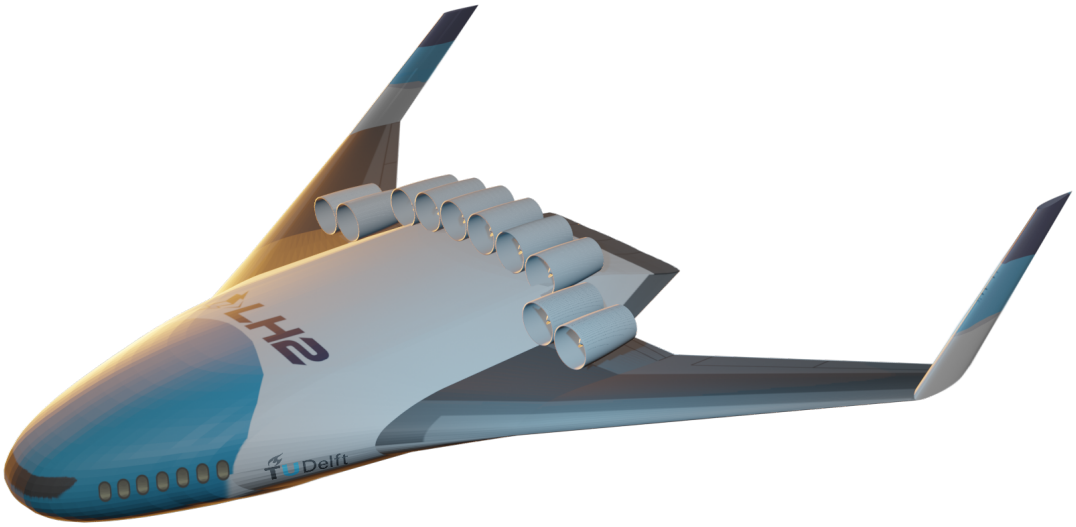


**Figure 19.3:** *External configuration of the Lightning2 Aircraft.*

# 20

# Requirements Compliance.

With the final conceptual design presented in this report, the project end-point is reached, that which falls within the scope of the Design Synthesis Exercise. This points grants the opportunity, and necessitates a review of the aircraft with regard to the set requirements at the start of the project. This chapter first explains and presents the requirements compliance matrix in Section 20.1. Requirements that are not relevant at this stage anymore, or were not formulated properly are discussed in Section 20.2. Subsequently, rationales are provided for requirements that are not met (or cannot be verified at this stage) accompanied by proposed modifications to meet them in Section 20.3.

## 20.1. Requirement Compliance Matrix

This section presents the requirements compliance matrix, depicted in Table 20.1. The requirements identified at the start of the Design Synthesis Exercise are reiterated here, without making any adjustments to the original.

In Table 20.1, the first column contains the requirement identification (ID). The adjacent column provides the full written-out requirement. The third column contains the check whether requirement is met and verified. A green colour indicates that the requirement is met, whereas a red colour indicates that the requirement not complied with. The latter can also occur if verification of the requirement cannot be performed at this stage. Lastly, column four indicates which specific section of the report should be referred to for details regarding the specific requirement compliance. Note that some requirements are cross out as they were not deemed applicable and that the unique requirement identifiers may not be reused.

**Table 20.1:** *Requirements compliance matrix.*

| ID | Name | Check | Section |
|---|---|---|---|
| | **Weight - WGT** | | |
| ~~MIS.WGT.1~~ | ~~The aircraft shall have a maximum take-off weight of TBD N.~~ | | |
| MIS.WGT.2 | The aircraft shall have a longitudinal centre of gravity range such that it does not tip over during loading and unloading on the ground. | | Section 9.2 |
| | **Noise regulations - REG** | | |
| MIS.REG.1 | The aircraft shall meet the Stage 5 / Chapter 14 noise requirements of ICAO. | | Subsection 12.1.3 |
| MIS.REG.1.1 | The maximum certified EPNdB of the aircraft at the lateral full-power measurement point shall be according to the table in Chapter 12 of Attachment 1 of Annex 16 to the Convention on International Civil Aviation Volume 1 (ICAO). | | Subsection 12.1.3 |
| MIS.REG.1.2 | The maximum certified EPNdB of the aircraft at the flyover reference noise measurement point shall be according to the table in Chapter 12 of Attachment 1 of Annex 16 to the Convention on International Civil Aviation Volume 1 (ICAO). | | Subsection 12.1.3 |
| MIS.REG.1.3 | The maximum certified EPNdB of the aircraft at the approach reference noise measurement point shall be according to the table in Chapter 12 of Attachment 1 of Annex 16 to the Convention on International Civil Aviation Volume 1 (ICAO). | | Subsection 12.1.3 |

| | | | |
|---|---|---|---|
| MIS.REG.1.4 | The sum of the differences at all three measurement points between the maximum noise levels and the maximum permitted noise levels specified in MIS.REG.1.1, MIS.REG.1.2, MIS.REG.1.3 shall not be less than 17 EPNdB. | | Subsection 12.1.3 |
| MIS.REG.1.5 | The maximum noise level at each of the three measurement points shall not be less than 1 EPNdB below the corresponding maximum permitted noise level specified in MIS.REG.1.1, MIS.REG.1.2, MIS.REG.1.3. | | Subsection 12.1.3 |
| MIS.REG.2 | The aircraft shall comply with the CS-25 amendment 27 regulations and Means of Compliance set by EASA. | | Subsection 12.1.3 |
| MIS.REG.3 | The airframe shall withstand the limit load factor specified in CS25.337. | | Subsection 8.3.7 |
| MIS.REG.4 | The aircraft shall comply with the size requirements set by the most limiting airport. | | Section 7.9 |
| MIS.REG.4.1 | The aircraft shall fit into the ICAO category C, with a width of at most 36 m to be able to operate at Rotterdam-The Hague airport. | | Section 7.9 |
| | **Sustainability - SUS** | | |
| MIS.SUS.1 | On-ground operation of the aircraft shall be without gas emissions. | | Section 15.1 |
| MIS.SUS.1.1 | Taxiing of the aircraft shall be without $NO_x$, $CO_2$, and any other green house gas (GHG) emissions. | | Section 15.1 |
| MIS.SUS.1.2 | During push back there shall be no $NO_x$, $CO_2$, and any GHG emissions. | | Section 15.1 |
| MIS.SUS.2 | All parts shall be made from environmentally friendly materials. | | Section 17.1 |
| ~~MIS.SUS.2.1~~ | ~~All relevant materials shall be produced with GHG emissions of TBD kg per kilogram of material.~~ | | |
| ~~MIS.SUS.2.2~~ | ~~All relevant materials shall be produced with toxic emissions of TBD kg per kilogram of material.~~ | | |
| MIS.SUS.3 | All aircraft parts shall be recycled or repurposed at end-of-life. | | Section 18.4 |
| MIS.SUS.4 | The propulsion system shall be environmentally friendly. | | Section 12.2 |
| MIS.SUS.4.1 | The propulsion system shall have an at least 50% reduction in $NO_x$ emission compared to emissions of new aircraft entered service in 2000. | | Section 12.2 |
| MIS.SUS.4.2 | The propulsion system shall be designed such that the overall fuel consumption can be further reduced by 10% within 15 years after service entry. | | Section 18.3 |
| MIS.SUS.4.3 | The propulsion system shall have an at least 45% reduction in $CO_2$ emissions compared to emissions of new aircraft entered service in 2000. | | Section 12.2 |
| MIS.SUS.5 | The overall fuel consumption of the aircraft shall be reduced by 10% compared to the A320. | | Section 12.2 |
| ~~MIS.SUS.6~~ | ~~The aircraft shall be manufactured with a TBD % of recycled materials.~~ | | |
| | **Organisaton - ORG** | | |
| MIS.ORG.1 | The conceptual design shall be finished within the time constraint of 10 weeks. | | N.A. |
| MIS.ORG.2 | The conceptual design shall be finished within the resource constraint of 10 students. | | N.A. |
| | **Aerodynamic Characteristics - AER** | | |
| MIS.AER.1 | The aircraft shall provide lift. | | Subsection 7.4.1 |
| MIS.AER.2 | The HLDs shall be able to increase $C_{L_{max}}$ | | N.A. |
| MIS.AER.3 | The airframe shall have a total drag coefficient, $C_D$, of TBD | | Subsection 7.4.2 |
| MIS.AER.4 | The aircraft shall have a minimum stall velocity $V_s$ according to CS25.103. | | Subsection 7.4.1 |
| ~~MIS.AER.5~~ | ~~The aircraft shall have a minimum stall AoA, of TBD degrees.~~ | | |

| | | | |
|---|---|---|---|
| | **Structural Support - STR** | | |
| MIS.STR.1 | The aircraft shall house a payload of 15 750 kg. | | Section 8.4 |
| MIS.STR.2 | The aircraft shall be able to house a payload volume of 127 $m^3$. | | Chapter 19 |
| MIS.STR.3 | The airframe shall house all necessary subsystems. | | Section 8.4 |
| MIS.STR.3.1 | The airframe shall have mounting points for the subsystems. | | Section 8.3 |
| MIS.STR.3.2 | The airframe shall protect all the subsystems from (hostile) environment. | | Section 8.4 |
| MIS.STR.4 | The airframe shall be able to sustain the ultimate design loads of 1.5 times the limit load as according to CS25.303. | | Subsection 8.3.7 |
| MIS.STR.4.1 | No element of the airframe shall experience plastic deformation under its ultimate design load. | | Subsection 8.3.7 |
| MIS.STR.4.2 | The landing gear shall be able to withstand the ultimate landing loads without failure. | | Subsection 9.4.1 |
| | **Thrust - THR** | | |
| ~~MIS.THR.1~~ | ~~The aircraft shall have a thrust of TBD N at cruise conditions.~~ | | |
| MIS.THR.2 | The aircraft shall have thrust such that requirement MIS.FLI.2 is satisfied. | | Section 12.3 |
| MIS.THR.3 | Propulsion system shall provide enough thrust in case of one engine inoperative to satisfy CS.121. | | Section 16.1 |
| | **Flight Performance - FLI** | | |
| MIS.FLI.1 | The aircraft shall have a maximum landing distance of 1400 m at sea level. | | Section 12.3 |
| MIS.FLI.2 | The aircraft shall have a maximum take-off distance of 2000 m at sea level. | | Section 12.3 |
| MIS.FLI.3 | The aircraft shall have an operational range of 3700 km at maximum payload. | | Chapter 2 |
| MIS.FLI.4 | The aircraft shall have a minimum cruise velocity of 0.7 Mach at cruise altitude. | | Section 6.3 |
| MIS.FLI.5 | The minimum cruise altitude of the aircraft shall be 609,6 m above mountainous areas as according to SARA.5015 regulation of EASA. | | Section 8.4 |
| MIS.FLI.6 | The aircraft shall be able to land on solid tarmac and asphalt. | | Section 9.4 |
| ~~MIS.FLI.7~~ | ~~The aircraft shall have a maximum Mach number of TBD.~~ | | |
| MIS.FLI.8 | The aircraft shall have a rate of climb according to CS25.111. | | Section 8.1 |
| MIS.FLI.9 | The approach velocity shall be 1.23 the stall speed at sea level, according to CS25.125 | | Section 12.3 |
| MIS.FLI.10 | The take-off velocity shall be according to CS25.107 | | Section 12.3 |
| | **Payload - PLD** | | |
| MIS.PLD.1 | The aircraft shall be able to carry payload of 15 750 kg. | | Chapter 19 |
| MIS.PLD.1.1 | The aircraft shall be able to transport 150 passengers with their luggage. | | Chapter 19 |
| MIS.PLD.1.2 | The aircraft shall be able to carry an additional payload of 2 % of the maximum take-off weight in addition to MIS.PLD.1.1. | | Section 10.3 |
| | **Maintenance - MTN** | | |
| MIS.MTN.1 | All critical components of the aircraft shall be accessible for inspection. | | Section 15.3 |
| MIS.MTN.2 | All critical parts of the aircraft shall be accessible for replacement and repair. | | Section 15.3 |
| MIS.MTN.3 | Engines of the aircraft shall be replaceable. | | Section 15.3 |
| | **Safety and Reliability - SAR** | | |
| MIS.SAR.1 | The aircraft shall have the dispatch reliability level of the industry standard 99.6%. | | Section 16.1 |
| MIS.SAR.2 | The aircraft shall have a sufficient safety level by adhering to the CS25 requirements. | | Section 8.1 |
| MIS.SAR.2.1 | The number of emergency exits shall be according to CS25.807. | | Chapter 19 |
| | **Stability - STA** | | |

| | | | |
|---|---|---|---|
| MIS.STA.1 | The aircraft shall be statically stable. | | Section 9.2 |
| MIS.STA.2 | The aircraft shall have a lateral centre of gravity range such that it does not tip over during turning or extreme crosswinds when on the ground. | | Section 9.4 |
| | **Control - CON** | | |
| MIS.CON.1 | The aircraft shall be controllable. | | Section 9.3 |
| MIS.CON.2 | The aircraft shall have an autopilot system. | | Section 14.5 |
| | **Customers - CUS** | | |
| STH.CUS.1 | The aircraft shall have a maximum unit cost of 100 million dollars. | | Section 3.2 |
| STH.CUS.2 | The aircraft shall have a maximum turnaround time of 120% with respect to the main competitors. | | Section 15.2 |
| STH.CUS.3 | The aircraft shall have an operational lifetime of 30 years. | | Chapter 2 |
| STH.CUS.3.1 | The aircraft shall be able to withstand fatigue loads for the operational lifetime. | | Chapter 21 |
| STH.CUS.4 | The aircraft design shall be finalised within five years. | | Section 3.4 |
| ~~STH.CUS.4.1~~ | The cutting edge technology used in the aircraft shall be implementable within five years. | | Chapter 21 |
| | **Citizens around the Airport - CIT** | | |
| STH.CIT.1 | The aircraft shall not release any debris in the environment during normal operation. | | Chapter 19 |
| STH.CIT.2 | The aircraft shall have a reduction in perceived noise of at least 65% compared to aircraft which entered service in 2000. | | Subsection 12.1.3 |
| | **Passengers - PAX** | | |
| STH.PAX.1 | The pressure inside of the cabin shall be equivalent to the pressure below 2500 m altitude during normal operation. | | Section 8.4 |
| STH.PAX.2 | The temperature inside of the cabin shall be between 17 and 24 degrees Celsius during normal operation. | | Chapter 19 |
| STH.PAX.3 | Passengers shall be comfortable in their seats. | | Chapter 19 |
| STH.PAX.3.1 | The passenger seats shall have a pitch of at least 86 cm. | | Chapter 19 |
| STH.PAX.3.2 | The passenger seat shall have a width of at least 48 cm. | | Chapter 19 |
| STH.PAX.4 | Materials used shall not be toxic for the passengers or the crew. | | Chapter 19 |
| | **Manufacturing Companies - MFC** | | |
| STH.MFC.1 | The aircraft shall be manufacturable. | | Chapter 17 |
| STH.MFC.2 | The aircraft shall be reproducible. | | Chapter 17 |
| STH.MFC.3 | The manufacturing process shall comply with CS25.605. | | Chapter 17 |

## 20.2. Requirement filtering

Some of the requirements that were set at the start of the project are outdated at this point in the design, either because the requirements were not quantifiable, or due to certain design choices. In this section a short justification will be given on why certain requirements have been deemed not applicable.

Requirement MIS.WGT.1 is not applicable because MTOW mainly influences the noise the aircraft produces. Since there is already a separate noise requirement, this requirement becomes obsolete.

Requirement MIS.SUS.2.1, MIS.SUS.2.2, MIS.THR.1, MIS.FLI.7, and MIS.SUS.6 are no longer applicable as these are mainly driven by the future design choices, therefore can not be specified beforehand.

Requirement MIS.AERO.5.1 is not applicable anymore because the stall angle is not something that is designed for.

## 20.3. Feasibility Analysis

Requirements MIS.SUS.1.1 and MIS.SUS.1.2 are currently not met as Lightning2 has to rely on its fuel cells to taxi around the airport. The fuel cells generate electricity using an chemical reaction which has as byproduct water vapour, which is classified as a GHG. To still comply with the requirements of the client, participating in the EU Emissions Trading System is required. Besides that, requirement MIS.SUS.2 cannot be met for now, since it is unrealistic to make all parts of the aircraft recyclable, however for the non-recyclable components, they will be repurposed at end-of-life.

Requirement MIS.SUS.2 is currently not met as the aircraft has to rely on primary aluminium for its load bearing structure due to regulations. The production of primary aluminium is a rather energy intensive process, which does not qualify as an environmentally friendly material. The same logic applies to the use of composite materials. Materials used in non load bearing components can be the so called environmentally friendly materials as discussed in Section 17.1.

Requirement MIS.AER.5 is a stall angle requirement that still had to be defined. As stated in Chapter 7 the cruise angle of attack is 3 degrees. While the stall angle of attack should not be near the optimal cruise angle, it should also not be near the angle of attack of all needed manoeuvres. For now this cannot be analysed as it is heavily dependant on further detailed design and testing of the prototype.

Requirement MIS.STR.4.2 states a TBD requirement for landing loads. While the structural weight of the landing gear is estimated during the Class II weight iteration, further design of the landing gear was omitted from the DSE design phase. The associated loads introduced in the remaining structure are taken into account during the design of the wingbox and the fuselage, which enables a later design of the landing gear.

Requirement MIS.SAR.1 states a dispatch reliability level of the industry standard. While during the design this safety level is taken into account but can only be analysed during the testing and certification phase of the design.

Requirement STH.CUS.3 requires an operational lifetime of 30 years. This requirement can only be assessed after detailed design of all components, where the maintenance aspect can be properly assessed. Critical parts of the aircraft that are prone to failure within 30 years should be replaceable.

Requirement STH.CIT.1 requires the aircraft to not release any debris in the environment during normal operation. While all aircraft parts are made to not deteriorate mid-flight, only during testing can this be validated.

Requirement STH.PAX.2 states the need for a comfortable cabin temperature between 17 and 24 degrees Celsius during normal operation. As the climate control system is not yet considered during this phase of the design, however in Section 6.4 it is stated that around 30 % of the fuel is converted to heat. The cooling needed for the fuel-cell can potentially be offset by bleeding some of this heat to the passenger cabin.

Finally requirement STH.PAX.4 requires used materials to not be toxic for the passengers or the crew. Usage of toxic materials is unavoidable in the form of solvents, hydraulic fluids, coolants and fuel. The usage of these materials should be addressed in the certification phase of the design.

# 21

# Continuation of the Lightning2 Program

Due to the time and resource limitations of this Design Synthesis Exercise, the design results remain preliminary. In order to obtain a final, airworthy, product, further development and design are necessary. This will have to be done after this DSE has finished.

The first step in this is the generation of inputs for the Class III weight estimation, as well as execution of it. With this more detailed weight estimation, several different analyses will be done. These include things like aerodynamic, noise and emissions analyses. It should be noted that even though the resulting design from the DSE is not final, no major changes can be implemented after the Class II weight estimation has been completed. Therefore, the design steps that are taken during the writing of this report are of high importance, since they heavily limit subsequent design changes.

With the results of the Class III weight estimation and detailed analyses, the pre-production, also known as Class IV, weight estimation can be done. During this estimation, inventory is made of the masses and moments of inertia and the different components and drawings of these components are made. This weight estimation is the final one that is done without the aircraft being built. After production the whole aircraft shall be put on a scale in order for the actual aircraft weight to be measured.

Certification and testing of the aircraft is also something that needs to be considered. Certification is an important step that is required for the aircraft to be allowed into service. This is a process that cannot be performed at a single moment in time. In reality it is intertwined in the detailed design process. This includes the extensive testing of different subsystem components as well as their integration.

The steps that have to be taken in order for the design to be finalised are shown in Figure 21.1. The Class III and Class IV weight estimations are not shown in the diagram, since they are not standalone design steps, but are more summaries of the design steps made so far. The general flow of Figure 21.1 is as follows: It starts with checking the design resulting from the DSE for compliance with the requirements that were set. Then more detailed analyses are performed in order to identify areas of the design that need to be further improved, after which the design is iterated in order to implement the findings. Then, as the design is final at that point in time, it will move to final testing and certification such that it is allowed to operate commercially. Production then starts, as well as commercial operation once the first units roll out of the assembly line. At that point, commercial support for customers as well as the flight training program will commence. Finally, as the aviation industry changes rapidly, adjustability of the aircraft is monitored continuously during its operational life, so that improvements can be made to ensure optimal efficiency. As during any design process, any changes that are made to the design during the detailed design phase are checked to see if they comply with the set requirements.

The steps shown in this flow chart are also depicted in the Gannt chart shown in Figure 21.2. As opposed to Figure 21.1, the Gannt chart shows the different steps in a time-dependent manner. The interdependency of the steps is removed in order to more clearly show how the detailed design phase will develop over the coming years. Together with the flow chart, this gives a clear, yet concise overview of the detailed design phase of the blended wing body concept proposed during this DSE project.

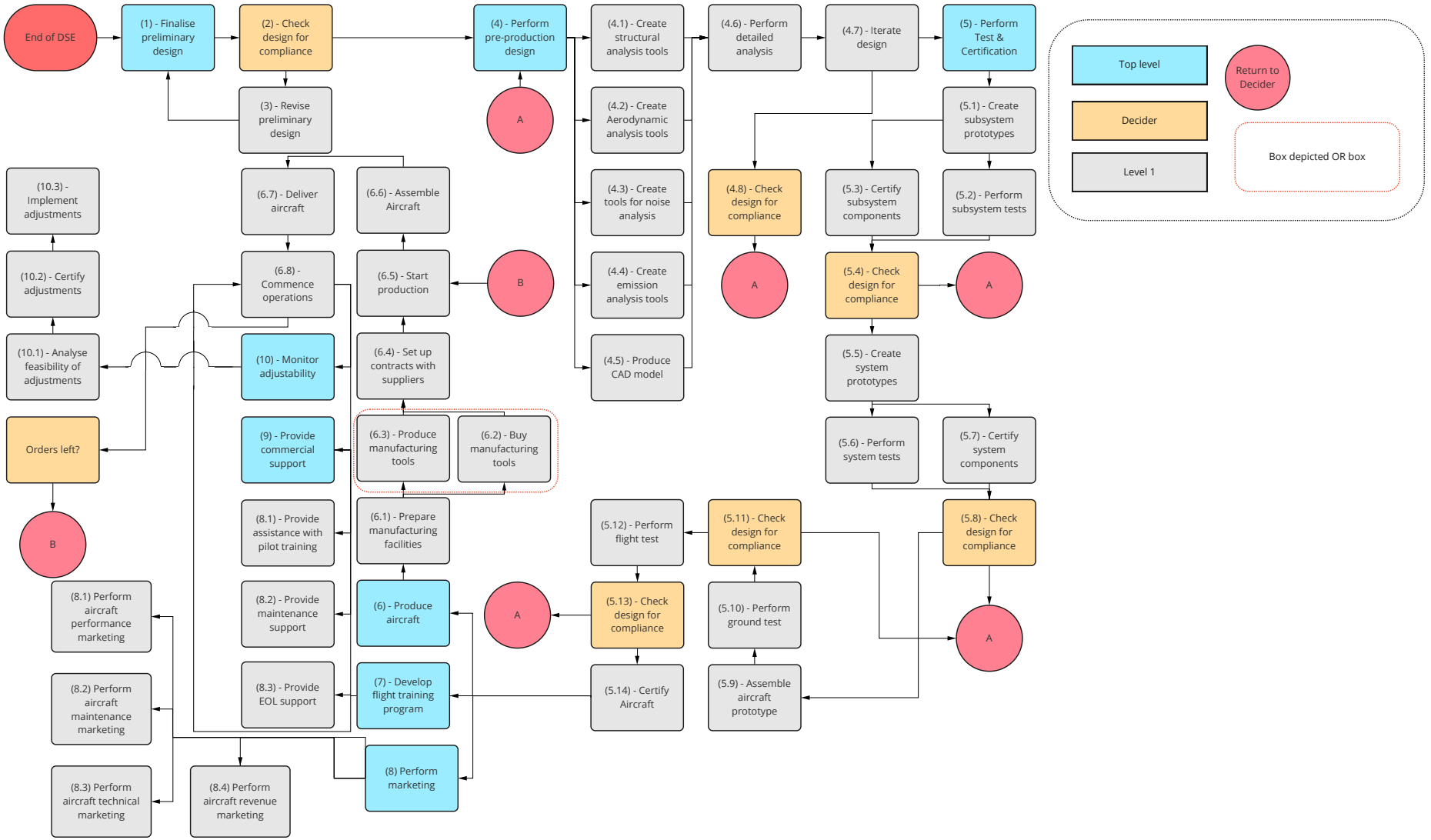


**Figure 21.1:** *Flow chart for the project continuation.*

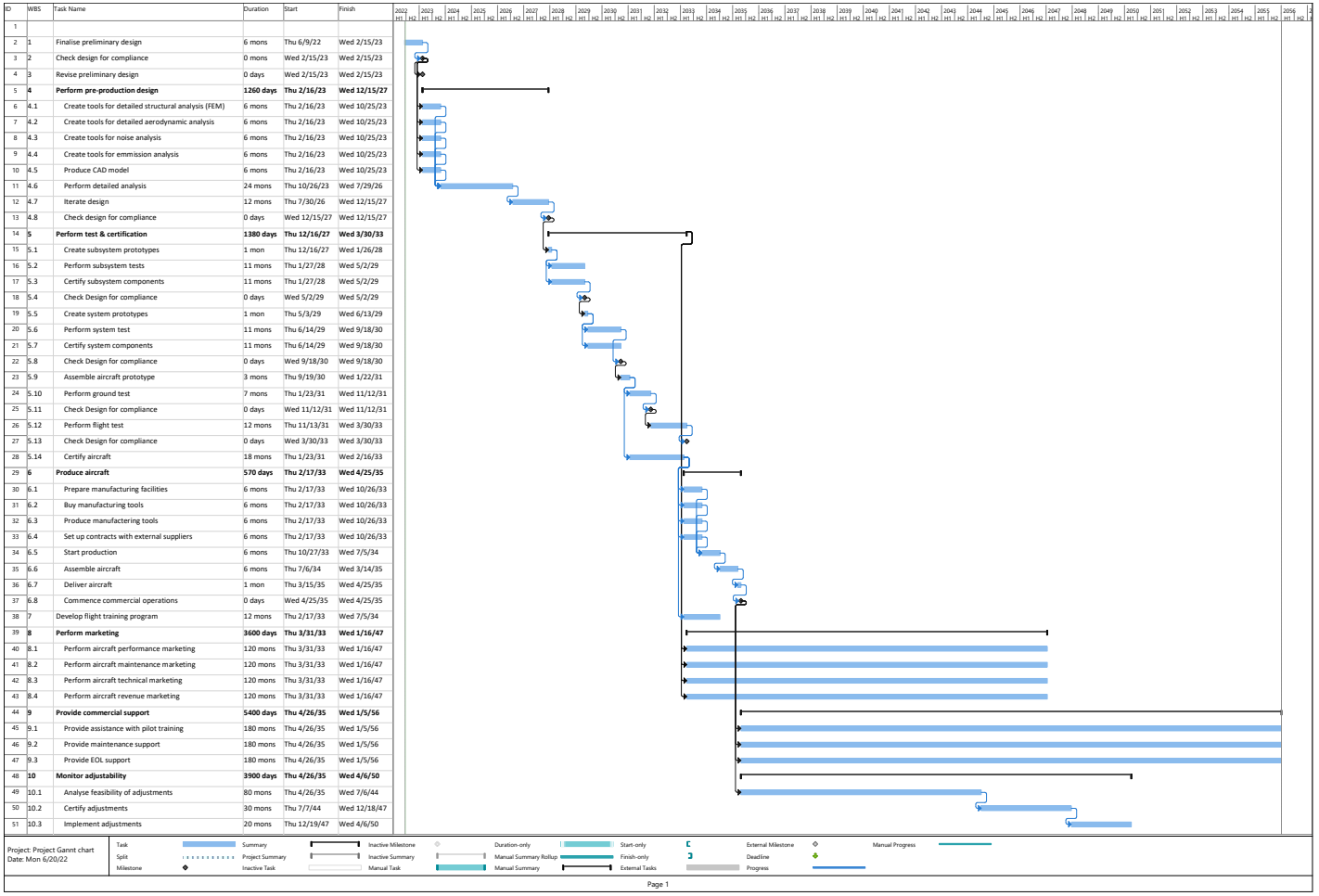

| ID | WBS | Task Name | Duration | Start | Finish |
|---|---|---|---|---|---|
| 1 | | | | | |
| 2 | 1 | Finalise preliminary design | 6 mons | Thu 6/9/22 | Wed 2/15/23 |
| 3 | 2 | Check design for compliance | 0 mons | Wed 2/15/23 | Wed 2/15/23 |
| 4 | 3 | Revise preliminary design | 0 days | Wed 2/15/23 | Wed 2/15/23 |
| 5 | **4** | **Perform pre-production design** | **1260 days** | **Thu 2/16/23** | **Wed 12/15/27** |
| 6 | 4.1 | Create tools for detailed structural analysis (FEM) | 6 mons | Thu 2/16/23 | Wed 10/25/23 |
| 7 | 4.2 | Create tools for detailed aerodynamic analysis | 6 mons | Thu 2/16/23 | Wed 10/25/23 |
| 8 | 4.3 | Create tools for noise analysis | 6 mons | Thu 2/16/23 | Wed 10/25/23 |
| 9 | 4.4 | Create tools for emmission analysis | 6 mons | Thu 2/16/23 | Wed 10/25/23 |
| 10 | 4.5 | Produce CAD model | 6 mons | Thu 2/16/23 | Wed 10/25/23 |
| 11 | 4.6 | Perform detailed analysis | 24 mons | Thu 10/26/23 | Wed 7/29/26 |
| 12 | 4.7 | Iterate design | 12 mons | Thu 7/30/26 | Wed 12/15/27 |
| 13 | 4.8 | Check design for compliance | 0 days | Wed 12/15/27 | Wed 12/15/27 |
| 14 | **5** | **Perform test & certification** | **1380 days** | **Thu 12/16/27** | **Wed 3/30/33** |
| 15 | 5.1 | Create subsystem prototypes | 1 mon | Thu 12/16/27 | Wed 1/26/28 |
| 16 | 5.2 | Perform subsystem tests | 11 mons | Thu 1/27/28 | Wed 5/2/29 |
| 17 | 5.3 | Certify subsystem components | 11 mons | Thu 1/27/28 | Wed 5/2/29 |
| 18 | 5.4 | Check Design for compliance | 0 days | Wed 5/2/29 | Wed 5/2/29 |
| 19 | 5.5 | Create system prototypes | 1 mon | Thu 5/3/29 | Wed 6/13/29 |
| 20 | 5.6 | Perform system test | 11 mons | Thu 6/14/29 | Wed 9/18/30 |
| 21 | 5.7 | Certify system components | 11 mons | Thu 6/14/29 | Wed 9/18/30 |
| 22 | 5.8 | Check Design for compliance | 0 days | Wed 9/18/30 | Wed 9/18/30 |
| 23 | 5.9 | Assemble aircraft prototype | 3 mons | Thu 9/19/30 | Wed 1/22/31 |
| 24 | 5.10 | Perform ground test | 7 mons | Thu 1/23/31 | Wed 11/12/31 |
| 25 | 5.11 | Check Design for compliance | 0 days | Wed 11/12/31 | Wed 11/12/31 |
| 26 | 5.12 | Perform flight test | 12 mons | Thu 11/13/31 | Wed 3/30/33 |
| 27 | 5.13 | Check Design for compliance | 0 days | Wed 3/30/33 | Wed 3/30/33 |
| 28 | 5.14 | Certify aircraft | 18 mons | Thu 1/23/31 | Wed 2/16/33 |
| 29 | **6** | **Produce aircraft** | **570 days** | **Thu 2/17/33** | **Wed 4/25/35** |
| 30 | 6.1 | Prepare manufacturing facilities | 6 mons | Thu 2/17/33 | Wed 10/26/33 |
| 31 | 6.2 | Buy manufacturing tools | 6 mons | Thu 2/17/33 | Wed 10/26/33 |
| 32 | 6.3 | Produce manufactering tools | 6 mons | Thu 2/17/33 | Wed 10/26/33 |
| 33 | 6.4 | Set up contracts with external suppliers | 6 mons | Thu 2/17/33 | Wed 10/26/33 |
| 34 | 6.5 | Start production | 6 mons | Thu 10/27/33 | Wed 7/5/34 |
| 35 | 6.6 | Assemble aircraft | 6 mons | Thu 7/6/34 | Wed 3/14/35 |
| 36 | 6.7 | Deliver aircraft | 1 mon | Thu 3/15/35 | Wed 4/25/35 |
| 37 | 6.8 | Commence commercial operations | 0 days | Wed 4/25/35 | Wed 4/25/35 |
| 38 | 7 | Develop flight training program | 12 mons | Thu 2/17/33 | Wed 7/5/34 |
| 39 | **8** | **Perform marketing** | **3600 days** | **Thu 3/31/33** | **Wed 1/16/47** |
| 40 | 8.1 | Perform aircraft performance marketing | 120 mons | Thu 3/31/33 | Wed 1/16/47 |
| 41 | 8.2 | Perform aircraft maintenance marketing | 120 mons | Thu 3/31/33 | Wed 1/16/47 |
| 42 | 8.3 | Perform aircraft technical marketing | 120 mons | Thu 3/31/33 | Wed 1/16/47 |
| 43 | 8.4 | Perform aircraft revenue marketing | 120 mons | Thu 3/31/33 | Wed 1/16/47 |
| 44 | **9** | **Provide commercial support** | **5400 days** | **Thu 4/26/35** | **Wed 1/5/56** |
| 45 | 9.1 | Provide assistance with pilot training | 180 mons | Thu 4/26/35 | Wed 1/5/56 |
| 46 | 9.2 | Provide maintenance support | 180 mons | Thu 4/26/35 | Wed 1/5/56 |
| 47 | 9.3 | Provide EOL support | 180 mons | Thu 4/26/35 | Wed 1/5/56 |
| 48 | **10** | **Monitor adjustability** | **3900 days** | **Thu 4/26/35** | **Wed 4/6/50** |
| 49 | 10.1 | Analyse feasibility of adjustments | 80 mons | Thu 4/26/35 | Wed 7/6/44 |
| 50 | 10.2 | Certify adjustments | 30 mons | Thu 7/7/44 | Wed 12/18/47 |
| 51 | 10.3 | Implement adjustments | 20 mons | Thu 12/19/47 | Wed 4/6/50 |



**Figure 21.2:** *Flow chart for the project continuation.*

# 22

# Conclusion

The goal for this design synthesis exercise, set 10 weeks ago, was to *design a new cutting-edge aircraft concept similar in size to the A320, which emits at least 50% less $NO_x$, 45% less $CO_2$, and 65% less perceived noise*. To achieve this, a blended wing body, named the Lightning2 was designed. The big advantage of a blended wing body is its aerodynamic shape, maximising lift and minimising drag. The propulsion, structures & materials, stability & control, and performance characteristics are established within this report.

The conceptual design of the Lightning2 was realised by an iterative process. The performance of the final conceptual design is reviewed to see if Lightning2 satisfies all requirements. The characteristics and performance of Lightning2 can be found in Table 22.1 and Table 22.2, respectively. Lightning2 makes major steps towards the set "Flightpath 2050" goals, as it produces no $CO_2$ or $NO_x$ during its operational life time. Not all requirements could be met, as some requirements can only be satisfied with a conventional aircraft and not a hydrogen blended wing body. However, all flight certification requirements set by CS-25 and ICAO are met. The weights of the conceptual design can be seen in Table 22.3.

**Table 22.1:** *Characteristics of Lightning2.*

| Parameter | Value |
|---|---|
| Number of passengers [-] | 150 |
| Payload [kg] | 15 750 |
| Unit manufacturing cost FY22 [million USD] | 46.14 |
| Length [m] | 34.4 |
| Wingspan [m] | 36.0 |
| Wing surface area [$m^2$] | 373.6 |
| Fuel type | Hydrogen |
| Fuel mass [kg] | 1 753.7 |
| Fuel cell | PEMFC |
| Number of engines | 10 |
| Maximum sea level thrust [kN] | 228.1 |

**Table 22.2:** *Performance of Lightning2.*

| Parameter | Value |
|---|---|
| Cruise altitude [m] | 10 972 |
| Cruise Mach [-] | 0.8 |
| Wing loading [$N/m^2$] | 2 150 |
| Thrust loading [-] | 0.249 |
| Take-off distance [m] | 1 307 |
| Landing distance [m] | 828 |
| Noise approach [dB] | 95.98 |
| Noise lateral [dB] | 94.25 |
| Noise flyover [dB] | 83.67 |
| $CO_2$ emissions [kg/km pax] | 0 |
| $NO_x$ emissions [kg/km pax] | 0 |
| Emissions [kg/km pax] | 0.0261 |

**Table 22.3:** *Weights of Lightning2.*

| Parameter | Value |
|---|---|
| MTOW [kg] | 82 267 |
| FW [kg] | 1 754 |
| OEW [kg] | 64 762 |

An extensive verification and validation has been performed on the methods and outcomes to provide significant confidence in the models used. Each line of code is verified using at least unit testing and benchmark testing to ensure that no mistakes are present in the models. The outcomes are compared with literature to ensure the

required accuracy. Finally, a sensitivity analysis was conducted from which was concluded that the fuel cell efficiency has major influences on the design and should therefore be closely monitored.

The financial feasibility of Lightning2 is established by performing a financial and market analysis. From the market analysis it is concluded that Lightning2 will mainly focus on the short-haul market which is dominated by low cost carriers, making it important that Lightning2 is price competitive. To realise Lightning2 an initial investment of 19.7 billion USD is required. Lightning2 has an average manufacturing unit cost of 46.14 million USD and an expected operating cost of 62 929 USD per nautical mile. It is expected to break even in 2046 with 448 aircraft sold. To make Lightning2 financially interesting for airlines, major investment are needed to quickly change the current kerosene airport infrastructure to a hydrogen infrastructure.

After 15 years an update will be given to the fuel cell used, reducing the fuel consumption with an additional 12.3%. Besides the sustainable operations of Lightning2, it is also ensured that the manufacturing and end-of-life is sustainable. It is inevitable to primarily use aluminium and composites as this is required by regulations. The processes to manufacture the parts will however not require more energy compared to current manufacturing methods. At the end-of-life, 100% of the aircraft, including the composites and fuel cells, is recycled, reused, or repurposed. The majority of the recycled raw material will be returned in the production cycle for non-load bearing structures.

Overall it can be concluded that lightning2 satisfies the mission statement of the design synthesis exercise. While the blended wing body concept with hydrogen propulsion seems ambitious, this report proves that major sustainable steps can be achieved with Lightning2 which is expected to enter in 2034.

While the next steps in realising Lightning2 were already elaborated upon in Chapter 21, some recommendations concerning the current conceptual design are stated below.

- Collaborate with General Electric regarding possibilities for electric ducted fans. As stated in Chapter 6, no current electric ducted fan designs for commercial aircraft are available on the market. A collaboration with General Electric is needed to design a electric ducted fan for the specific thrust requirements of Lightning2.
- More research has to be conducted in the effects of BLI on the thrust required, drag reduction and the structural requirements of the fan blades to withstand the distorted air.
- Find manufactures and off the shelf components for propulsion system parts such as the cooling system and compressor.
- Perform a detailed heat management analysis. Electrical components such as the fuel cell and motor produce heat which needs to be removed. Some research in this has been performed in this report but this should be extended.
- Detailed research into the effects of ejecting water vapour into the stratosphere. Experts remain unsure of the exact effects of ejecting water vapour into the stratosphere, whether this is harmful to the environment.
- Look into the effects of using a multi-cell wing box. This can reduce the shear in the vertical plane of the wingbox possibly leading to a weight reduction.
- Investigate the use of composites in the wingbox and fuselage structure.

# Bibliography


[1] A. Sgueglia and et al. “Exploration and Sizing of a Large Passenger Aircraft with Distributed Ducted Electric Fans”. In: *AIAA - Scitech 2018* (2018).

[2] H.H. Abada. “Turboelectric Distributed Propulsion System for NASA Next Generation Aircraft”. In: *Browse all Theses and Dissertations* (2017).

[3] Ira H. Abbott and Albert E. Von Doenhoff. *Theory of wing sections : including a summary of airfoil data*. first. Mineola: Dover Publications, 1959.

[4] G.H. Abumeri, L.H. Kuguoglu, and C.C. Chamis. *Composite Fan Blade Design for Advanced Engine Concepts*. Technical Memorandum NASA/TM-2004-212943. Cleveland, Ohio, United States: National Aeronautics and Space Administration, 2004.

[5] *Airbus A320 Flight Crew Operating Manual*. Rev. 23. Airbus. 2004.

[6] Daniel Albalate, Germà Bel, and Xavier Fageda. “Competition and cooperation between high-speed rail and air transportation services in Europe”. In: *Journal of Transport Geography* 42 (2015), pp. 166–174.

[7] John D. Anderson. *Fundamentals of Aerodynamics*. sixth. Mcgraw-Hill Education, 2016.

[8] S M Arnold et al. “Spherical Cryogenic Hydrogen Tank Preliminary Design Trade Studies”. In: *48th AIAA/ASME/ASCE/AHS/ASC Structures, Structural Dynamics, and Materials Conference*. 2007.

[9] E. Asmatulu, M. Overcash, and J. Twomey. “Recycling of Aircraft: State of the Art in 2011”. In: *Journal of Industrial Engineering* (2013).

[10] V. Babu. *Fundamentals of Propulsion*. first. Cham, Switzerland: Springer, 2022.

[11] T. Bednarek et al. *Historical Analysis of FCH 2 JU Stationary Fuel Cell Projects*. JCR Technical Report. 2021.

[12] A. Birolini. “Reliability Engineering : Theory and Practice”. In: eighth. Berlin, Germany: Springer, 2017. Chap. Basic Concepts, Quality & Reliability (RAMS) Assurance of Complex Equipment & Systems.

[13] Bombardier Inc. *2018 Financial Report*. Financial Report. Bibliothèque et Archives nationales du Québec, 2019.

[14] Alessandro Bombelli. *Lecture 3 - Airline business models*. Brightspace: `https://brightspace.tudelft.nl/d2l/le/content/397910/viewContent/2489463/View`. Delft University of Technology, AE3501-19, Accessed on 26-9-2020. 2021.

[15] Clark Borst. *Air Traffic Control and Management*. Brightspace: `https://brightspace.tudelft.nl/d2l/le/content/397980/viewContent/2283297/View`. Delft University of Technology. AE4302 Avionics and Operations. 2022.

[16] Clark Borst. *Instrument Landing Systems*. Brightspace: `https://brightspace.tudelft.nl/d2l/le/content/397980/viewContent/2283291/View`. Delft University of Technology. AE4302 Avionics and Operations. 2022.

[17] Clark Borst. *Terrestrial radio-navigation systems*. Brightspace: `https://brightspace.tudelft.nl/d2l/le/content/397980/viewContent/2283288/View`. Delft University of Technology. AE4302 Avionics and Operations. 2022.

[18] G D Brewer. *Hydrogen Aircraft Technology*. CRC Press, 1991.

[19] Malcom Brown and Roelof Vos. “Conceptual Design and Evaluation of Blended-Wing Body Aircraft”. In: *2018 AIAA Aerospace Sciences Meeting*. 2018.

[20] UK Government Department for Business Innovation & Skills. “UK Aerospace Maintenance, Repair, Overhaul & Logistics Industry Analysis”. In: *Department for Business, Innovation & Skills* (2017).

[21] V.H.L. Cheng et al. “Flight-Deck Automation for Trajectory-Based Surface Operations”. In: *American Institute of Aeronautics and Astronautics* (2008).

[22] W. Cinibulk. *Aircraft Electrical Wire*. [PowerPoint Slides]. Accessed: 03-06-2022. 2001.

[23] Clean Hydrogen Joint Undertaking. *Hydrogen-powered aviation : a fact-based study of hydrogen technology, economics, and climate impact by 2050*. Report. Publications Office of the European Union, 2020.

[24] Regina R. Clewlow, Joseph M. Sussman, and Hamsa Balakrishnan. “The impact of high-speed rail and low-cost carriers on European air passenger traffic”. In: *Transport Policy* 33 (2014), pp. 136–143.

[25] R. Curran et al. “Integrating Aircraft Cost Modeling into Conceptual Design”. In: *CONCURRENT ENGINEERING: Research and Applications* (2005).

[26] H.D. Curtis. *Fundamentals of Aircraft Structural Analysis*. first. Chicago, Illinois, United States: Irwin, 1997.

[27] Karen A. Deere et al. “Computational Analysis of Powered Lift Augmentation for the LEAPTech Distributed Electric Propulsion Wing”. In: *AIAA - Aviation Forum - 2017* (2017).

[28] Maria Delgado et al. “Dynamic Modeling and Simulation of an Optimized Proton Exchange Membrane Fuel Cell System”. In: *ASME International Mechanical Engineering Congress and Exposition, Proceedings*. 2007.

[29] Y. Denieul. “Preliminary Design of Control Surfaces and Laws for Unconventional Aircraft Configurations”. Accessed: 16-06-2022. PhD thesis. Preliminary Design of Control Surfaces and Laws for Unconventional Aircraft Configurations, 2016.

[30] H Derking, L van ter Torgt, and M Keezer. *Cryoworld: Liquid Hydrogen Storage: Status and Future Perspectives*. PowerPoint Presentation. 2019.

[31] J. van Dommelen and R. Vos. “Conceptual design and analysis of blended-wing-body aircraft”. In: *Journal of Aerospace Engineering* 228 (2014).

[32] N.H.M. van den Dungen. “Synthesis of an Aircraft Featuring a Ducted-Fan Propulsive Empennage”. MA thesis. Delft University of Technology, 2017.

[33] ECAC-CEAC. *Reports on Standard Method of Computing Noise Contours around Civil Airports*. Applications Guide. Neuilly-sur-Seine Cedex, France: European Civil Aviation Conference, 2016.

[34] U.S. Department of Energy. “Multi-Year Research, Development, and Demonstration Plan”. In: *Energy Efficiency & Renewable Energy* (2017).

[35] M.J. Eslamibidgolia et al. “How theory and simulation can drive fuel cell electrocatalysis”. In: *Nano Energy* 29 (2016). Accessed: 11-05-2022.

[36] European Aviation Safety Agency. *Easy Access Rules for Large Aeroplanes (CS-25) (Initial issue)*. first. EASA. Brussels, Belgium, 2018.

[37] European Commission, Directorate-General for Mobility and Transport, Directorate-General for Research and Innovation. *Flightpath 2050 : Europe’s vision for aviation : maintaining global leadership and serving society’s needs*. Publications Office, 2011.

[38] J.L. Felder, H.D. Kim, and G.V. Brown. “An Examination of the Effect of Boundary Layer Ingestion on Turboelectric Distributed Propulsion Systems”. In: *Aerospace Sciences Meeting including the New Horizons Forum and Aerospace Exposition* (2011).

[39] Raluca-Andreea Felseghi et al. “Hydrogen Fuel Cell Technology for the Sustainable Future of Stationary Applications”. In: *Energies* 12.23 (2019).

[40] D.F. Finger et al. “Cost Estimation Methods for Hybrid-Electric General Aviation Aircraft”. In: *Asia Pacific International Symposium On Aerospace Technology* (2019).

[41] P. Footohi, A. Bouskela, and S. Shkarayev. “Aerodynamic Characteristics of the Blended-Wing-Body VTOL UAV”. In: *Journal of Aerospace Engineering and Mechanics* (2020).

[42] D Giancoli. *Physics for scientists and engineers*. fifth. Pearson, 2020.

[43] C Goldberg et al. “Economic Viability Assessment of NASA’s Blended Wing Body N3-X Aircraft”. In: *53rd AIAA/SAE/ASEE Joint Propulsion Conference*. 2017.

[44] Hongyi Gu and Yulai Wan. “Can entry of high-speed rail increase air traffic? Price competition, travel time difference and catchment expansion”. In: *Transport Policy* 97 (2020), pp. 55–72.

[45] S. Gudmundsson. *General Aviation Aircraft Design (Second Edition)*. second. Amsterdam, the Netherlands: Butterworth-Heinemann, 2021.

[46] M.D. Guynn and E.D. Oison. *Evaluation of an Aircraft Concept With Over-Wing, Hydrogen-Fueled Engines for Reduced Noise and Emissions*. Technical Memorandum NASA/TM-2002-211926. Hampton, Virginia, United States: National Aeronautics and Space Administration, 2002.

[47] G.K.W Kenwayand R. Henderson et al. “Reducing Aviation’s Environmental Impact Through Large Aircraft For Short Ranges”. In: *48th AIAA Aerospace Sciences Meeting Including the New Horizons Forum and Aerospace Exposition* (2010).

[48] International Civil Aviation Organization. *Annex 16 to the Convention on International Civil Aviation: Environmental Protection Volume I - Aircraft Noise*. Online: `https://brightspace.tudelft.nl/d2l/le/content/415039/viewContent/2366784/View`. Eight Edition. 2017.

[49] Y. Isik. “ARINC 629 Data Bus Standard on Aircrafts”. In: *Civil Aviation School, Anadolu University* (2021).

[50] C.N. Jardine. “Calculating the Environmental Impact of Aviation Emissions”. In: *Environmental Change Institute* (2005).

[51] Y. Jin et al. “Modeling of Ducted-Fan and Motor in an Electric Aircraft and a Preliminary Integrated Design”. In: *SAE Int. J. Aerosp.* 11 (2018).

[52] W S Johnson et al. “Wrinkling of Composite Sandwich Structures Under Compression”. In: *Journal of Composites Technology & Research* 17 (Oct. 1995).

[53] T. Kadyk et al. “Analysis and Design of Fuel Cell Systems for Aviation”. In: *Energies* (2018).

[54] Ramin Karim et al. “Positioning Embedded Software Maintenance within Industrial Maintenance”. In: *2008 IEEE International Conference on Software Maintenance*. 2008, pp. 440–443.

[55] Mustafa Keçeci, C.O. Colpan, and T.H. Karakoç. “Reducing the fuel consumption and emissions with the use of an external fuel cell hybrid power unit for electric taxiing at airports”. In: *International Journal of Hydrogen Energy* (2022).

[56] E. Keen and W. Mason. “A Conceptual Design Methodology for Predicting the Aerodynamics of Upper Surface Blowing on Airfoils and Wings”. In: *AIAA* (2005).

[57] H.J.M. Kok, M. Voskuijl, and M.J.L. van Tooren. “Distributed Propulsion featuring Boundary Layer Ingestion Engines for the Blended Wing Body Subsonic Transport”. In: *American Institute of Aeronautics and Astronautics* (2010).

[58] A. Kollmuss and J. Lane. “Carbon Offsetting & Air Travel”. In: *Stockholm Environment Institute* (2008).

[59] Zhang Kun et al. “Recyclable thermo-insulating panels made by reversible gelling of dispersed silica aerogel microparticles”. In: *Journal of Sol-Gel Science and Technology* (2022).

[60] M.J. van Laar et al. *The Design of a Cutting Edge Low-Emission Low-Noise Aircraft Baseline Report*. Report. Delft, The Netherlands: Delft University of Technology, 2022.

[61] I. Langella. *Lecture-5 : Aero Engines - examples*. Brightspace: `https://brightspace.tudelft.nl/d2l/le/content/213451/viewContent/1472042/View`. AE-2230-II Propulsion and Power, Delft Technical University, Accessed: 27-05-2022. 2021.

[62] J. Larminie and A. Dicks. *Fuel Cell Systems Explained*. second. Hoboken, New Jersey, United States: John Wiley & Sons, 2013.

[63] RONGSHAN LI and YU LU. “Research on the Over-outsourcing in Aviation Manufacturing Industry—Case Analysis based on the Boeing 787”. In: *WSEAS Transactions on Business and Economics* (2007). DOI: `10.37394/23207.2020.17.49`.

[64] Xiaolu Li et al. “Recyclable flame-retardant epoxy composites based on disulfide bonds: Flammability and recyclability”. In: *Composites Communications* 25 (2021).

[65] Florian Linke et al. “GLOWOPT - A new approach towards global-warming-optimized aircraft design”. In: *1st Aerospace Europe Conference (AEC)*. Jan. 2020.

[66] C. Liu et al. “A preliminary method to estimate impacts of inlet flow distortion on boundary layer ingesting propulsion system design point performance”. In: *Journal of Aerospace Engineering* 228(9) (2013). Accessed: 27-05-2022.

[67] C. Liu et al. “Thermal cycle analysis of turboelectric distributed propulsion system with boundary layer ingestion”. In: *Aerospace Science and Technology* 27 (2013).

[68] C. Liu et al. “Turboelectric Distributed Propulsion System Modelling for Hybrid-WingBody Aircraft”. In: *Joint Propulsion Conference & Exhibit* 48 (2012).

[69] B Mohr et al. “Design of a 450-passenger blended wing body aircraft for active control investigations”. In: *AIAA - Aviation Forum - 2017* (2017).

[70] Elon Musk. “Hyperloop Alpha”. In: *SpaceX: Hawthorne, CA, USA* (2013).

[71] National Academies of Sciences, Engineering, and Medicine. *Commercial Aircraft Propulsion and Energy Systems Research*. Washington, DC: The National Academies Press, 2016.

[72] M. Nita and D. Scholz. *Estimating the Oswald Factor from Basic Aircraft Geometrical Parameters*. Deutsche Gesellschaft für Luft- und Raumfahrt - Lilienthal-Oberth e.V., 2012.

[73] P Nolte et al. “Quantitative Assessment of Technology Impact on Aviation Fuel Efficiency”. In: *Air Transport and Operations Symposium*. 2012.

[74] P. Okonkwo and H. Smith. “Review of Evolving Trends in Blended Wing Body Aircraft Design”. In: *Progress in Aerospace Sciences* (2016).

[75] P. Okonkwo and H. Smith. “Review of evolving trends in blended wing body aircraft design”. In: *Progress in Aerospace Sciences* (2016).

[76] F. Oliviero. *Aircraft Aerodynamic Analysis - Lift & Drag*. Online PowerPoint: `https://brightspace.tudelft.nl/d2l/le/content/415039/viewContent/2366782/View`. Accessed: 03-06-2022. 2021.

[77] F. Oliviero. *Aircraft aerodynamic analysis: Mobile surfaces of the wing*. Brightspace: `https://brightspace.tudelft.nl/d2l/le/content/415039/viewContent/2366784/View`. Delft University of Technology. Aerospace Design and Systems Engineering Elements II AE2111-II. 2022.

[78] F. Oliviero. *Requirement Analysis and Design principles for A/C stability & control (Part 2)*. Brightspace: `https://brightspace.tudelft.nl/d2l/le/content/419892/viewContent/2368598/View`. Delft University of Technology.AE3211-I - Systems Engineering and Aerospace Design. 2022.

[79] Esfandiar Pakdel et al. “Recent progress in recycling carbon fibre reinforced composites and dry carbon fibre wastes, Resources, Conservation and Recycling”. In: *Chemical Engineering and Processing: Process Intensification* 166 (2021). ISSN: 0921-3449.

[80] Bruno G. Pollet, Iain Staffell, and Jin Lei Shang. “Current status of hybrid, battery and fuel cell electric vehicles: From electrochemistry to market prospects”. In: *Electrochimica Acta* 84 (2012), pp. 235–249.

[81] R.J. Hamann et al. *Systems Engineering & Technical Management Techniques: Lecture Notes*. Online. Accessed: 11-05-2022. 2006.

[82] R.Vos and J. A. Melkert. *Wing and Propulsion System Design*. Brightspace: `https://brightspace.tudelft.nl/d2l/le/content/415039/viewContent/2366784/View`. Delft University of Technology. Aerospace Design and Systems Engineering Elements I AE1222-II. 2022.

[83] Naveed U. Rahman and James F. Whidborne. “Propulsion and Flight Controls Integration for a Blended-Wing-Body Transport Aircraft”. In: *Journal of Aircraft, Vol. 47, No. 3* (2010).

[84] Calvin Rans. *Structural Analysis and Design 2020/2021 Lecture Notes*. Online PowerPoints: `https://brightspace.tudelft.nl/d2l/home/292976`. Accessed: 13-6-2022. 2020.

[85] D. Raymer. *Aircraft Design: A Conceptual Approach*. sixth. Reston, Virginia, United States: American Institute of Aeronautics and Astronautics, 2018.

[86] P. Roling. *Airfield perfomance*. Brightspace: `https://brightspace.tudelft.nl/d2l/le/content/293140/viewContent/2084485/View`. Delft University of Technology. AE2230-I Flight & Orbital Mechanics. 2022.

[87] P. Roling. *Lecture 13 - Airport of the future*. Brightspace: `https://brightspace.tudelft.nl/d2l/le/content/397912/viewContent/2228670/View`. Delft University of Technology. AE3502-14 Airport Planning, Design and Operations. 2022.

[88] P. Roling. *Lecture 8 - Emissions*. Brightspace: `https://brightspace.tudelft.nl/d2l/le/content/397912/viewContent/2228664/View`. Delft University of Technology. AE3502-14 Airport Planning, Design and Operations. 2022.

[89] R. Roos. "Study of experimentally blended wings". In: *Honors research projects* (2017).

[90] J Roskam. *Airplane Design part VIII: Airplane Cost Estimation: Design, Development, Manufacturing and Operating*. Lawrence, Kansas, United States: DARcorporation, 1990.

[91] J. Roskam. *Airplane Design Part I: Preliminary Sizing of Airplanes*. Revised edition. Lawrence, Kansas, United States: DARcorporation; Revised edition, 2017.

[92] Ros Rosli et al. "A review of high-temperature proton exchange membrane fuel cell (HT-PEMFC) system". In: *International Journal of Hydrogen Energy* 42 (July 2016), pp. 9293–9314.

[93] Royal Schiphol Group. *Sustainable taxiing and the Taxibot*. Accessed on 10-05-2022. 2020.

[94] D.A. Sagerser, S. Lieblein, and R.P. Kkebs. *Empirical Expressions for Estimating Length and Weight of Axial-Flow Components of VTOL Powerplants*. Technical Memorandum NASA-TM-X-2406. Cleveland, Ohio, United States: National Aeronautics and Space Administration, 1971.

[95] Oliverio Esteban Velázquez Salazar, Julien Weiss, and François Morency. "Development of blended wing body aircraft design". In: *CASI 62nd Aeronautics Conference and AGM*. Montréal, Canada, 2015.

[96] Yash Sanghai. "Techno-Economic Analysis of Hydrogen Fuel Cell Systems Used as an Electricity Storage Technology in a Wind Farm with Large Amounts of Intermittent Energy". Masters Thesis. Cambridge, Massachusetts: University of Massachusetts Amherst, 2013.

[97] Sara Bagassi, Francesca Lucchi, Franco Persiani. *Aircraft Preliminary Design: a windowless concept*. Report. Forlì, Italy: University of Bologna, 2015.

[98] B. Sarlioglu. *Electrification of Aircraft and Vehicles Current Status and Future Trends*. [PowerPoint Slides]. Accessed: 02-06-2022. 2017.

[99] R.K. Schmidt. "A Semi-Analytical Weight Estimation Method for Oval Fuselages in Novel Aircraft Configurations". MA thesis. Technical university of Delft, Aerospace Engineering, 2013.

[100] Dieter Scholz. "Aircraft Design". In: Hamburg Open Online University, 2022. Chap. Empennage Sizing.

[101] A. Sgueglia. "Methodology for sizing and optimising a Blended Wing-Body with distributed electric ducted fans". PhD thesis. Institut Supérieur de l'Aéronautique et de l'Espace, 2019.

[102] D. Simons et al. "Noise breakdown of landing aircraft using a micrphone array and airframe noise model". In: *46th International Congress and Exposition on Noise Control Engineering Taming Noise and Moving Quiet* (2017).

[103] J. Sinke. *AE3211-II Reader: Chapter 10 Lean Manufacturing*. Brightspace: `https://brightspace.tudelft.nl/d2l/le/content/419893/viewContent/2616707/View`. Delft University of Technology. AE3211-II Production of Aerospace Systems. 2022.

[104] J. Sinke. *AE3211-II Reader: Chapter 7 Riveting & Bolting*. Brightspace: `https://brightspace.tudelft.nl/d2l/le/content/419893/viewContent/2608956/View`. Delft University of Technology. AE3211-II Production of Aerospace Systems. 2022.

[105] Yann D. Staelens and Ron F. Blackwelder. "Novel Pitch Control Effectors for a Blended Wing Body Airplane in Takeoff and Landing Configuration". In: *AIAA 2007-683* (2007).

[106] K.D. Subodh and J.G. Kaufman. “Recycling Aluminum Aerospace Alloys”. In: *The Minerals, Metals & Materials Society* (2007).

[107] Athanasios Synodinos, Rod Self, and Antonio Torija. “Noise assessment of aircraft with distributed electric propulsion using a new noise estimation framework”. In: *24th International Congress on Sound and Vibration (ICSV)*. July 2017.

[108] A. Thirkell, R. Chen, and I. Harrington. “A Fuel Cell System Sizing Tool Based on Current Production Aircraft”. In: *SAE Technical Paper* (2017).

[109] S. T. Thompson et al. “Direct hydrogen fuel cell electric vehicle cost analysis: System and high-volume manufacturing description, validation, and outlook”. In: *Journal of Power Sources* 399 (2018).

[110] Simon T. Thompson et al. “Direct hydrogen fuel cell electric vehicle cost analysis: System and high-volume manufacturing description, validation, and outlook”. In: *Journal of Power Sources* 399 (2018).

[111] van Laar, M.J. et al. *Midterm report*. Technical Report. Delft, The Netherlands: Delft University of Technology, 2022.

[112] D Verstraete. “The Potential of Liquid Hydrogen for long range aircraft propulsion”. MA thesis. Cranfield University School of Engineering, 2009.

[113] Augusto Voltes-Dorta and Eliad Becker. “The potential short-term impact of a Hyperloop service between San Francisco and Los Angeles on airport competition in California”. In: *Transport Policy* 71 (2018), pp. 45–56.

[114] R. Vos and M Hoogreef. *Lecture 7 - Landing Gear and Empennage Design*. Brightspace: `https://brightspace.tudelft.nl/d2l/le/content/407821/viewContent/2282380/View`. Delft University of Technology. AE1222-II Aerospace Design & Systems Engineering Elements. 2022.

[115] R. Vos and J.A. Melkert. *Wing and Propulsion System Design*. Brightspace: `https://brightspace.tudelft.nl/d2l/le/content/213451/viewContent/1472042/View`. AE1222-II Aerospace Design and Systems Engineering Elements I. Delft University of Techonoly. Accessed: 29-05-2022. 2019.

[116] D.G. Vutetakis. “Applications – Transportation | Aviation: Battery”. In: *Encyclopedia of Electrochemical Power Sources* (2009).

[117] T. Wan and B. Song. “Aerodynamic Performance Study of a Modern Blended-Wing-Body Aircraft Under Severe Weather Situations”. In: *American Institute of Aeronautics and Astronautics* (2011).

[118] Philip Andrew Weed. “Hybrid Wing-Body Aircraft Noise and Performance Assessment”. Masters Thesis. Cambridge, Massachusetts: Massachusetts Institute of Technology, 2010.

[119] J.R. Welstead and J.L. Felder. “Conceptual Design of a Single-Aisle Turboelectric Commercial Transport with Fuselage Boundary Layer Ingestion”. In: *American Institute of Aeronautics and Astronautics* (2016).

[120] M.M. Whiston et al. “Expert assessments of the cost and expected future performance of proton exchange membrane fuel cells for vehicles”. In: *Proceedings of the National Academy of Sciences* 116 (2019).

[121] C Winnefeld et al. “Modelling and Designing Cryogenic Hydrogen Tanks for Future Aircraft Applications”. In: *Energies* 11.105 (2018).

[122] B. Yildiz et al. “A Generic Approach to Analyze the Impact of a Future Aircraft Design on the Boarding Process”. In: *Energies* (2018).

[123] M. Zhang et al. “Assessment Method of Fuel Consumption and Emissions of Aircraft during Taxiing on Airport Surface under Given Meteorological Conditions”. In: *Sustainability* (2019).

[124] William E. Zorumski. *Aircraft Noise Prediction Program Theoretical Manual Part 2*. Technical Memorandum NASA-TM-83199-PT-2. Hampton, Virginia: National Aeronautics and Space Administration, 1982.